
Late Pleistocene paleoceanography of the Subarctic Pacific
derived from the diatom record

Kumulative Dissertation
zur Erlangung des akademischen Grades eines
Doktors der Naturwissenschaften
– Dr. rer. nat. –

Am Fachbereich Geowissenschaften
Der Universität Bremen

vorgelegt von

Jian Ren
Bremerhaven, 2015

Gutachter der Dissertation:
Prof. Dr. Ralf Tiedemann
Prof. Dr. Bernhard Diekmann

Erklärung

Hiermit versichere ich an Eides statt, die vorliegende Arbeit, abgesehen von der Beratung durch meine akademischen Lehrer, selbständig und ohne Zuhilfenahme fremder als der hier angegebenen Quellen angefertigt zu haben.

Bremerhaven, 03. 09. 2015

Jian Ren

Meinen Eltern

献给我的父母

Abstract

Paleoceanography and climate variability of the Late Pleistocene is of vital importance to understand the mechanisms of glacial-interglacial cycles and abrupt climate changes during deglaciations. In relation to the paleoceanography studies carried out in the North Atlantic, rather few recent research has been done in the North Pacific. Developments of sea surface temperature and sea ice in the past provide crucial information on paleoceanographic variability. The aim of this thesis is to establish a diatom-based transfer function for sea surface temperature and to reconstruct the Late Pleistocene paleoceanographic history based on diatom assemblages, in order to improve the understanding of the North Pacific's role in the global glacial-interglacial climate changes. The thesis consists of three studies, of which the results are presented in three manuscripts.

In the first study, a new diatom data set was generated from 422 surface sediments, covering a broad range of environmental variables of the northern North Pacific, the Sea of Okhotsk and the Bering Sea. The diatom biogeographic distribution patterns of 38 species and species groups were mapped. Statistical analysis discloses that 32 species and species groups have strong correspondence with the pattern of summer sea surface temperature (SSST). This close relationship between diatom assemblages and the SSST is useful in deriving a transfer function in the northern North Pacific for the quantitative paleoceanographic studies. In addition, the relative abundance of the sea ice indicator diatoms *Fragilariopsis cylindrus* and *F. oceanica* of >20% in the diatom composition is used to represent the winter sea ice maximum extent in the Bering Sea.

In the second research project, a new diatom-based transfer function for SSST reconstructions was established based on 206 surface sediment samples with 32 species and species groups recovered in the northern North Pacific and its marginal seas. The SSST was estimated by three different techniques: the Imbrie and Kipp Method (IKM), the Modern Analog Technique (MAT) and Artificial Neural Network technique (ANN). All the SSST estimates for surface samples derived from three methods show high correlations with the modern observations. The transfer functions based on IKM, MAT and ANN were tested on a sediment core retrieved from the western North Pacific for the last 180 ka (ka=10³ yr). The SSST reconstruction, although with low glacial-interglacial temperature amplitudes of 1.5-2 °C, displays clear climate variability patterns. The reconstructed SSST is consistent with the local planktonic $\delta^{18}\text{O}$ record and the NGRIP $\delta^{18}\text{O}$ profile, indicating its potential for paleoceanographic reconstruction in the region.

In the third study, diatom records from both the eastern and western North Pacific demonstrate glacial-interglacial variability for the last 160 ka. The diatom-derived SSSTs show uninterrupted temperature reconstructions in the northern North Pacific, covering the whole last glacial-interglacial cycle for the first time in the region. The sea ice diatom and cold water species imply ice-free environment for the last 160 ka in the eastern and western North Pacific open ocean. A possible sea ice expansion during Heinrich Event 1 is indicated by high abundance of cold water diatoms as well as sea ice biomarker from previous studies.

An ocean basin-wide east-lead-and-west-lag phenomenon has been discovered in the eastern and western North Pacific during the Termination I and II. It is likely that the mountain glaciers in northwestern America responded faster to the increased summer insolation during the terminations, and discharged huge amount of melting water into the nearby open ocean, which consequently changed the surface environment earlier in the eastern North Pacific

The studies of this thesis document the diatom distribution in the northern North Pacific surface sediments and discover a close relationship between the diatom assemblages and the SSST, which is fundamental for a quantitative paleoceanographic study based on diatom fossils. Accordingly, a new diatom-based transfer function for SSST reconstructions is established and applied to sediment cores, providing continuous SSST records for the first time in the northern North Pacific for the last 160 ka. The reconstructed SSST records show similar patterns with the global climate variability records elsewhere. During the terminations, diatom records also display a basin wide lead-and-lag phenomenon, implying possible local imprints on global climate signals.

Kurzfassung

Paläozeanographie und Klimavariabilität des späten Pleistozäns sind von erheblicher Bedeutung für das Verständnis der Mechanismen von Glazial-Interglazial-Zyklen und dem abrupten Klimawandel während der Deglaziation. Im Verhältnis zu den bisherigen paläozeanographischen Studien aus dem Nordatlantik fand bisher eher wenig solche Forschung im Nordpazifik statt. Die Entwicklung von Meeresoberflächentemperaturen und Meereisverbreitung in der Vergangenheit bieten maßgebliche Informationen über die paläozeanographische Variabilität. Ziel dieser Doktorarbeit ist es, eine Diatomeen-basierende Transferfunktion für Oberflächentemperaturen zu etablieren und die spätpleistozäne Geschichte basierend auf Diatomeen-Assoziationen zu rekonstruieren, um dadurch das Verständnis um die Rolle des Nordpazifiks im globalen Glazial-Interglazial-Klimawandel zu erweitern. Die Doktorarbeit beinhaltet drei Studien, deren Resultate in drei Manuskripten präsentiert werden.

In der ersten Studie wird ein neuer Diatomeen-Datensatz aus 422 Sedimentoberflächenproben generiert, der eine breite Spanne von Umweltvariablen des nördlichen Nordpazifiks, des Ochotskischen Meeres sowie des Beringmeeres umfasst. Das biogeographische Verteilungsmuster von 38 Diatomeen-Arten und Artengruppen wird kartographiert. Statistische Analyse enthüllt, dass 32 Arten und Artengruppen eine starke Verbindung zum Oberflächentemperaturverteilungsmuster ausweisen. Diese nahe Beziehung zwischen Diatomeen-Vergesellschaftung und Oberflächentemperatur ist hilfreich hinsichtlich der Ableitung einer Transferfunktion für quantitative paläozeanographische Studien im nördlichen Nordpazifik. Zusätzlich wird die relative Häufigkeit der Meereis-Indikator-Diatomeen *Fragilariopsis cylindrus* und *F. oceanica* von mehr als 20% der Gesamt-Diatomeen-Assoziation genutzt, um die maximale Wintermeereisausdehnung im Beringmeer zu repräsentieren.

Im zweiten Forschungsprojekt wird eine neue Diatomeen-basierende Transferfunktion zur Rekonstruktion von Sommermeeresoberflächentemperaturen (SMOT) auf der Grundlage von 206 Sedimentoberflächenproben mit 32 Arten und Arten-Gruppen aus dem nördlichen Nordpazifik und seinen Randmeeren etabliert. Die SMOT werden mit drei verschiedenen statistischen Verfahren ermittelt: der Imbrie-und-Kipp Methode (IKM), der Modern-Analogue-Technique (MAT) und dem Künstlichen Neuralen Netzwerk (KNN). Alle SMOT-Berechnungen aus Sedimentoberflächenproben mittels der drei Verfahren zeigen eine hohe Korrelation mit heutigen Messungen an der Meeresoberfläche der jeweiligen Probenposition. Die auf IKM, MAT und KNN basierenden Transferfunktionen werden an einem Sedimentkern vom westlichen Nordpazifik getestet, der die letzten 180 ka (tausend Jahre) Sedimentationsgeschichte beinhaltet. Die SMOT Rekonstruktion zeigt klare Muster der Klimavariabilität, obwohl die Glazial-interglazial-Amplitude nur 1,5 bis 2°C beträgt. Die rekonstruierten SMOT stimmen dabei mit den regionalen planktischen $\delta^{18}\text{O}$ -Aufzeichnungen sowie dem NGRIP $\delta^{18}\text{O}$ -Profil überein, was ihr Potential für paläozeanographische Rekonstruktionen in der Region aufzeigt.

In der dritten Studie legen Diatomeen-Aufzeichnungen vom östlichen und westlichen Nordpazifik die Glazial-Interglazial-Variabilität der letzten 160 ka dar. Die Diatomeen-Abgeleiteten SMOT zeigen eine

lückenlose Temperaturrekonstruktion des nördlichen Nordpazifiks und decken dabei zum ersten Mal vollständig den letzten Glazial-Interglazial-Zyklus in dieser Region ab. Meereis-Indikator-Diatomeen und Kaltwasserarten deuten auf eisfreie Umweltbedingungen im offenen Ozean des westlichen und östlichen Nordpazifiks während der letzten 160 ka hin.

Eine mögliche Meereis-Expansion während Heinrich-Ereignis 1 wird durch eine große Häufigkeit von Kaltwasser-Diatomeen sowie Meereis-Biomarkern vorangegangener Studien angezeigt. Ein ozeanbeckenweites Ost-führt-West-folgt Phänomen wurde während der glazialen Terminationen I und II im östlichen und westlichen Nordpazifik entdeckt. Es ist hierbei wahrscheinlich, dass die Bergvergletscherungen auf dem nordwestlichen amerikanischen Kontinent schneller auf erhöhte Sommerinsolation während der Terminationen reagierten und enorme Mengen an Schmelzwasser in den angrenzenden Ozean abführten, was infolgedessen schon früh die Umweltbedingungen im Oberflächenwasser des östlichen Nordpazifiks änderte.

Die Studien dieser Doktorarbeit dokumentieren die Diatomeen-Verteilung in Oberflächensedimenten des nördlichen Nordpazifiks und decken eine enge Beziehung zwischen Diatomeen-Vergesellschaftungen und SMOT auf, welche grundlegend für eine quantitative paläozeanographische Studie basierend auf fossilen Diatomeen ist. Dementsprechend wird eine neue Diatomeen-basierende Transferfunktion für SMOT-Rekonstruktionen etabliert und auf Sedimentkerne angewendet, was zum ersten Mal überhaupt vollständige SMOT-Aufzeichnungen für die letzten 160 ka im Nordpazifik bereitstellt. Die rekonstruierten SMOT-Aufzeichnungen zeigen vergleichbare Muster mit Aufzeichnungen globaler Klimavariabilität. Während der glazialen Terminationen zeigen die Diatomeen-Aufzeichnungen ein beckenweites Ost-führt-West-folgt Phänomen, welches eine mögliche lokale Prägung auf das globale Klimasignal impliziert.

Acknowledgements

First and foremost, I would like to thank my two supervisors Dr. Rainer Gersonde and Prof. Dr. Ralf Tiedemann for offering me the opportunity to do my PhD on this intriguing topic at Alfred Wegener Institute Helmholtz Center for Polar and Marine Research (AWI). Thank you for your sincere support and kindly help throughout my study. Special thanks go to Rainer, who invited me to the INOPEX cruise and advised my research work, for inspiring ideas, professional discussions, constructive comments and tremendous amount of time and efforts dedicated. I am also truly grateful for the financial support for my PhD from Prof. Dr. Gerald Haug from Universität Potsdam. Prof. Dr. Bernhard Diekmann is thanked for reviewing my thesis.

I am deeply indebted to Dr. Oliver Esper for helping me with every detail about diatom identification and transfer functions, which benefit my study greatly. In particular, I incredibly acknowledge Dr. Constance Sancetta, who enlightens me with carefulness and encourages me all the time. Oliver and Connie, without your patience and dedication, my PhD study would have been much harder. Prof. Dr. Ruediger Stein, Dr. Andrea Abelmann, Dr. Kirsten Fahl, Dr. Frank Lamy, Dr. Rainer Sieger, Dr. Lester Lembke-Jene and Dr. Gerhard Kuhn from Marine Geology group are thanked for sharing nice scientific papers and your considerateness. Prof. Michael Sarnthein from Universität Kiel is thanked for fruitful discussion on the stratigraphy of studied cores, and Dr. Joël Guiot from Aix-Marseille Université is acknowledged for explanation on ANN applications. I thank Dr. Frank Schmieder from Universität Kiel for kindly offering Fe XRF data of sediment cores. I also thank Prof. Anne de Vernal from Université du Québec à Montréal, Dr. John Barron from USGS, and Dr. Eric Galbraith from McGill University and Prof. Kozo Takahashi from Kyushu University for our beneficial discussion and talks. Many thanks go to Stephan Heckendorff, who devoted much time to solve my problems on ODV application. I thank Ute Bock, Rita Fröhlking and Michael Seebeck for lab assistance, as well as the cruise members of INOPEX and KALMAR for providing material for my PhD study. I really appreciate our secretary Aysel Sorensen and Susanne Steinfeld and Heidi Trage from Universität Bremen for your patience and helps for administration works. Karin Leiding from AWI Library is also thanked for your kindness.

Special acknowledgement goes to the Helmholtz Graduate School for Polar and Marine Research (POLMAR) for enrolling me as a student member and for providing various interesting and beneficial lectures on science and soft skills, and to the AWI DokTeam and Dr. Sabine Kasten, Dr. Claudia Hanfland and Dr. Claudia Sprengel for your support and encouraging words.

I am thankful that my friends in and outside Germany always backed me when I was in trouble and eased me when anxious. I thank AWI Chinese friends Haiyan, Hao, Shuang, Wenshen, Xun, Wei and Yubin for the countless wonderful days and nights we shared together, curing my homesickness. I thank Barteck Kotrys and Christian Stepanek, my roommates for one year and friends forever, for the interesting discussions about this colorful and diverse world and for tasty foods and of course vodka. I also thank Xiaowei, Jie, Fangliang, Xi, Pengfei, Zhouyang, Jun, ViviQ, ElaineX, Ryan and Xuan for everlasting warm

greetings and encouragement from homeland. Many thanks go to my colleagues from Geowissenschaft department, Edith, Hartmut, Innes, Jenia, Johannes, Lars, Marie, Michael, Nadine, Sarah, Tanja, Thomas, Verena and all other AWI comrades, for making a friendly and homelike working environment. Xiaoping, Huadong, Xiaotong, Tong, Xiaoxia, Mike, Xuezhu, Xu, Qiang, Chen, Yameng, Tingting, Qun, Sven, Yongshen, Qinghua, Dong, Rong, Youji, Weixia, Hongkun, Hongwen and Nanjun and your families and all other friends too numerous to mention individually by name are acknowledged as well. I am grateful to my international roommates, Bartek, Shuang, Gaston, Johannes, Laura and Hartmut. You all and *Linzer str. 7* will be part of my memory forever.

I would like to thank Prof. Hui Jiang, Prof. Min Liu and Dr. Longbin Sha from East China Normal University (ECNU), Shanghai, Dr. Jianfang Chen, Dr. Haiyan Jin and Dr. Lihua Ran from the Second Institute of Oceanography (SIO), Hangzhou, Dr. Yuanhui Huang from the First Institute of Oceanography (FIO), Qingdao, for your significant scientific support and encouragement.

Last but absolutely not least, I sincerely thank my parents and my beloved Kunkun, for your endless support, your patience, your understanding, your considerateness and for so many things too plentiful to describe here. Without you, I can hardly make it through. For my whole life, I owe you a debt of gratitude for what you have done and haven't done. I love you!

寒窗数载终破晓。对我的父母和女友困困，除了谢意和歉意，我笔尖词穷。感谢这些年来你们无尽的付出和漫长的等待，感谢你们的耐心和体贴，感谢你们默默的鼓励和支持，感谢你们源源不断的爱。谢谢你们，我爱你们！

Contents

<u>Abstract</u>	<u>i</u>
<u>Kurzfassung</u>	<u>iii</u>
<u>Acknowledgements</u>	<u>v</u>
<u>Chapter 1: Introduction</u>	<u>1</u>
1.1 Motivation and objectives	1
1.2. The northern North Pacific and its marginal seas	4
<i>1.2.1. Modern oceanographic settings and climate condition</i>	<i>4</i>
<i>1.2.2. Relevant paleoceanography and marine micropaleontology studies</i>	<i>7</i>
1.3. Diatom and its application in paleoceanography	9
<u>Chapter 2: Material and Methods</u>	<u>11</u>
2.1. Material	11
<i>2.1.1. Surface samples</i>	<i>11</i>
<i>2.1.2. Sediment cores</i>	<i>11</i>
2.2. Methods	13
2.3. Diatom based transfer function for summer sea surface temperature (SSST)	15
2.4. Core chronology	19
<u>Chapter 3: Diatom distributions in northern North Pacific surface sediments and their relationship to modern environmental variables</u>	<u>23</u>
3.1 Introduction	23
3.2 Regional setting	24
3.3 Material and methods	27
3.4 Results	33
3.5 Discussion	47
3.6 Conclusions	55
Supplementary material	57
<u>Chapter 4: Diatom-based transfer function for the estimation of sea surface temperatures in the northern North Pacific: development, calibration and caveats</u>	<u>61</u>
4.1 Introduction	61
4.2 Sediment material and its relation to modern oceanography	64
4.3 Methods	66
4.4 Results	71

4.5 Discussion	83
4.6 Conclusions	86
<u>Chapter 5: Late Pleistocene palaeoceanographic variability in the northern North Pacific for the last 160 ka: evidences from diatom records</u>	<u>89</u>
5.1 Introduction	89
5.2 Oceanography settings	91
5.3 Material and methods	92
5.4 Results	98
5.5 Discussion	101
5.6 Conclusions	112
<u>Chapter 6: Conclusion and Perspectives</u>	<u>113</u>
6.1. Conclusions	113
6.2. Future perspectives	117
6.2.1. <i>Improvement of SSST reconstruction</i>	<i>117</i>
6.2.2. <i>Sea ice reconstruction</i>	<i>117</i>
6.2.3. <i>Paleoceanography in the Bering Sea</i>	<i>118</i>
<u>Data handling</u>	<u>121</u>
<u>References</u>	<u>122</u>
<u>Appendix</u>	<u>141</u>

Chapter 1 Introduction

1.1. Motivation and objectives

1.1.1. Motivation

The North Pacific is one of the largest ocean basins, which contains more than 25% of the world ocean volume (Zahn et al., 1991). Nowadays it is characterized by an extremely low salinity surface layer (permanent halocline), preventing water column vertical mixing and ocean-atmosphere gas and heat exchange, which influences marine productivity and determines global CO₂ concentration (Haug et al., 1999; Sarnthein et al., 2004). The fresh water flow through the Bering Strait from the North Pacific to the North Atlantic is assumed to be a factor that stabilizes the global climate variability (Keigwin and Cook, 2007). Formation and maintenance of this fresh water layer are affected by several factors, among which are sea ice and sea surface temperature (SST). Therefore, the development history of sea ice and SST are of vital importance to understand the role the North Pacific plays in the global oceanographic and climatic changes, especially for the last glacial-interglacial cycle. However, the Late Pleistocene paleoceanography in the North Pacific is not well studied. For instance, only few reliable SST records are reconstructed in the area (Fig. 1.1; Margo Project Members, 2009). The poorly developed paleoceanographic research is attributed partly to the shallow carbonate compensation depths (CCD; ~3500 m, Berger and Winterer, 1974), resulting in the absence of calcareous fossils preserved in the sediments for ¹⁴C dating and geochemistry studies, and partly to the uncertainty of reservoir ages in the area, which ranges between 700-900 years according to different studies (e.g. Southon et al., 1990; Keigwin et al., 1992; Galbraith, 2006; Caissie et al., 2010; Davies et al., 2011; Max et al., 2012).

The Northern Hemisphere inter-ocean teleconnections are of great interest to have a comprehensive knowledge of the transmission mechanisms of climate events between ocean basins, such as the North Pacific and North Atlantic (Max et al., 2012). In spite of the fact that the paleoceanographic variability of the North Pacific has similar pattern to those of the North Atlantic (Kotilainen and Shackleton, 1995), Greenland (Hendy and Kennett, 1999; Max et al., 2014) and even the Antarctic (Jaccard et al., 2005; Galbraith et al., 2008), the synchronicity of abrupt changes (e.g. the last deglaciation) in these areas is still controversial. While some studies imply that the climate shift from the cold Heinrich Event 1 (H1) to the warm Bølling-Allerød (B/A) in the North Pacific is synchronous to the North Atlantic (Galbraith et al., 2007; Max et al., 2012; Lam et al., 2013), the other researches suggest an earlier response (Nakagawa et al., 2003; Gebhardt et al., 2008; Maier et al., 2015). To clear up the dissimilarity of these results, more high resolution and well dated sediment samples are required.

In order to elucidate the importance of the northern North Pacific in past and present global climate development and to fill the knowledge gaps of this region, several cruises were carried out in recent years, focusing on different timescales. The Integrated Ocean Drilling Program (IODP) Expedition 323 and 341 aim at the Neogene paleoceanography in the Bering Sea and the southern Alaska margin, respectively

(Expedition 323 Scientists, 2009; Expedition 341 Scientists, 2014), while two cruises with R/V *Sonne*, the Innovative NOrth Pacific EXperiment (INOPEX) and the Kurile-Kamchatka and ALeutean MARginal (KALMAR), target mainly on the last glacial-interglacial transition in the same region (Dullo et al., 2009; Gersonde, 2012).

This thesis is partially based on the samples from INOPEX and KALMAR to decipher the paleoceanography in the northern North Pacific and the Bering Sea for the last 160 ka (ka=10³ yr), by using diatom fossils preserved in the sediments, which is a powerful proxy especially in this region devoid of calcareous components.

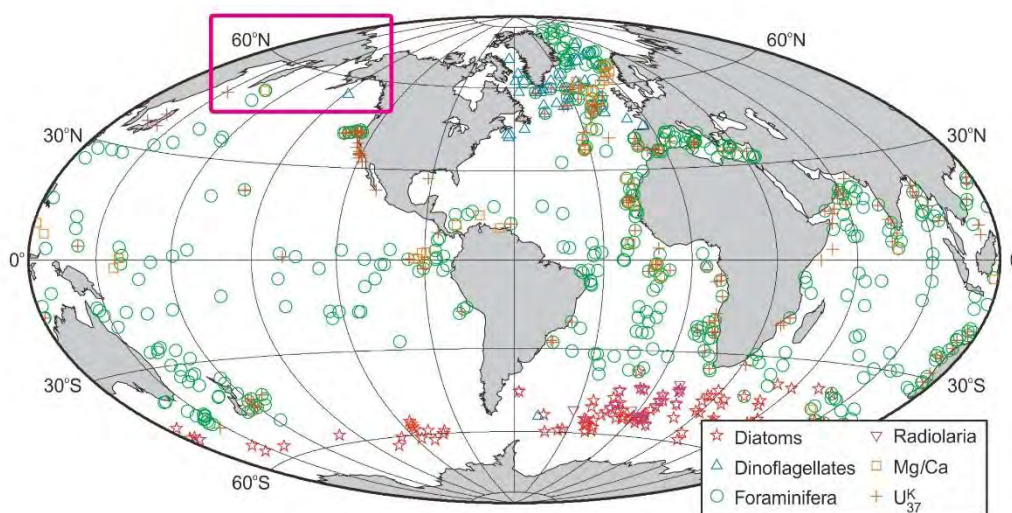


Fig. 1.1 Last glacial SST reconstruction stations of Multiproxy Approach for the Reconstruction of the Glacial Ocean Surface project (MARGO). The red square indicates the northern North Pacific, where only few reliable SST estimations are available (modified after MARGO project members, 2009).

1.1.2. Objectives

The main aim of this thesis is to improve the understanding of Late Pleistocene glacial-interglacial paleoceanographic variability in the northern North Pacific based on diatom records. Therefore detailed objectives are set to achieve this aim.

1) To document the modern diatom distribution in the surface sediment in the northern North Pacific which is the base for the quantitative reconstruction of paleo-sea-surface-environment (e.g. temperature, sea ice concentration) and furthermore to disclose the relationships between the diatom distribution and the environmental variables (e.g. sea surface temperatures, salinities, nutrients) and to detect the major factors which determine the diatom distributions in the northern North Pacific.

2) To establish a reliable diatom reference data set and to verify transfer functions by different methods and to validate the reconstructions of target environmental variables (e.g. temperature, sea ice concentration) by apply them to sediment core records.

3) To reconstruct the paleo-environmental variability in the northern North Pacific for the past 160 ka

(late MIS 6 to Holocene) and to investigate the consistence and disparity of the eastern and western North Pacific.

1.1.3. Synopsis

In the following parts of the introduction, the modern surface oceanography and atmospheric patterns of the northern North Pacific are introduced (*Subchapter 1.2.1*) and the previous relevant paleoceanography studies related the thesis are also briefly reviewed (*Subchapter 1.2.2*). An overview of diatoms as a proxy in paleoceanographic research is presented in *Subchapter 1.3*.

The material and methods used in the thesis are described in *Chapter 2*. The main research results are presented in *Chapter 3-5*, which are either published or in preparation for submission. And finally, the conclusions are summarize and future outlooks are demonstrated in *Chapter 6*. The *Appendix* consists of supplementary data for the manuscripts and additional publications I participated during my PhD study.

The detailed goals of three manuscripts are as listed below.

In *Chapter 3*: Ren, J., Gersonde, R., Esper, O., Sancetta, C., 2014. Diatom distributions in northern North Pacific surface sediments and their relationship to modern environmental variables. *Palaeogeography, Palaeoclimatology, Palaeoecology*, 402, 81–103, doi: 10.1016/j.palaeo.2014.03.008.

We study totally 422 surface samples, which cover the entire northern North Pacific including the Bering Sea and the Sea of Okhotsk, to map the modern distribution of diatom in the area. We statistically analyse the diatom data set, together with the diatom flux data from the sediment traps in the area, to discuss the relationships between the diatom distribution and the environmental variables (e.g. sea surface temperatures, sea ice concentration, salinities, nutrients, mixed layer depths). We also reveal the factors which fundamentally control the distributions of diatom species in the North Pacific.

In *Chapter 4*: Ren, J., Gersonde, R., Esper, O., Sancetta, C. Diatom-based transfer function for the estimation of sea surface temperatures in the northern North Pacific: development, calibration and caveats. To be submitted to *Palaeogeography, Palaeoclimatology, Palaeoecology*.

We develop a new diatom reference data set for quantitative reconstruction of summer sea surface temperature (SSST) in the northern North Pacific. We test three methodologically different transfer function techniques on the reference data set to investigate their performance. We also apply them to a selected sediment core to validate the reliability of the transfer function.

In *Chapter 5*: Ren, J., Gersonde, R., Esper, O., Sancetta, C., Tiedemann, R. Late Pleistocene palaeoceanographic variability in the northern North Pacific for the last 160 ka: evidences from diatom records. To be submitted to *Quaternary Research*.

We provide reconstructed SSST of the northwestern and northeastern North Pacific based on diatom transfer functions, which are for the first time continuous temperature reconstructions in the study area for the last glacial-interglacial cycle. We also present indicator diatom species for sea ice and different water

masses. These results enable us to improve the understanding the role the North Pacific played in the global glacial-interglacial cycle. We also discuss the basin-wide synchronous and asynchronous responses to global climate change in the northwestern and northeastern North Pacific.

1.1.4. Authors' contribution

In **Chapter 3**: I took the surface sediment samples and made quantitative slides for diatom study. I counted all the slides and integrated our original diatom data with the data provided by C. Sancetta. I ran the statistical analysis, supported by O. Esper, and carried out the interpretation of diatom data with contribution from R. Gersonde. I drafted the original manuscript. All co-authors reviewed and discussed the manuscript.

In **Chapter 4**: I sub-sampled most of the core sediment and made quantitative slides for diatom study. I did all diatom counts under microscope. I revised the diatom reference data set and tested the transfer function, with assistance from O. Esper. R. Gersonde and O. Esper discussed the establishment of transfer function and the core age model. I wrote the original manuscript, which was reviewed by all co-authors.

In **Chapter 5**: I took most of the sediment core samples and made quantitative slides for diatom study. I counted all the slides and analyzed the diatom data. I established part of the age model of the sediment core. I drafted the entire manuscript and discussed with O. Esper, R. Gersonde and C. Sancetta.

1.2. The northern North Pacific and its marginal seas

1.2.1. Modern oceanographic settings and climate condition

The North Pacific Ocean is divided into the Subarctic Gyre (Dodimead et al., 1963) and the Subtropical Gyre (e.g. Qiu, 2002; Fig. 1.2) by the Subarctic Front, which is defined as steep gradients of temperature and salinity where the cold and fresh water of the Subarctic Gyre from the north meets the warm and salty Subtropical water to the south (Aydin et al, 2004). The Kuroshio Current (KC) brings warm and salty water-masses from tropical Pacific to the Subtropical Gyre via its eastward extension, the Kuroshio Extension (KE; Kawai, 1972). The Kuroshio Extension turns to the broad and sluggish North Pacific Current (NPC) near the International Date Line (White et al., 1982; Qiu, 2002). At the North America coast, the eastward North Pacific Current partly turns southward, becoming the California Current (CC), and partly runs northward and forms the Alaska Current (AC; Qiu, 2002). The Subarctic Gyre consists of two subgyres, the Alaska Gyre (AG) in the east and the Western Subarctic Gyre (WSG) in the west (Fig. 1.2). The Alaska Gyre is centered at the Gulf of Alaska. The Alaska Stream (AS) originates from the northern branch of the Alaska Gyre and flows along the Aleutian Islands. The water exchange between the North Pacific and the Bering Sea occur mainly via the western Aleutian Islands, due to the shallow passes of the eastern parts (Stabeno et al., 1999; Takahashi, 2005). The Western Subarctic Gyre is located at the junction area of the Bering Sea, the Sea of Okhotsk and the North Pacific (Fig 1). The Alaska Stream joins the East Kamchatka Current (EKC) from the Bering Sea, as it encounters the Kamchatka

Peninsula and turns southwestward along the continent. The Oyashio Current (OC) is formed when the East Kamchatka Current meets with the water-mass from the Sea of the Okhotsk. Off Hokkaido, the Oyashio Current becomes the eastward Subarctic Current (SC), running along the Subarctic Front (Favorite et al., 1976; Fig. 1.2). An anticlockwise gyre, the Bering Sea Gyre (BSG), is formed in the Bering Sea, above the Bering Basin, along the outline of the continental slope (Fig. 1.2; Ohtani et al., 1972). A part of the water-mass from the Bering Sea Gyre originates the East Kamchatka Current along the Siberian coast, while the other part becomes eastward to join the coastal currents along the Alaska on the Bering Shelf. The unidirectional northward outflow is detected from the Bering Sea to the Chukchi Sea of the Arctic Ocean with an amount of 0.85 Sv (Coachman, 1993; Takahashi, 2005). Additionally, a sharp salinity gradient exists along the Bering Shelf slope due to the river runoff from the nearby continents and sea ice melt (Takenouti and Ohtani, 1974). Similar to the Bering Sea, an anticlockwise gyre, the Okhotsk Gyre (OG) dominates the surface currents system of the Sea of Okhotsk (Fig 1). The Sea of Okhotsk receives water-mass from the North Pacific originated from the East Kamchatka Current and from the Sea of Japan via the Soya Strait (Takizawa, 1982).

In present day, no seasonal or perennial sea ice is found in the open ocean Pacific (Fig. 1.2; Dodimead et al., 1963). However, approximately one-third of the Bering Sea, mainly above the Bering Shelf, is covered by winter sea ice. The advance of the sea ice starts at the Bering Strait in November and extends

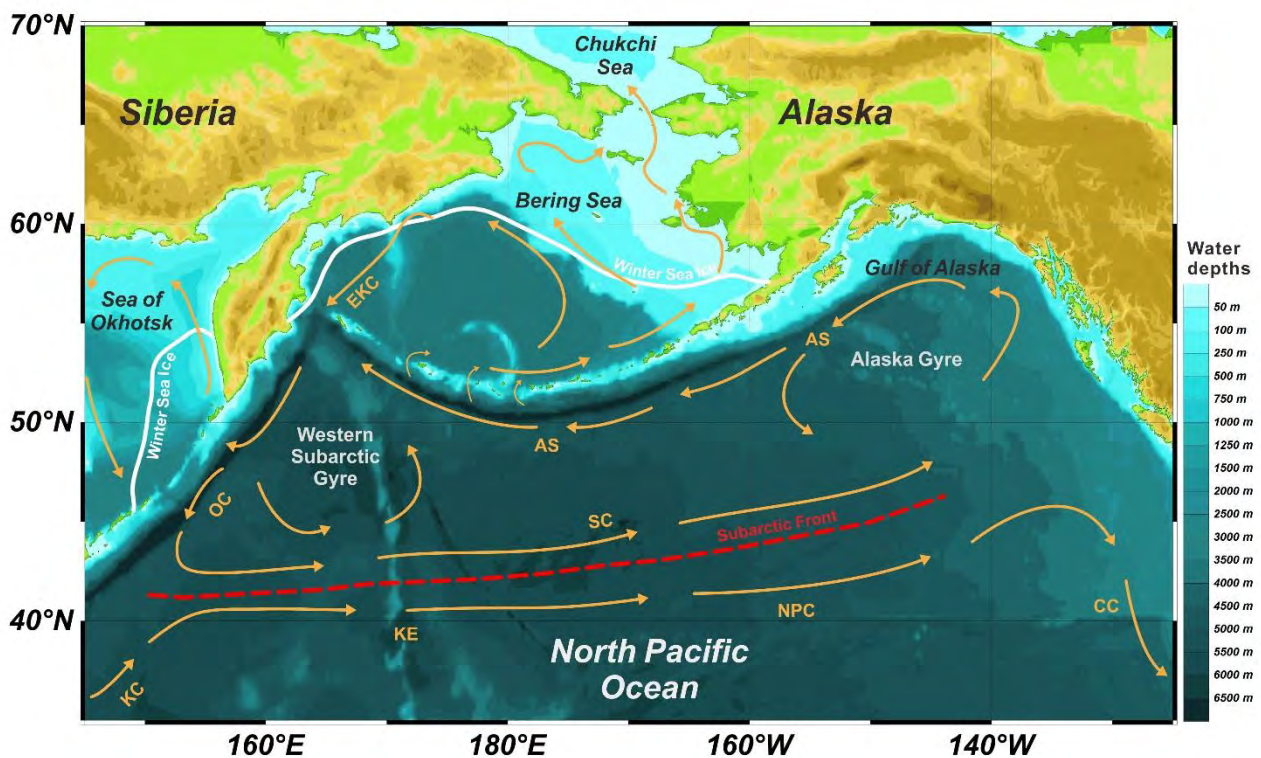


Fig. 1.2 Modern surface circulation of the northern North Pacific, the Bering Sea and the Sea of Okhotsk, shown in orange arrows: AS-Alaska Stream; CC-California Current; EKC-East Kamchatka Current; KC-Kuroshio Current; NPC-North Pacific Current; OC-Oyashio Current; SC-Subarctic Current. The Winter Sea Ice boundary (Averaged 15% sea ice concentration of March of 1982-1991; Raynolds et al., 2002) and the Subarctic Front (Aydin et al., 2004) are indicated by the white lines and red dash line, respectively.

to its southern maximum in March-April and disappears completely in July (Niebauer, 1980, 1983). In contrast, the Bering Basin experiences no seasonal ice cover, although it may be influenced by the drifting ice (Sancetta, 1981). Similarly, the Sea of Okhotsk experiences the winter sea ice, which covers about 75% of the sea (Fig. 1.2; Parkinson et al., 1987). The sea ice occurs in coastal areas in November and extends to its maximum in mid-March, while an ice-free environment appears during the summer (Parkinson and Gratz, 1983; Parkinson et al., 1987).

The upper water column of the modern North Pacific is dominated by a permanent halocline (North Pacific Halocline, at ~150 m water depth), preventing the nutrient and gas exchange between the fresh surface layer and the cold and salty deep ocean (Gargett, 1991). The upper water column is further stabilized by a seasonal thermocline at 50 m water depth in summer (Gargett, 1991). This stratification is maintained by riverine input from the surrounding continents, particularly from the east and north, and low evaporation rate (Warren, 1983; Emile-Geay et al., 2003). Thereby, the deep water formation in the North Pacific is impeded by this fresh surface layer and thus the intermediate water, named North Pacific Intermediate Water (NPIW), is only generated in the Sea of Okhotsk when coastal polynyas occur during the winter sea ice formation (Talley, 1993).

The northern North Pacific open ocean and the oceanic part of the Bering Sea are described as a High-Nutrient-Low-Chlorophyll regime (HNLC), where macro-nutrients are insufficiently consumed throughout the year (Banse and English, 1999; Tsuda et al, 2007). It is hypothesized that iron limitation is the major cause of the low phytoplankton growth in this area (Martin and Fitzwater, 1988) and validated by *in situ* iron enrichment experiments (e.g. Tsuda et al., 2003).

Table 1.1 Minimum and maximum sea surface temperatures (SST) and corresponding months in different areas of North Pacific Ocean (data derived from World Ocean Atlas 1994; Levitus and Boyer, 1994).

Area	SST _{min}	SST _{min} month	SST _{max}	SST _{max} month	ΔSST _{max-min}
Bering Basin	1.53	March	9.36	August	7.83
Bering Shelf	-0.04	March	8.42	August	8.46
Sea of Okhotsk	-0.99	February	10.85	September	11.84
North Pacific open ocean	7.94	March	17.07	August	9.06
NP north of 40°N (subarctic)	4.79	March	13.34	September	8.55
NP south of 40°N (subtropical)	13.83	March	24.11	August	10.28
All	2.57	March	12.01	August	9.44

North Pacific is characterized by significant seasonal SST variability. The average summer (July, August and September) and winter (January, February and March) SST difference of the whole study area is 9.44 °C, while the maximum seasonal contrast of 11.84 °C is found in the Sea of Okhotsk (Table 1.1). These oceanographic features are likely to be associated with temporal and spatial large-scale atmospheric variability, i.e. the Aleutian Low (AL), the Pacific Decadal Oscillation (PDO), the Pacific/North America (PNA) teleconnection mode and further, the Arctic Oscillation (AO) and the El Niño-Southern Oscillation

(ENSO). The PNA and PDO are indices related to the SST seesaw between the central North Pacific and the west American coasts (Mantua et al., 1997; Mantua and Hare, 2002; Overland et al., 2002). The PDO pattern is also found during the Holocene along the margins of the eastern North Pacific (Barron and Anderson, 2011). Furthermore, studies show the location and strength of the AL centers influence the winter climate and sea ice distribution in the North Pacific and the Bering Sea by the storm tracks, which brings warmer moisture into the area (Shinji, 1972; Overland and Pease, 1982; Luchin et al., 2002; Rodionov et al., 2007). As suggested by Rodionov et al. (2007), the annual variability of the Bering Sea climate is primarily determined by the AL position. In a global view, the shift of the AL is further associated with the ENSO and AO conditions (Niebauer, 1998; Overland et al., 1999). In the geological scale, the AL plays a role in shaping the state of the sea ice extent in the Bering Sea and the sea of Okhotsk during the Last Glacial Maximum (LGM) and the Holocene (Katsuki et al., 2009; 2010).

1.2.2. Relevant paleoceanography and marine micropaleontology studies

For paleoceanographic research, marine micropaleontology has long been proved a useful tool to estimate the SST, sea ice and salinity variability in the past (e.g. CLIMAP Project Members, 1976, 1984; Karpuz and Schrader, 1990; Pflaumann et al., 1996, 2003; Sarnthein et al., 2004; Esper and Gersonde, 2014a, b). As a basic study of these quantitative reconstructions, the relationships between surface species distributions and modern environmental variables are of vital importance (Birks, 2010). A few studies focusing on the assemblages of radiolarian, diatoms and dinoflagellate cysts in the surface sediments have been carried out in the northern North Pacific (e.g. Sachs, 1973a; Sancetta, 1982; Bonnet et al., 2012). However, most of them have only regional coverage rather than the entire northern North Pacific. While modern radiolarian assemblages has been investigated by Abelmann and Nimmergut (2005) in the Sea of Okhotsk, diatom distributions were studied by Sancetta (1981, 1982) and Caissie (2012) in the Bering Sea, by Shiga and Koizumi (2000) and Tsoy et al. (2009) in the Sea of Okhotsk, and by Lopes et al. (2006) in the northeast Pacific. In these regional researches, local signals might be overweighed and thus bias the results. In addition, several studies that cover the northern North Pacific suffers from sparse samples (Sachs, 1973a on radiolarian; Bonnet et al., 2012 on dinoflagellate cysts). Despite the broader coverage of the diatom assemblages in the surface samples surveyed by Sancetta (1981, 1982) and Sancetta and Silvestri (1986), the surface data set is impaired by the deficiency of samples from the eastern North Pacific. Nevertheless, most studies discover a close relationship between the diatom assemblages and the water mass distribution, which is generally controlled by SST.

The glacial-interglacial SST variability is critical to the understanding of the Late Pleistocene paleoceanography and paleoclimate (Kucera et al., 2005a). Additionally, reconstructed SSTs provide crucial information to validate the performance of climate models and hence improve the future climate predictions (MARGO Project Members, 2009). In contrast to the North Atlantic and Southern Ocean, the Late Pleistocene SST history in the northern North Pacific is less well studied. The available SST studies

from the northern North Pacific open ocean (de Vernal and Pedersen, 1997; Max et al., 2012; Harada et al., 2012), the Bering Sea (Caissie et al., 2010) and the Sea of Okhotsk (Ternois et al., 2000; Harada et al., 2004) only concentrate on the last 30 to 40 ka, particularly on the Termination I, due to the dissolution of carbonate components in the glacial sediment. Few SST records cover longer time spans (Kiefer et al., 2001; Gebhardt et al., 2008; Haug and Sarnthein, 2005; Harada et al., 2006, 2008; Seki et al., 2009; Max et al., 2014). However, these records are discontinuous between terminations (Gebhardt et al., 2008; Max et al., 2014), in low resolution (Haug 2000; Kiefer et al., 2001) or characterized by a warmer-than-present-day LGM (Harada et al., 2008), preventing a comprehensive and precise picture of the Late Pleistocene SST variability of the northern North Pacific. Nevertheless, these SST records show millennial scale fluctuations similar with those of the North Atlantic and the Greenland ice cores (Kiefer et al., 2001; Gebhardt et al., 2008; Max et al., 2012). Whether the millennial scale climate variabilities and trends in these areas are synchronous with those from the Northern Hemisphere has been discussed by several studies on sediment cores, demonstrating contrasting conclusions (Kiefer et al., 2001; Kim et al., 2004; Kiefer and Kienast, 2005; Max et al., 2012). Likewise, climate models also show contradictory results (Saenko et al., 2004; Okumura et al., 2009; Okazaki et al., 2010), implying complicate mechanisms of oceanic and atmospheric teleconnections between ocean basins. Further detailed study on the global teleconnection has been hampered by the lack of carbonate material for ^{14}C dating and uncertainty of the ^{14}C reservoir age in the North Pacific (Sarnthein et al., 2004).

Beside age uncertainty, inconsistency between SST reconstructions based on different proxies, which represent temperatures of variable dwell depths and blooming seasons, might also bias the inter-ocean-basin comparison. The SST reconstructions of Termination I of MD01-2415 from the Detroit Seamount, northwestern North Pacific, estimated by the SIMMAX transfer function and Mg/Ca ratio of planktonic foraminifera, are featured by Mg/Ca SSTs with high frequent fluctuations and more stable and warmer SIMMAX SSTs (Sarnthein et al., 2006; Gebhardt et al., 2008). Seki et al. (2009) also discuss the discordance between the alkenone-derived and TEX_{86} SSTs reconstructed in the Sea of Okhotsk, arguing a shift of coccolithophore growing season from autumn to summer and hence alter the representing alkenone SST. In order to discern the modern production season of marine micro-planktons, samples of a few sediment traps from the northern North Pacific open ocean (Sancetta, 1992; Takahashi, 1997; Tsoy and Wong, 1999; Onodera et al., 2005), the Bering Sea (Onodera and Takahashi, 2009) and the Sea of Okhotsk (Seki et al., 2007) thus have been analyzed. Yet it is hardly possible to clarify the blooming seasons in the past.

The northern North Pacific sea ice development in the Late Pleistocene has long been studied using ice rafted debris (IRD) and sea ice related microfossils. Gebhardt et al. (2008) and Katsuki et al. (2003) propose sea ice or drifted ice extent to the northwestern North Pacific during the Termination I and Marine Isotope Stage (MIS) 2 and 3, while in the northeastern counterpart the sea ice transfer function based on dinoflagellate cysts indicates a half-year sea ice cover duration (de Vernal and Pedersen, 1997). However,

these sea ice proxies are indirectly related to sea ice and microfossils also suffer from dissolution, which might distort paleoenvironment reconstructions. In recent years, a novel geochemical biomarker, C₂₅ monounsaturated hydrocarbon (IP₂₅), has been developed to reconstruct paleo sea ice (Belt et al., 2007). IP₂₅ in surface sediments is in consistent with the modern sea ice edge and thus provides the potential for sea ice extent reconstruction in the Bering Sea and the northern North Pacific (Cassie et al., 2012; Méheust et al., 2013; Stoyanova et al., 2013). IP₂₅ from sediment cores highlights that sea ice occurs in the northern North Pacific during the LGM and H1, while it is only discovered in the northwestern North Pacific in the Younger Dryas (YD) cold event (Max et al., 2012; Méheust, 2014), which is in accord with the suggestion that northeastern North Pacific is less affected by the sea ice (Sancetta, 1985).

1.3. Diatom and its application in paleoceanography

Diatoms are microscopic unicellular algae with approximately 10⁵ species (Round and Crawford, 1989), which are distributed in nearly all environments where water is present (Round et al., 1990; Smol and Stoermer, 2010). They are featured by siliceous cell walls, termed frustules, which are formed by absorption of silicate from surrounding water mass. A diatom frustule consists of two valves (namely epivalve and hypovalve) and cingula (or girdle). Structures of valves vary between species, which is the foundation for diatom taxonomy identification. Furthermore, diatoms are photosynthetic and therefore dwell in the photic zone where light is accessible (~30-40 m in temperate ocean; Round and Crawford, 1989).

Diatoms have been discovered for about 200 years and efficiently studied only after the development of fully corrected optical microscopes (Smol and Stoermer, 2010). It is unknown when people start to use the occurrence and abundance of diatom to investigate environmental changes. But certainly diatom usage for environment soared with the upsurge of interest in surface water acidification and with availability of high-speed computers for multivariate statistical analysis in the mid to late 20th century (Birks, 2010; Smol and Stoermer, 2010). For paleoceanography, pioneer researchers studied the relationship between diatom distribution and oceanographic environments (e.g. Smayda, 1958; Jousé et al., 1971; Guillard and Kilham, 1977), which becomes the groundwork for paleoceanographic reconstructions. An early intention for paleo-SST estimation was carried out by Kanaya and Koizumi (1966), using the abundance ratio of warm and cold diatom species, named *Td* index. This empirical method, albeit imprecise, was since then continually applied in paleoceanography (e.g. Barron, 1992, 1995; Koizumi and Sakamoto, 2003; Koizumi, 2008; Koizumi and Yamamoto, 2015). For more accurate reconstructions, Imbrie and Kipp (1971) generated a statistical method, using factor analysis and regression of factor loadings against SST at the same locations (Sancetta, 1999). Such numerical methods, named transfer function later, are widely used in paleoceanography reconstruction (i.e. SST, salinity, sea ice concentration) in different ocean basin (e.g. Sancetta, 1979; Koç Karpuz and Schrader, 1990; Crosta et al., 1998; Zielinski et al., 1998; Jiang et al., 2002; Gersonde et al., 2003, 2005; Esper and Gersonde, 2014a, b; Sha et al., 2014, 2015), providing important

views on regional and global paleoclimate change. Interestingly, state-of-the-art geochemistry techniques have been developed since the last decade for ^{14}C dating (Ingalls et al., 2004) and $\delta^{15}\text{N}$ (Brunelle et al., 2007) based on diatom-bound organic material and for $\delta^{30}\text{Si}$ and $\delta^{18}\text{O}$ from diatom siliceous frustule (De La Rocha et al., 1998; Swann and Leng, 2009), which undoubtedly promote paleoceanographic studies and improve our comprehension for global environmental variability.

Diatoms siliceous frustules are the dominant component of opal deposition in the high latitude oceans (Gersonde, 1990 and references therein), presenting valuable material for paleoceanography in these area, including the North Pacific where calcareous fossils are sparse. In the North Pacific, the diatoms from water column (e.g. Venrick, 1971), sediment traps (e.g. Tsoy and Wong, 1999; Onodera and Takahashi, 2009) and surface sediments (e.g. Kanaya and Koizumi, 1966; Jousé et al., 1971; Sancetta, 1982; Sancetta and Silvestri, 1986; Lopes et al., 2006) have been studied in the past decades. However, due to the lack of carbonate in the sediments for ^{14}C dating and the uncertainty of reservoir ages (as mentioned in **Subchapter 1.1.1**), only few sediment cores focusing on diatoms composition are studied, most of which either extend only to the last termination (Barron et al., 2003, 2009; Caissie et al., 2010; Smirnova et al., 2015) or cover a longer time period but in low resolution (Sancetta and Silvestri, 1984, 1986; Katsuki et al., 2003; Koizumi and Yamamoto, 2015). As a consequence, few diatom transfer functions has been developed in the northern North Pacific (Sancetta, 1979), lagging far behind its global counterparts. In contrast, recent studies on diatom derived isotope records ($\delta^{15}\text{N}$, $\delta^{30}\text{Si}$, $\delta^{18}\text{O}$) show potential capability to deepen the understanding of the paleoceanography in this region (Brunelle et al., 2010; Maier et al., 2013, 2015; Swann and Snelling, 2015).

Chapter 2 Material and methods

2.1. Material

2.1.1. Surface samples

The surface material of this study consists of 422 surface samples recovered from the entire northern North Pacific, including the Bering Sea and the Sea of Okhotsk (Fig. 2.1). Among them, 263 samples were taken from a former study by Sancetta and Silvestri (1986), which are trigger-weight and piston-core top samples. The other 159 surface sediment samples, studied at Alfred Wegener Institute Helmholtz Center for Polar and Marine Research (AWI), were collected during cruises INOPEX (Gersonde, 2012), KALMAR (Dullo, et al., 2009), KOMEX (Dullo, et al., 2004) and several Canadian expeditions (M. Henry and A. de Vernal, personal communication), which were retrieved by multicorer and represent the topmost 1 cm of the sediment. The location information is listed in Appendix (Table A1).

Although no direct dating for the surface sediment samples is available, it is assumed that they represent the environment of an average of the past decades, thanks to low sedimentation rates in the area.

Table 2.1 Sediment cores studied in the thesis.

Core	Latitude	Longitude	Water depth	Recovery	Studied section	Studied period	Coring device ^a
MD01-2416	51°16.08'N	167°43.50'E	2317 m	44.75 m	0-12 m	6-176 ka BP	GPC
MD02-2489	54°23.40'N	148°55.26'W	3640 m	29.80 m	0-19 m	8-152 ka BP	GPC
RAMA44	53°N	164°39.20'E	2980 m	3.84 m	0-0.78 m	2-14 ka BP	PC
SO202-12-1	54°03.04'N	179°05.24'E	2109 m	10.69 m	0-6.7 m	1.6-67 ka BP	KAL
SO202-18-6	60°07.60'N	179°26.61'W	1107 m	7.21 m	0-6.92 m	5.4-13 ka BP	KAL

^a Coring device: GPC-Giant Piston Core; PC-Piston Core; KAL-Giant Box Core

2.1.2. Sediment cores

In this thesis, in total 5 sediment cores from the northern North Pacific have been investigated (Table 2.1; Fig. 2.1), including 3 cores from the North Pacific open ocean (MD01-2416, MD02-2489 and RAMA 44) and 2 cores from the Bering Sea (SO202-12-1 and SO202-18-6). Giant piston core MD01-2416 and MD02-2489 were retrieved from the Detroit Seamount, Northwestern Pacific and from the Patton Seamount, Northeastern Pacific during the IMAGES VII WEPAMA cruise by R/V *Marion Dufresne* in 2001 and 2002, respectively (Bassinot and Baltzer, 2002). RAMA 44 was taken on Scripps Institution of Oceanography RAMA Expedition at the crest of Meiji Seamount, Northwestern Pacific by R/V *Thomas Washington* in 1980 (Keigwin, 1987). In addition, giant box core SO202-12-1 and SO202-18-6 were recovered from the Bowers Ridge and the shelf break of Bering Shelf, respectively, during the SO202-INOPEX cruise by R/V *Sonne* in 2009 (Gersonde, 2012).

The sediment of MD01-2416 dominantly consists of diatom bearing and diatomaceous olive gray clay and silty clay, interbedded with diatomaceous ooze. The sediment is similar in MD02-2489 by the observation of smear slides and diatom slides under the microscope, although no core description is available as this core was retrieved in the transit gap between two cruises (M. Sarnthein, personal communication). The sediment of RAMA44 and SO202-12-1 is composed of diatom bearing and diatomaceous dark olive gray clay and olive gray clay interrupted by diatomaceous ooze. Owing to its closer location to the terrestrial input, the sediment of SO202-18-6 comprises coarser material, i.e. sandy mud and silty clay. Ash layers are found in all five cores. Most of them are not observed under the microscope of diatom slides due to the sampling interval, except four samples of pure volcanic glass shards are encountered in MD02-2489. In general, two layer of laminated sediments are found in SO202-12-1 and SO202-18-6, corresponding to the B/A event and the early Holocene (Gersonde, 2012; Kuehn et al., 2014). These laminae represent diatomaceous ooze in which diatom valves are significantly well preserved.

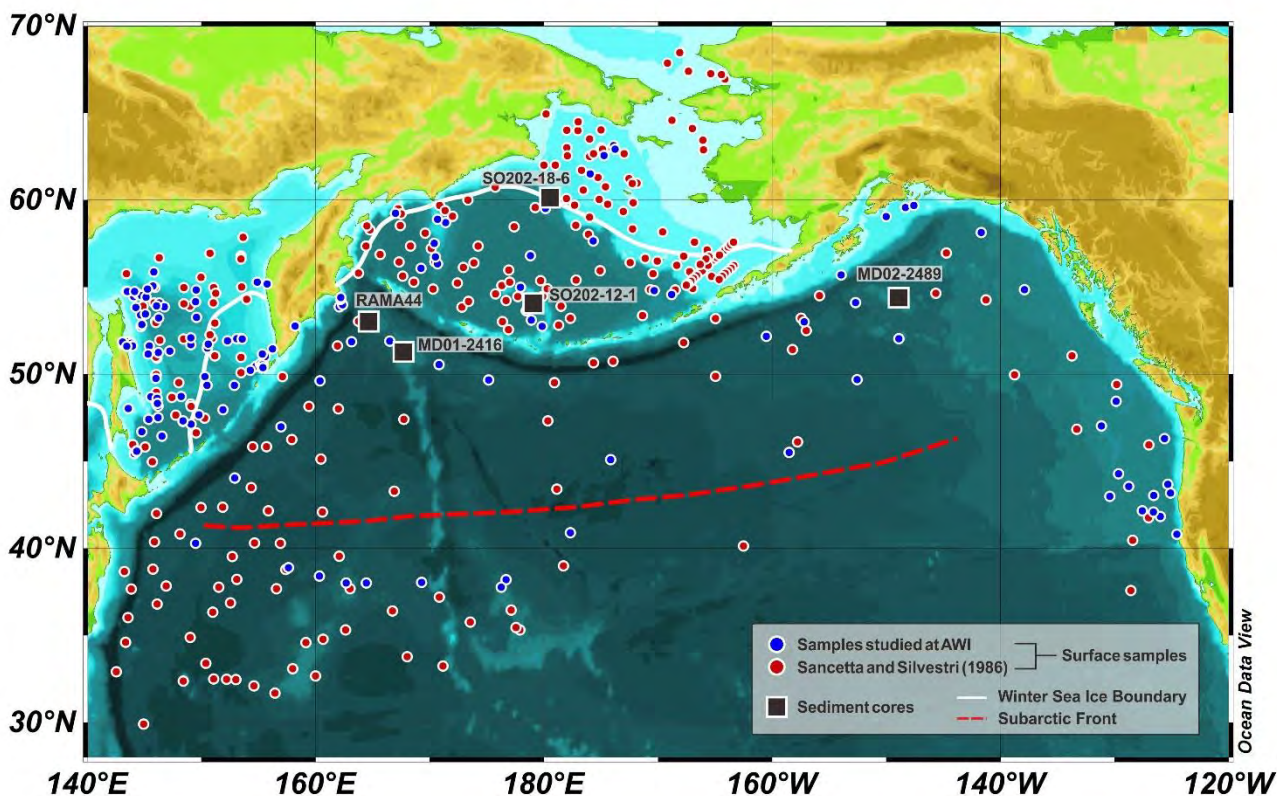


Fig. 2.1 Distribution map of 422 surface samples in the North Pacific Ocean (blue and red circles). Sediment cores are indicated by black squares. The winter sea ice edge (March of 1982–1991; Reynolds et al., 2002) and the Subarctic Front (Aydin et al., 2004) are shown as the solid white and dashed red lines, respectively.

The sections of MD01-2416 and MD02-2489 studied in this thesis cover the period from Marine Isotope Stage 6 (MIS 6) to mid-Holocene, allowing investigations on glacial-interglacial paleoceanography variability in the northern North Pacific (Table 2.1; Fig. 4.2; Fig. 5.2). Both RAMA44 and SO202-18-6 document the diatom variability of past 14 ka, while SO202-12-1 extends back to 70 ka BP (Table 2.1).

2.2. Methods

2.2.1. Preparation of diatom study slides

For the surface samples, topmost 1 cm of the sediment were gathered to represent the modern environment. For the sediment core samples, sub-samples were collected as 1-cm slices at 10 cm interval throughout the cores. Additionally, in order to precisely capture the abrupt climate change during Termination I, sampling interval was increased to 5 cm for MD01-2416, MD02-2489 and SO202-12-1 at the corresponding H1-B/A boundary. For the thick laminae section (thickness >200 cm) in SO202-18-6, the sampling interval is reduced to ca. 50 cm to protect the intact laminated material for future study. In total 565 samples, including 159 surface samples and 406 core samples, were taken for diatom study.

The cleaning of the sediment samples and the preparation for permanent mounts for light microscopy are according to a routine method established at the Alfred Wegener Institute Helmholtz Center for Polar and Marine Research (AWI; Gersonde and Zielinski, 2000). All samples were freeze-dried in the first place. 0.5 g of sediment (in few times 0.2, 0.3 or 0.4 g, dependent on sample's availability) were treated in a 400 ml beaker with ca. 15 ml of hydrogen peroxide (H₂O₂, 35%) and ca. 15 ml of concentrated hydrochloric acid (HCl) and heated at ca. 150 °C to enhance the reaction and evaporate the peroxide. After completion of the reaction, demineralized water was added up to 400 ml. The water was mildly removed by a water jet pump after a settling time of 24 h. The washing process was repeated 9 to 10 times until all acid residue was cleaned and a part of the clay fraction was removed. The acid-free residue was then transferred to a 50 Nalgene bottle and diluted exactly to 50 ml for storage. Two or three drops of neutralized formaldehyde (CH₂O) were added for preservation.

For quantitatively diatom estimation, microscopic slides with evenly distributed diatom valves were made. Three grease-free round cover glasses with diameter of 1.8 cm were placed in a petri dish (diameter: 4.8 cm, inner wall height: 1.7 cm) filled with demineralized water. In order to mount the diatom valves to the cover glasses, a small portion of gelatin (0.085 g/l) was added to the petri dish. The filled Nalgene bottle was shaken carefully to re-suspend the sample residue. A defined aliquot, which was dependent on the corresponding diatom concentration, was taken from the center of the evenly suspended sample residue by an automatic pipette and then randomly suspended in the petri dish. After a settling time of 2 h, the water in the petri dish was removed by a strip of absorptive paper. When the petri dish was fully dried (generally after 24 h air drying), two cover glasses was chosen for permanent mounting using the mounting media Meltmount ($n_D^{20} \sim 1.662$, toluene as solvent). The material on the cover glass was covered by gelatin to prevent shifting during the mounting process. All slides were labeled and stored in slides boxes.

2.2.2. Diatom identification and microscopic estimation

The diatom counting procedure followed the steps established by Schrader and Gersonde (1978). An average of 400 diatom valves in several traverses across the slide was counted for each sample with a Zeiss

Axioskop microscope at $\times 1000$ magnification with apochromatic optics. Diatom valves and fragments were counted according to the criteria set by Schrader and Gersonde (1978) and Zielinski (1993). These criteria were slightly revised by adding in endemic species, in order to be applied to countings on North Pacific diatoms (Table 2.2).

Diatoms were counted to species or species group level. The diatom were identified according to the following literature: Sancetta (1982), Akiba (1986), Sancetta (1987), Medlin and Priddle (1990), Hasle and Syverstsen (1997), Witkowski et al. (2000) and Onodera and Takahashi (2007). In total 140 taxa were identified.

The preservation state of diatom valves was recorded during diatom identification under the microscopy. Five categories of preservation were established based on the description by Zielinski (1993): Good (1): assemblage consists both of heavily and weakly silicified diatom species with no dissolution of the areolae or the valve margin or fragmentation, Moderate (3): both heavily and weakly silicified species are present but the latter show marked dissolution of the areolae or the valve margin or fragmentation and Poor (5): assemblage dominated by heavily silicified species with dissolution of the areolae or the valve margin and many fragmented valves. Categories 2 and 4 represent intermediate conditions.

2.2.3. Data preparation

The raw diatom valve counts were converted to percentage abundance. In order to avoid terrestrial and lateral influences, all the fresh, brackish and benthic species were excluded and relative percentages were recalculated. Some diatom taxa were combined as groups. For instance, *Chaetoceros* resting spores were combined into the group *Chaetoceros* resting spores, which cannot be identified to species level due to the absence of setae. Thus, only 38 species and species groups were used in the further statistical analysis.

For the statistical analysis, a further logarithm-based transformation, as suggested by Zielinski et al. (1998), was applied in order to down-weight the most abundant species, such as *Neodenticula seminae*, which accounts for up to 80% of the total assemblage in some samples. The following equation is used:

$$L = \text{LOG}_{10} (\text{relative abundance} \times 10 + 1) \quad (1)$$

To calculate diatom valve concentration (valves per gram dry sediment), an equation developed by Esper et al. (2010) was used:

$$\text{Diatom valves/gram} = (1/w) \times (csa/ta) \times (sv/split) \times (dvn/tn) \quad (2)$$

where w is the dried sample weight in grams, csa is the area of the cover slide (254.5 mm^2), ta is the area of one counted traverse (3.6 mm^2), sv is the volume of processed diatom suspension (50 ml), $split$ is the volume of suspension split onto the cover slide (from 1.4 to 9.8×10^{-2} ml), dvn is the total counted diatom valve number and the tn is the number of fully counted traverses.

2.2.4. Statistical methods

Q-mode factor analysis was used to simplify the surface diatom data set into a small number of

varimax factors and to identify the most dominant species by a software package from Sieger et al. (1999).

Canonical Correspondence Analysis (CCA), a direct gradient analysis to investigate the variation in the modern biological assemblages that could be explained by the corresponding environmental variables, was chosen to statistically detect the influences of environmental variables on the distribution of diatom species, by using the CANOCO program (version 4.5; ter Braak and Smilauer, 2002). A forward selection then was used to rank the importance of the environmental variables for determining the diatom species distribution or to reduce the insignificant variables (if the statistical significance level, e.g. p -value >0.05).

Nine modern environmental variables were selected for CCA: the summer sea surface temperatures from World Ocean Atlas 1994 (WOA94; Levitus et al., 1994); summer sea surface salinity from World Ocean Atlas 2005 (Antonov et al., 2006); the mean annual sea surface concentration of dissolved nitrate (NO_3), phosphate (PO_4) and silicate (SiO_4) from World Ocean Atlas 2005 (Garcia et al., 2006) (all above at 10m water depth); summer and winter sea ice concentration (SSIC and WSIC) from NOAA Optimum Interpolation (OI) Sea Surface Temperature Version 2 (Reynolds et al., 2002) and summer and winter mixed layer depths (MLD) from World Ocean Atlas 1994 (Monterey and Levitus, 1997). All the data sets have a $1^\circ \times 1^\circ$ spatial resolution, which guarantees the data quality. The selected environmental variables for each surface sample are listed in Appendix (Table A1). In this study summer means July, August and September and winter stands for January, February and March.

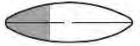
2.3. Diatom based transfer function for summer sea surface temperature (SSST)

2.3.1. Transfer function methods

In this thesis, three methods are used to for the SSST reconstruction: IKM (Imbrie and Kipp, 1971), MAT (Hutson, 1980) and ANN (Malmgren et al., 2001). These transfer functions basically represent three different methods to associate a specific diatom assemblage preserved in sediment with an SSST and to estimate SSSTs based on this relationship.

The Imbrie and Kipp Method (IKM) was developed by Imbrie and Kipp (1971) and Klován and Imbrie, (1971). The IKM is based on the principal components analysis (PCA) or factor analysis as expressed in Imbrie and Kipp (1971). In principle it aims to reduce the complexity of the data set by clustering different taxa into several groups of species (components or factors), which relate to specific environmental variables. Each environmental variable is then related to these factors by linear or quadratic regression. The relationship between the environmental variable and diatom assemblage is thus represented by this regression equation and consequently it is used to estimate SSST of sediment core records. The IKM is widely used in the world oceans for temperature and sea ice reconstructions (e.g. CLIMAP, 1976; 1984; Koç Karpuz and Schrader, 1990), especially in the Southern Ocean (e.g. Zielinski et al., 1998; Abelmann et al., 1999; Esper and Gersonde, 2014a, b).

Table 2.2 Criteria of North Pacific diatom counting.

Diatom groups ^a	Illustration of criteria ^b	Counted as	Counting standards ^a
Centrales	Coscinodiscineae Valve view	 1	In a valve view, centric diatoms, e.g. <i>Actinocyclus</i> sp., <i>Coscinodiscus</i> sp. and <i>Thalassiosira</i> sp., are counted, when more than half of the valve is presented.
		 0	
	Coscinodiscineae Girdle view	 2	In a girdle view, centric diatoms are counted, when more than half of the valve (either epivalve or hypovalve) is presented. Note that girdle bands (copulae) are never counted.
		 1	
		 0	
	Biddulphiineae Girdle view mostly	 1	Centric diatoms with high elevations (horns), e.g. <i>Odontella</i> sp., are counted when more than half of the valve with horn is presented.
		 0	
	Rhizosoleniineae Girdle view only	 1	Centric diatoms with processes, e.g. <i>Rhizosolenia</i> sp., are counted when valve with process is presented.
		 2	
	Pennales	Araphidineae: Diatomaceae	 1
 1/2			
 0			
Raphidineae: Bacillariaceae		 1	Pennate diatoms with canal raphe (e.g. <i>Fragilariopsis</i> sp, <i>Nitzschia</i> sp.) are counted when more than half of the valve or when only central parts is presented.
 0			
Raphidineae: Naviculaceae	 1	Pennate diatoms with monoraphe (e.g. <i>Achenanthes</i> sp., <i>Cocconeis</i> sp.) and biraphe (e.g. <i>Navicula</i> sp.) are counted when central part or more than half of the valve is presented.	
	 0		
	 0		
	 0		

^a Diatom groups after Simonsen (1979).^b Illustration of criteria and counting standards modified after Zielinski (1993) for the North Pacific diatoms.

The Modern Analog Technique (MAT) was first used by Hutson (1980). The primary assumption of MAT is that analogous micropaleontological assemblages dwell in a similar environment. Therefore, the degree of similarity between the fossil assemblage from the sediment cores and the modern assemblage from the surface sediment samples are employed to determine the modern analogs of the fossil assemblage. The target environmental variable is then estimated via these modern analogs. In order to reduce the bias from samples with low similarity, a large number of surface sediment samples covering wide ranges of environmental conditions is required. The MAT has been successfully applied to temperature and sea ice reconstructions by dinoflagellate cysts of the Northern Hemisphere (de Vernal et al., 2001, 2005) as well as by diatoms in the Southern Ocean (Esper and Gersonde, 2014a, b).

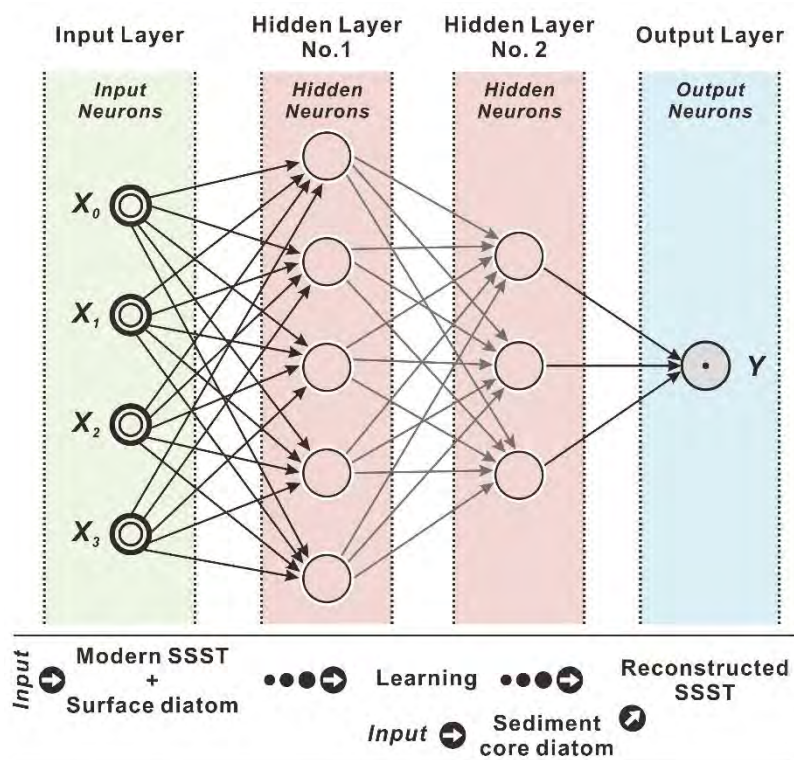


Fig. 2.2 Schematic diagram of artificial neural network (ANN). Circles represent different neurons, while color bars indicate various layers. The arrows show data interaction between neurons. The conceptual procedure of diatom SSST reconstruction based on ANN is presented in the bottom panel.

The artificial neural network (ANN) was introduced to paleoceanography Malmgren and Nordlund (1996) and was employed to reconstruct SSST by Malmgren et al. (2001). In general, the ANN uses a back propagation (BP) neural network (Malmgren and Nordlund, 1997; Crosta and Koç, 2007), in which a set of processing units (neurons) identify the relationship between input variables (i.e. diatom abundances) and output variables (i.e. SSST) by interconnecting each neurons via hidden neurons in hidden layers (Fig. 2.2; Malmgren and Nordlund, 1997; Kucera et al., 2005b). After this “learning” process, the network is capable to estimate the SSST with input data from sediment cores. The ANN is independent from the size of the reference data set by means of extrapolation. Due to its complexity, however, the ANN is considered a methods of black box. In addition, the learning process consumes more time compared with other transfer

function methods (Crosta and Koç, 2007). Therefore only several studies have used the ANN for paleo-environment reconstructions (e.g. Kucera et al., 2005b; Bonnet et al., 2010).

2.3.2. Transfer function settings

1) All diatom abundance data were transformed by logarithm according to equation (1) in order to reduce the bias from extremely abundant species (e.g. *N. seminae*). A recent study in the Southern Ocean also suggests that logarithmized data show more reliable performance in transfer functions (Esper and Gersonde, 2014b).

2) MAT and ANN were performed on the free software R (<http://www.r-project.org>) with the Analogue package (Simpson, 2007; Simpson and Oksanen, 2011) and the Neuralnet package (Günther and Fritsch, 2010), respectively, while IKM was applied by PaleoToolBox (<http://www.pangaea.de/Software/PaleoToolBox>), a software package developed by Sieger et al. (1999).

3) Reconstructions from IKM are calculated with three factors, which explain 84.2% of the total variance in diatom assemblages (**Chapter 3**). Instead of linear regression, quadratic regression is used to deduce SSST reconstructions since most diatom species and species groups are unimodally distributed against the SSSTs (**Chapter 3**).

4) Reconstructions from MAT are deduced based on the Squared Chord Distance (Prell, 1985; Overpeck et al., 1985):

$$D_{ij} = \sum_{k=1}^m (\sqrt{p_{ik}} - \sqrt{p_{jk}})^2 \quad (3)$$

where m is the total number of diatom taxa, p_{ik} and p_{jk} are the relative abundance of diatom taxon k in fossil assemblage i (sediment core sample) and modern assemblage j (surface sample), and then D_{ij} is the squared chord distance between assemblages i and j . D_{ij} is a statistical similarity indicator between two samples. Therefore the smaller the squared chord distance, the more analogous the two samples are.

The number of the best analogs used in the transfer function is determined by the lowest result of leave-one-out cross validation (LOO) and max bias (Simpson and Oksanen, 2011) from a set of 10 analogs.

5) Reconstructions from ANN are developed by Resilient Back Propagation, which is revised from normal Back Propagation (BP) network. This method is faster than other BP networks (Günther and Fritsch, 2010). One hidden layer and 20 hidden neurons are set to construct the neural network.

2.3.3. Transfer function development

To run a reliable transfer function, the reference data set has to be carefully selected. Therefore the original reference data set is revised according to several standards (details are presented in **Chapter 4**):

- 1) Samples with diatom valves significantly altered by dissolution (preservation category 4 and 5) are excluded.
- 2) Samples overrepresented in certain area, which might bias the homogeneity of sample distribution, are ruled out.

- 3) Samples with outliers of certain species (i.e. extreme higher or lower abundance compared to samples from the similar environment) are eliminated.

In addition, diatom species and species groups with negligible relationship with the SSST are excluded from the original reference data set to reduce the bias from their non-SSST signal.

The final reference data set is then randomly split into two parts of calibration (80%) and verification (20%) subsets for training and testing, respectively (Kucera et al., 2005b). Some studies also suggest a separation with 5/6 and 1/6 (e.g. Bonnet et al., 2010). However, this separation rule is rather empirical than strict (J. Guiot, personal communication). This is also a way to reduce the spatial autocorrelation (Telford, 2006; Birks, 2010).

To evaluate the performance of the transfer functions, the root mean squared errors of predictions are calculated between the observed and estimated SSSTs from the calibration and verification data set, namely $RMSEP_{cal}$ and $RMSEP_{veri}$, respectively. The corresponding coefficients of determination (R^2_{cal} and R^2_{veri}) are applied as well. Low RMSEPs and high R^2 indicate a good performance of the transfer function.

The RMSEPs of the transfer functions are then used as a systematic error for the reconstructions of sediment cores.

2.4. Core chronology

The age models of the last 30 ka and 50 ka of MD01-2416 and MD02-2489, respectively, are based on accelerator mass spectrometry (AMS) ^{14}C dating on the planktonic foraminifer *Neogloboquadrina pachyderma* (s) by Sarnthein et al. (2007, 2013, 2015). They used a method of ^{14}C plateau tuning to constrain the Termination I of two cores (Fig. 2.3). The ^{14}C plateaus discovered in these cores were tuned to a high resolution ^{14}C record of a limnological laminated core from Lake Suigetsu, Japan, dated independently by varve counting (Bronk Ramsey et al., 2012). The ^{14}C dating points not defined in the ^{14}C plateaus were calibrated to calendar ages with CALIB 7.0 (Stuiver and Reimer, 1993) with the Marine 13 calibration curve (Reimer et al., 2013), using the reservoir ages determined by Sarnthein et al. (2015) according to the nearest ^{14}C plateau (Maier et al., 2015). The correlation between the benthic $\delta^{18}O$ records of MD01-2416 (Gebhardt et al., 2008) and LR04 global benthic $\delta^{18}O$ stack (Lisiecki and Raymo, 2005) and independently dated geomagnetic paleointensity and inclination events (Gebhardt et al., 2008) were used to establish the age model of MD01-2416 for the last 180 ka BP beyond the limit of ^{14}C dating (**Chapter 4**). For MD02-2489, the Ca and Fe intensity (Gebhardt et al., 2008; Schmieder et al., unpublished data) measured by the X-Ray Fluorescence (XRF) Core Scanner I at Bremen University (Röhr and Abrams, 2000) were visual matched with the carbonate content and the magnetic susceptibility (Rea et al., 1995; McDonald, 1997; McDonald et al., 1999), respectively, of the nearby core ODP887 (54°21.92'N, 148°26.78'W, water depth 3647 m), extending back to 290 ka BP (**Chapter 5**). The age model of ODP887 was determined by assigning to the LR04 global benthic $\delta^{18}O$ stack (Lisiecki and Raymo, 2005) by Galbraith et al. (2008).

Two INOPEX cores, SO202-12-1 and SO202-18-6, were initially dated by ^{14}C dating based on planktonic foraminifer *Neogloboquadrina pachyderma* (s) and calibrated with CALIB 7.0 (Stuiver and Reimer, 1993) and the INTCAL13 calibration curve (Reimer et al., 2013), using a reservoir age of 700 yr (Kuehn et al., 2014; Abelmann et al., unpub. data). Then the laminae of SO202-18-6 were correlated to the NGRIP ice core $\delta^{18}\text{O}$ record (NGRIP members, 2004) by layer counting to calculate the local reservoir ages from the B/A to the early Holocene and therefore the age model of SO202-18-6 was updated (Kuehn et al., 2014) to ca. 14 ka BP. Similarly, the age model of SO202-12-1 were renewed by correlation with SO202-18-6 by using the boundaries of laminae, XRF Ca/Ti ratios and distinct ash layers (Kuehn et al., 2014). The rest of SO202-12-1 was extrapolated to 70 ka BP with the closest sedimentation rate.

The age model of RAMA44 has been established by Keigwin et al. (1992) by ^{14}C dating based on *Globigerina bulloides* and mix planktonic foraminifer with 700 yr reservoir age. To convert the traditional ages to calendar ages, this age model is recalibrated with CALIB 7.0 (Stuiver and Reimer, 1993) and the MARINE13 calibration curve (Reimer et al., 2013), using a constant reservoir age of 700 yr. It then extends to 17 ka BP.

All the age models were established by linear interpolation between the calibrated calendar ages.

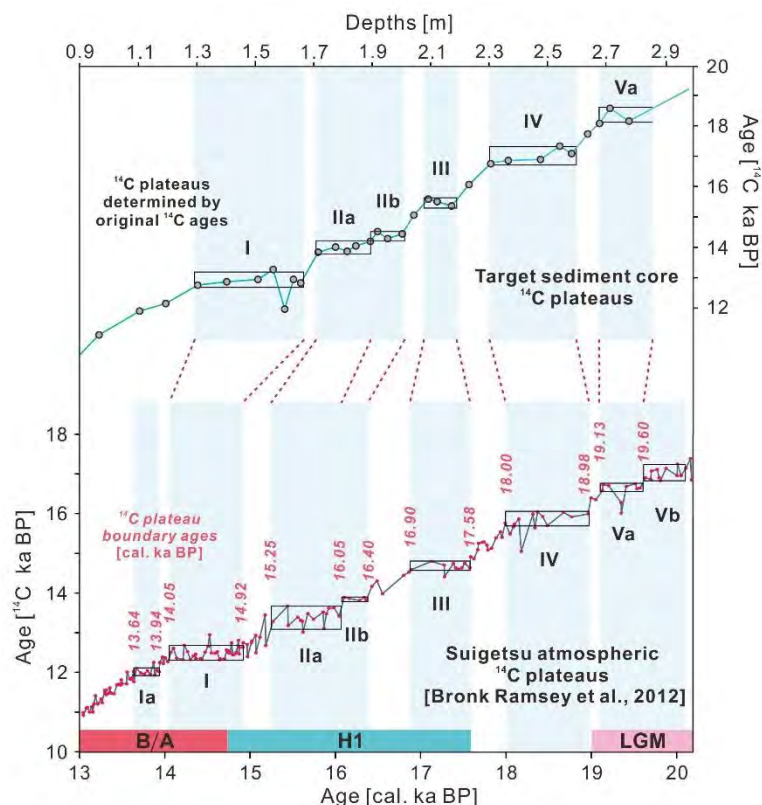


Fig. 2.3 Schematic diagram of ^{14}C plateau tuning methods for MD01-2416 and MD02-2489 (modified after Sarnthein et al., 2015). Planktic ^{14}C plateaus of MD01-2416 and MD02-2489 (horizontal boxes; upper panel) are tuned to atmospheric ^{14}C plateau suite of Lake Suigetsu, Japan (horizontal boxes in lower panel; Bronk Ramsey et al. 2012). The ^{14}C plateaus are assigned by Roman numbers according to Sarnthein et al. (2015) and are highlighted by boxes and blue bars. Climate events are shown in the bottom: LGM- Last Glacial Maximum, H1- Heinrich event 1, B/A- Bølling/Allerød.

Chapter 3. Diatom distributions in northern North Pacific surface sediments and their relationship to modern environmental variables

Jian Ren^a, Rainer Gersonde^a, Oliver Esper^a, Constance Sancetta^b

^aAlfred Wegener Institute Helmholtz Centre for Polar and Marine Research, Am Handelshafen 12, D-27570 Bremerhaven, Germany (Correspondence to J. Ren: jian.ren@awi.de)

^bMoreland Hills, OH 44022, U.S.A.

Published in *Palaeogeography, Palaeoclimatology, Palaeoecology* (2014), doi: 10.1016/j.palaeo.2014.03.008

Abstract

In order to map the modern distribution of diatoms and to establish a reliable reference data set for paleoenvironmental reconstruction in the northern North Pacific, a new data set including the relative abundance of diatom species preserved in a total of 422 surface sediments was generated, which covers a broad range of environmental variables characteristic of the subarctic North Pacific, the Sea of Okhotsk and the Bering Sea between 30° and 70°N. The biogeographic distribution patterns as well as the preferences in sea surface temperature of 38 diatom species and species groups are documented. A Q-mode factor analysis yields a three-factor model representing assemblages associated with the Arctic, Subarctic and Subtropical water mass, indicating a close relationship between the diatom composition and the sea surface temperatures. The relative abundance pattern of 38 diatom species and species groups was statistically compared with nine environmental variables, i.e. the summer sea surface temperature and salinity, annual surface nutrient concentration (nitrate, phosphate, silicate), summer and winter mixed layer depth and summer and winter sea ice concentrations. Canonical Correspondence Analysis (CCA) indicates 32 species and species groups have strong correspondence with the pattern of summer sea surface temperature. In addition, the total diatom flux data compiled from ten sediment traps reveal that the seasonal signals preserved in the surface sediments are mostly from spring through autumn. This close relationship between diatom composition and the summer sea surface temperature will be useful in deriving a transfer function in the subarctic North Pacific for the quantitative paleoceanographic and paleoenvironmental studies.

The relative abundance of the sea-ice indicator diatoms *Fragilariopsis cylindrus* and *F. oceanica* of >20% in the diatom composition is used to represent the winter sea ice edge in the Bering Sea. The northern boundary of the distribution of *F. doliolus* in the open ocean is suggested to be an indicator of the Subarctic Front, while the abundance of *Chaetoceros* resting spores may indicate iron input from nearby continents and shelves and induced productivity events in the study area.

3.1. Introduction

Reliable data sets of diatom species composition in ocean surface sediments are widely used for paleoceanographic reconstruction in the Southern Ocean (e.g. Zielinski and Gersonde, 1997; Crosta et al.,

1998; Zielinski et al., 1998; Esper and Gersonde, 2014a) and in the North Atlantic Ocean (e.g. Koc Karpuz and Schrader, 1990). In contrast, only a few investigations were published in the North Pacific decades ago (Kanaya and Koizumi, 1966; Jousé et al., 1971; Sancetta, 1979, 1981, 1982). Recent studies are either based on sparse samples (e.g. Kazarina and Yushina, 1999) or focus on minor regions (e.g. Shiga and Koizumi, 2000 and Tsoy et al., 2009 on the Sea of Okhotsk; Lopes et al., 2006 on coastal North America). The pioneer statistical analysis based on diatom species from surface samples of the entire North Pacific was done by Sancetta (1979). However, only few samples from the Bering Sea, especially from the Bering Shelf, which is covered by sea ice seasonally, were included in her study. Later work expanded the data set in the marginal seas (Sancetta, 1981) and the subarctic Pacific (Sancetta and Silvestri, 1986).

As one of the High Nutrient Low Chlorophyll (HNLC) regions, the North Pacific plays a role in controlling the glacial-interglacial atmospheric CO₂ concentration variability by plankton productivity shifts, which are limited by iron availability, and by ocean stratification, which may reduce CO₂ leak from deep ocean to atmosphere (Sigman et al., 2004; Haug et al., 2005; Jaccard et al., 2005). Furthermore, the atmospheric vapor and water flow from the North Pacific through the Bering Strait to the Arctic and hence the North Atlantic may stabilize the global climate variability by the salinity and heat balance (Keigwin and Cook, 2007). Thus, in order to understand the North Pacific's role in shaping global climatic and oceanographic changes, the history of paleo-sea-surface-temperature and winter sea ice distribution is of vital importance (e.g. Gebhardt et al., 2008; Max et al., 2012). Therefore, a high quality and comprehensive diatom based data set is needed for paleoceanographic reconstruction, due to the restricted occurrence of calcareous fossils and hence reconstructions based on corresponding geochemical proxies in this area.

In this paper, we present the diatom distribution in northern North Pacific sediments, including the Sea of Okhotsk and the Bering Sea. In total 422 surface samples, including 263 samples from Sancetta and Silvestri (1986) are studied here, covering the Subarctic Front system (Fig. 3.1a). Statistical analysis, such as Q-mode analysis and Canonical Correspondence Analysis, is applied to the diatom data set, in order to reveal the relationships between the diatom distribution and the environmental variables (e.g. sea surface temperatures, sea ice concentration, salinities, nutrients, mixed layer depths) and to detect the primary factors which determine the diatom species and their abundance distributions in the North Pacific.

3.2. Regional setting

3.2.1. North Pacific open ocean

The northern North Pacific open ocean can be subdivided by the Subarctic Front into the Subarctic Gyre (Dodimead et al., 1963) and the northern part of the Subtropical Gyre (e.g. Qiu, 2002; Fig. 3.1b). The Subarctic Front, located between 40°N and 44°N in the western and central North Pacific, is characterized by an abrupt change in temperature and salinity where the cold and fresh water of the subarctic gyre from the north meets the warm and salty subtropical water to the south (Yuan and Talley, 1996; Aydin et al., 2004). The average maximum surface temperature gradient of the Subarctic Front is 0.44 °C /10 km, while

the salinity gradient is 0.087‰/10 km (at 10 m water depth; Yuan and Talley, 1996).

South of the Subarctic Front, the Kuroshio Extension (KE) constitutes the northwestern boundary current of the Subtropical Gyre (Kawai, 1972). The Kuroshio Extension is an eastward extension of the Kuroshio Current (KC; Qiu, 2000). Around the International Date Line, the Kuroshio Extension broadens to form the sluggish North Pacific Current (NPC; White et al., 1982; Qiu, 2002). The North Pacific Current bifurcates when it encounters the North America coast. Whereas the southern branch forms the coastal California Current (CC), the northern branch turns northward and originates the Alaska Current (AC; Qiu, 2002).

The Subarctic Gyre consists of two subgyres, the Alaska Gyre (AG) in the east and the Western Subarctic Gyre (WSG) in the west (Dodimead et al., 1963). The northern rim of the Alaska Gyre is the Alaska Stream (AS), which flows southwestward along the Aleutian Islands, bringing the fresher North Pacific surface water into the Bering Sea mainly through the western Aleutian Islands (Fig. 3.1b).

The East Kamchatka Current (EKC) originates from the Bering Sea and flows along the Kamchatka peninsula, forming the western boundary of the Western Subarctic Gyre. The East Kamchatka Current meets with the waters from the Sea of Okhotsk and forms the Oyashio Current (OC). Off Hokkaido, around 42°N, the Oyashio Current turns eastward, becoming the Subarctic Current (SC), which runs along the Subarctic Front (Fig. 3.1b; Favorite et al., 1976).

As an ocean of vast area, significant contrasts are found between the eastern and western parts of the surface North Pacific. Due to the currents system, the western North Pacific has a sharper temperature gradient than the eastern North Pacific (Fig. 3.1b). Higher concentrations of macronutrient (nitrate, phosphate and silicate), iron and chlorophyll are recorded in the western North Pacific, while no substantial difference are found between primary productivity in the western and eastern North Pacific (Fig. 3.2; Shiimoto et al., 1998; Harrison et al., 1999; Lam et al., 2006; Lam and Bishop, 2008). The mixed layer depth is shallower in summer and deeper in winter in the western North Pacific than in the eastern counterpart (Fig. 3.2; Harrison et al., 1999).

No winter sea ice is found in the modern open ocean.

3.2.2. Bering Sea

A large-scale cyclonic gyre, the Bering Sea Gyre (BSG), is formed in the Bering Sea, along the margin of the continental slope (Fig. 3.1b; Ohtani et al., 1972). The Bering Slope Current (BSC) flows northward along the shelf-slope break and bifurcates at around 58°N (Stabeno and Reed, 1994). A part of the Bering Sea Current turns westward to originate the East Kamchatka Current along the Siberian coast, while the other part joins the unidirectionally northerly outflow from the Bering Strait into the Chukchi Sea of the Arctic Ocean with an amount of 0.85 Sv (Coachman, 1993; Takahashi, 2005).

Most of the Bering Shelf is covered by sea ice in winter, comprising approximately 1/3 of the Bering Sea. The seasonal advance of the sea ice starts at the Bering Strait in November and extends to its southern

maximum in March-April (Fig. 3.1b). Sea ice has completely disappeared from the Bering Sea by July (Niebauer, 1980, 1983). In contrast, the Bering Basin experiences no ice cover, although it may be influenced by drifting ice (Sancetta, 1981). As a consequence of the river runoff from the nearby continents and melting of sea ice, a sharp salinity gradient is found along the Bering Shelf slope (Takenouti and Ohtani, 1974).

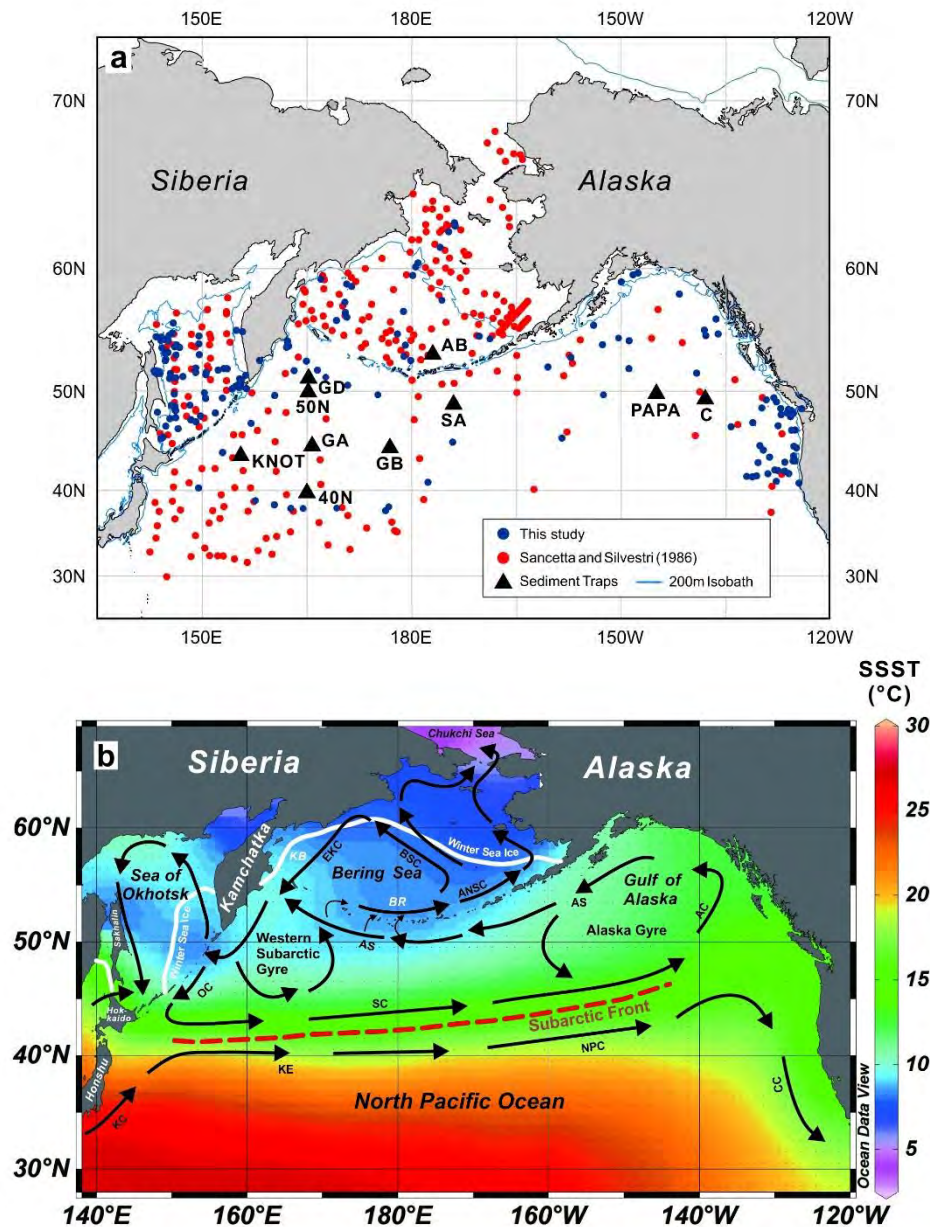


Fig. 3.1 a) Distribution map of 422 surface samples in the North Pacific Ocean (blue and red circles). Black triangles indicate the sediment traps mentioned in the Discussion. b) Current system in the North Pacific Ocean (black arrows). The winter sea ice edge (March of 1982-1991; Reynolds et al., 2002) and the Subarctic Front (Aydin, et al., 2004) are indicated by the solid white and dashed red lines, respectively. The summer sea surface temperature from WOA94 is indicated as a background (Levitus et al., 1994). Currents system: AC: Alaska Current; ANSC: Aleutian North Slope Current; AS: Alaska Stream; BSC: Bering Slope Current; CC: California Current; EKC: East Kamchatka Current; KC: Kuroshio Current; KE: Kuroshio Extension; NPC: North Pacific Current; OC: Oyashio Current; SC: Subarctic Current. Topography: BR: Bowers Ridge; KB: Komandorsky Basin.

3.2.3. Sea of Okhotsk

Similar to the Bering Sea, a cyclonic gyre, the Okhotsk Gyre (OG) dominates the surface current system (Fig. 3.1b). A part of the surface water runs into the North Pacific to rejoin the Kuroshio Current and form the Oyashio Current (Favorite et al., 1976; Alfultis and Martin, 1987; Ternois et al., 2001). In addition to the North Pacific water, the Sea of Okhotsk receives another water source from the Japan Sea through Soya Strait (Takizawa, 1982).

The Sea of Okhotsk has seasonal sea ice in winter, covering about 75% of the sea (Fig. 3.1b; Parkinson et al., 1987). The sea ice begins to form in coastal areas in November, extends to its maximum coverage usually in mid-March, and by June retreats to a few coastal regions, leading to an ice-free environment during the summer (Parkinson and Gratz, 1983; Parkinson et al., 1987).

The cooling and freshening water mass from the Sea of Okhotsk is considered to be a source of North Pacific Intermediate Water (Yasuda, 2004), which could be important for CO₂ absorption and climate variability.

3.3. Material and methods

3.3.1. Material

A total of 422 surface sediment samples were recovered from the northern North Pacific including the Bering Sea and the Sea of Okhotsk, covering an area between 140°E-120°W and 30°N-70°N (Fig. 3.1a). Among them, 263 samples (named as SanSamp hereafter) were from a former study by Sancetta and Silvestri (1986). The other 159 surface sediment samples, studied at Alfred-Wegener-Institute (named as AWISamp hereafter), were collected during cruises INOPEX (Gersonde, 2012), KALMAR (Dullo, et al., 2009), KOMEX (Dullo, et al., 2004) and several Canadian expeditions. The SanSamp are trigger-weight and piston-core top samples, while AWISamp are retrieved by multicorer and represent the topmost 1 cm of the sediment.

In order to rule out disturbed sediments, the seafloor was inspected by the ATLAS PARASOUND system prior to the retrieval of the AWISamp (Dullo, et al., 2004, 2009; Gersonde, 2012). SanSamp material was examined in smear slides for evidence of displaced material. A few SanSamp samples from the region of Bowers Ridge and the Bering Basin may have post-depositional effects, such as dissolution, winnowing or turbidity flows, that increase the relative abundance for some species (such as *Rhizosolenia hebetata*). However, because they do not have a significant effect upon the statistical analysis, we have decided to keep them in order to display the complete data set.

Due to low sedimentation rates in the area, although no direct dating for the sediment samples is available, it is assumed that they represent the environment of an average of approximately the past century.

3.3.2. Data preparation

The data of SanSamp were obtained from Sancetta and Silvestri (1986). Slide preparation and

counting methods for the SanSamp material are described in Sancetta (1981), Sancetta and Silvestri (1986). For AWISamp, quantitative diatom slides were prepared according to the standard procedure established at the Alfred-Wegener-Institute (Gersonde and Zielinski, 2000). Diatom counting was done following the description by Schrader and Gersonde (1978). An average of 400 diatom valves was counted for each sample using a Zeiss Axioskop microscope at $\times 1000$ magnification. The identification methods of SanSamp and AWISamp are similar.

Diatoms were identified to species or species group level. The identifications were done according to the following literature: Sancetta (1982), Akiba (1986), Sancetta (1987), Medlin and Priddle (1990), Hasle and Syverstsen (1997), Witkowski et al. (2000) and Onodera and Takahashi (2007). In total 140 taxa were originally identified in AWISamp, while 51 species and 1 group of benthic diatoms is reported in SanSamp. Diatom taxa found in SanSamp and AWISamp are basically consistent. In order to combine the two data sets, 49 common taxa were selected for further study (see List S1 for taxonomic details). Some taxa were combined as groups in SanSamp, therefore we also grouped them in AWISamp.

Asteromphalus brookei and *A. robustus* are combined and identified as *Asteromphalus* group.

Chaetoceros resting spores were combined into the group *Chaetoceros* resting spores. The *Chaetoceros* specimens observed belong to the subgenus *Hyalochaetae*, whose spores cannot be identified to species level due to the absence of setae.

Although the two species could be clearly separated, *Fragilariopsis cylindrus* and *F. oceanica* were combined in SanSamp. Consequently, the two species are grouped in the whole data set.

For the same reason, *Rhizosolenia hebetata* f. *hebetata* and *Rhizosolenia hebetata* f. *semispina* were combined as *Rhizosolenia hebetata* group.

Thalassionema nitzschioides consists of a few varieties (Zielinski and Gersonde, 1997; Tanimura, 1999; Hasle, 2001). Two varieties, *Thalassionema nitzschioides* var. *lanceolata* and *Thalassionema nitzschioides* var. *parva*, are not included in the data set. Therefore, here *Thalassionema nitzschioides* refers only to *Thalassionema nitzschioides* var. *nitzschioides*.

Thalassiosira antarctica var. *borealis* resting spores are easily confused with *T. gravida* resting spores due to their similar structures (Syverstsen, 1979; Sancetta, 1982; Hasle and Syverstsen, 1997). Therefore, the two species are grouped in the whole data set.

All the fresh, brackish and benthic species were excluded and relative percentages were recalculated, in order to avoid terrestrial and lateral influences. Hence, only 38 species and species groups were used in the further statistical analysis. The abundance of selected 38 taxa or taxon groups was compared against summer sea surface temperature (Table 3.1).

The raw counts were converted to percentage abundance to map the diatom distributions. For the statistical analysis, a further logarithm-based transformation, as suggested by Zielinski et al. (1998), was

Table 3.1 Thirty-eight diatom species/species groups and their relation to summer sea surface temperatures.

Species or species group	Abbrev.	Temperature Range (°C)	Temperature Maximum (°C)	Remarks ^a
<i>Actinocyclus curvatulus</i>	Acurv	8-26	8.5-10	
<i>Actinocyclus ochotensis</i>	Aocho	7.5-26	8-10.5	
<i>Actinocyclus octonarius</i>	Actocto	16-27	22-26	ww
<i>Alveus marinus</i>	Amari	19.5-27	22-27	ww
<i>Asteromphalus robustus</i> + <i>A. brookei</i>	Aster	8-27	22-27	
<i>Azpeitia nodulifera</i>	Anodu	16-27	24-27	ww
<i>Azpeitia tabularis</i>	Atabu	7-27	19-26	
<i>Bacterosira bathyomphala</i>	Bbath	5-12.5	7.5-12	cw, end
<i>Chaetoceros</i> resting spore	Chaet	5-26.5	7.5-21	ne
<i>Coscinodiscus marginatus</i>	Cmarg	6.5-22	10-14	
<i>Coscinodiscus oculus-iridis</i>	Cocul	7-26.5	8-10	
<i>Coscinodiscus radiatus</i>	Cradi	12.5-27	22-26	ww
<i>Fragilariopsis doliolus</i>	Fdoli	8-26.5	16-22	ww
<i>Fragilariopsis oceanica</i> + <i>F. cylindrus</i>	Foccy	5-12.5	5-8	si
<i>Hemidiscus cuneiformis</i>	Hcune	15-27	26-26.5	ww
<i>Neodenticula seminae</i>	Nsemi	7.5-21	8-15	end
<i>Nitzschia bicapitata</i>	Nbica	9-27	22.5-27	ww
<i>Nitzschia sicula</i>	Nsicu	9-26.5	20-26	ww
<i>Odontella aurita</i>	Oauri	5-25.5	5-9.5	ne
<i>Porosira glacialis</i>	Pglac	5-22	5-10	cw
<i>Rhizosolenia bergonii</i>	Rberg	19-27	22.5-27	ww
<i>Rhizosolenia hebetata</i> f. <i>hebetata</i> + <i>R. hebetata</i> f. <i>semispina</i>	Rhehe	6-22	6.5-10	
<i>Rhizosolenia setigera</i>	Rseti	9-27	18-27	ww
<i>Rhizosolenia styliformis</i>	Rstyl	7-26.5	7-10	ww
<i>Roperia tessellata</i>	Rtess	13-27	20.5-26	ww
<i>Stellarima stellaris</i>	Sstel	7-27	24-26	
<i>Stephanopyxis turris</i>	Sturr	6-26	8-22.5	
<i>Thalassionema nitzschioides</i>	Tnitz	5-27	11.5-23.5	
<i>Thalassiosira antarctica</i> var. <i>borealis</i> resting spore	Tabsp	5-24	7-10	cw, end
<i>Thalassiosira eccentrica</i>	Tecce	8-27	19-27	ww
<i>Thalassiosira hyalina</i>	Thyal	5-12.5	6-8.5	cw, end
<i>Thalassiosira leptopus</i>	Tlept	8.5-27	22-26	ww
<i>Thalassiosira lineata</i>	Tline	8.5-27	20-26	ww
<i>Thalassiosira nordenskiöldii</i>	Tnord	5-16	5-8.5	cw, end
<i>Thalassiosira oestrupii</i>	Toest	8.5-27	13-21	ww
<i>Thalassiosira pacifica</i>	Tpaci	5.5-21.5	21	
<i>Thalassiosira trifulta</i>	Ttrif	8-24	8.5-15	
<i>Thalassiothrix longissima</i>	Tlong	7-26.5	8.5-9	

^a cw=cold water; end=endemic; ne=neritic; si=sea ice; ww=warm water

employed in order to down-weight the most abundant species, such as *Neodenticula seminae*, which accounts for up to 80% of the total assemblage in some samples. The following equation is used:

$$L = \text{LOG}_{10} (\text{relative abundance} \times 10 + 1)$$

The AWISamp diatom data set is being stored in the Pangaea databank (www.pangaea.de) and is available upon request.

3.3.3. Environmental variables

The selected environmental variables consist of the summer sea surface temperatures (TEMP; at 10m water depth; Fig. 3.1b) from World Ocean Atlas 1994 (WOA94; Levitus et al., 1994); summer sea surface salinity (SALINITY; at 10m water depth; Fig. 2a) from World Ocean Atlas 2005 (Antonov et al., 2006); the mean annual sea surface concentration of dissolved nitrate (NO₃; Fig. 3.2b), phosphate (PO₄; Fig. 3.2c) and silicate (SiO₄; Fig. 3.2d) from World Ocean Atlas 2005 (all at 10m water depth; Garcia et al., 2006); summer and winter sea ice concentration (SSIC and WSIC; sea ice concentration is the relative amount of area covered by ice in a certain grid, which is generally presented in percentage; Fig. 3.2e and 3.2f) from NOAA Optimum Interpolation (OI) Sea Surface Temperature Version 2 (Reynolds et al., 2002) and summer and winter mixed layer depths (MLD; mixed layer is an ocean surface layer with homogenous temperature and density. Its depth variation has impact on phytoplankton bloom; Fig. 3.2g and 3.2h) from World Ocean Atlas 1994 (Monterey and Levitus, 1997). All the data sets have a 1°×1° spatial resolution, which guarantees the data quality (see the references above). The selected environmental variables for each sample are listed in Appendix A (Table S1). In this study summer means July, August and September and winter stands for January, February and March.

The summer sea surface temperatures (SSSTs) from WOA94 were chosen instead of the updated versions of World Ocean Atlas (i.e. WOA2001, WOA2005, WOA2009) due to the recent warming in the Bering Sea, where a transition from an Arctic environment to a subarctic condition is under way (e.g. Overland and Stabeno, 2004; Grebmeier et al., 2006). The SSSTs derived from WOA09 are >0.5 °C higher in the western Bering Sea than the SSSTs from WOA94 (Fig. 3.3). These warming signals, if assigned to surface sediment samples which represent the last hundred years or more, may bias the paleotemperature reconstruction to a warmer environment. Therefore, we selected the WOA94, whose measurements were performed mainly in the 1970's before the onset of warming in the Bering Sea (Levitus et al., 1994). For the same reason, we selected the SSIC and WSIC data from 1982 to 1991 rather than the full temporal range from 1982 to 2011 (Reynolds et al., 2002).

3.3.4. Statistical methods

A Q-mode factor analysis was employed to simplify the complex diatom data set into a small number of varimax factors and to identify the most dominant species by using a software package from Sieger et al. (1999).

In order to detect the influences of environmental variables on the distribution of diatom species, the CANOCO program (version 4.5; ter Braak and Smilauer, 2002) was chosen for the statistical analysis. A Detrended Correspondence Analysis (DCA) was applied to determine whether a diatom species

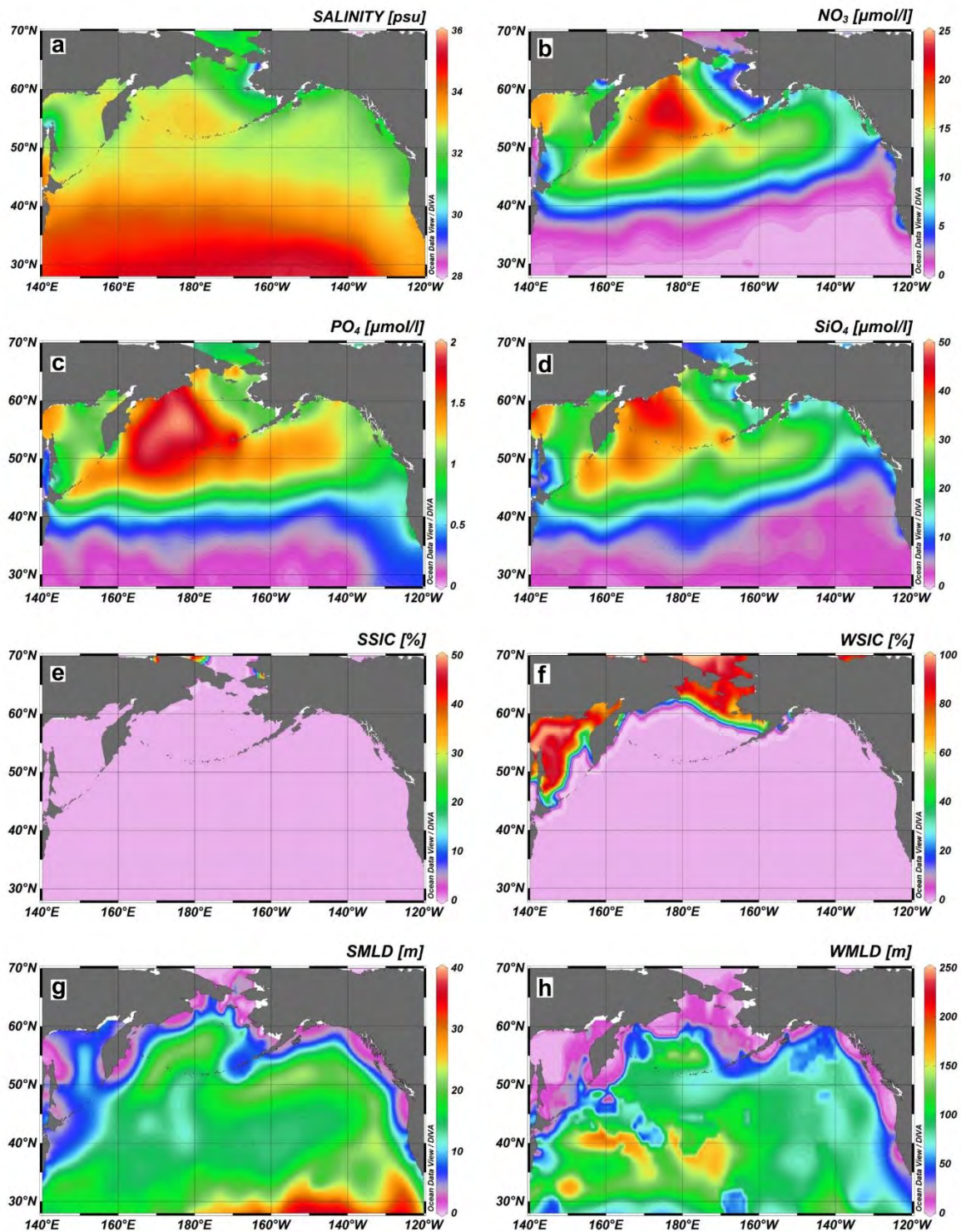


Fig. 3.2 Environmental variables of the surface water layer of the study area. They are the summer sea surface salinity (SALINITY; a), the mean annual sea surface concentration of dissolved of nitrate (NO₃; b), phosphate (PO₄; c) and silicate (SiO₄; d), the summer and winter sea ice concentration (SSIC and WSIC; e and f) and the summer and winter mixed layer depth (SMLD and WMLD; g and h). a-d are from 10 m water depths.

distribution is a unimodal or a linear pattern. The DCA shows a first gradient of standard deviation (SD) length of 3.295 (Table 3.2), indicating a unimodal diatom distribution (ter Braak and Prentice, 1994). Therefore the non-linear methods of correspondence analysis (CA) and canonical correspondence analysis (CCA) are preferable for our data set. In contrast to the CA, the CCA is a direct gradient analysis to investigate the variation in the biological assemblages that could be explained by the corresponding environmental variables. Hence the direct analysis is likely to be more effective than the traditional indirect methods, if the environmental data are available (ter Braak and Prentice, 1988). The CCA was thus applied to the logarithm-transformed diatom relative abundances with the nine environmental variables listed above. The resulting ordination diagrams of CCA show the main pattern of variation in diatom assemblages as influenced by the environmental variables and the distributions of the species along each environmental variable (ter Braak and Verdonschot, 1995). In this case, the environmental vectors point in the general direction of maximum environmental change across the diagram, and their lengths are approximately proportional to the rate of change in that direction (Birks et al., 1990). The angles between vectors indicate correlations between individual environmental variables. A positive correlation is reflected by an angle smaller than 90° and the smaller the angle, the closer the positive relation of the two variables. A negative correlation is suggested by an angle larger than 90° , while little relation between two variables is indicated by 90° . A forward selection was used to rank the importance of the environmental variables for determining the diatom species distribution or to reduce the insignificant variables (if the statistical significance level, e.g. p -value >0.05).

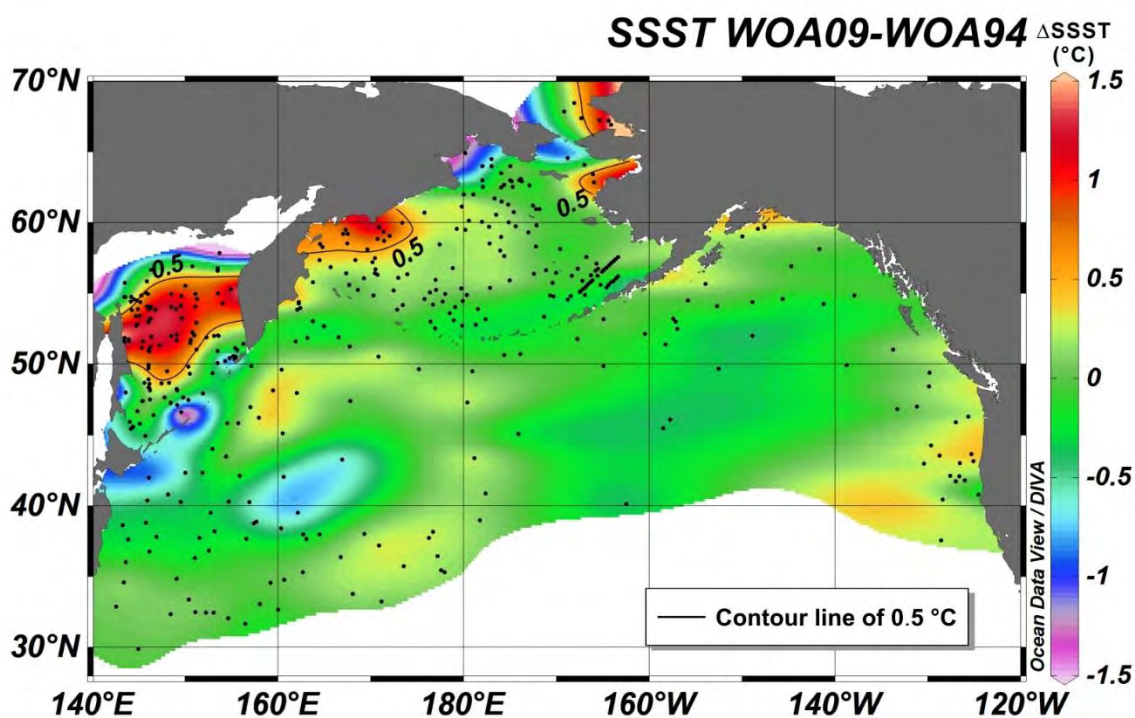


Fig. 3.3 Summer sea surface temperature differences between WOA09 and WOA94, showing a warming in the western Bering Sea and the middle Sea of the Okhotsk. Surface samples are indicated by dots.

Table 3.2 Results of the Detrended Correspondence Analysis (DCA).

Axes	1	2	3	4	Total inertia
Eigenvalues	0.412	0.062	0.052	0.034	1.06
Lengths of gradient	3.295	1.950	1.302	1.290	
Cumulative percentage variance of species data	38.9	44.7	49.7	52.8	
Sum of all eigenvalues					1.06

3.4. Results

3.4.1. Diatom distribution

The biogeographic distribution of 38 diatom species and species groups from 422 surface samples was investigated and mapped. Most of the species show clear distribution patterns corresponding to environmental variables, mainly the surface temperatures and the sea ice distribution. Species such as *Actinocyclus octonarius*, *Alveus marinus*, *Azpeitia nodulifera*, *Hemidiscus cuneiformis*, *Rhizosolenia bergonii*, *R. setigera* and *Thalassiosira leptopus* are only found south of the Subarctic Front, while *Bacterosira bathyomphala*, *Fragilariopsis cylindrus*, *F. oceanica*, *Porosira glacialis*, *Thalassiosira hyalina* and *T. nordenskiöldii* occur exclusively north of the winter sea ice edge (Fig. 3.4). *Actinocyclus curvatulus*, *Coscinodiscus marginatus*, *Neodenticula seminae* and *Thalassiosira trifulta* are frequently encountered between the winter sea ice edge and the Subarctic Front (Fig. 3.4).

3.4.2. Q-mode factor analysis

Q-mode analysis based on 422 surface samples detected 3 factors, which explain 84.2% of the total variance in diatom assemblages.

3.4.2.1. Arctic Factor

Factor 1 accounts for 39.8% of the total variance. The assemblage is restricted to the Bering Shelf, the Kuril Islands and the marginal Sea of Okhotsk, where the SSSTs are below 10 °C (Fig. 3.5). It reaches highest score values in the Chukchi Sea and on the Bering Shelf. The southern boundary is close to the maximum extent of the winter sea ice and occurs parallel to the East Kamchatka and the Oyashio Currents (Fig. 3.5). Therefore, Factor 1 is named Arctic Factor. The Arctic Factor is dominated by *B. bathyomphala*, *F. oceanica*, *F. cylindrus*, *T. antarctica* var. *borealis* resting spore, *T. hyalina* and *T. nordenskiöldii*, with minor contributions from *P. glacialis* (Table 3.3). Most of them are all sea ice related species (Sancetta, 1982).

Bacterosira bathyomphala is a cold water species endemic to the Northern Hemisphere (Hasle and Syvertsen, 1997). Hasle (1990) reported that *B. bathyomphala* dominated in the ice-edge zone during the spring bloom in the Barents Sea, indicating it is a sea ice related species. It is only found in our samples

from the Sea of Okhotsk and the Bering Sea, where SSST ranges between 5-12.5 °C in summer (Table 3.1; Fig. 3.6). In the Sea of Okhotsk, *B. bathyomphala* is abundant on the northern and western slopes (5-40%),

Table 3.3 Results of Q-mode analysis. Species/species groups with high values are bold and underlined, while species with high scores in more than one factors are bold and italic.

Diatom species/groups	Arctic Factor	Subarctic Factor	Subtropical Factor
Acurv	-0.018	<i>-0.341</i>	<i>0.18</i>
Aocho	-0.016	<i>-0.156</i>	-0.037
Aocto	-0.01	0.073	<i>0.179</i>
Aster	-0.025	-0.014	0.118
Anodu	-0.017	0.076	<i>0.184</i>
Atabu	-0.047	0.028	<i>0.277</i>
Bbath	<i>0.328</i>	-0.038	-0.061
Chaet	<i>0.391</i>	-0.116	<i>0.166</i>
Cmarg	-0.064	<i>-0.226</i>	0.04
Cocul	0.011	<i>-0.13</i>	0.01
Cradi	-0.05	0.052	<i>0.307</i>
Sstel	-0.01	-0.019	0.117
Nsemi	0.067	<i>-0.561</i>	0.014
Hcune	-0.019	0.06	<i>0.161</i>
Nbica	-0.009	0.061	<i>0.153</i>
Foccy	<i>0.488</i>	0.103	-0.047
Amari	-0.018	0.076	<i>0.18</i>
Nsicu	-0.009	0.026	0.069
Oauri	0.169	-0.054	-0.001
Pglac	<i>0.178</i>	-0.003	-0.031
Fdoli	-0.055	0.07	<i>0.337</i>
Rberg	-0.012	0.045	<i>0.115</i>
Rhehe	0.022	<i>-0.335</i>	-0.017
Rseti	-0.005	0.044	0.1
Rstyl	0.017	-0.025	0.052
Rtess	-0.026	0.06	<i>0.187</i>
Sturr	0.007	0.012	0.061
Tnitz	<i>0.281</i>	0.052	<i>0.346</i>
Tabsp	<i>0.328</i>	-0.039	-0.044
Tecce	-0.007	0.041	<i>0.292</i>
Tpaci	0.014	0.013	0.029
Thyal	<i>0.294</i>	0.115	0.005
Tnord	<i>0.382</i>	0.044	-0.03
Toest	-0.022	-0.103	<i>0.331</i>
Ttrif	0.011	<i>-0.457</i>	0.03
Tlept	-0.004	0.03	0.074
Tline	-0.005	0.062	<i>0.225</i>
Tlong	-0.03	<i>-0.22</i>	<i>0.158</i>

while it is rare in the central basin. It also appears on the edge of the Bering Shelf in the Bering Sea.

The sea ice indicator species (Hasle and Syvertsen, 1997), *F. cylindrus* and *F. oceanica*, are restricted to the winter sea ice area, i.e. north of the winter sea ice edge in the Bering Sea and the Sea of Okhotsk (Fig. 3.4). They are the predominant species in waters overlying the Bering Shelf (up to 80%) and less common along the Kamchatka Peninsula and in the marginal Sea of Okhotsk. *F. cylindrus* is a bipolar species while *F. oceanica* is endemic to the Northern Hemisphere (Medlin and Priddle, 1990; Hasle and Syvertsen, 1997; Lundholm and Hasle, 2010). Their maximum abundance occurs at SSSTs between 5-8 °C and they are absent where SSST exceeds 12.5 °C (Table 3.1; Fig. 3.6).

Porosira glacialis occurs in bipolar cold water regions and is frequently found in sea ice (Grant and Hasle, 1976; Hasle and Syvertsen, 1997; Pike et al., 2009). In this study, it is mainly restricted to the Bering and Okhotsk Seas, where SSST ranges between 5-10 °C (Fig. 3.6), and is quite rare in the North Pacific open ocean (Fig. 3.4). In the Bering Sea, *P. glacialis* has relatively high abundance north of the winter sea ice edge (up to 8%) and is somewhat more common in the Komandorsky Basin than in the Bering Basin (up to 4%). It appears in the western Sea of Okhotsk with abundances less than 2%.

Three *Thalassiosira* taxa - *T. antarctica* var. *borealis* resting spore, *T. hyalina* and *T. nordenskiöldii* - are all restricted to the Northern Hemisphere (Hasle and Syvertsen, 1997). They display highest relative abundance on the Bering Shelf, along the Kamchatka Peninsula and off the Kuril Islands (Fig. 3.4). These areas, either north of the winter sea ice edge or influenced by the Oyashio Current, are controlled by cold water masses. Therefore these three species inhabit cold environments. The peak abundances of *T. nordenskiöldii* and *T. hyalina* are referable to SSSTs between 5-8.5 °C whereas *T. antarctica* var. *borealis* resting spore prefers 7-10 °C (Table 3.1; Fig. 3.6).

3.4.2.2. Subarctic Factor

Factor 2, accounting for 25.4% of the total variance. It covers most the subarctic region between the winter sea ice edge and the Subarctic Front (Fig. 3.5). The high scores of the assemblage is centered in the Bering Basin and the Alaskan Gyre. Minor high values are also found in the Western Subarctic Gyre and in the central Sea of Okhotsk. It covers most of the subarctic region and thus indicates the subarctic environment. The Subarctic Factor is dominated by *A. ochotensis*, *C. marginatus*, *C. oculus-iridis*, *N. seminae*, *R. hebetata* group and *T. trifulta* (Table 3.3).

Actinocyclus ochotensis occurs in low abundance (<3%) and is sporadically distributed in the area except in the Bering Basin (Fig. 3.4). High relative abundance can be related to an SSST range from 8 to 10.5 °C (Table 3.1; Fig. 3.6).

Coscinodiscus marginatus is rare in the marginal seas except at several stations in the Bering Basin. It appears north of the Subarctic Front in the open North Pacific (10-14 °C; Fig. 3.6).

Coscinodiscus oculus-iridis is sporadically distributed in the study area. Similar to *C. marginatus*, it reaches higher abundance around the Bowers Ridge and Aleutian Arc. It dwells in a temperature range between 7 to 26.5 °C and reaches a maximum abundance at SSSTs between 8-10 °C (Table 3.1; Fig. 3.6).

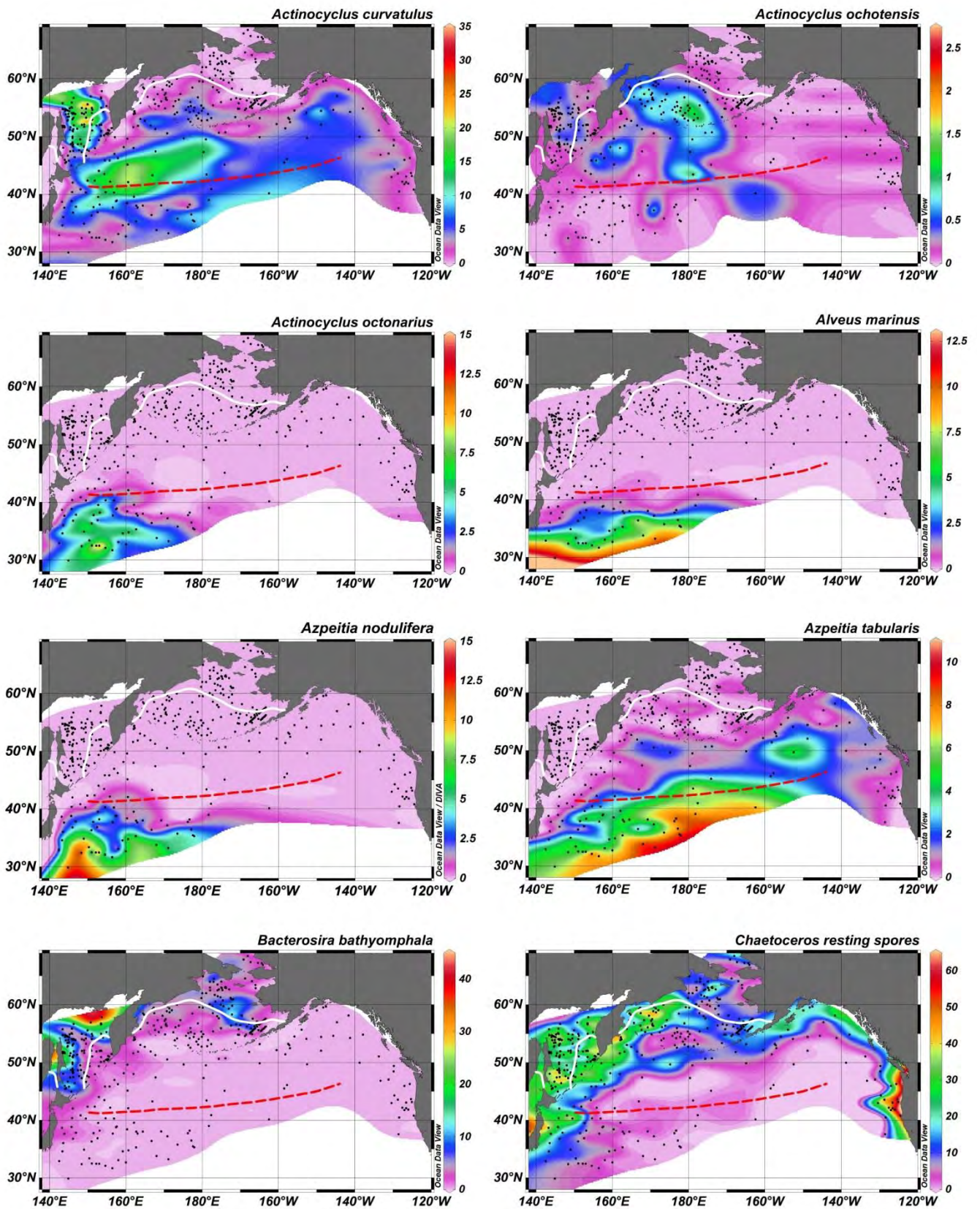


Fig. 3.4 Relative abundance maps of 36 selected diatom species and species groups. The color bar at the right side of each species shows the relative abundances. The white line indicates the winter sea ice edge (Reynolds et al., 2002) and the red dashed line represents the Subarctic Front (Aydin, et al., 2004).

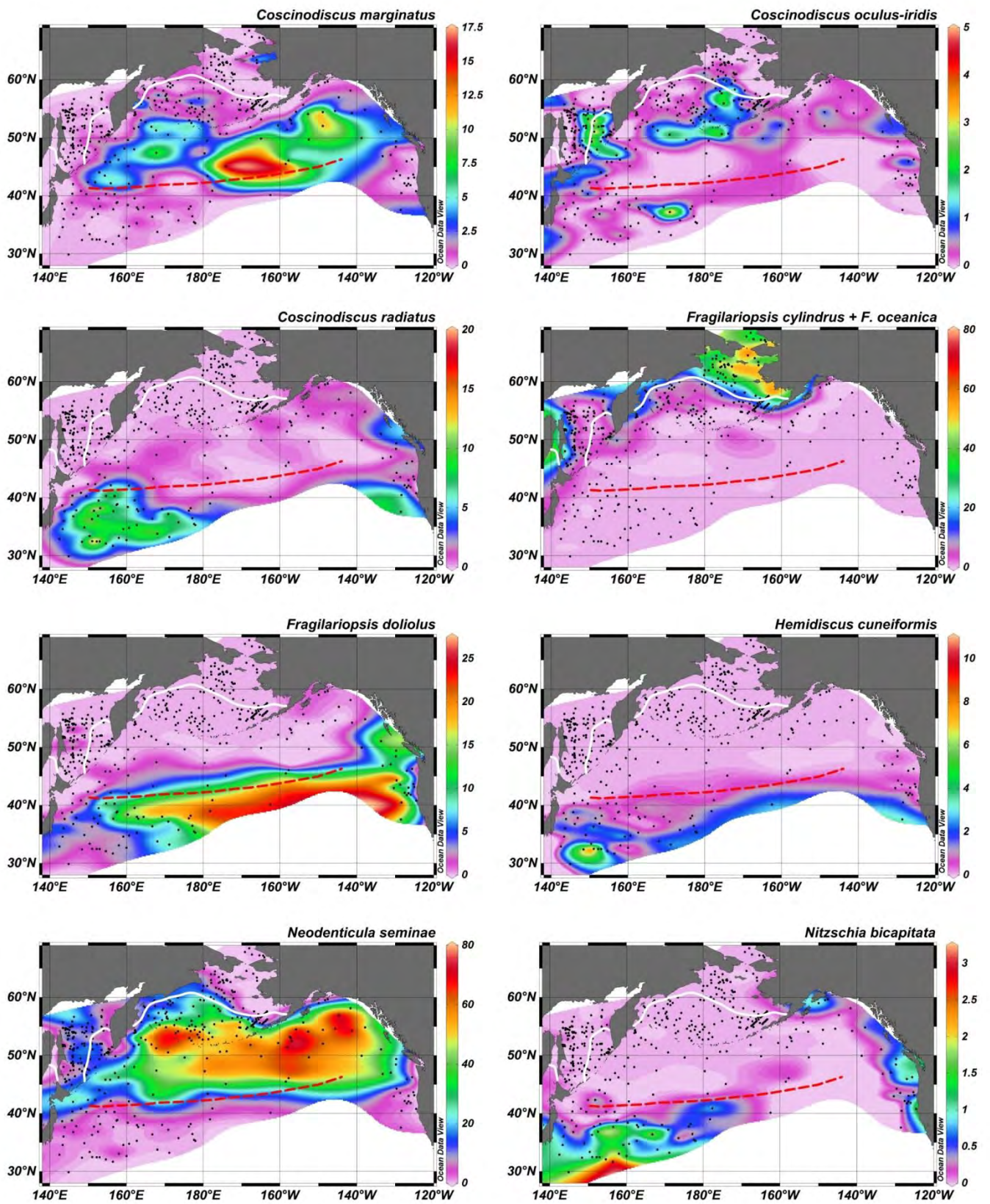


Fig. 3.4 (continued)

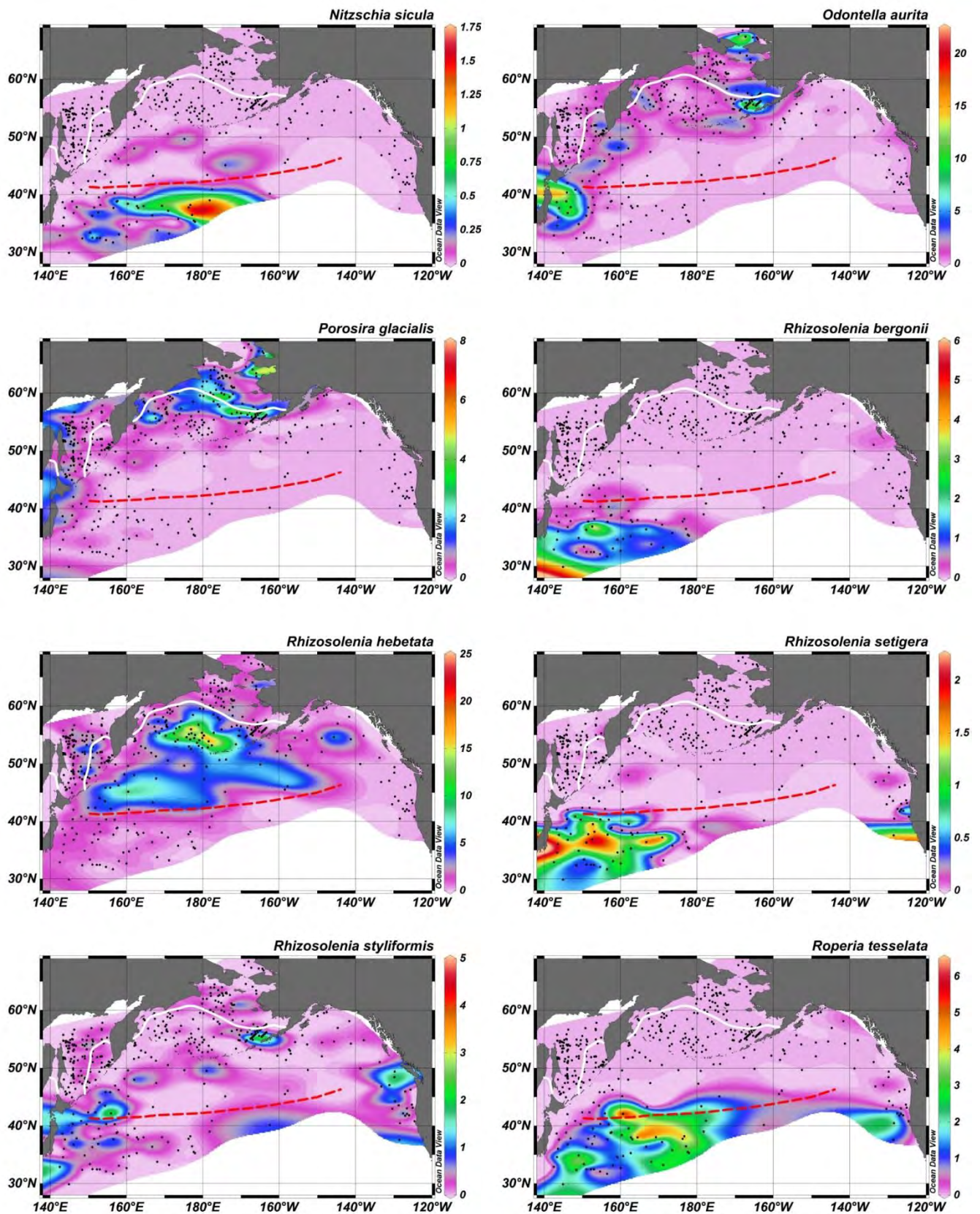


Fig. 3.4 (continued)

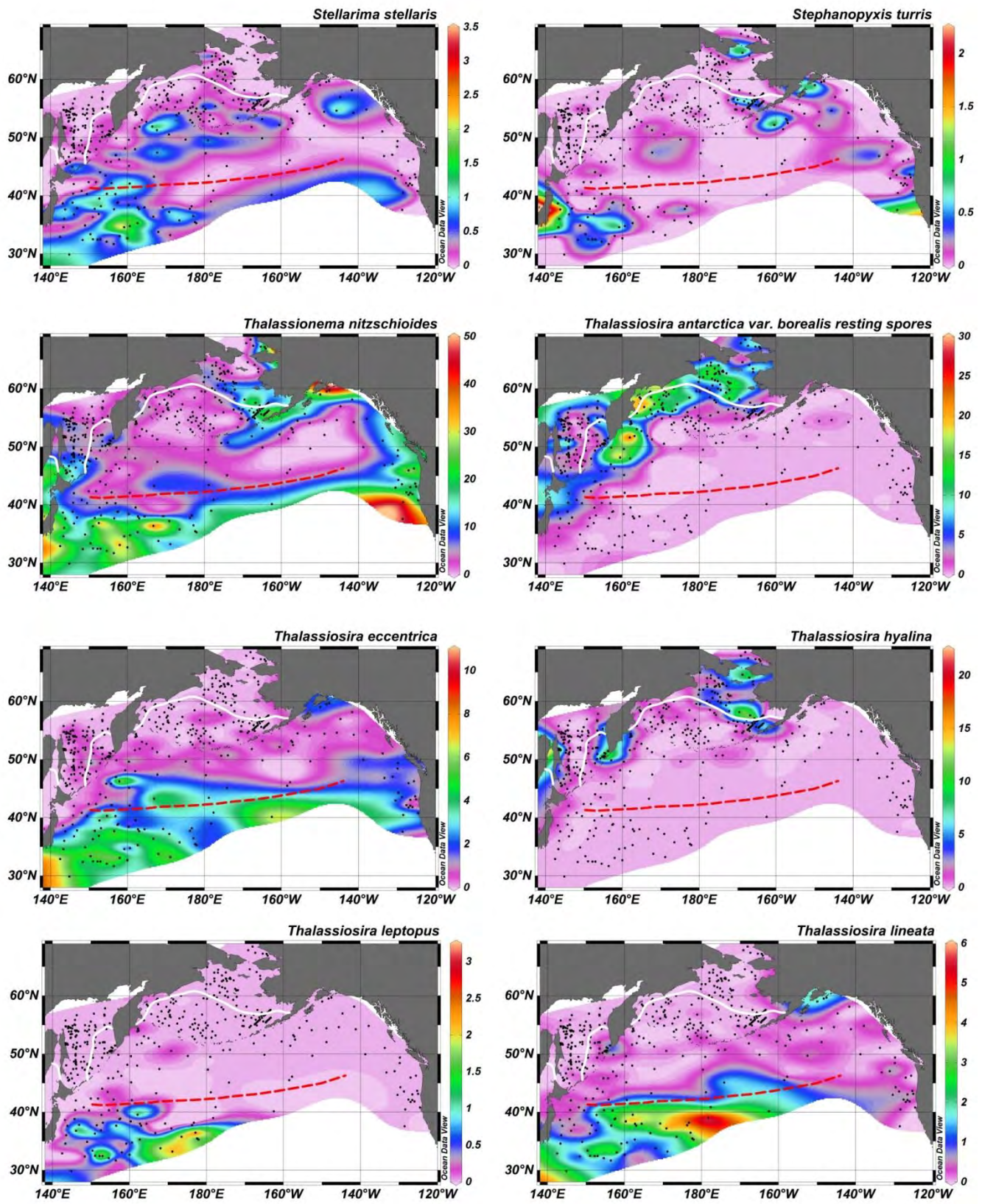


Fig. 3.4 (continued)

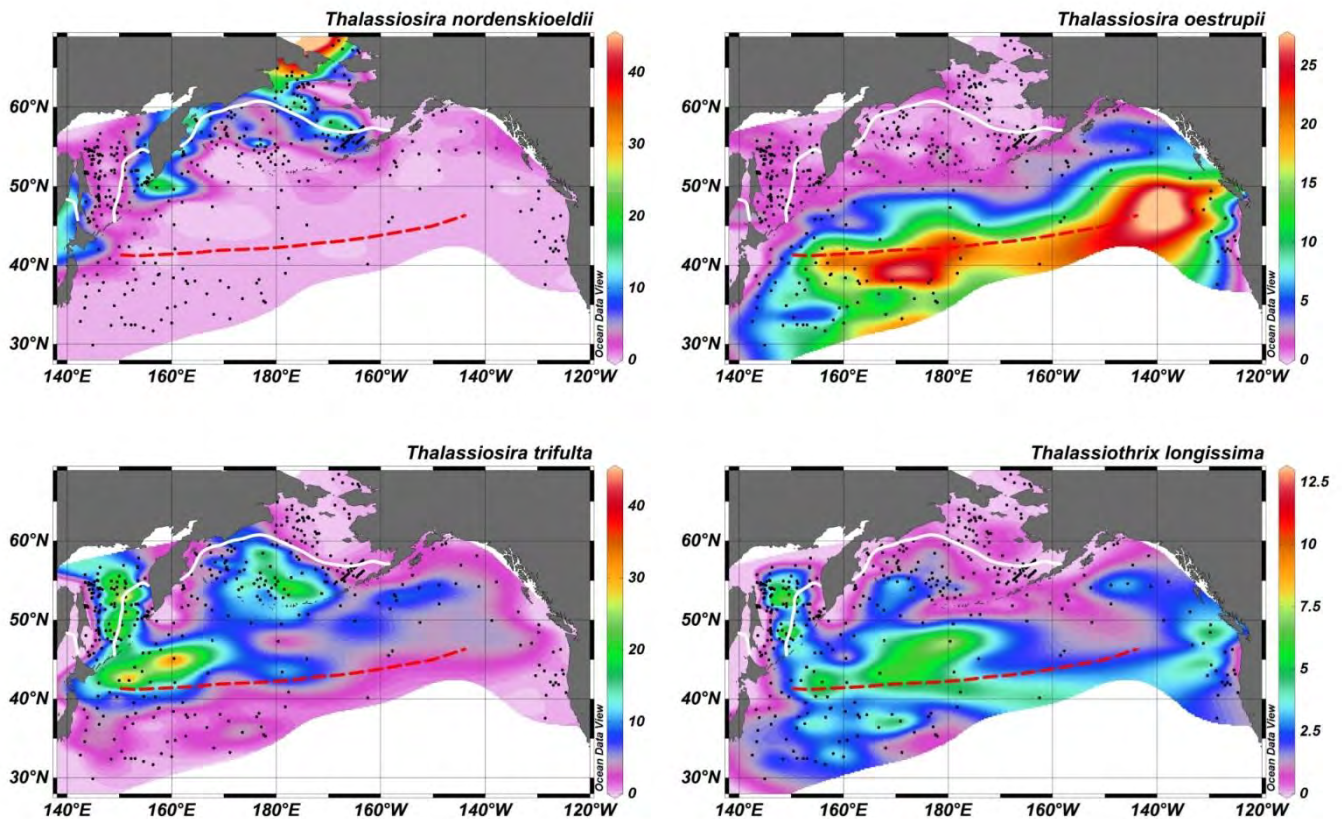


Fig. 3.4 (continued)

Neodenticula seminae is the most dominant species of the Subarctic Factor as well as the entire study area. It is rarely encountered outside the North Pacific region (Semina, 1981; Shimida et al., 2006). Except the samples from the Bering Shelf and subtropical North Pacific, *N. seminae* contributes at least 20% to the subarctic assemblage. The samples recovered along the Aleutian Current, from the Gulf of Alaska to the Bowers Ridge, contain >50% *N. seminae*. The distribution of *N. seminae* lies between the 8 °C isotherm, which overlies the continental slope, and 15 °C isotherm which corresponds to the Subarctic Front (Fig. 3.4). In the samples from the Sea of Okhotsk, it is generally less than 20%. High abundance (>10%) appears between 8 to 15 °C (Table 3.1; Fig. 3.6).

Rhizosolenia hebetata group is encountered between the winter sea ice edge and the Subarctic Front (SSST 6-22 °C; Fig. 3.6). At sites in the North Pacific open ocean, less than 5% of the diatom assemblages consist of *Rhizosolenia hebetata* group.

The heavily silicified *Thalassiosira trifulta* is another dominant species in the Subarctic Zone. It is abundant (up to 25%) in samples from the centers of the Bering and Okhotsk seas. Two peak values (up to 36%) are found along the west end of the Subarctic Front. *T. trifulta* appears between 8-24 °C (Table 3.1; Fig. 3.6).

3.4.2.3. Subtropical Factor

Factor 3, which explains 19% of the total variance, covers the entire area south of the Subarctic Front (Subtropical Factor; Fig. 3.5). It also extends north to the Gulf of Alaska along the coast of North America.

The highest score values occur in the southwest of the study area, where the warm Kuroshio and North Pacific Currents have the strongest influence. The Alaska Gyre brings warm waters from the Subarctic Front northward and accumulates them in the Gulf of Alaska, where the SSTs are higher than that of the counterpart in the western part of the study area, the Western Subarctic Gyre (Fig. 3.5). The assemblage is mostly composed of warm-water species, *Alveus marinus*, *Azpeitia nodulifera*, *A. tabularata*, *C. radiatus*, *F. doliolus*, *T. eccentrica*, *T. lineata*, *T. oestrupii* and *R. tessellata*. Minor species include *Actinocyclus octonarius*, *H. cuneiformis*, *N. bicapitata* and *R. bergonii* (Table 3.3). Among them, *Alveus marinus*, *Azpeitia nodulifera*, *H. cuneiformis*, *R. bergonii* and *T. oestrupii* are tropical species but also occur in subtropical region (Jousé et al., 1971; Muhina, 1971).

Actinocyclus octonarius is only found in the samples of the southwestern North Pacific, south of Subarctic Front, where the SSTs range between 16 to 27 °C (Table 3.1; Fig. 3.4 and 3.6).

Other warm water related species, *Alveus marinus* and *Azpeitia nodulifera*, show similar distribution patterns to *Actinocyclus octonarius*. They occur at SSTs >16 °C (Table 3.1; Fig. 3.4 and 3.6).

Azpeitia tabularis displays a broad range of occurrence, from the Bering Basin (8 °C) to the subtropical North Pacific (27 °C). It is, however, more abundant (>5%) south of the Subarctic Front with an SST range of 19-26 °C (Table 3.1; Fig. 3.4 and 3.6).

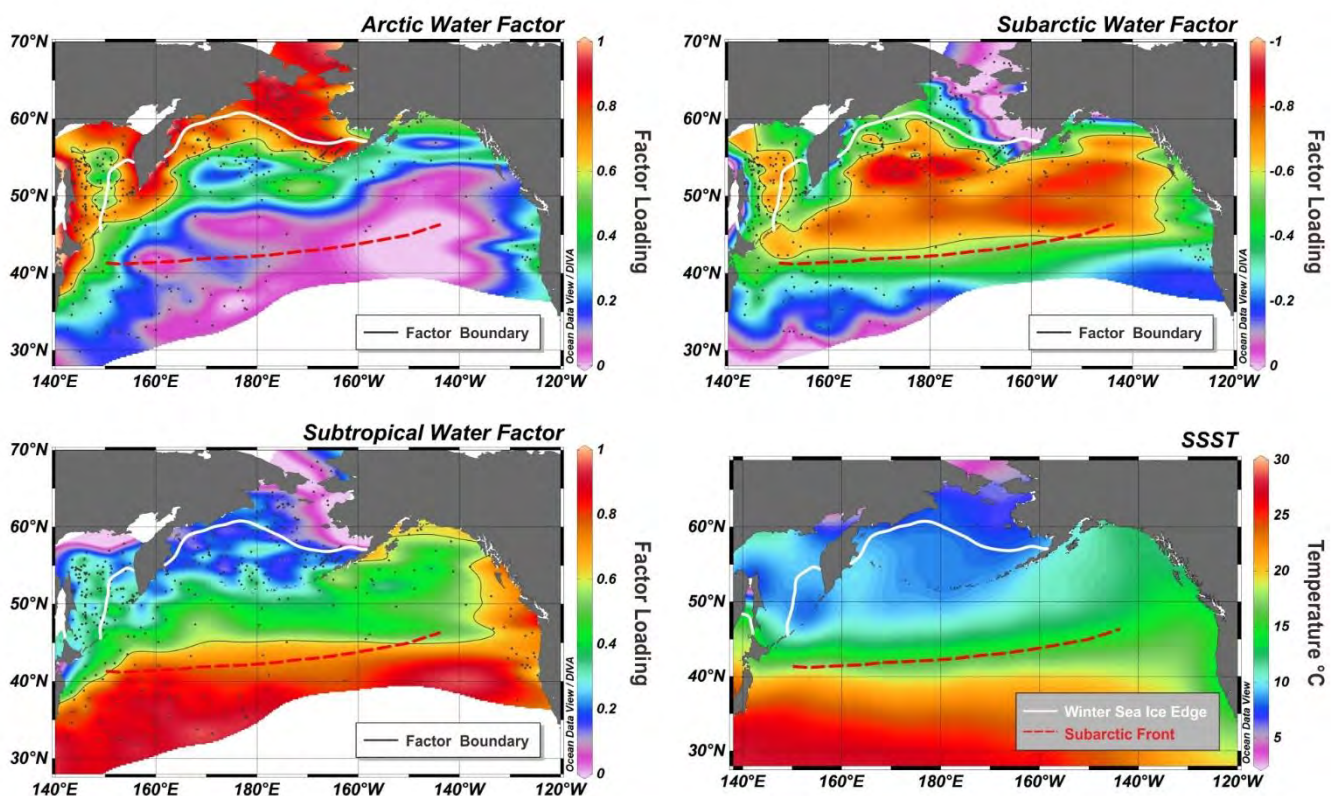


Fig. 3.5 Three factors yielded by Q-mode factor analysis, representing the Arctic, Subarctic and Subtropical water mass, respectively. The summer sea surface temperature pattern from WOA94 (Levitus et al., 1994) is shown as a reference.

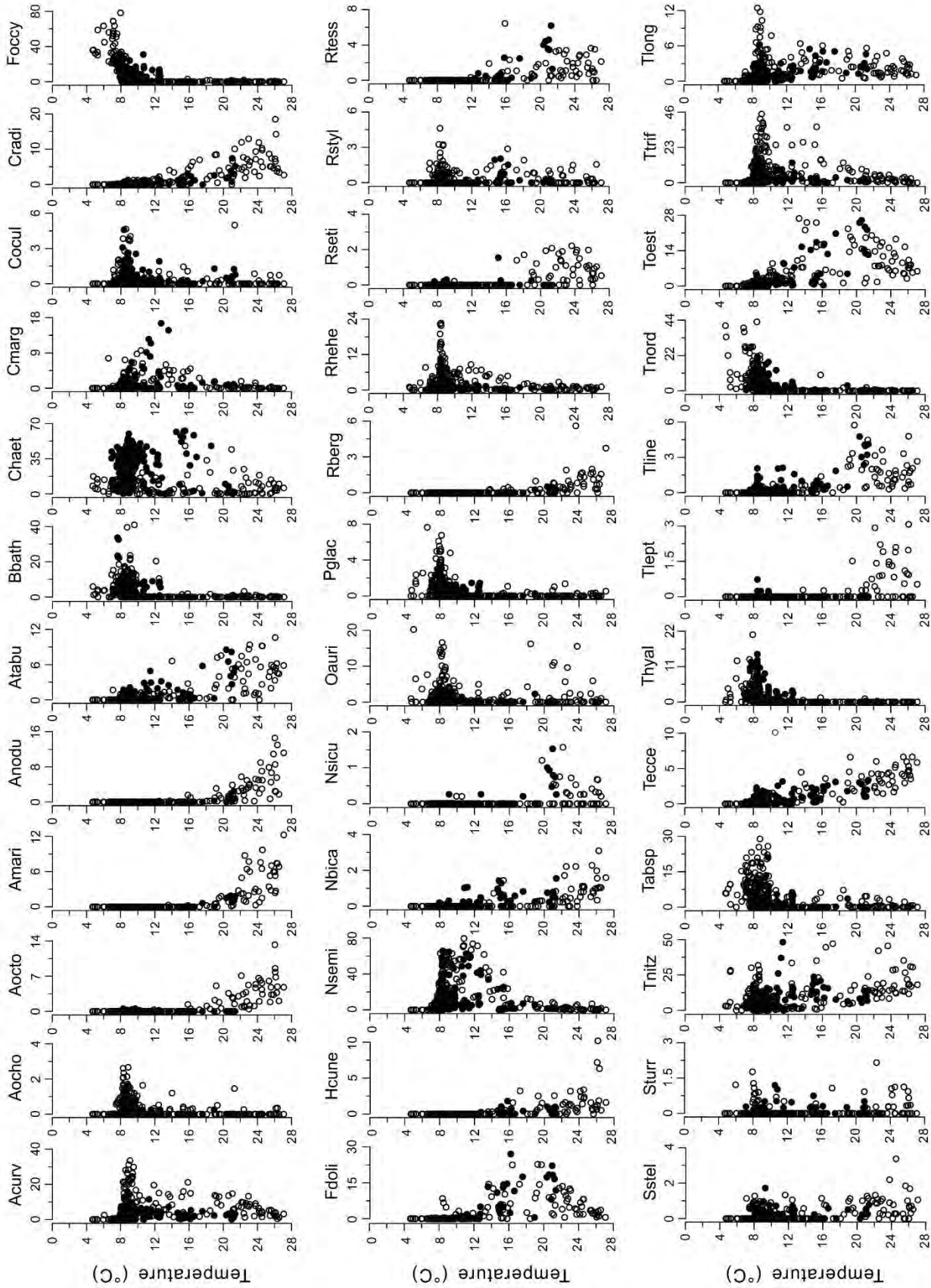


Fig. 3.6 Relative abundances of the 36 diatom species and species groups against summer sea surface temperature. Open circles represent samples from Sancetta and Silvestri (1986), while closed circles represent samples from this study. Abbreviations of diatom names are referred to Table 3.1.

The warm water related species, *C. radiatus*, *F. doliolus* and *H. cuneiformis* are only found in samples south of the Subarctic Front. *Coscinodiscus radiatus* is abundant in the western North Pacific between 30-40° N and is also encountered in a few samples close to the American coast (Fig. 3.4), while *F. doliolus* occurs in high concentrations across the subtropical North Pacific, except samples near Japan (Fig. 3.4). *Hemidiscus cuneiformis* only occurs in southernmost samples, indicating a temperature preference of >15 °C (Table 3.1; Fig. 3.6).

Nitzschia bicapitata appears southwest of the Subarctic Front (Fig. 3.4). It is also found in samples along the coasts of North America (Fig. 3.4). It is relatively abundant at temperatures between 22.5 to 27 °C (Table 3.1; Fig. 3.6).

Rhizosolenia bergonii only occurs south of the Subarctic Front (Fig. 3.4). It is relatively more abundant in the western subtropical North Pacific. *Rhizosolenia bergonii* prefers a warmer environment, >22.5 °C (Table 3.1; Fig. 3.6).

The typical warm-water species *R. tesselata* is present exclusively at sites south of the Subarctic Front, where SSTs are >13 °C (Fig. 3.6).

Three *Thalassiosira* species, *T. eccentrica*, *T. lineata* and *T. oestrupii* are encountered south of the Subarctic Front, indicating warm water masses. *T. eccentrica* and *T. lineata* are also found in low relative abundance in the samples from the Gulf of Alaska (Fig. 3.4). *T. eccentrica* and *T. lineata* reach maximum values between 19 to 27 °C (Table 3.1; Fig. 3.6), while *T. oestrupii* prefers a relatively cooler environment (13-21 °C ; Table 3.1; Fig. 3.6).

3.4.2.4. Other species

Four taxa score high values in more than one factor due to their occurrence in a wide area (*A. curvatulus*, *Chaetoceros* resting spores, *Thalassionema nitzschioides* and *Thalassiothrix longissima*. Fig. 3.4, Table 3.3). Nine species do not show clear factor scores, either due to their low relative abundance (*Asteromphalus* group, *N. sicula*, *R. setigera* and *Thalassiosira leptopus*) or their scattered distribution (*Odontella aurita*, *R. styliiformis*, *Stellarima stellaris*, *Stephanopyxis turris* and *T. pacifica*).

In our surface samples, *Actinocyclus curvatulus* is mainly distributed in the Sea of Okhotsk and western North Pacific (Fig. 3.4). Values >5% of the total assemblage occur between SSTs of 8 and 26 °C in the study area; the maximum value is concentrated around 9 °C (Fig. 3.6).

Chaetoceros resting spores occur in the coastal regions of the western and eastern North Pacific (Fig. 3.4), where biological productivity is high (Sancetta, 1981), the upwelling system is strong (Lopes et al., 2006) and lateral advection of iron from nearby continental shelves is sufficient (Lam et al., 2006; Lam and Bishop, 2008). *Chaetoceros* resting spores have a broad temperature range between 5-26.5 °C (Table 3.1; Fig. 3.6).

Thalassionema nitzschioides occurs in the North Pacific and in adjacent seas with high relative abundance (up to 50%). It is distributed from the Chukchi Sea to the subtropical North Pacific. It has maximal values in the Gulf of Alaska and west of North America while it also dominates the western

subtropical North Pacific (Fig. 3.4). No preference of SSST is indicated (Fig. 3.6).

Thalassiothrix longissima displays an evenly distributed pattern in the study area, except the Bering Shelf. It is common in the central Sea of Okhotsk (up to 12%) and in the middle of the North Pacific (up to 8%; Fig. 3.4). Therefore it occurs in a temperature range from 7 to 26.5 °C (Table 3.1; Fig. 3.6).

Odontella aurita is found from the Chukchi Sea, southeastern Bering Sea, off the Kuril Islands and east of Japan. It has a wide temperature range from 5 to 25.5 °C in summer (Fig. 3.6).

Rhizosolenia styliformis and *Stephanopyxis turris* show no distinct distribution patterns and have low relative abundance. They occur in samples from the southeastern Bering Sea, east of Japan, the Gulf of Alaska and west of the North America. It seems that they tolerate a wide range of temperature (SSST between 7-26.5 and 6-26 °C, respectively).

Stellarima stellaris appears throughout the study region with low abundance (less than 2%). The maximum values are found southwest of the Subarctic Front (Fig. 3.4). It thus shows no clear SSST preference (Fig. 3.6).

Nitzschia sicula, *R. setigera* and *T. leptopus* are subtropical species as they only occur south of the Subarctic Front (Fig. 3.4). They are relatively abundant in the western subtropical North Pacific, while only a few *R. setigera* are found in coastal samples off North America. *N. sicula* and *T. leptopus* thrive in environments warmer than 20 °C, whereas *R. setigera* prefers a warmer environment, >18 °C (Table 3.1; Fig. 3.6).

3.4.3. CCA results

In order to clarify the main influential environmental variable on diatom distribution, we carried out the CCA in addition to the diatom distribution mapping and the Q-mode analysis. The CCA based on 38 selected species and species groups from 422 samples shows that the first four axes explain 47.1% of the species variance, constrained by nine selected environmental variables, with 35.4% of the variance explained by the first axis and 7.4% explained by the second one (Table 3.4; Table S1). Axes 3 and 4 represent 4.3% of the variance and thus are considered less important (Table 3.4). The forward selection indicates that most environmental variables are statistically significant with a p-value <0.05.

Table 3.4 Results of Canonical Correspondence Analysis (CCA) for the first 4 axes.

Axes	1	2	3	4	Total inertia
Eigenvalues	0.376	0.078	0.028	0.018	1.06
Species-environment correlations	0.957	0.745	0.734	0.713	
Cumulative percentage variance					
of species data	35.4	42.8	45.4	47.1	
of species-environment relation	72.3	87.3	92.7	96.1	

The distribution pattern of environmental variables can be plotted as vectors in the CCA ordination diagram (Fig. 3.7a and 3.7b). Summer sea surface temperature (TEMP) is closely related to salinity (SALINITY) and slightly related to summer and winter mixed layer depths (SMLD and WMLD), while nutrient variables (NO_3 , PO_4 and SiO_4) point in the opposite direction. These vectors indicate that the dissolved nutrients and summer and winter sea ice concentrations (SSIC and WSIC) increase when TEMP decreases.

The CCA scatter diagram for samples versus environmental variables shows distribution patterns along the canonical axes (Fig. 3.7a). The samples from the subtropical North Pacific have high positive values (>0.5) on the first canonical axis, while the samples in the Bering Sea and the Sea of Okhotsk score negatively on this axis (<0). The samples from the Bering Shelf also have high scores on the second canonical axis (>0.5) corresponding to the areas with maximum winter sea ice concentration.

The first axis accounts for 72.3% of the canonical variance (Table 3.4). It is positively correlated with TEMP ($r=0.981$), followed by SALINITY (0.832), WMLD (0.779) and SMLD (0.509). Dissolved nutrients ($r<-0.582$) and WSIC and SSIC ($r<-0.109$) are negatively correlated with Axis 1 (Table 3.5). The second axis explains 15% of the canonical variance (Table 3.4). It is positively correlated with WSIC ($r=0.572$; Table 3.5). The CCA diagram shows that the samples from the Bering Shelf seasonally covered by sea ice have the highest positive values on Axis 2 (Fig. 3.7a). The second axis has a negative relationship with dissolved nutrients ($r<-0.423$) and WMLD and SMLD ($r<-0.448$) while no clear correlation is found between Axis 2 and TEMP and SALINITY.

Table 3.5 Correlation between the first and second CCA-axes and the nine selected environmental variables.

Environmental Variables ^a	First CCA Axis ^b	Second CCA Axis ^b
TEMP	0.981	0.020
WSIC	-0.471	0.572
SSIC	-0.109	0.290
SALINITY	0.832	-0.301
NO_3	-0.582	-0.602
PO_4	-0.696	-0.514
SiO_4	-0.610	-0.423
WMLD	0.779	-0.448
SMLD	0.509	-0.590

^a TEMP: summer sea surface temperature; SALINITY: summer sea surface salinity; WSIC and SSIC: winter and summer sea ice concentration, respectively; WMLD and SMLD: winter and summer mixed layer depths

^b These values are the correlation coefficient for linear regressions between environmental variables and CCA scores.

In the CCA diagram, the diatom species are positioned based on their relationship to the environmental variables in the ordination diagram (Fig. 3.7b; Table S2). Since Axis 1 is highly correlated with TEMP, diatom species preferring relatively high surface water temperatures are generally positioned to the right of CCA Axis 1, including *Alveus marinus*, *Azpeitia nodulifera*, *R. bergonii*, *H. cuneiformis*, *R. setigera*, *N. sicula*, *T. leptopus*, *Actinocyclus octonarius*, *R. tessellata*, *N. bicapitata*, *F. doliolus*, *C. radiatus*,

Azpeitia tabularis, *T. lineata*, *T. eccentrica*. These species are abundant in the sites south of the Subarctic Front, being influenced by subtropical water masses (Fig. 3.4). In contrast, sea ice and Arctic species are located in the opposite direction of CCA Axis 1, such as *T. hyalina*, *F. oceanica*, *F. cylindrus*, *T. nordenskieoldii*, *P. glacialis*, *B. bathyomphalus* and *T. antarctica* var. *borealis* resting spores. These species are also positioned in the positive direction of sea ice variables (Fig. 3.7b), indicating a high correlation with sea ice distribution. They are found mainly on the Bering Shelf, the area seasonally covered by sea ice (Fig. 3.4). Between these two assemblages of diatoms lie the subarctic species, such as *R. hebetata*, *N. seminae*, *C. oculus-iridis*, *T. trifulta*, *C. marginatus* and *A. curvatulus*. They dominate the diatom composition in the subarctic area (Fig. 3.4). Species with no clear correlation to any of the environmental variables are also encountered in the middle of the Axis 1. These are *Asteromphalus* group, *Stellarima stellarima*, *Stephanopyxis turris*, *R. styliformis*, *T. pacifica* and *T. longissima*, which are either rare in abundance or are sporadically distributed (Fig. 3.4 and 3.7b). *Chaetoceros* species resting spores and *T. nitzschioides* appear throughout the study area, showing no specific environment preference (Fig. 3.4).

The forward selection also shows the strongest correlation between TEMP and the diatom species distribution (Table 3.6).

Table 3.6 The results of Forward Selection of nine selected environmental variables. The ranking of each parameter according to the marginal and conditional effects are shown.

Marginal Effects		Conditional Effects		
Variable ^a	λ	Variable ^a	λ	<i>p</i> -value
TEMP	0.37	TEMP	0.37	0.002
SALINITY	0.29	NO ₃	0.05	0.002
WMLD	0.26	WSIC	0.02	0.002
PO ₄	0.25	SiO ₄	0.04	0.002
NO ₃	0.20	WMLD	0.01	0.002
SiO ₄	0.20	SALINITY	0.02	0.002
SMLD	0.13	PO ₄	0.01	0.002
WSIC	0.11	SSIC	0	0.010
SSIC	0.01	SMLD	0	0.488

^a TEMP: summer sea surface temperature; SALINITY: summer sea surface salinity; WSIC and SSIC: winter and summer sea ice concentration, respectively; WMLD and SMLD: winter and summer mixed layer depths

3.5. Discussion

3.5.1. Total diatom peak flux

In order to summarize the seasonal signals preserved in the surface sediments, we compiled the monthly total diatom flux data from ten sediment traps located in the North Pacific (Fig. 3.1a) based on previous studies (Takahashi, 1997; Tsoy and Wong, 1999; Onodera et al., 2005; Onodera and Takahashi, 2009).

Monthly total diatom peak flux mostly appears in April with two minor occurrences in August and October (Fig. 3.8). Long period sediment trap results reveal a total diatom flux with spring and autumn peaks (AB and SA; Onodera and Takahashi, 2009). So do the data from short-term traps (Takahashi, 1997; Tsoy and Wong, 1999; Onodera et al., 2005), although the timings of autumn maxima vary more than those of spring maxima (Takahashi, 1997). In spite of the high flux in August, the summer flux of July is relatively low due to the intensified stratification (Fig. 3.8; Onodera and Takahashi, 2009).

In the sediment traps from the open ocean and the Western Subarctic Gyre (i.e. GB, SA, 40N, KNOT, GA, GD, 50N; Fig. 3.1a), the total diatom fluxes peak in spring (April, May, June), summer (mainly August) and autumn (mainly October). The winter fluxes almost disappear in these areas (Fig. 3.8). In contrast, diatom fluxes from the Alaska Gyre are stable throughout the year, with small peaks in May and November (Fig. 3.8). The opal flux in the same area has a maximum from May to September (Wong et al., 1999). High fluxes in the Bering Sea appear often in August (AB; Onodera and Takahashi, 2009). In the Sea of Okhotsk, the opal fluxes appear in late spring and summer (Seki et al., 2007).

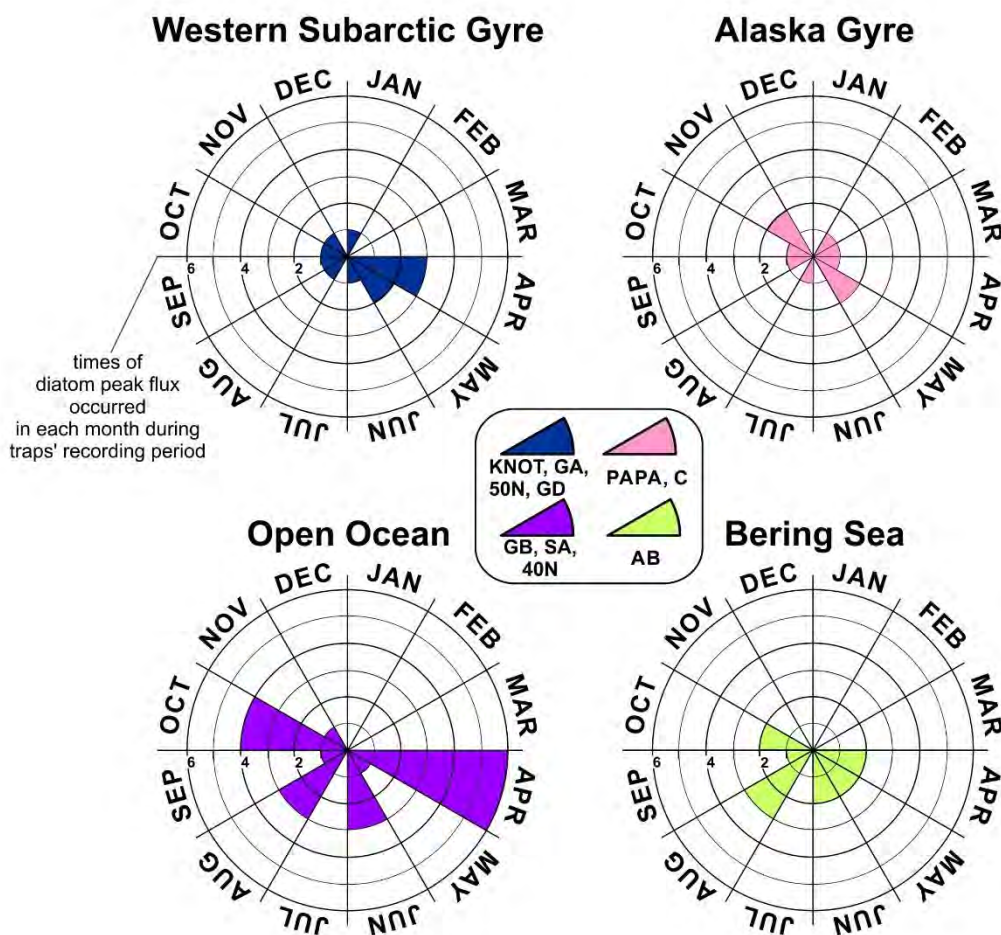


Fig. 3.8 The rosegram of total monthly diatom peak flux. The numbers indicate the times of diatom peak flux occurred in each month during traps' recording period. The station names are shown as well. The total diatom flux data are collected from Takahashi, 1997 (Station PAPA and C); Tsoy and Wong, 1999 (Station GB, GD and GA); Onodera et al., 2005 (Station 40N, KNOT and 50N) and Onodera and Takahashi, 2009 (Station SA and AB)

Consequently, the seasonal signals preserved in the surface sediments mainly result from production during spring through autumn. Most of our surface samples are located in the regions with spring and summer fluxes, i.e. the Western Subarctic Gyre, the Bering Sea and the Sea of Okhotsk (Fig. 3.1a). Therefore, spring to summer signals may be chosen as the target for paleoenvironmental reconstruction.

In general, annual mean diatom fluxes of the western North Pacific are 2 to 4 times higher than that of the eastern counterpart (e.g. Onodera et al., 2005), probably due to richer nutrient concentrations in the western part and to its proximity to Asian dust sources and continental inputs (Shiomoto et al., 1998; Harrison et al., 1999; Lam et al., 2006; Lam and Bishop, 2008).

In terms of species abundance, *N. seminae* contributes more than 70% of annual diatom flux in all sediment traps except KNOT and 40N (Onodera et al., 2005). The high abundance in the sediment is thus an accurate reflection of the species dominance in the water column.

3.5.2. Diatom species distribution

3.5.2.1. Subtropical North Pacific open ocean

The Subtropical assemblage is dominated by typical warm water species, such as *Alveus marinus*, *Azpeitia nodulifera*, *A. tabularis*, *C. radiatus*, *F. doliolus*, *H. cuneiformis*, *Rhizosolenia bergonii*, *Roperia tessellata*, *T. lineata* and *T. eccentrica*. These species have a surface temperature preference $>16\text{ }^{\circ}\text{C}$ (Fig. 3.6) and thus geographically decrease dramatically north of the Subarctic Front (Fig. 3.4). Kazarina and Yushina (1999) grouped similar species into the subtropical and the tropical assemblage, with a temperature coverage from 13 to 26 $^{\circ}\text{C}$, which is in accordance with our study. Among them, *Alveus marinus*, *Azpeitia nodulifera*, *F. doliolus*, *H. cuneiformis*, *Rhizosolenia bergonii* and *Roperia tessellata* are defined as warm water species by Kanaya and Koizumi (1966). Koizumi and Sakamoto (2003) took this warm species group and made a ratio of warm/cold species to estimate sea surface temperature. In this study, these species, except *F. doliolus*, show maximum values in the western subtropical Pacific (Fig. 3.4), where the warm and salty Kuroshio Current starts to form the Kuroshio Extension (Fig. 3.1b) with a SSST $>20\text{ }^{\circ}\text{C}$. In this region, certain species are employed to trace the Kuroshio Current (e.g. Jiang et al., 2006).

The CCA shows that *F. doliolus* has lower score in the direction of environmental vector TEMP than the other warm species mentioned above (Fig. 3.7b), indicating that it prefers a relatively lower temperature. *Fragilariopsis doliolus* was found to be abundant in the transition zone between the subtropical and subarctic gyres (Venrick, 1971). It accounts for 3-20% of the diatom composition of surface samples south of the Subarctic Front and disappears abruptly in the northern samples (Fig. 3.4). Off Oregon and California, *F. doliolus* is also associated with the boundary of the Central Gyre, the synonym of the North Pacific Subtropical Gyre (Sancetta, 1992; Barron et al., 2003; Barron and Bukry, 2007). Thus the northern boundary of the distribution of *F. doliolus* in the open ocean is suggested to be an indicator of the Subarctic Front, where the water masses from subtropical and subarctic sources mix. This is supported by the sediment trap study from Station 40 (40 $^{\circ}$ N, 165 $^{\circ}$ E, 2986 m trap depth; Fig. 3.1a; Onodera et al., 2005),

located south of the Subarctic Front. *Fragilariopsis doliolus* was dominant in Station 40N when the subtropical water mass was present, whereas *N. seminae* replaced *F. doliolus* when the cold Oyashio water prevailed (Onodera et al., 2005).

3.5.2.2. Subtropical North Pacific coasts

Compared with the subtropical North Pacific open ocean, more coastal, fresh- and brackishwater species are encountered in samples off coasts, such as *Achnanthes* spp, *Coconeis* spp, *Fragilaria* spp and *Nitzschia* spp. Off the coast of western North America, Lopes et al. (2006) suggest that these species are transported by coastal river plumes from the coastal area to the offshore areas (e.g. the Columbia River, the Eel River). Therefore lateral transport is not negligible in the study area. The dominant species in the area are *Chaetoceros* resting spores, *T. nitzschioides*, *N. seminae* and *F. doliolus*, in accordance with the sediment trap observations in the same region (Sancetta, 1992; Tsoy and Wong, 1999; Onodera et al., 2005).

The blooming of *Chaetoceros* spp. may depend upon iron supply to the North Pacific (Tsuda et al., 2003). *Chaetoceros* species produce spores when nutrients are depleted following the upwelling season (Margalef, 1978). It is hence used as an indicator of upwelling and production (e.g. Margalef, 1978; Sancetta, 1981; Abrantes, 1988). Our results off the coast of western North America show that the relative abundance of *Chaetoceros* spores declines dramatically (from 60% to 1.5%) in samples further away from the coast, where low productivity and less seasonal variability occurs. This is in accord with the results from Lopes et al. (2006). The western margin of the North Pacific and the Bering Sea also show high abundance of *Chaetoceros* resting spores in sediments (up to 60%; Fig. 3.4). It is in agreement with the results shown by Koblenz-Mishke et al. (1970), that this is an area with high average annual primary productivity, due to the vertical mixing and continental inputs nearby (Sancetta, 1981). Yuan and Zhang (2006) suggest high correlations between Asian dust events and biological productivity in the western North Pacific, although the relationship between the aeolian dust and *Chaetoceros* species is relatively low. The iron addition from the aeolian dust could trigger the bloom of *Chaetoceros* species, hence the high amount of the resting spores in the sediments (Tsuda et al., 2003). In the North Pacific, *Chaetoceros* resting spores generally are abundant in the neritic regions, where high nutrient and iron concentrations are supported by input from proximate continents and shelves (Fig. 3.4; Lam and Bishop, 2008; Serno et al., 2014). Therefore, the abundance of *Chaetoceros* resting spores may indicate iron input and induced productivity events in the study area.

Thalassionema nitzschioides is considered to be a wide distributed species in low latitudes (Hasle and Syvertsen, 1997). In coastal areas, it is used as an upwelling indicator (e.g. Margalef, 1978; Abrantes, 1988; Abrantes et al., 2007). In our samples, it is as abundant in the oligotrophic open ocean as it is in the coastal zone (Fig. 3.4), indicating that it tolerates low nutrients more than the coastal diatom species, while in the strong upwelling regions it is likely diluted by other bloom species (e.g., *Chaetoceros*) in response to nutrient input (Lopes et al., 2006).

3.5.2.3. Subarctic North Pacific

The Subarctic North Pacific is dominated by *N. seminae* with secondary *A. curvatulus*, *A. ochotensis*, *C. marginatus* and *T. trifulta* (Fig. 3.4).

Neodenticula seminae is widely distributed in the subarctic North Pacific, accounting for >40% of the diatom composition in surface sediments and sediment traps (e.g. this study; Kanaya and Koizumi, 1966; Sancetta, 1982; Kazarina and Yushina, 1999; Onodera and Takahashi, 2009). *Neodenticula seminae* reaches maximum values in the northwestern North Pacific, the Gulf of Alaska and along the Aleutian Islands (Fig. 3.4). Sancetta (1982) proposed it as a tracer of the Alaska Stream, where it comprises >50% of the diatom abundance. The summer silicate concentration in the Gulf of Alaska is high (>10 $\mu\text{mol}\cdot\text{L}^{-1}$), indicating the relationship between the silicate concentration and the abundance of *N. seminae*. The results of the CCA also show *N. seminae* follows the same vector as nutrients (Fig. 3.7b), implying the distribution of heavily silicified *N. seminae* is constrained by the nutrients pattern (e.g. SiO_4 ; Shimada et al., 2006). *Neodenticula seminae* almost disappears south of the Subarctic Front (Fig. 3.4). Together with *F. doliolus*, we use them to define the transition zone between the subtropical and subarctic water masses.

Four samples from the coastal area of the Gulf of Alaska contain extremely high abundance of *T. nitzschioides* (>15%), especially two stations near the coast (up to 50%). It is very likely that they are influenced by the local upwelling system.

3.5.2.4. Bering Sea and Sea Ice

The Bering Sea diatom assemblages are divided along the Bering Slope. The so-called Bering Basin assemblage (Sancetta, 1981; Kazarina and Yushina, 1999) is similar to the subarctic North Pacific assemblage discussed above, including dominant *N. seminae*, *R. hebetata* group and *T. trifulta*. These heavily silicified species are supported by the high summer silicate concentration (>10 $\mu\text{mol}\cdot\text{L}^{-1}$) encountered in the area. The area is influenced by the Alaska Stream via straits along the Aleutian Islands and thus is well traced by *N. seminae*.

Rhiosolenia hebetata group, mainly *R. hebetata* f. *hebetata*, appearing in cold northern regions (Hasle and Syvertsen, 1997), is similar in its distribution pattern to *N. seminae*, although in relatively lower abundance. It almost disappears south of the Subarctic Front (Fig. 3.4). Being associated with the subarctic water, it is regarded as an indicator of the Alaska Stream and the Subarctic Front (Sancetta, 1979; Lopes et al., 2006). The highest values found close to the Bowers Ridge (up to 20%) is likely due to the concentration by the current winnowing (Sancetta, 1982). Caissie et al. (2010) considered *R. hebetata* as a productivity indicator. Our results show that the abundance of *R. hebetata* in the subarctic Pacific may not only relate to high productivity, because it occurs in low relative abundance along the Kamchatka Peninsula and Kuril Islands, an area with high productivity (Koblentz-Mishke et al., 1970). A study from the northeast subarctic Pacific also implies a relation between *R. hebetata* and open oligotrophic waters (Lopes et al., 2006).

Sancetta (1981) defined the diatom assemblage above the Bering Shelf as the Sea Ice Assemblage,

including *F. cylindrus*, *F. oceanica*, *T. antarctica* var. *borealis* resting spores, *T. hyalina* and *T. nordenskiöldii* (Fig. 3.4). The similar composition is also reported from the North Atlantic (e.g. Koç Karpuz and Schrader, 1990; Jiang et al., 2001). Within this assemblage, *F. cylindrus* and *F. oceanica* are true sea ice species, being found within the base of the sea ice (Horner and Alexander, 1972; Poulin, 1990). *Fragilariopsis cylindrus* has a bipolar distribution. Together with *Fragilariopsis curta*, which is endemic to the Southern Hemisphere, it has been used as a sea ice extent indicator in the Southern Ocean, where abundance of 3% coincides well with Antarctic winter sea ice (Gersonde and Zielinski, 2000). In the Bering Sea, a relative abundance of 20% of *F. cylindrus* and *F. oceanica* and the maximum extent of the winter sea ice (sea ice concentration >15%) are geographically well matched (Fig. 3.4). Furthermore, most samples experiencing winter sea ice (sea ice concentration >15%) contain more than 20% of *F. cylindrus* and *F. oceanica* (Fig. 3.9). Caissie et al. (2010) used the relative abundance of *Fragilariopsis* species (mainly *F. cylindrus* and *F. oceanica* in the Bering Sea) to reconstruct the sea ice duration during the year. Although some relationship is detected in this study, the interpretation needs caution when applied to paleoenvironment reconstruction. These diatom assemblages are controlled by the spring and summer blooms rather than simply the annual sea ice duration. Therefore, the sea ice diatoms in this study are used as a sea ice extent indicator rather than a sea ice duration proxy.

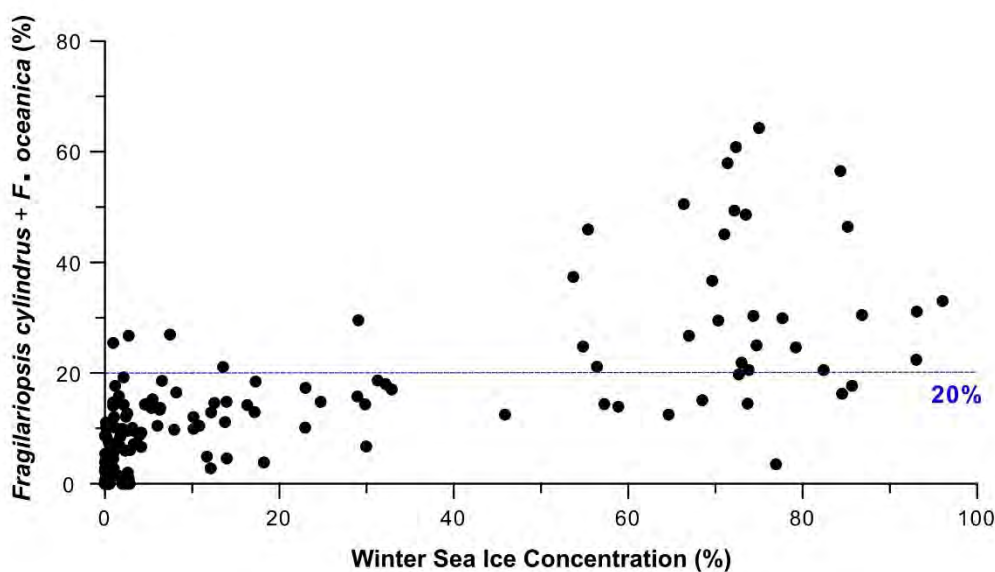


Fig. 3.9 Relative abundance of *Fragilariopsis cylindrus* and *F. oceanica* from the Bering Sea against winter sea ice concentration. The blue dot lines indicate the relative abundances of both species which coincide well with the winter sea ice edge.

The relative abundance of *F. cylindrus* and *F. oceanica* decreases gradually with the distance from the maximum extent of the winter sea ice (Fig. 3.10). The relationship between the relative abundance of sea ice species and the distance from the sea ice edge could be applied to estimate sea ice extent in the past.

Paralia sulcata and *Melosira sol*, together with minor contributions from coastal pennate species, such as *Delphineis surirella* and *Delphineis kippae*, are abundant on the Bering Shelf (in general 20-30%,

up to 55%). *Paralia sulcata* is a benthic species but quite common in coastal area and is possibly cosmopolitan (Crawford, 1979; Round et al., 1990; Hasle and Syvertsen, 1997). It is sometimes found in the neritic plankton and is very common along the south-eastern shores of the North Sea (Hendy, 1964) as well as in the northern part of the South China Sea, where the SSST is *ca.* 29 °C (Jiang et al., 2004). In addition, it is also the main constituent of the Norwegian-Atlantic Current assemblage with relatively warm-water temperatures in the Nordic Seas (Koç Karpuz and Schrader, 1990). *Delphineis surirella* and *D. kippae* are found living attached to the littoral sediments (Sancetta, 1982; Witkowski et al., 2000) and are very common along the coasts of the southern North Sea and the Atlantic coasts of Europe (e.g. Hendy, 1964). Thus, these neritic species occurring on the Bering Shelf are actually cosmopolitan throughout the world coastal ocean. The distribution of these species is probably controlled by light availability as a

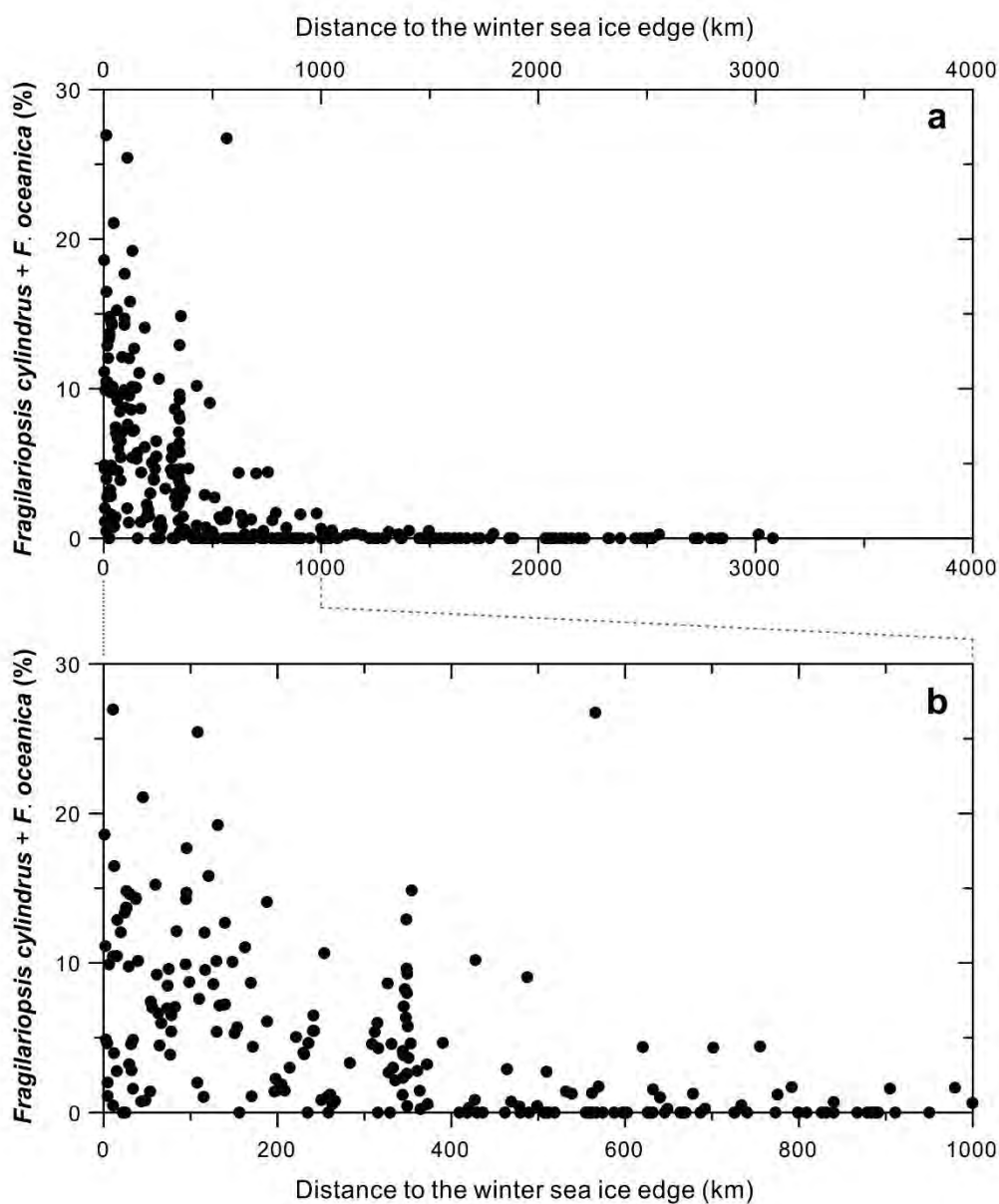


Fig. 3.10 a) The relationship between the relative abundance of *Fragilariopsis cylindrus* and *F. oceanica* and the distance to the winter sea ice edge (km). b) is an expansion of a) to magnify the relationship in the first 1000 km.

function of water depth rather than sea surface temperatures. However, the unique topography in the North Pacific and its marginal seas make these species a major component on the Bering Shelf, which is covered by sea ice during winter. This, as a consequence, will bias the statistical analysis of diatom distribution and environmental variables if they are included in the data set. For instance, *P. sulcata* shows a maximum value against cold temperature in a previous study by Kazarina and Yushina (1999). Jiang et al. (2001) also show that biased results occur when applying the CCA to species like *P. sulcata* and *D. surirella*. Therefore, these species are excluded from the database for the statistical analysis. However, the unique habitat of these species, being constrained to certain water depths, which is used to indicate sea level changes and the influence of coastal water (e.g. Huang et al., 2009), can be applied in sediment cores from the Bering Sea as well (Sancetta, 1983a).

3.5.2.5. Sea of Okhotsk

The Okhotsk Sea assemblage is mainly composed of *A. curvatulus*, *Thalassiosira trifulta*, *Chaetoceros* resting spores, *B. bathyomphala*, *N. seminae* and to a lesser degree, *Thalassionema nitzschioides*, in agreement with previous studies (e.g. Tsoy et al., 2009). *Actinocyclus curvatulus* and *T. trifulta* are also abundant in the subarctic assemblage. In the Q-mode analysis, these two species show high scores in both subarctic and subtropical factors (Table 3.3), due to their bimodal distribution (Fig. 3.4). Since they decrease from the central Sea of Okhotsk to the shelf, it is proposed that they are more pelagic species (Sancetta, 1982).

In the Sea of Okhotsk, Shiga and Koizumi (2000) grouped *B. bathyomphala* with the sea-ice species. Since the relative abundance of certain percentage (e.g. 6%) of *B. bathyomphala* coincides with the maximum winter sea ice extent (Fig. 3.4), it is likely to be a sea ice extent indicator of the region. However, *B. bathyomphala* is described as a neritic species (Sancetta, 1982 and references therein). It has been found abundant on the northern and western slopes of Sea of Okhotsk with depths shallower than 500m and rare in the deep central basin (Fig. 3.4; this study; Sancetta, 1982). Due to the fresher and cooler water mass there, winter sea ice mainly occurs on the shelf area, which coincidentally meets the relative abundance of certain percentage (e.g. 6%) of *B. bathyomphala*. In addition, the CCA shows *B. bathyomphala* has a lower value on the WSIC arrow than *F. cylindrus* and *F. oceanica*, implying that it prefers less sea ice than *F. cylindrus* and *F. oceanica* (Fig. 3.7b). Therefore *B. bathyomphala* could hardly be applied as a pure sea ice indicator before ruling out the influence from water depths.

Thalassionema nitzschioides is abundant in the southern coastal area, indicating the influence of the warm and saline water mass from the Sea of Japan through the Soya Strait (Sancetta, 1981).

3.5.3. Implications for paleoenvironment reconstructions

The results of the CCA and forward selection on the relative abundances of 38 diatom species and groups from 422 surface samples indicate a strong relationship between diatom species distribution and the summer sea surface temperature. Among them, 32 species and species groups are linearly or

unimodally distributed against the SSTs. The Q-mode analysis, which yields 3 factors corresponding to different water masses, also implies that the diatom distributions are mainly controlled by the SST patterns, in agreement with earlier studies in this area (Kanaya and Koizumi, 1966; Jousé et al., 1971; Sancetta, 1981, 1982; Sancetta and Silvertri, 1986; Kazarina and Yushina, 1999; Tsoy et al., 2009). The significant relationship between SST and diatom distribution supports establishment of a transfer function for paleotemperature reconstructions in the northern North Pacific area.

The CCA results reveal a less prominent impact on the diatom distribution by nutrients and winter sea ice concentration, especially in the subarctic area, where the high amount of nutrients support the highly silicified diatoms, such as *N. seminae*, *C. marginatus* and *T. trifulta* (Fig. 3.7b; Table 3.5). This, as well as skeletal morphology of *N. seminae* (Shimada et al., 2006), may imply additional information on nutrient supply during the glacial and interglacial periods.

The distribution of *F. cylindrus* and *F. oceanica* for the Bering Sea coincides well with the winter sea ice edge and therefore is used as an indicator to estimate the extent of winter sea ice.

These implications could be applied to previous paleoceanographic reconstructions based on diatom in the northern North Pacific, of which diatom composition of the late Pleistocene record are similar to surface sample results (Barron et al., 2003; Katsuki et al., 2003; Katsuki and Takahashi, 2005; Barron and Bukry, 2007; Barron et al., 2009; Katsuki et al., 2009; Caissie et al., 2010). This may improve our understanding of North Pacific paleoceanographic variability.

3.6. Conclusions

This study documents the diatom distribution in surface sediments of the northern North Pacific. Thirty-eight diatom species from 422 surface samples throughout the area show a clear distribution pattern.

Three assemblages are distinguished by Q-mode factor analysis, representing different water masses. The Arctic Assemblage, which is restricted to the area covered by sea ice seasonally, is dominated by sea ice related diatoms (e.g. *F. cylindrus*, *F. oceanica*) and cold water species (e.g. *B. bathyomphala*, *P. glacialis*, *T. antarctica* var. *borealis* resting spore, *T. hyalina* and *T. nordenskiöldii*). Between the winter sea ice edge and the Subarctic Front lies the Subarctic Assemblage, which includes *A. ochotensis*, *C. marginatus*, *C. oculus-iridis*, *N. seminae*, *R. hebetata* group and *T. trifulta*. The Subtropical Assemblage occurs south of the Subarctic Front, representing the warm water masses. Thus it is characterized by warm species, such as *Alveus marinus*, *Azpeitia nodulifera*, *A. tabulata*, *C. radiatus*, *F. doliolus*, *R. tessellata*, *T. eccentrica*, *T. lineata* and *T. oestrupii*.

A relative abundance of 20% *F. cylindrus* and *F. oceanica* is used to establish the maximum extent of winter sea ice in the Bering Sea. The northern boundary of the distribution of *F. doliolus* in the open ocean is suggested to be an indicator of the Subarctic Front.

The total diatom flux data from ten sediment traps reveal that the seasonal signals preserved in the surface sediments are mostly from spring through autumn, and indicate that the spring to summer signals

should be a main target for paleoenvironment reconstruction.

The Canonical Correspondence Analysis has been applied to analyze the relationship between relative diatom abundance and nine environmental variables. The result shows that the 32 species and species groups in the northern North Pacific are mainly related to the summer sea surface temperature, while sea ice concentrations play a minor role.

The new data set studied here covers the whole northern North Pacific and its marginal seas. The close relationship between diatom composition and the summer sea surface temperature will be useful in deriving a transfer function in this area for quantitative paleoceanographic and paleoenvironmental studies.

Acknowledgements

This paper is a contribution to the INOPEX (Innovative North Pacific EXperiment) project funded by the Bundesministerium für Bildung und Forschung (the German Ministry of Education and Research). Gerald H. Haug from Potsdam Universität and ETH Zürich is thanked for the financial funding for J. Ren. Surface samples were taken from several cruises, e.g. INOPEX, KALMAR, KOMEX. We thank the scientific and technical staff on shipboard. We would like to acknowledge Maryse Henry and Anne de Vernal from GEOTOP for offering the surface samples from the Canadian cruises. We are also grateful to Ute Bock and Stephan Heckendorff from AWI for the technical assistances. We thank John Barron and one anonymous reviewer for constructive comments.

Supplementary material to Manuscript I

List S1. Taxonomy

Based on the classification in Hasle and Syvertsen (1997).

CENTRIC DIATOMS

ORDER Biddulphiales

Suborder Coscinodiscineae

Family Thalassiosiraceae

- Genus *Bacterosira* Gran 1900
Bacterosira bathyomphala (Cleve) Syvertsen & Hasle 1993
- Genus *Porosira* Jørgensen 1905
Porosira glacialis (Grunow) Jørgensen 1905
- Genus *Thalassiosira* Cleve 1873 emend. Hasle 1973
Thalassiosira antarctica var. *borealis* Comber 1896
Thalassiosira eccentrica (Ehrenberg) Cleve 1904
Thalassiosira pacifica Gran & Angst 1931
Thalassiosira hyalina (Grunow) Gran 1897
Thalassiosira nordenskiöldii Cleve 1873
Thalassiosira oestrupii (Ostenfeld) Hasle 1972
Thalassiosira trifulta Fryxell in Fryxell & Hasle 1979
Thalassiosira leptopus (Grunow) Hasle & Fryxell 1977
Thalassiosira lineata Jousé 1968
Thalassiosira spp

Family Stephanodiscaceae

- Genus *Cyclotella* (Kützing) Brébisson 1838
Cyclotella spp
- Genus *Stephanodiscus* Ehrenberg 1845
Stephanodiscus spp

Family Melosiraceae

- Genus *Melosira* Agardh 1824
Melosira sol (Ehrenberg) Kützing 1849
- Genus *Paralia* Heiberg 1863
Paralia sulcata (Ehrenberg) Cleve 1873
- Genus *Stephanopyxis* (Ehrenberg) Ehrenberg 1845
Stephanopyxis turris (Greville et Walker-Arnott) Ralfs 1861

Family Coscinodiscusceae

- Genus *Coscinodiscus* Ehrenberg 1839 emend. Hasle & Sims 1986
Coscinodiscus marginatus Ehrenberg 1844
Coscinodiscus oculus-iridis (Ehrenberg) Ehrenberg 1854
Coscinodiscus radiatus Ehrenberg 1840

Family Stellarimaceae

- Genus *Stellarima* Hasle and Sims 1986
Stellarima stellaris (Roper) Hasle & Sims 1986

Family Hemidiscaceae

- Genus *Actinocyclus* Ehrenberg 1837
Actinocyclus curvatulus Janisch in A. Schmidt et al. 1874-1959
Actinocyclus ochotensis Jousé 1968
Actinocyclus octonarius Ehrenberg 1838
- Genus *Azpeitia* M.Peragallo in Tempère & Peragallo 1912
Azpeitia nodulifera (A. Schmidt) Fryxell & Sims in Fryxell et al. 1986
Azpeitia tabularis (Grunow) Fryxell & Sims in Fryxell et al. 1986
- Genus *Hemidiscus* Wallich 1860
Hemidiscus cuneiformis Wallich 1860
- Genus *Roperia* Grunow ex Pelletan 1889
Roperia tessellata (Roper) Grunow ex Pelletan 1889
- Family** Asterolampraceae
- Genus *Asteromphalus* Ehrenberg 1844
Asteromphalus brookei Bailey 1856
Asteromphalus robustus Castracane 1875
- Family** Heliopeltaceae
- Genus *Actinoptychus* Ehrenberg 1843
Actinoptychus senarius (Ehrenberg) Ehrenberg 1843
Actinoptychus vulgaris Schumann 1867
- Suborder** Rhizosoleniineae
- Family** Rhizosoleniaceae
- Genus *Rhizosolenia* Brightwell 1858
Rhizosolenia bergonii Peragallo 1982
Rhizosolenia hebetata Bailey 1856 forma *hebetata*
Rhizosolenia hebetata Bailey 1856 forma *semispina* (Hensen) Gran 1904
Rhizosolenia setigera Brightwell 1858
Rhizosolenia styliformis Brightwell 1858
Rhizosolenia spp
- Suborder** Biddulphiineae
- Family** Chaetocerotaceae
- Genus *Chaetoceros* Ehrenberg 1844
Chaetoceros spp
- Family** Eupodiscaceae
- Genus *Odontella* Agardh 1832
Odontella aurita (Lyngbye) Agardh 1832

PENNATE DIATOMS

ORDER Bacillariales

Suborder Fragilariineae

Family Thalassionemataceae

- Genus *Thalassionema* Grunow ex Mereschowsky 1902
Thalassionema nitzschioides (Grunow) Mereschowsky 1902
- Genus *Thalassiothrix* Cleve & Grunow 1880
Thalassiothrix longissima Cleve & Grunow 1880

Suborder Bacillariineae**Family** Bacillariaceae

- Genus *Alveus* Kaczmarska & Fryxell, 1996
Alveus marinus Kaczmarska & Fryxell, 1996
- Genus *Fragilariopsis* Hustedt in Schmidt emend. Hasle 1993
Fragilariopsis cylindrus (Grunow) Krieger in Helmcke & Krieger 1954
Fragilariopsis doliolus (Wallich) Medlin & Sims 1993
Fragilariopsis oceanica (Cleve) Hasle 1965
- Genus *Neodenticula* Akiba & Yanagisawa 1986
Neodenticula seminae (Simonsen and Kanaya) Akiba & Yanagisawa 1986
- Genus *Nitzschia* Hassall, 1845
Nitzschia bicapitata Cleve 1901
Nitzschia sicula (Castracane) Hustedt 1958

Table S1. Species scores of the CCA

Species or species group	Abbreviation	1 st Axis	2 nd Axis
<i>Actinocyclus curvatus</i>	Acurv	0.0275	-0.7866
<i>Actinocyclus ochotensis</i>	Aocho	-0.5287	-2.2592
<i>Actinocyclus octonarius</i>	Actocto	2.758	1.2169
<i>Alveus marinus</i>	Amari	3.2769	1.4505
<i>Asteromphalus robustus</i> + <i>A. brookei</i>	Aster	1.3969	-0.59
<i>Azpeitia nodulifera</i>	Anodu	3.2078	1.328
<i>Azpeitia tabularis</i>	Atabu	1.5505	-0.669
<i>Bacterosira bathyomphala</i>	Bbath	-0.8732	0.8244
<i>Chaetoceros</i> resting spore	Chaet	-0.4228	0.2741
<i>Coscinodiscus marginatus</i>	Cmarg	-0.0526	-2.4299
<i>Coscinodiscus oculus-iridis</i>	Cocul	-0.3979	-1.1018
<i>Coscinodiscus radiatus</i>	Cradi	1.7786	0.0133
<i>Fragilariopsis doliolus</i>	Fdoli	1.9337	0.3125
<i>Fragilariopsis oceanica</i> + <i>F. cylindrus</i>	Foccy	-0.9567	1.416
<i>Hemidiscus cuneiformis</i>	Hcune	2.9023	1.1509
<i>Neodenticula seminae</i>	Nsemi	-0.3899	-1.0794
<i>Nitzschia bicapitata</i>	Nbica	2.3651	0.9142
<i>Nitzschia sicula</i>	Nsicu	2.8564	0.9397
<i>Odontella aurita</i>	Oauri	-0.5007	0.1926
<i>Porosira glacialis</i>	Pglac	-0.8567	0.9094
<i>Rhizosolenia bergonii</i>	Rberg	3.1494	1.3402
<i>Rhizosolenia hebetata</i> f. <i>hebetata</i> + <i>R. hebetata</i> f. <i>semispina</i>	Rhehe	-0.3867	-1.3828
<i>Rhizosolenia setigera</i>	Rseti	2.8816	1.057
<i>Rhizosolenia styliformis</i>	Rstyl	0.217	-0.3363
<i>Roperia tessellata</i>	Rtess	2.6735	0.9004
<i>Stellarima stellaris</i>	Sstel	0.8812	-0.8678
<i>Stephanopyxis turris</i>	Sturr	0.8108	0.4446
<i>Thalassionema nitzschioides</i>	Tnitz	-0.0578	0.5749
<i>Thalassiosira antarctica</i> var. <i>borealis</i> resting spore	Tabsp	-0.7698	0.829
<i>Thalassiosira eccentrica</i>	Tecce	1.0311	0.0157
<i>Thalassiosira hyalina</i>	Thyal	-1.0003	1.6172
<i>Thalassiosira leptopus</i>	Tlept	2.7853	1.4667
<i>Thalassiosira lineata</i>	Tline	1.5153	0.5355
<i>Thalassiosira nordenskiöldii</i>	Tnord	-0.8891	0.9914
<i>Thalassiosira oestrupii</i>	Toest	0.518	-0.4681
<i>Thalassiosira pacifica</i>	Tpaci	0.3306	0.8899
<i>Thalassiosira trifulta</i>	Ttrif	-0.2504	-1.1296
<i>Thalassiothrix longissima</i>	Tlong	0.1853	-0.9254

Chapter 4. Diatom-based transfer function for the estimation of sea surface temperatures in the northern North Pacific: development, calibration and caveats

Jian Ren^a, Rainer Gersonde^a, Oliver Esper^a, Constance Sancetta^b

^aAlfred Wegener Institute Helmholtz Centre for Polar and Marine Research, Am Handelshafen 12, D-27570 Bremerhaven, Germany (Correspondence to J. Ren: jian.ren@awi.de)

^bMoreland Hills, OH 44022, U.S.A.

Ready to submit to Palaeogeography, Palaeoclimatology, Palaeoecology

Abstract

A new diatom-based transfer function for summer sea surface temperature (SSST) reconstructions for the northern North Pacific, the Bering Sea and the Sea of Okhotsk, has been developed from 206 surface sediment samples with 32 taxa and taxa groups. In order to avoid recent ocean warming, observed modern temperatures before 1994 were chosen as reference instead of more recent data. The SSST estimations by the Imbrie and Kipp Method (IKM), Modern Analog Technique (MAT) and Artificial Neural Network (ANN) show high correlations with the modern SSST. IKM estimates were performed by three factors and quadratic regression with root mean square errors of prediction on calibration data set (RMSEP_{cal}) of 1.29 °C. MAT reconstructions were best with five analogs resulting in the RMSEP_{cal} of 1.26 °C. ANN results were calculated by one hidden layer and twenty hidden neurons, showing the lowest RMSEP_{cal} of 0.02 °C. The transfer functions were applied to a sediment core retrieved from the northwestern North Pacific, covering the last 180 ka. The estimates show a clear glacial-interglacial pattern, which correlates well with the local planktic $\delta^{18}\text{O}$ record as well as the NGRIP $\delta^{18}\text{O}$ profile. All calculated communalities values of down-core samples are >0.65, thus no-analog was not found. In addition, the mean distance (dissimilarity index) of the majority of down-core samples are smaller than the threshold, indicating reliable results. The averaged estimates of the MAT and ANN display better performance and thus are suggested for Late Quaternary paleotemperature reconstructions in the North Pacific. The low glacial-interglacial temperature amplitudes of 1.5-2 °C are similar with previous estimates based on different proxies and methods in the study area. The robustness test also displays the reliability of the SSST reconstructions based on the calibration data set. The low glacial-interglacial SSST amplitude may imply the shift of diatom blooming season from cold late spring/early summer in modern time towards relative warm later summer during glacial period, thus changing the estimates towards warmer temperatures. The lack of cold endmembers in the reference dataset and the dissolution of sea ice diatoms may also influence the SSST reconstructions.

4.1. Introduction

One task of Late Quaternary paleoenvironmental reconstructions is the estimation of sea surface temperatures (SST) and their glacial-interglacial variability. Such data may constrain paleo-modeling and

thus help to validate the set-up and the performance of models used for future climate predictions (e.g. Jiang et al., 2005; Menviel et al., 2011). They also provide basic data on the distribution of cold and warm water masses and their variability at Quaternary time scales. Such information is crucial for the understanding of the physical parameters of the Quaternary ocean surface and related ocean circulation (e.g. MARGO Project Members, 2009). Paleotemperatures can be reconstructed by different methods, including micropaleontological (e.g. transfer functions on microfossils) and geochemical (e.g. Mg/Ca; Alkenone; TEX₈₆) approaches. Here we focus on the development of a transfer function-based temperature reconstruction. The Imbrie and Kipp Method (IKM; Imbrie and Kipp, 1971; Klován and Imbrie, 1971) and the Modern Analog Technique (MAT; Hutson, 1980), directly based on the composition and distribution of microfossil assemblages, are widely and successfully used in the world oceans (e.g. CLIMAP project members, 1976; Moore et al., 1980; Esper and Gersonde, 2014a, b). In contrast, the Artificial Neural Network (ANN) uses a group of interconnected processing units (neurons) to learn details of input dataset and to construct a network for reconstruction. Although it is nearly a black-box method, it also performs well for paleotemperature reconstructions (Guiot and de Vernal, 2007 and references therein). Chen et al. (2005) and Guiot and de Vernal (2007) suggest that MAT and ANN should be used as the standard reconstruction methods, while IKM is least successful, probably due to the fact that it uses linear technique to calibrate non-linear environmental changes (Kucera et al., 2005b). Marine diatoms are widely distributed and are phototrophic algae dwelling in the surface ocean, thus are sensitive to environmental changes in the sea surface. Therefore diatom assemblages are useful for past SST reconstructions (Zielinski and Gersonde, 1997; Esper and Gersonde, 2014b). Diatom reference data sets for paleotemperature reconstruction are broadly developed for the Southern Ocean (e.g. Zielinski and Gersonde, 1997; Esper et al., 2010) and the North Atlantic Ocean (e.g. Koç Karpuz and Schrader, 1990; Andersen et al., 2004) and successfully applied for Quaternary temperature estimation (e.g. Zielinski et al., 1998; Esper and Gersonde, 2014a, b). To date, a first diatom transfer function for the North Pacific has been developed by Sancetta (1979). However, this transfer function considers only a relatively small set of reference sites from the Sea of Okhotsk, the Bering Sea and the adjacent passage to the Arctic Ocean. Thus reference samples from cold areas required for reconstruction of colder (glacial) conditions are not well represented.

The North Pacific is a key area for comprehending glacial-interglacial climatic and oceanographic changes (e.g. Jaccard et al., 2005; Keigwin et al., 2007; Gebhardt et al., 2008; Max et al., 2012). Hence, the paleotemperature variability in the North Pacific is of vital importance. However, quantitative reconstructions based on calcareous fossils are sparse (e.g. Gebhardt et al., 2008; Cassie et al., 2010; Max et al., 2012), due to the absence of carbonate resulted from shallow carbonate compensation depths (CCD; ~3500 m, Berger and Wintereer, 1974). Therefore quantitative reconstructions based on siliceous fossils are needed for paleoceanographic studies. Radiolarian data set has been established in the North Pacific (e.g. Moore, 1973). However, some radiolarian species dwell at a wide range of depths and thus make the transfer functions for surface temperature questionable (Sancetta, 1979). Thus diatom-based

paleoceanographic reconstruction is one of the best options in the northern North Pacific.

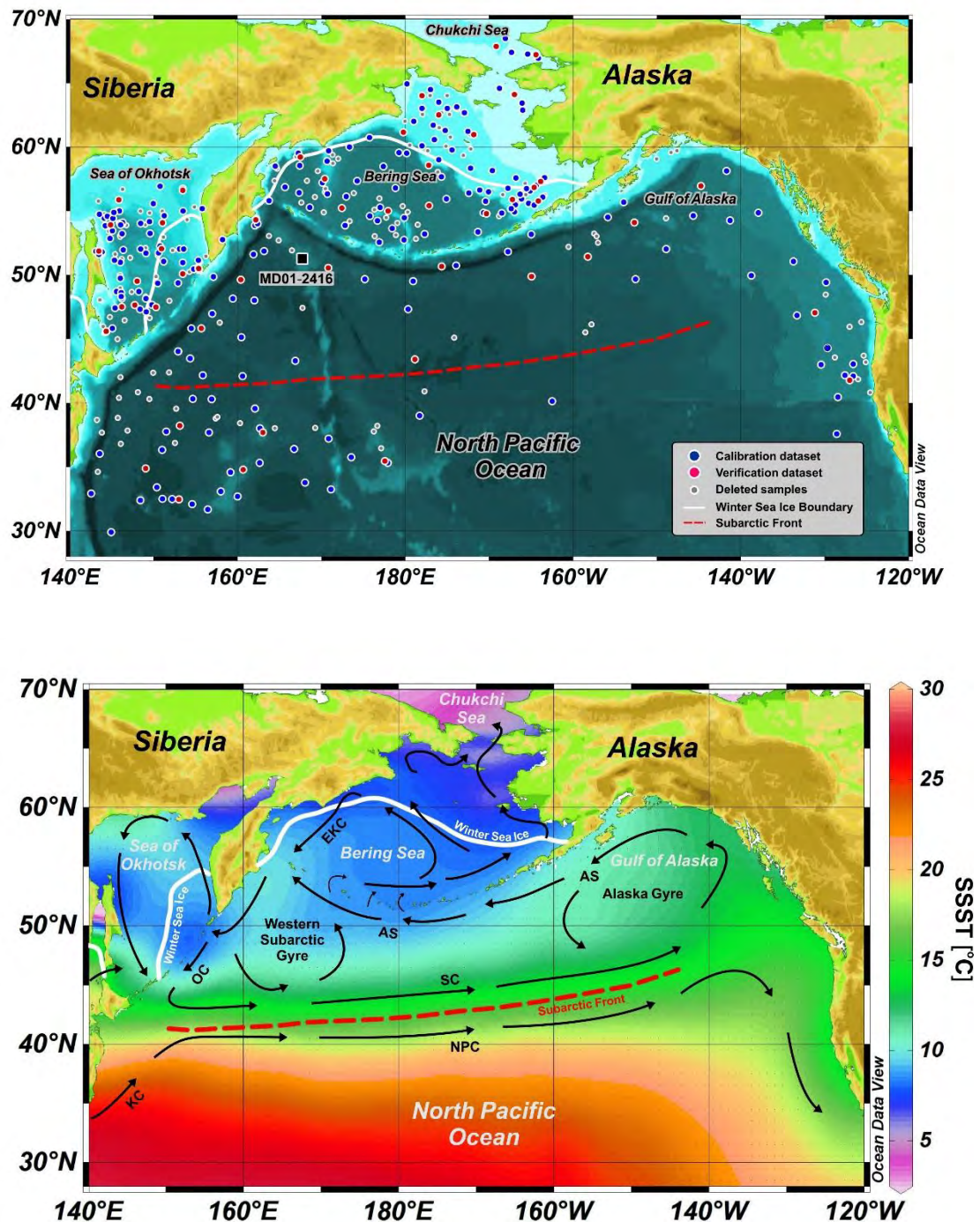


Fig. 4.1 (Top) Distribution map of 422 surface samples in the North Pacific Ocean. Blue and red circles represent the calibration data set and verification data set, respectively, while smaller gray dots were excluded from the final data set. (Bottom) Currents system in the North Pacific Ocean (black arrows). The summer sea surface temperature (July, August and September) from WOA94 is indicated as a background (Levitus and Boyer, 1994). The Winter Sea Ice boundary (Averaged 15% sea ice concentration of March of 1982-1991; Reynolds et al., 2002) and the Subarctic Front (Aydin et al., 2004) are indicated by the white lines and red dash line, respectively. AS: Alaska Stream; EKC: East Kamchatka Current; KC: Kuroshio Current; NPC: North Pacific Current; OC: Oyashio Current; SC: Subarctic Current.

Here we present a new diatom reference data set for quantitative reconstruction of glacial-interglacial variability of summer sea surface temperature (SSST) in the subarctic Pacific and the Bering Sea, from 30°N to 70°N, covering the subtropical, the subarctic and the arctic oceans (Fig. 4.1). The new data set is applied to a down-core record retrieved from Detroit Seamount, northwestern Pacific, with the IKM, MAT and ANN, three methodologically different techniques, to validate the reliability of each transfer function technique. This provides a new baseline for paleoceanographic reconstruction of the Quaternary Arctic North Pacific.

4.2. Sediment material and its relation to modern oceanography

4.2.1. Sediment material

The initial diatom reference data set is based on a total of 422 surface sediment samples recovered in the North Pacific and its marginal seas (Fig. 4.1; *Chapter 3*). Among them, 263 samples (named as SanSamp hereafter) were from a former study by Sancetta and Silvestri (1986), all representing core tops. The other 159 surface sediment samples, most of which were retrieved from multicorer, studied at the Alfred-Wegener-Institute (named as AWISamp hereafter), were collected during cruises KOMEX (Dullo et al., 2004), KALMAR (Dullo et al., 2009), INOPEX (Gersonde, 2012) and several Canadian expeditions. The information of sample locations and their corresponding environment variables is listed in Appendix A1 of *Chapter 3*.

All the samples are the topmost sediments of multicore, piston core and trigger core, thus we assume they represent the modern environment, although no direct dating is available.

In order to test the transfer functions, the upper section (12 m) of a giant piston core, MD01-2416, retrieved from Detroit Seamount (51°16.08'N, 167°43.50'E, 2317 m water depth), northwestern North Pacific was chosen (Fig. 4.1). The upper 12 m of the core document the last 180 ka ($k_a=10^3$ yr), spanning the late part of Marine Isotope Stage (MIS) 6 to the middle Holocene (Sarthein et al., 2007; Gebhardt et al., 2008; see 3.5). Sub-samples for diatom analysis were collected as 1-cm slices at 5 cm and 10 cm intervals throughout the core.

4.2.2. Oceanography settings

The surface circulation of the North Pacific consists of the Subarctic Gyre (Dodimead et al., 1963) and the Subtropical Gyre (Qiu, 2002; Fig. 4.1). It is divided by the Subarctic Front, which is characterized by steep gradients of temperature and salinity (Aydin et al., 2004). The Kuroshio Current (KC) brings warm and salty water masses from the tropical Pacific to the Alaska Gyre (AG), a subgyre of the Subarctic Gyre, via the North Pacific Current (NPC; White et al., 1982; Qiu, 2002; Fig. 4.1). The Alaska Stream (AS) from the Alaska Gyre transports the water masses into the Bering Sea via the Aleutian Islands (Stabeno et al., 1999; Takahashi, 2005), forming a cyclonic gyre in the Bering Sea (Ohtani et al., 1972; Fig. 4.1). Here,

a part of the water masses flows unidirectionally through the Bering Strait to the Chukchi Sea of the Arctic Ocean, while another part originates as the East Kamchatka Current (EKC) along the Siberian coast and runs back to the North Pacific (Coachman, 1993; Takahashi, 2005). The East Kamchatka Current partly enters the Sea of Okhotsk and generates another cyclonic gyre. The Oyashio Current (OC) is formed when the East Kamchatka Current meets with water masses from the Sea of Okhotsk. Off Hokkaido, the Oyashio Current becomes the eastward-flowing Subarctic Current (SC), running along the Subarctic Front (Favorite et al., 1976; Fig. 4.1).

Approximately one-third of the Bering Sea and three-fourths of the Sea of Okhotsk are covered by winter sea ice from November to July, with a March-April maximum extent (Niebauer, 1980; 1983; Parkinson and Gratz, 1983; Parkinson et al., 1987; Fig. 4.1).

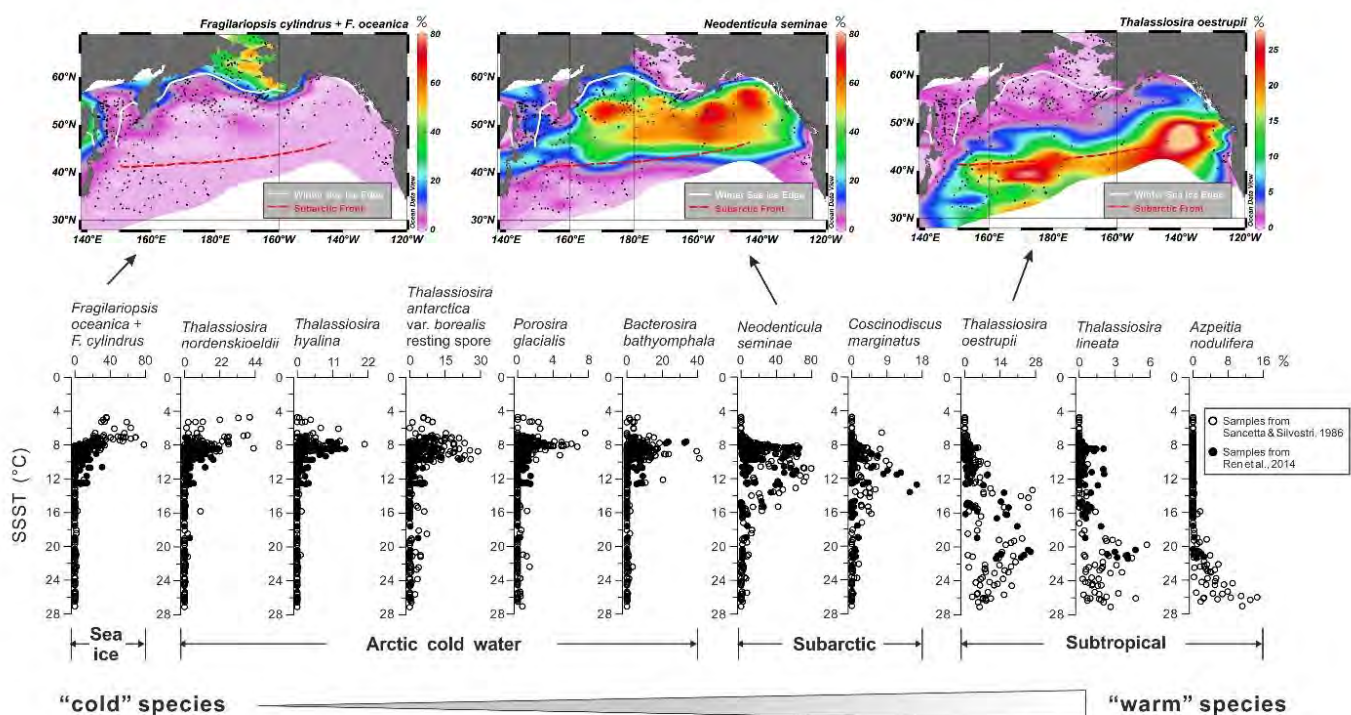


Fig. 4.2 Relative abundance of selected diatom species and species groups in relation to the summer sea surface temperature (SSST). The distribution patterns show specific temperature preference for each species. The distribution map of *Fragilariopsis cylindrus* and *F. oceanica*, *Neodenticula seminae* and *Thalassiosira oestrupii* are displayed on the top panel. The winter sea ice edge (March of 1982–1991; Reynolds et al., 2002) and the Subarctic Front (Aydin et al., 2004) are indicated by the solid white and dashed red lines, respectively.

4.2.3. Relationship between diatom distribution and modern oceanography

The relationship between diatom composition from surface sediment samples and North Pacific modern oceanography is discussed in **Chapter 3**. Except cosmopolitan species, most diatom show clear distribution patterns which are constrained by SSST (Fig. 4.2). A Q-mode factor analysis was applied to the total 422 sample data set, including 38 species and species groups (D422/38), by **Chapter 3**. It yields three factors representing diatom assemblages (factors) associated with the Arctic, Subarctic and Subtropical water masses, respectively, indicating a close relationship between diatom composition and

sea surface temperatures (**Chapter 3**). Furthermore, Canonical Correspondence Analysis (CCA) also indicates 32 diatom species and species groups have strong correspondence with the SSST pattern (**Chapter 3**). On the other hand, sea-ice-related species, like *Fragilariopsis cylindrus* and *F. oceanica* (Horner and Alexander, 1972; Poulin, 1990), have a distribution pattern limited to the winter sea ice edge and the related water mass.

4.3. Methods

4.3.1. Sample dealing

The SanSamp treatment, diatom slide preparation and counting methods are presented in Sancetta (1981), Sancetta and Silvestri (1986). For AWISamp and downcore samples, diatom slides were quantitatively made following the standard procedure established at the Alfred-Wegener-Institute (Gersonde and Zielinski, 2000). Diatom counts were according to the description by Schrader and Gersonde (1978). An average of 400 diatom valves was counted for each sample with a Zeiss Axioskop microscope at $\times 1000$ magnification.

The preservation state of the diatom samples can provide additional information on the selective dissolution of diatoms which may bias the reference data set. Five categories of preservation were established based on the description by Zielinski (1993). The categories are:

Good (1): assemblage consists both of heavily and weakly silicified diatom species with no dissolution of the areolae or the valve margin or fragmentation; Moderate (3): both heavily and weakly silicified species are present but the latter show marked dissolution of the areolae or the valve margin or fragmentation; Poor (5): assemblage dominated by heavily silicified species with dissolution of the areolae or the valve margin and many fragmented valves. Categories (2) and (4) represent intermediate conditions.

Diatom preservation was only examined in AWISamp, while SanSamp has no clear dissolution information. The samples in categories 4 and 5 were defined as highly affected by dissolution and were deleted from the reference data set. In order to reduce the dissolution bias of SanSamp, we assumed that any samples within 100 km distance from stations highly affected by dissolution in AWISamp were also poorly preserved and hence were deleted.

4.3.2. Data preparation and processing

Diatoms were identified to species or species group level. Taxonomies are discussed in detail in **Chapter 3**. Two surface sample sets were merged and 49 common taxa were selected. Some taxa were combined as groups (see **Chapter 3**) resulting in 38 species and species groups for this study.

A logarithm-based transformation on percentage abundance, as suggested by Zielinski et al. (1998), was applied in order to down-weight the most abundant species, such as *Neodenticula seminae*, which accounts for 80% of the total assemblage of some samples. The following equation is used:

$$L = \text{LOG}_{10}(\text{relative abundance} \times 10 + 1)$$

4.3.3. Environmental data

The sea surface temperature data (at 10m water depth) were retrieved from World Ocean Atlas 1994 (WOA94; Levitus and Boyer, 1994), whose measurements were performed mainly in the 1970's before the onset of warming in the Bering Sea (Levitus and Boyer, 1994). In general, SSST was chosen as a target for paleoenvironmental reconstruction due to the fact that diatom export in the northern North Pacific and its marginal seas usually occurs in summer (July, August and September; see **Chapter 3**). The modern SSST in the study area ranges from 4.7 °C in the Chukchi Sea to 27 °C in the western North Pacific off Japan. The modern SSST of the core location is ca. 9.1 °C .

4.3.4. Methods of quantitative SSST reconstruction

In this study, three methods are applied to the paleo-SSST estimation: IKM (Imbrie and Kipp, 1971), MAT (Hutson, 1980) and ANN (Malmgren et al., 2001). These methods represent three different approaches to relate a specific diatom assemblage to an SSST.

1) The Imbrie and Kipp Method (IKM) developed by Imbrie and Kipp (Imbrie and Kipp, 1971; Klován and Imbrie, 1971) is widely used in the world oceans (e.g. CLIMAP, 1976; 1984; Koç Karpuz and Schrader, 1990), especially in the Southern Ocean (e.g. Zielinski et al., 1998; Abelmann et al., 1999; Esper and Gersonde, 2014a). In principle, the IKM is to reduce the dimensionality of the dataset, which is similar to the Weighted Average (WA) and Weighted Average Partial Least Square (WAPLS) (Guiot and de Vernal, 2007; Birks, 2010). Therefore we chose IKM as a representative of this group of methods. IKM allows a good understanding of the calibration process. It uses Q-mode factor analysis (CABFAC) to separate the informative signals from statistical noise by reducing the dimension of the reference data set to several factors. A multiple regression (REGRESS) then results in a paleoenvironment-equation based on the relation between the factors and the modern environmental variables. In the third step (THREAD), the sediment core samples are separated into the factors of the reference data set by CABFAC and the target paleoenvironmental variable is calculated by the paleoenvironment-equation. A communality factor is calculated by IKM to determine the fit between the reference data set and the sediment core data, in order to rule out the no-analog cases between modern diatom assemblages and the down core assemblages (Esper and Gersonde, 2014a). In IKM, it is assumed that the species linearly respond to an environmental parameter, which is not frequently observed in nature. Although the calibration process may potentially bias the estimated SSST, IKM uses a novel data pre-treatment that improves its competence to deal with unimodal relationships (Kucera et al., 2005b).

IKM is applied by using the software package PaleoToolBox developed by Sieger et al. (1999) (<http://www.pangaea.de/Software/PaleoToolBox>). In this study, three factors and quadratic regression are selected for SSST reconstruction.

2) Another method is the Modern Analog Technique (MAT; Hutson, 1980), which is based on the degree of similarity between the fossil assemblage from the sediment cores and the modern assemblage

from the surface sediment samples. The assumption is that similar diatom assemblages should form in a similar environment and thus a specific environmental parameter of the fossil assemblage could be estimated via their modern analogs. Therefore, a large number of surface sediment samples covering wide ranges of environmental conditions is required. The best analogs are selected from the reference data set by using the Squared Chord Distance, which has been verified to be most effective (e.g. Prell, 1985; Overpeck et al., 1985). The observed values of the target environmental variables (e.g. SSST) are then averaged as the estimated values of the corresponding down-core samples. Prell (1985) has summed up the pros and cons of MAT. The advantages of MAT are a) species percentage data are used without special data processing, maintaining the original data set, b) estimates of environmental variables are directly averages of the observed values of the best analogs, keeping the calculation simple and fast, c) every step of calculation is transparent, d) increase or decrease of the reference data set is easily handled as no paleoenvironment-equation is used in MAT, and e) no-linear relationship between species and environmental variables is suitable for MAT. The disadvantages are a) dependency on the large and geographically and ecologically balanced data set for enough best analogs for reconstruction, and b) determination of the best analogs is arbitrary due to the lack of a statistical threshold.

Furthermore, Telford and Birks (2005) argue that MAT is significantly influenced by autocorrelation, the tendency of neighboring sites to resemble each other rather than randomly selected sites, which might overestimate the estimates and deteriorate the quality of the paleoenvironmental reconstruction. In order to reduce the bias from autocorrelation, a canonical correspondence analysis (CCA) is utilized to detect the relationship between diatom assemblages and environmental variables (Telford, 2006).

A set of 10 analogs are applied. The number of the best analogs used in the transfer function is determined by the lowest result of leave-one-out cross validation (LOO; Simpson and Oksanen, 2011). The free software R (<http://www.r-project.org>) is used to perform MAT with the Analogue package (Simpson, 2007; Simpson and Oksanen, 2011).

3) The artificial neural network (ANN) is introduced to reconstruct paleo-SSST by Malmgren et al. (2001). The ANN usually uses a back propagation (BP) neural network, which assumes that there is a relationship between the distributions of modern assemblages and the physical and chemical properties of the environment (Malmgren and Nordlund, 1997; Crosta and Koç, 2007). The ANN autonomously identifies the relationship by a set of processing units (neurons) in different hidden layers, which interconnect input variables (i.e. diatom counts) with one or more output variables (environmental parameter(s)) via the neural network (Malmgren and Nordlund, 1997; Kucera et al., 2005b). The neural network is established by learning processes of each neuron, which minimize prediction error for each sample in the reference data set (Kucera et al., 2005b). ANN allows extrapolation of the modern data set even if it is in small size. However, unlike MAT and IKM, the calibration process of ANN (learning) is nearly a black box, making it hard to understand the resulting network. In addition, the complexity of the learning process causes the process significantly time-consuming.

Resilient back propagation were used for ANN reconstruction, which is a revised BP network which has been proved to be fastest compared with others (Günther and Fritsch, 2010). Twenty hidden neurons in one hidden layer were set to construct the neural network. The free software R (<http://www.r-project.org>) was employed to run ANN with the Neuralnet package (Günther and Fritsch, 2010).

In this study we compare the performance of the three methods from their application to the same data set. In order to verify the calibration results, we randomly split the reference data set into two pairs of calibration (5/6) and verification (1/6) subsets (J. Guiot, personal communication).

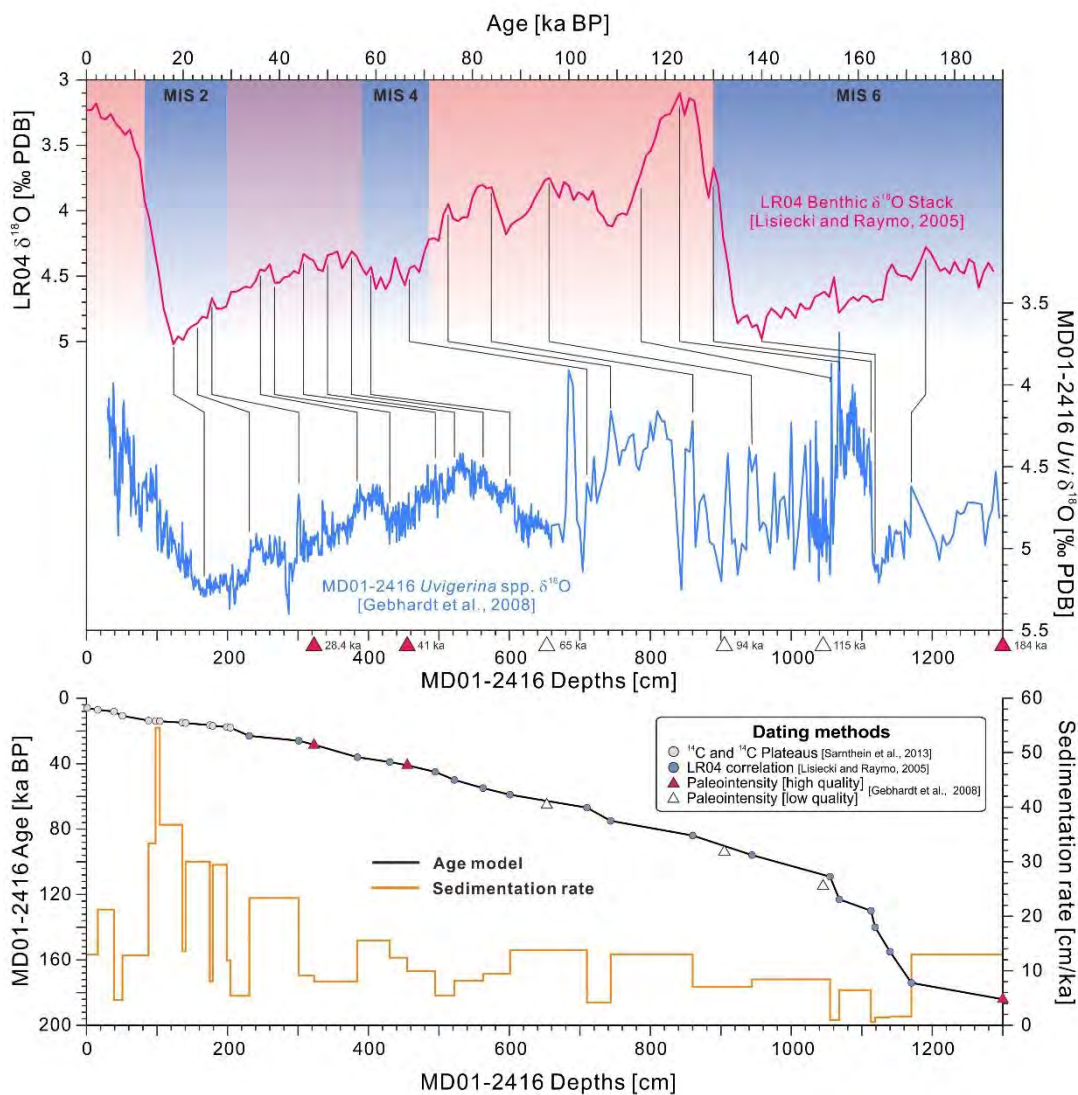


Fig. 4.3 (Top) Graphic correlations between benthic $\delta^{18}\text{O}$ of MD01-2416 (*Uvigerina* spp.; Gebhardt et al., 2008) and LR04 global benthic $\delta^{18}\text{O}$ stack (Lisiecki and Raymo, 2005). Shaded bars indicate the Marine Isotope Stages according to Lisiecki and Raymo (2005). The red and white triangles represent the paleointensity events with high and low quality, respectively (Gebhardt et al., 2008). (Bottom) Age model of MD01-2416. The gray circles are ^{14}C dating points and ^{14}C plateau boundaries listed in Table 1, while the red triangles display the paleointensity control points with high quality. The graphic correlations of benthic $\delta^{18}\text{O}$ for dating are shown in blue circles. The paleointensity datings with low quality are plotted in white triangles as well to show the small difference of different dating methods. The sedimentation rates are displayed in the bottom panel.

Table 4.1 Age control points for MD01-2416.

Depths (cm)	Calendar ages (ka BP)	Sedimentation rates (cm/ka)	Dating methods	References
0.75	5.900		¹⁴ C calibration ^a	Sarnthein et al., 2004; Maier et al., 2015
16	7.077	12.957	¹⁴ C calibration ^a	Sarnthein et al., 2004; Maier et al., 2015
39	8.161	21.218	¹⁴ C calibration ^a	Sarnthein et al., 2004; Maier et al., 2015
51	10.754	4.628	¹⁴ C calibration ^a	Sarnthein et al., 2004; Maier et al., 2015
88	13.640	12.821	Suigetsu varve ^b	Sarnthein et al., 2007; 2013
98	13.940	33.333	Suigetsu varve ^b	Sarnthein et al., 2013
104	14.050	54.545	Suigetsu varve ^b	Sarnthein et al., 2007; 2013
136	14.920	36.782	Suigetsu varve ^b	Sarnthein et al., 2007; 2013
140.50	15.250	13.636	Suigetsu varve ^b	Sarnthein et al., 2007; 2013
175	16.400	30.000	Suigetsu varve ^b	Sarnthein et al., 2013
179	16.900	8.000	Suigetsu varve ^b	Sarnthein et al., 2007; 2013
199	17.580	29.412	Suigetsu varve ^b	Sarnthein et al., 2007; 2013
204	18.000	11.905	Suigetsu varve ^b	Sarnthein et al., 2013
230.93	22.992	5.395	LR04 ^c	this study
301.18	26.002	23.337	LR04 ^c	this study
323	28.400	9.099	Paleointensity ^d	Gebhardt et al., 2008
384.28	36.047	8.014	LR04 ^c	this study
430.16	38.998	15.550	LR04 ^c	this study
455	41	12.406	Paleointensity ^d	Gebhardt et al., 2008
494.72	44.993	9.946	LR04 ^c	this study
522	49.970	5.482	LR04 ^c	this study
562.71	54.938	8.195	LR04 ^c	this study
600.78	58.981	9.415	LR04 ^c	this study
710.03	66.925	13.754	LR04 ^c	this study
743.71	74.983	4.178	LR04 ^c	this study
859.96	83.913	13.019	LR04 ^c	this study
944.05	95.881	7.026	LR04 ^c	this study
1054.96	109.067	8.412	LR04 ^c	this study
1068.09	122.989	0.944	LR04 ^c	this study
1113.01	129.940	6.462	LR04 ^c	this study
1118.86	140.017	0.581	LR04 ^c	this study
1140.07	155.009	1.415	LR04 ^c	this study
1170.43	173.997	1.599	LR04 ^c	this study
1300	184	12.952	Paleointensity ^d	Gebhardt et al., 2008

^a ¹⁴C ages of samples were corrected for 570 ± 140 ya reservoir age, which was determined by Sarnthein et al. (2013) according to the nearest ¹⁴C plateau, and converted into calendar ages by CALIB 7.0 (Stuiver and Reimer, 1993) with the Marine13 calibration curve (Reimer et al., 2013).

^b ¹⁴C plateaus were correlated to atmospheric ¹⁴C plateaus from Lake Suigetsu (Bronk Ramsey et al., 2012) to determine the plateau boundaries.

^c Graphic correlation were applied between benthic $\delta^{18}\text{O}$ records (*Uvigerina* spp.) of MD01-2416 (Gebhardt et al., 2008) and LR04 global stack (Lisiecki and Raymo, 2005).

^d Only high quality of magnetic signals were chosen as age control points (see Gebhardt et al., 2008).

4.3.5. Core chronology

The age model of MD01-2416 has been developed by Sarnthein et al. (2005, 2007), Gebhardt et al. (2008) and Sarnthein et al. (2013) by using the ^{14}C plateau boundaries and the joint geomagnetic and $\delta^{18}\text{O}$ records, and by Galbraith et al. (2008), which is derived from minimum tuning to glacial terminations I to V. These two age models, however, are different from each other on several Marine Isotope Stages (MIS; Gebhardt et al., 2008). In addition, the former age model is based on low resolution planktonic $\delta^{18}\text{O}$ records (Imbrie et al., 1992; Bassinot et al., 1994) and the latter one is correlated with EPICA Dome C record in the Southern Hemisphere (EDC; EPICA Community Members, 2004), both of which may bias the accuracy of the age model.

In order to avoid the contradictions of different age models, we established a new age model for MD01-2416 by 1) AMS ^{14}C dating (Sarnthein et al., 2004) and ^{14}C plateau boundaries developed by Sarnthein et al. (2007; 2013), by correlating marine ^{14}C plateaus to atmospheric ^{14}C plateaus from Lake Suetsu (Bronk Ramsey et al., 2012), for the last 18 ka BP (see Maier et al., 2015), by 2) graphic correlation between benthic $\delta^{18}\text{O}$ records of MD01-2416 and LR04 global stack (Lisiecki and Raymo, 2005), and 3) by independently dated geomagnetic paleointensity and inclination events (Gebhardt et al., 2008) for the last 180 ka BP (Table 4.1; Fig. 4.3). For the AMS ^{14}C dating, a reservoir age of 570 ± 140 year was applied to CALIB 7.0 (Stuiver and Reimer, 1993) with the Marine13 calibration curve (Reimer et al., 2013). The paleomagnetic intensity minima events with high quality, as defined by Gebhardt et al. (2008), were chosen as extra dating points, including the Mono Lake (28.4 ka BP), Laschamp (41 ka BP) and Icelandic Basin (184 ka BP). Linear interpolation has been applied between the dating points.

The high sedimentation rates in the upper part of the core (e.g. 55 cm/ka; Fig. 4.3) may result from the sample stretching during the coring. Széreméta et al. (2004) estimate an oversampling or stretching range from 30% to 37% in the upper core using the same giant piston corer on the R/V *Marion Dufresne*. For ages > 30 ka BP, the sedimentation rates are generally lower than 20 cm/ka (Fig. 4.3).

4.4. Results

4.4.1. Development of a diatom reference data set for paleotemperature reconstructions

In general, the total 422 sample data set, including 38 species and species groups (D422/38) shows a good relationship between diatom assemblage composition and sea surface temperatures (cf. **Chapter 3**). However, the unmodified data set contains assemblages biased by strong dissolution and hence could exhibit a poor relationship to the SSST in certain regions (Zielinski et al., 1998). Species independent of SSST such as taxa indicating the neritic and upwelling environment (e.g. *Chaetoceros* spp. group and resting spores; Sancetta, 1982) and cosmopolitan taxa (e.g. *Thalassionema nitzschioides* group; Sancetta, 1982) also have an impact on paleotemperature reconstruction. In order to reduce the error introduced by biased information and to develop diatom reference data set for D422/38 we excluded the following

samples and taxa from the D422/38 data set:

A total of 21 samples with diatom assemblages affected by significant dissolution (preservation category 4 and 5) were excluded. They are distributed in the middle of the North Pacific and also appear in the Northwestern and -eastern Pacific (Fig. 4.1). Another 35 samples with outliers of certain species, *Fragilariopsis cylindrus*, *F. oceanica*, *F. doliolus*, *Nitzschia bicapitata*, *Porosira glacialis*, *Rhizosolenia bergonii*, *Thalassiosira antarctica* var. *borealis* resting spore, *T. lineata* and *T. oestrupii*, were deleted. Most of these samples were located off Japan, in the western North Pacific and off western North America in the eastern North Pacific, while a few were found in the Sea of Okhotsk and in the middle of the North Pacific (Fig. 4.1). The reduced data set became D366/38.

Samples in the D366/38 data set are over represented by the Sea of Okhotsk and the Bering Sea with SSST lower than 10 °C (Fig. 4.1), which could result in less reliable or less accurate calibration by enlarging the cold and sea ice signal and downweighing the information in the remaining part of the data set (Kucera et al., 2005b). Therefore, some of the samples from the Sea of Okhotsk (53 among 125 samples) and the Bering Sea (58 among 151 samples) were geographically evenly deleted according to the suggestion by Kucera et al. (2005b) that should the diatom reference data set be balanced in ecological and geographical coverage.

Chaetoceros spp. resting spores and *T. nitzschioides* (here this species refers only to *Thalassionema nitzschioides* var. *nitzschioides*) are abundant and their distributions have little relationship with the SSST (**Chapter 3**); they were therefore excluded from the reference data set. Transfer functions based on diatoms without *Chaetoceros* spp. resting spores were also proposed by Schrader and Koç Karpuz (1990) for the Norwegian-Iceland Sea and Zielinski et al. (1998) and Esper and Gersonde (2014a, b) for the Southern Ocean, respectively, since the taxonomy and the distribution of *Chaetoceros* spp. resting spores are poorly studied. Although there is no theoretical reason for excluding rare species (Kucera et al., 2005b), four species (*Asteromphalus* group, *Stellarima stellaris*, *Stephanopyxis turris*, *Thalassiosira pacifica*) were deleted from the data set in order to reduce the possible bias due to their low signal to noise ratio.

After the exclusion of 111 samples and 6 taxa and taxa groups, a diatom reference data set was established with 255 samples and 32 taxa and taxa groups (D255/32). According to the 5/6 and 1/6 ratio mentioned above, they were further separated into D_{cal}206/32 for calibration (training) and D_{veri}49/32 for verification (testing) for the establishment of diatom transfer functions (Fig. 4.1).

4.4.2. Establishment of the transfer function

To establish a transfer function with a least error, several criteria were applied to determine the performance of the transfer functions for each method. The Root Mean Square Error of Prediction (RMSEP_{cal} and RMSEP_{veri}) are the standard deviation of the difference between observed and estimated values, based on the calibration and verification data sets, respectively. Similarly, R^2_{cal} and R^2_{veri} correspond to the coefficient of determinations between observations and estimates on the calibration and verification

data sets. High R^2 and low RMSEPs indicate a good performance of a transfer function.

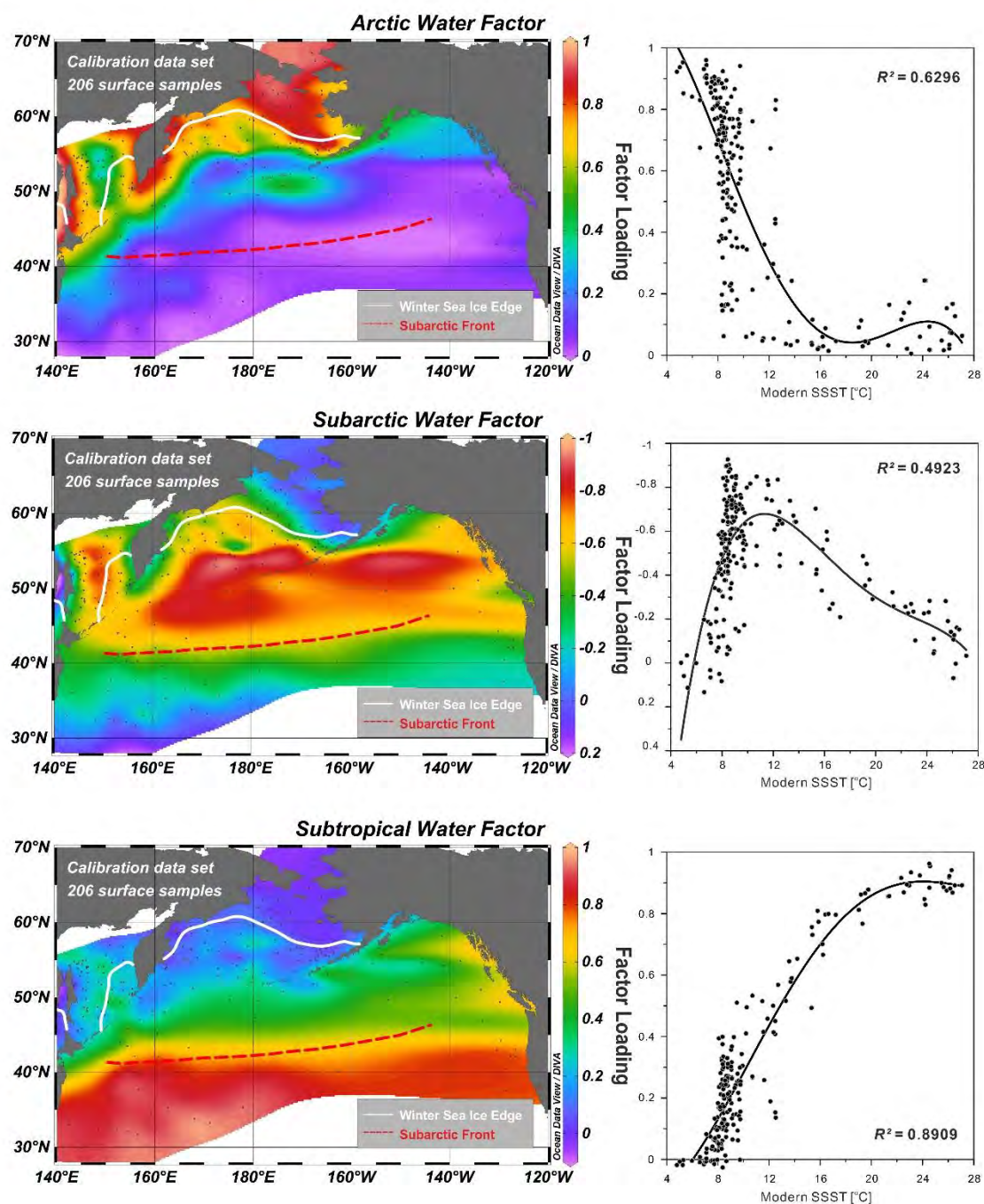


Fig. 4.4 Geographical distribution of the factor loadings of the Q-mode factor analysis on the reference data set of 206 samples. Three factors are displayed: Arctic Water Factor, Subarctic Water Factor and Subtropical Water Factor. Black dots in the maps indicate sample locations. The correlations between the modern SSST and the factor loadings are shown on the right panel. .

4.4.2.1. IKM

Q-mode analysis based on calibration data set of 206 surface samples detected 3 factors, which explain 83.6% of the total variance in diatom assemblages. This results is consistent with the results derived from 422 surface samples (*Chapter 3*).

Factor 1 (Arctic Factor), accounting for 35.97% of the total variance, covers the Bering Shelf and the

Table 4.2 Results of Q-mode analysis on calibration data set of 206 surface samples. Diatom species/species groups with high loading values are bold and underlined, while species with high scores in more than one factors are bold and italic.

Diatom species/groups	Arctic Factor	Subarctic Factor	Subtropical Factor
<i>Actinocyclus curvatulus</i>	-0.002	<u>-0.334</u>	<u>0.215</u>
<i>Actinocyclus ochotensis</i>	-0.02	<u>-0.135</u>	-0.014
<i>Actinocyclus octonarius</i>	0.017	0.092	<u>0.235</u>
<i>Alveus marinus</i>	0.011	0.091	<u>0.214</u>
<i>Azpeitia nodulifera</i>	0.012	0.089	<u>0.217</u>
<i>Azpeitia tabularis</i>	-0.016	0.032	<u>0.303</u>
<i>Bacterosira bathyomphala</i>	<u>0.357</u>	-0.059	-0.024
<i>Coscinodiscus marginatus</i>	-0.043	<u>-0.228</u>	0.024
<i>Coscinodiscus oculus-iridis</i>	0.018	<u>-0.134</u>	0.007
<i>Coscinodiscus radiatus</i>	-0.02	0.046	<u>0.347</u>
<i>Fragilariopsis doliolus</i>	-0.029	0.051	<u>0.346</u>
<i>Fragilariopsis oceanica</i> + <i>F. cylindrus</i>	<u>0.573</u>	0.11	0.005
<i>Hemidiscus cuneiformis</i>	0.006	0.071	<u>0.185</u>
<i>Neodenticula seminae</i>	0.082	<u>-0.58</u>	0.014
<i>Nitzschia bicapitata</i>	0.01	0.062	<u>0.163</u>
<i>Nitzschia sicula</i>	0.004	0.029	0.069
<i>Odontella aurita</i>	0.207	-0.059	-0.004
<i>Porosira glacialis</i>	<u>0.211</u>	0.005	-0.014
<i>Rhizosolenia bergonii</i>	0.006	0.053	<u>0.133</u>
<i>Rhizosolenia hebetata</i> f. <i>hebetata</i> + <i>R. hebetata</i> f. <i>semispina</i>	0.048	<u>-0.314</u>	-0.001
<i>Rhizosolenia setigera</i>	0.011	0.055	0.126
<i>Rhizosolenia styliformis</i>	0.015	-0.029	0.059
<i>Roperia tessellata</i>	-0.001	0.054	<u>0.176</u>
<i>Thalassiosira antarctica</i> var. <i>borealis</i> resting spore	<u>0.361</u>	-0.041	-0.005
<i>Thalassiosira eccentrica</i>	0.033	0.04	<u>0.336</u>
<i>Thalassiosira hyalina</i>	<u>0.353</u>	0.112	0.025
<i>Thalassiosira leptopus</i>	0.007	0.033	0.083
<i>Thalassiosira lineata</i>	0.023	0.057	<u>0.232</u>
<i>Thalassiosira nordenskiöldii</i>	<u>0.431</u>	0.002	-0.028
<i>Thalassiosira oestrupii</i>	0.018	-0.123	<u>0.353</u>
<i>Thalassiosira trifulta</i>	0.021	<u>-0.462</u>	0.032
<i>Thalassiothrix longissima</i>	-0.01	<u>-0.221</u>	<u>0.196</u>

marginal Sea of Okhotsk, where winter sea ice exists. The factor loadings and observed SSTs are highly correlated ($R^2=0.63$; Fig. 4.4). The diatom assemblage is characterized by sea ice related species (*Fragilariopsis cylindrus*, *F. oceanica*) and cold water species (*Bacterosira bathyomphala*, *Porosira glacialis*, *Thalassiosira antarctica* var. *borealis* resting spore, *T. hyaline*, *T. nordenskiöldii*). Factor 2 (Subarctic Factor) accounts for 29.27% of the total information explained. It is restricted between the

winter sea ice edge and the Subarctic Front (Fig. 4.4). The diatom assemblage is dominated by subarctic species: *Actinocyclus ochotensis*, *Coscinodiscus marginatus*, *C. oculus-iridis*, *Neodenticula seminae*, *Rhizosolenia hebetata* group and *T. trifulta* (Table 4.2). Factor 3 (Subtropical Factor) explains 18.32% of the total variance. It is mainly located in the area south of the Subarctic Front with an extension reaching the north of the Gulf of Alaska along the coast of North America (Fig. 4.4). The factor loadings highly correlate with SSSTs ($R^2=0.89$). The assemblage mainly consists of warm-water diatoms: *Alveus marinus*, *Azpeitia nodulifera*, *A. tabulata*, *C. radiatus*, *F. doliolus*, *T. eccentrica*, *T. lineata*, *T. oestrupii*. In addition, *Actinocyclus octonarius*, *H. cuneiformis*, *N. bicapitata*, *R. bergonii* and *R. tessellata* have minor contribution (Table 4.2).

The estimate of IKM displays a R^2_{cal} of 0.94, a $\text{RMSEP}_{\text{cal}}$ of 1.29 °C and a standard error of estimate (SEE) of 1.29 °C on the calibration data set, while it performs better on the verification set with a R^2_{veri} of 0.96, a $\text{RMSEP}_{\text{veri}}$ of 1.12 °C and an SEE of 1.12 °C (Table 4.3). However, the warm and cold endmembers are not well reconstructed (Fig. 4.5).

4.4.2.2. MAT

High accuracy of the prediction by MAT is achieved with certain numbers of best analogs. In order to find the optimal number of analogs suitable for our study, root mean square error of prediction (RMSEP) of leave-one-out cross validation (LOO), R^2 and maximum bias (ter Braak and Juggins, 1993) were calculated to indicate the quality of each analog. For the first 10 analogs, both 4 and 5 analogs show high values of R^2 and low RMSEP of LOO and maximum bias (Fig. 4.6). Here we selected 5 closest analogs to estimate the SSSTs. The MAT reconstruction shows a slightly better correlation between the estimated and observed SSSTs, with a R^2_{cal} of 0.95 and a $\text{RMSEP}_{\text{cal}}$ of 1.26 °C on the calibration set and a R^2_{veri} of 0.96 and a $\text{RMSEP}_{\text{veri}}$ of 1.00 °C on the verification set (Table 4.3, Fig. 4.5). The MAT estimate has a low accurate prediction on warm samples (22 to 26°C) and better results on cold stations (4.7 to 10°C; Fig. 4.5).

4.4.2.3. ANN

The number and types of the neurons included in the network of ANN has to be selected carefully and separately for each data set (Kucera et al., 2005b). However the selection is also empirical. Kucera et al. (2005b) apply one or two hidden layers and about 16 hidden neurons to the South Atlantic foraminifera data set (n=321 samples) for the ANN-based reconstructions. Since the time consumption for ANN learning is proportional to the number of hidden layers and neurons, here we chose one hidden layer with 20 logarithmic neurons according to Kucera et al. (2005b) in order to run the reconstruction efficiently. The configuration of the network also includes 33 input neurons (32 for diatom species data and 1 for modern SSST data) and 1 linear output neuron for the SSST prediction. The learning threshold was set to stop learning when the prediction error is lower than 0.01. We ran ANN on the calibration and verification data sets for 10 times with 10 replications for each time. All ANN reconstructions were calculated as 10 averages of the replications of lowest $\text{RMSEP}_{\text{cal}}$ in each run in order to reduce the bias from greatly varying

network configurations (Kucera et al., 2005b). Among three methods, ANN displays the best correlation ($R^2_{\text{cal}}=0.99$) and lowest $\text{RMSEP}_{\text{cal}}$ (0.02°C) on the calibration set, although it could be a result of

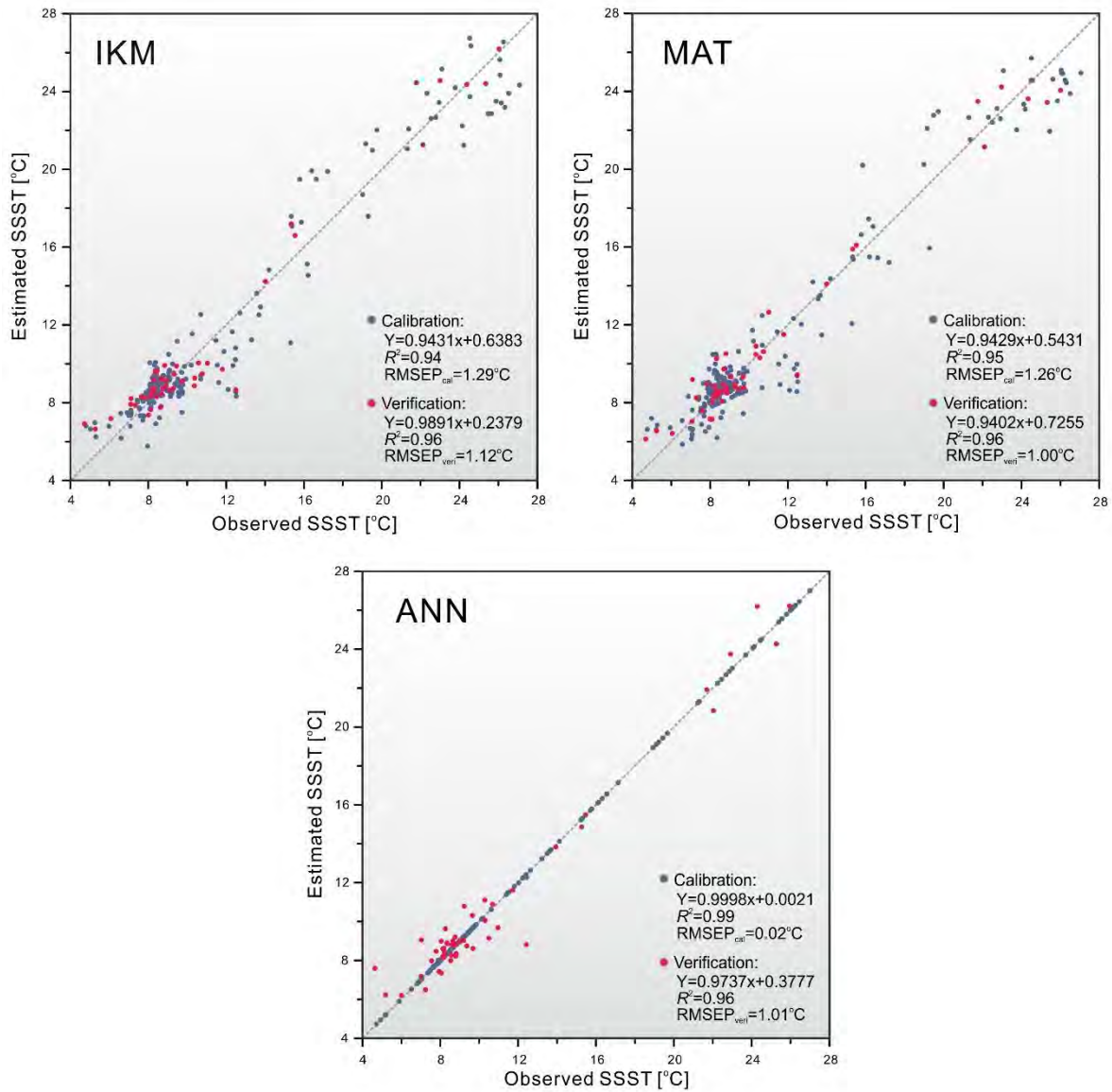


Fig. 4.5 Regression plots for the three transfer function methods for SSST reconstructions. Blue and red dots represent the calibration and verification data set, respectively. RMSEP: root mean square error of prediction. $\text{RMSEP}_{\text{cal}}$ and $\text{RMSEP}_{\text{veri}}$ are calculated based on calibration and verification data set, respectively.

Table 4.3 Results of validation tests for the SSST reconstructions based on IKM, MAT and ANN. R^2_{cal} and R^2_{veri} correspond to the correlation coefficient between observed values from calibration and verification dataset, respectively, and estimated values. $\text{RMSEP}_{\text{cal}}$ and $\text{RMSEP}_{\text{veri}}$ are the standard deviation of the difference between observed and estimated values, calculated by dividing the database in calibration and verification data sets.

	R^2_{cal}	R^2_{veri}	$\text{RMSEP}_{\text{cal}}$ (°C)	$\text{RMSEP}_{\text{veri}}$ (°C)
IKM	0.94	0.96	1.29	1.12
MAT	0.95	0.96	1.26	1.00
ANN	0.99	0.96	0.02	1.01

overestimation by fitting every detail of the calibration data set, including the noises (Guiot and de Vernal, 2007). The ANN verification data set shows a reasonable correlation ($R^2_{\text{veri}}=0.96$) and relatively low $\text{RMSEP}_{\text{veri}}$ (1.00°C ; Table 4.3). It also performs better on both warm and cold samples than IKM and MAT (Fig. 4.5).

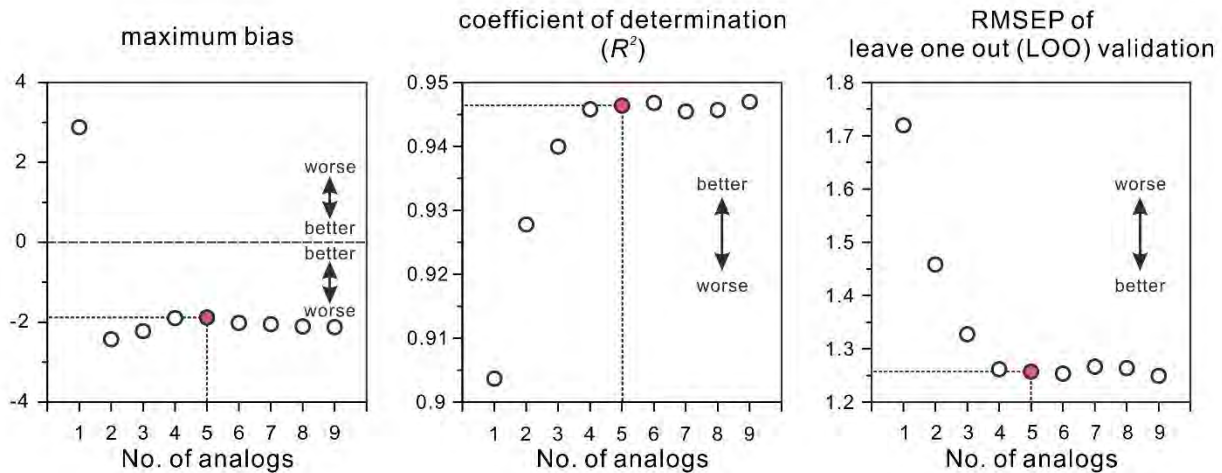


Fig. 4.6 Selection of the best analogs of MAT reconstructions. Maximum bias, coefficient of determination and root mean square error of prediction (RMSEP) by leave one out validation are used to determine the best analogs, which are indicated by red circles.

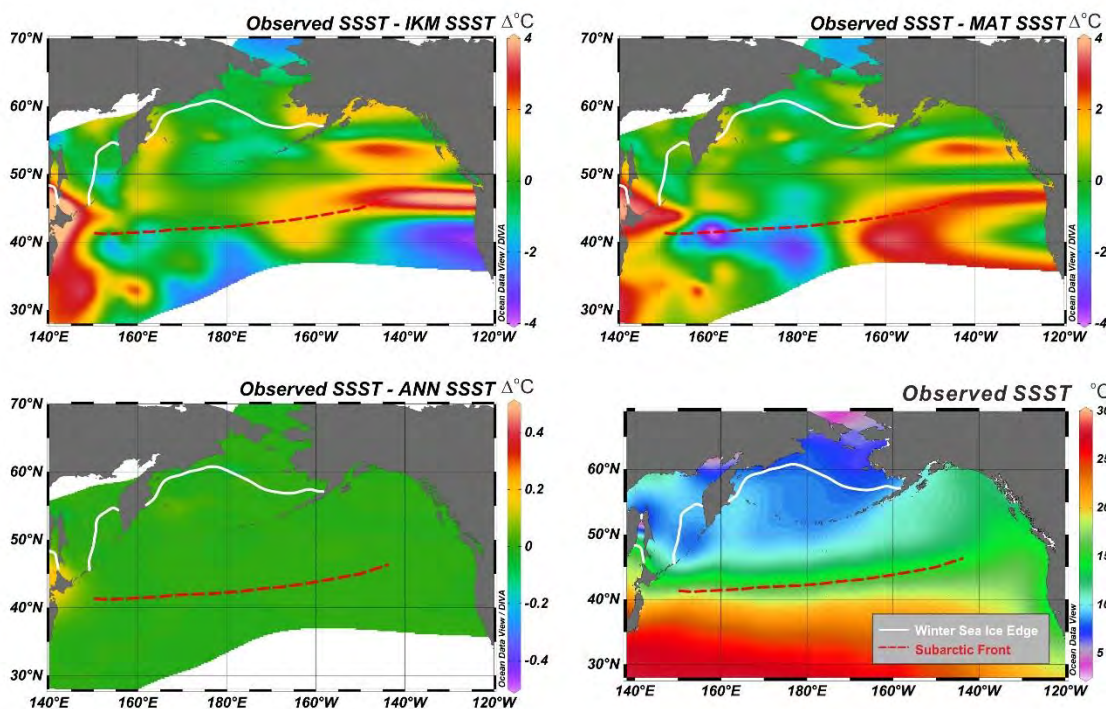


Fig. 4.7 Comparison between the modern summer sea surface temperature (SSST; Levitus and Boyer, 1994) and the SSST reconstructed by IKM, MAT and ANN. The winter sea ice edge (March of 1982–1991; Reynolds et al., 2002) and the Subarctic Front (Aydin et al., 2004) are indicated by the solid white and dashed red lines, respectively. The summer sea surface temperature pattern from WOA94 (Levitus and Boyer, 1994) is shown at the right-bottom as a reference.

In general, the performances of the three methods exhibit a good linear correlation between observed and estimated SSTs. However, the reconstructions of IKM overestimate the cold endmembers in the Chukchi Sea and underestimate the warm endmembers (Fig. 4.7). MAT estimates suffer the similar shortcomings (Fig. 4.7). Both methods have good results in the Bering Basin. The result of ANN indicates the best SST reconstruction, although SSTs around Japan are overestimated (Fig. 4.7).

4.4.3. Testing the transfer function on sediment core MD01-2416

4.4.3.1. Diatom assemblage of MD01-2416

Diatoms from the North Pacific core MD01-2416 are abundant, with concentrations ranging from 20 to 80×10^6 valves/g dry sediment. The diatom concentration peaks occur during the Bølling/Allerød (B/A) and MIS 5, corresponding to high productivity in the warm period (Fig. 4.8). On the contrary, diatoms are in low abundance during the cold period (ca. 10×10^6 valves/g dry sediment) and the Holocene (ca. 15×10^6 valves/g dry sediment).

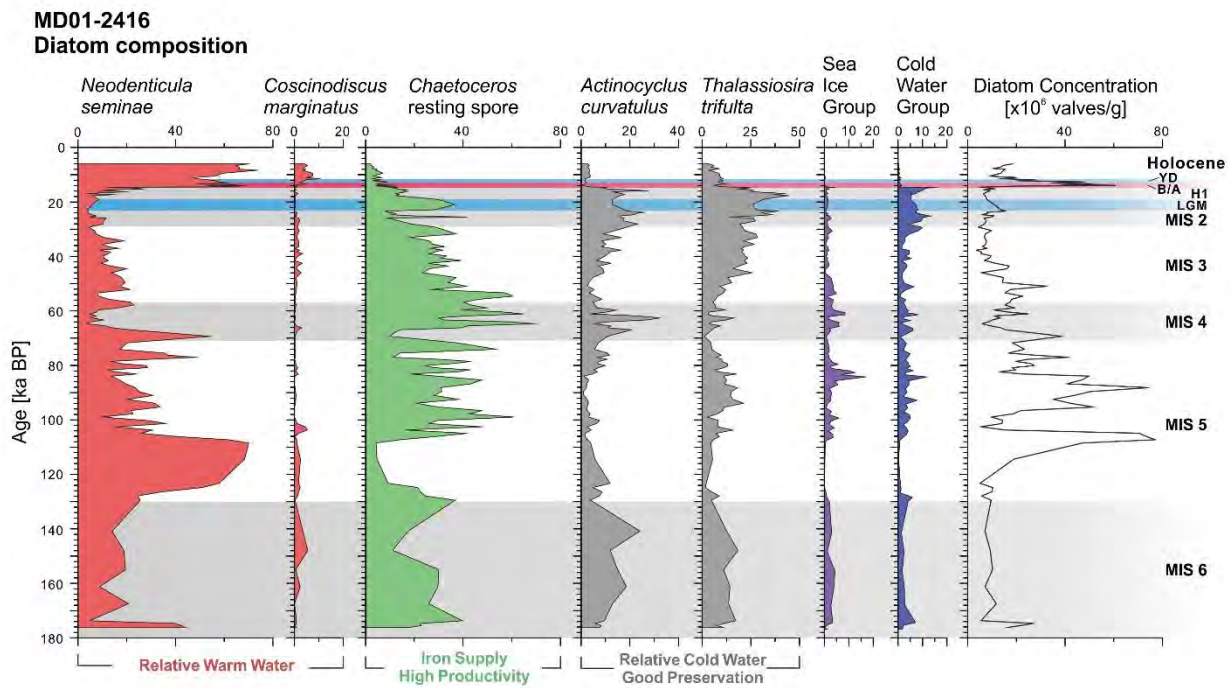


Fig. 4.8 Diagram of relative abundances of selected diatom species and species groups. The cold water group includes *Bacterosira bathyomphala*, *Porosira glacialis*, *Thalassiosira antarctica* var. *borealis* r. sp., *T. bulbosa*, *T. hyaline*, *T. nordenskiöldii*. The sea ice group consists of *Fragilariopsis cylindrus* and *F. oceanica*. The diatom concentration is shown in the right panel. The Marine Isotope Stages and other climate events are indicated in shaded bars.

In total 48 taxa were distinguished from MD01-2416, excluding fresh water species which were deposited via lateral transportation. The diatom assemblages are dominated by the relatively warm water species *N. seminae* (60%) and a minor proportion of *Coscinodiscus marginatus* (5-7%) during MIS 1 and MIS 5, while *Chaetoceros* resting spores (30-60%), *Thalassiosira trifulta* (2.5-42%), *Actinocyclus*

curvatulus (2-30%), the cold water species group (1-13%; including *Bacterosira bathyomphala*, *Porosira glacialis*, *T. antarctica* var. *borealis* r. sp., *T. bulbosa*, *T. hyalina*, *T. nordenskiöldii*) and the sea ice species group (0.5-16%; including *Fragilariopsis cylindrus*, *F. oceanica*) are more abundant during the colder MIS 2, MIS 3 and MIS 4 (Fig. 4.8). The diatom assemblages of MD01-2416 are composed of three factors derived from IKM. While the Subarctic and Subtropical Factor have high loadings during the interglacial period, the Arctic Factor dominates the glacial interval.

The diatoms in the samples of the Last Glacial Maximum (LGM) are mostly moderately dissolved (preservation category 3 and 4), including the fragile sea ice indicators (*F. cylindrus* and *F. oceanica*). In contrast, the heavily silicified species, *A. curvatulus* and *T. trifulta*, display their maxima during the same period (Fig. 4.8).

4.4.3.2. Diatom-based quantitative SSST reconstructions

The SSST reconstruction of MD01-2416 was calculated with the $D_{cal}206/32$ data set. The diatom SSST records reconstructed by the three different methods are shown in Fig. 4.9. All three reconstructions display the same trends with similar degree of variability, indicating reliable estimates. The SSSTs by the IKM and MAT are more constant during the glacial period, while the ANN record has higher fluctuations. The highest temperatures occur in MIS 5.5 (113-130 ka BP; Fronval and Jansen, 1997) in the reconstructions by IKM and MAT, with the warmer one of 11.6 °C in the MAT, while the estimate from ANN is 10.6 °C (Fig. 4.9). Warm temperatures, ca. 10 °C, also appear during the B/A and the Holocene. The LGM (19-23 ka BP; Kucera et al., 2005a) is the coldest period with an average temperature of 8.3 °C

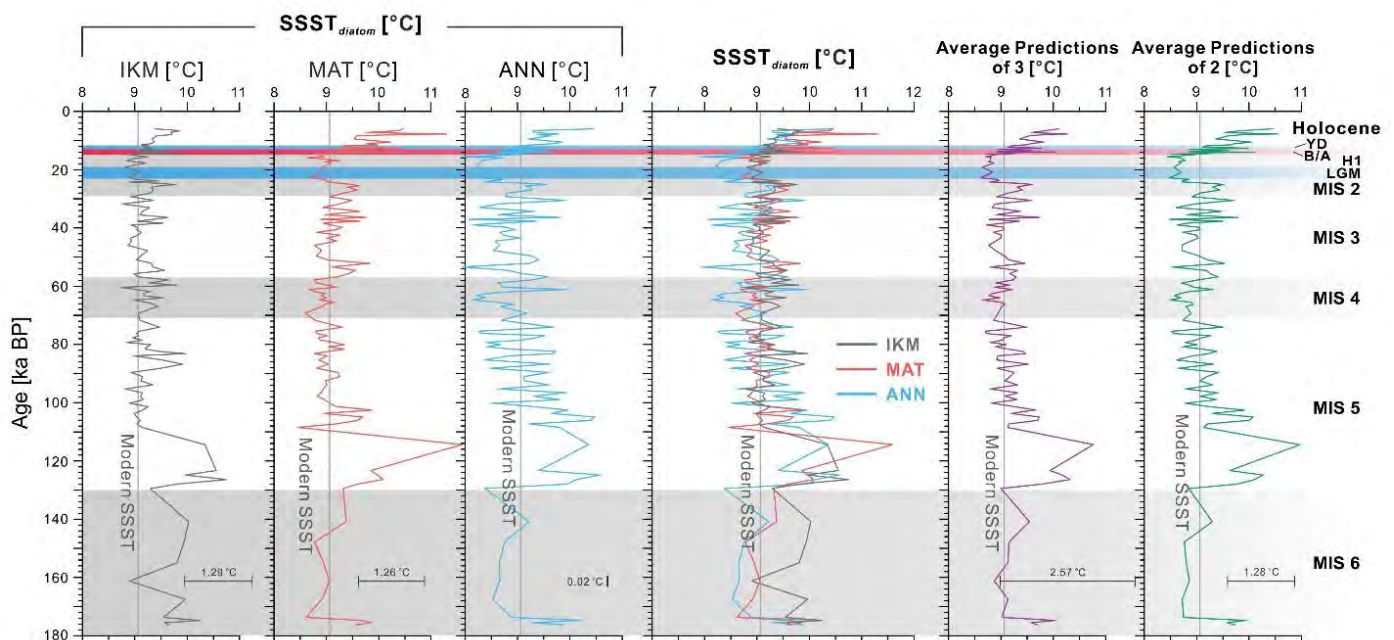


Fig. 4.9 Reconstructions of SSSTs derived from $D_{cal}206/32$ calibration data set by IKM, MAT and ANN. The averaged estimates by IKM/MAT/ANN and MAT/ANN are shown in the right panel. The modern SSST on the coring site is displayed. The error bars indicate systematic errors, which are represented by $RMSEP_{cal}$ in Table 4.3. The Marine Isotope Stages and other climate events are shown in shaded bars.

by the ANN, 8.8 °C by the MAT and 8.9 °C by the IKM. Therefore the glacial-interglacial differences in SSSTs are 2-3 °C by the ANN and MAT and 1.6 °C by the IKM (Fig. 4.9).

A sudden SSST increase of 1 to 2 °C is seen in all records during Termination I (Fig. 4.9). The warming starts at 14.8 ka BP in the reconstructions of IKM and MAT, while the ANN shows an earlier onset at 15.6 ka BP and a significant rise of temperature at *ca.* 14.6 ka BP. This warming is synchronous with the abrupt increase of the warm species *N. seminae* at 14.6 ka BP coinciding with the onset of the B/A warming period. The Younger Dryas (11.7-12.9 ka BP; Rasmussen et al., 2006) is reconstructed by the MAT with a temperature increase of 1.5 °C prior to a 1 °C cooling, whereas a minor warming of 0.8 °C followed by a 0.5 °C drop of temperature is shown in the estimate of ANN and a stable temperature in the IKM (Fig. 4.9). During 11 to 6 ka BP, the early Holocene records increase modestly in the IKM and fluctuate within 2 °C in the MAT and ANN.

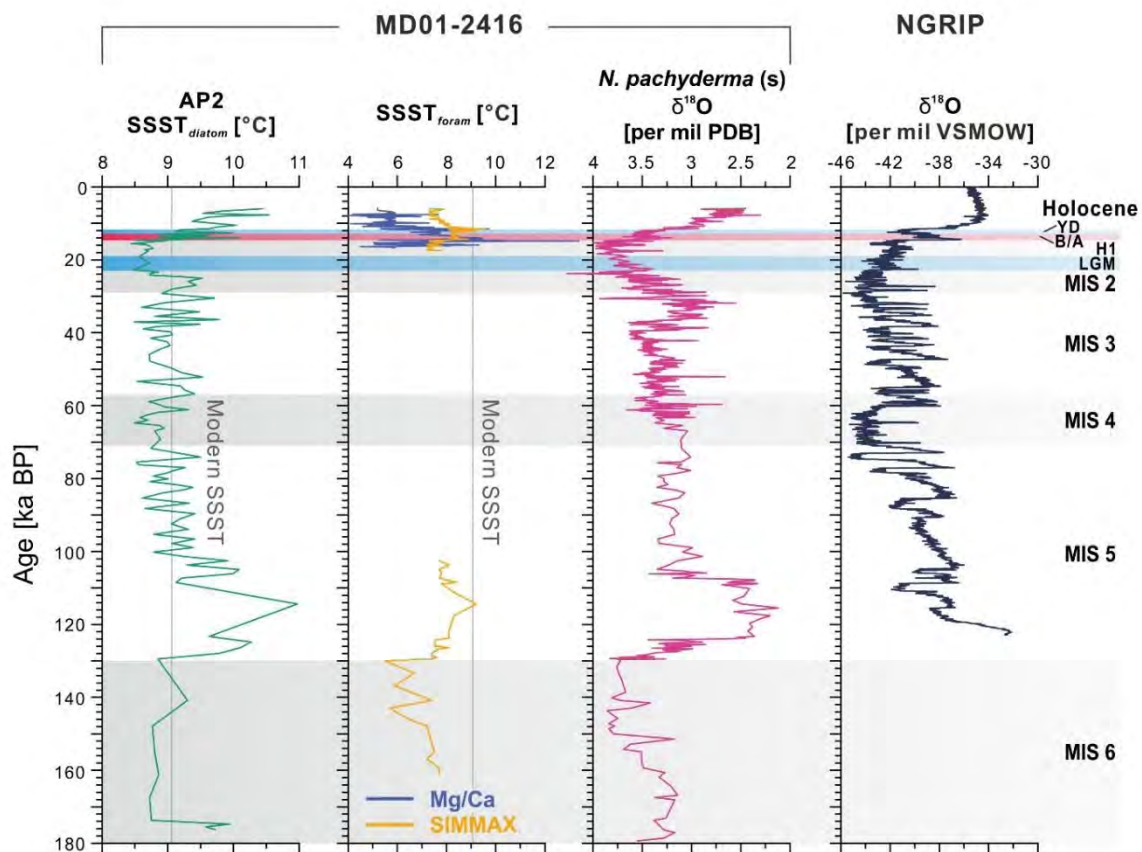


Fig. 4.10 Comparison of the diatom based SSST reconstructions with other proxies for the last 160kyr. The averaged estimate by MAT and ANN (AP2) in this study is shown. The δ¹⁸O of *N. pachyderma* (sinistral) and SSST reconstructions from SIMMAX and Mg/Ca are from Gebhardt et al. (2008). The 50 years mean oxygen isotope record is displayed as well for comparison (North Greenland Ice Core Project Members, 2007). The Marine Isotope Stages and other climate events are highlighted in shaded bars.

All results show a warm temperature of *ca.* 9 °C during MIS 3, which is equivalent to the modern SSST of 9.1 °C. Furthermore, MIS 4 also has a relatively high temperature of *ca.* 9 °C (Fig. 4.9). It is likely that the dissolution of sea ice diatoms plays a role in biasing the results. The lack of cold endmembers,

with coldest samples of $4.7\text{ }^{\circ}\text{C}$, in the calibration data set is another possible reason to get high glacial estimates.

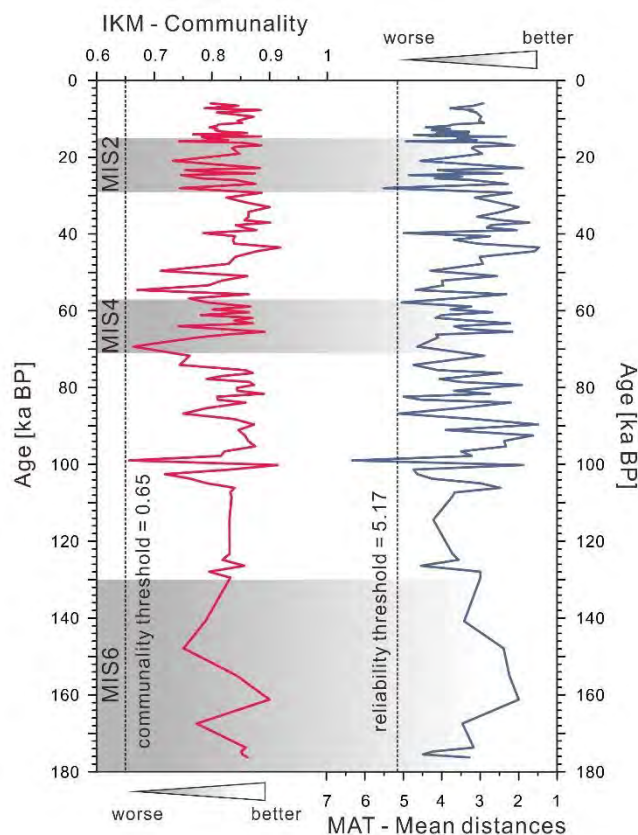


Fig. 4.11 Quality control of the transfer function results for MD01-2416. High communnality values of IKM and low mean distances of MAT indicate better reconstructions. The communnality threshold is set at 0.65, while the reliability threshold of MAT is calculated as the mean distance of the whole reference data set minus the standard deviation.

A multi-method strategy is suggested to enhance the reliability of the reconstructions, because different methods may capture complementary information from the complex relationships between diatom assemblages and the corresponding environmental variables, in our case the temperature (Racca et al., 2001; Kucera et al., 2005b; Guiot and de Vernal, 2007). Therefore we averaged the estimates by the IKM, MAT and ANN (=AP3, Averaged Prediction of 3 methods; systematic error of $2.57\text{ }^{\circ}\text{C}$), as well as the latter two (=AP2, Averaged Prediction of 2 methods; systematic error of $1.28\text{ }^{\circ}\text{C}$), due to the poorest performance of the IKM. The result shows an agreement between AP2 and AP3, while AP2 covers a wider SSST range than AP3 (Fig. 4.9). In general, AP2 and AP3 (APs hereafter) have fluctuations similar to the estimates from each method, with slightly higher glacial-interglacial amplitudes (Fig. 4.9). Moreover, the APs are in line with the planktonic $\delta^{18}\text{O}$ record from the same core (Gebhardt et al., 2008), including the warm pulse during MIS 3 (Fig. 4.10). Finally, the APs correlate generally well with the NGRIP $\delta^{18}\text{O}$ record, especially Termination I (NGRIP members, 2004; Fig. 4.10). Therefore, the average estimates of the MAT and ANN are suggested as the most reliable paleotemperature reconstructions in the northern North Pacific.

4.4.4. Quality control and robustness of the down-core SSST reconstructions

For down-core reconstructions, the IKM SSST estimates can be assessed by the communality for each down-core assemblage, which is the sum of squares of the factors estimates for each sample, representing the success of the varimax factors in accounting for sample's assemblage (Sachs et al., 1997). If the communality value is less than 0.5, the corresponding assemblage is considered as a no-analog assemblage, which should be ruled out of the reference data set for reconstruction. Most communality values of MD01-2416 are between 0.7 and 0.95, while only three samples show relative low communality (between 0.65 and 0.7; Fig. 4.11). Therefore no-analogs are not encountered in the sediment record.

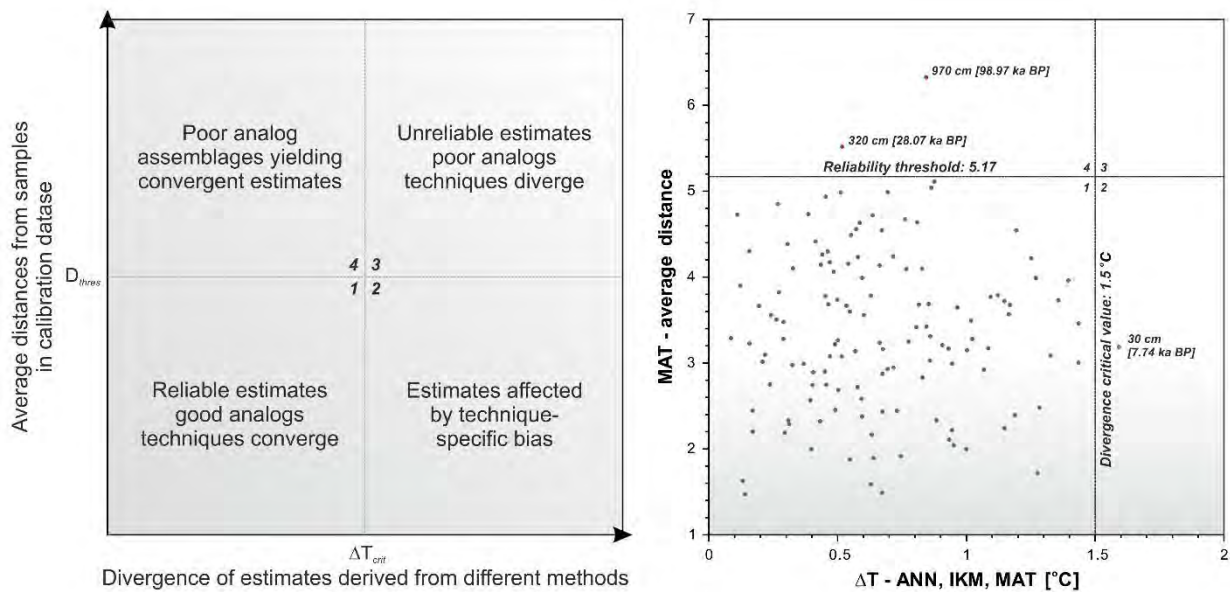


Fig. 4.12 (Left) A conceptual model for the assessment of the reliability of the SSST estimates developed by Kucera et al. (2005b). **(Right)** The conceptual model applied to MD01-2416 SSST reconstructions. The model is based on the division of the bivariate space of an estimate of how well is a fossil sample performed in the calibration data set (e.g. a dissimilarity coefficient/similarity index/communality) and a measure of divergence among reconstructions from different techniques (ΔT). Here we used the dissimilarity coefficient of MAT and the difference between the lowest and the highest SSST reconstructions by the three transfer function techniques. The reliability threshold is set at 5.17 (see text) and the divergence critical value is 1.5 °C. Two samples with poor analogs are displayed in red.

The quality of MAT reconstructions can be evaluated by the mean distances of the selected analogs. Here we defined a reliability index (threshold) to determine a no-analog or poor analog situation according to de Vernal et al. (2005), which is derived from the difference between the mean distance of the calibration data set and the standard deviation. In our $n=206$ data set, the mean distance was 14.55, with a standard deviation of 9.38. The threshold of reliability was thus set by the mean minus the standard deviation (5.17 in this study), below which the distance was considered to be reliable for reconstruction. Furthermore, mean distances smaller than half the threshold value represents good analog (Vernal et al., 2005; Esper and Gersonde, 2014a, b). All the mean distance values of MD01-2416 are below the reliability threshold,

except two samples (Fig. 4.11). Neither the communality of IKM nor the mean distance of MAT indicates the poor analogs of the transfer function are related to glacial-interglacial patterns (Fig. 4.11).

In order to assess the robustness of the SSST reconstructions, we plotted all down-core samples in the conceptual model developed by Kucera et al. (2005b; Fig. 4.12). The divergences among estimates from three different techniques are between 0 and 2 °C, while the average distances from the samples in the calibration data set are below 7 (Fig. 4.12). Only two samples (depths of 320 cm/28.07 ka BP and 970 cm/98.97 ka BP) have average distances higher than the threshold of the calibration data set (5.17). These samples with poor analog assemblages are found in MIS 2 and MIS 5, respectively, probably due to reworking or selective dissolution. If the critical value of temperature divergence is set to 1.5 °C (beyond the systematic errors of each technique), the majority of the samples are within the threshold, indicating a good convergence of different techniques. Therefore our results, although with low glacial-interglacial SSST amplitudes, show the robustness of the SSST reconstructions based on the calibration data set $D_{cal206/32}$.

4.5. Discussion

4.5.1. Comparison with other SSST reconstructions in the northern North Pacific

The diatom based SSST reconstructions reflect the global climate variability for the last 180 ka (Fig. 4.9; Fig. 4.10). Compared to previous SSST estimates in the northern North Pacific, the SSST from this study shows similar patterns but also several discrepancies.

SSST estimates have been applied to the same sediment core based on planktonic foraminifera (Mg/Ca and SIMMAX; Gebhardt et al., 2008). Neither reconstruction extends to the glacial period due to carbonate dissolution, whereas the SIMMAX estimates do cover parts of Termination II and MIS 5.5. However, the SSSTs of the two methods display significant differences during Termination I and the Holocene, which are attributed to the different living depths of individual foraminifera species (Sarnthein, et al., 2004; Gebhardt et al., 2008). The SIMMAX was defined for 10m water depth identical to the diatom reconstructions in this study. Therefore, its reconstruction shows similar temperature patterns with our study during Termination II and MIS 5.5 (Fig. 4.10), although the accurate temperatures are 1-2 degrees lower, probably because the reconstruction is based on a North Atlantic database, which has different foraminiferal composition from the North Pacific (Gebhardt et al., 2008). The SSSTs derived from Mg/Ca indicate the temperatures close to the halocline (Gebhardt et al., 2008) and hence result in a striking discrepancy between the subsurface and surface environment.

Sancetta (1979) has applied a temperature transfer function based on diatoms to a northern North Pacific sediment core (V21-151, 52.27°N, 163.63°E, 5055m water depth), nearby MD01-2416, showing a slight temperature difference, *ca.* 2.6 °C, between the modern and the LGM (18 ka BP, as defined therein). It is in agreement with our results although the summer temperatures for her reconstruction are *ca.* 2 degrees higher than reported here, which is probably caused by the lack of samples representing the cold

environment in the northern Bering Sea in the reference data set (data set SSST min=8 °C; Sancetta, 1979).

Another siliceous microfossil group, radiolaria, was studied by Sachs (1973a, b), Moore (1973, 1978), and Robertson (1975) in this area, using factor analysis and regression analysis to quantitatively reconstruct isotherm maps for the LGM. Based on these data sets, a glacial-interglacial cooling of 4 °C in summer and annual surface temperature in the northeastern North Pacific has been found by Moore (1973) and Sabin and Pisias (1996), respectively. These cores are located in the Transition Zone, close to the Subarctic Front, which is characterized by steep gradients of temperature (Dodimead et al., 1963), therefore they are sensitive to temperature shifts and hence recorded high glacial-interglacial temperature differences.

Organic-walled dinoflagellate cysts also provide useful information for paleoceanographic variability reconstruction in the North Pacific (Bonnet et al., 2012). de Vernal et al. (1997) argued that previous reconstructions were challenged due to the lack of polar environments in the reference data sets. They thus merged Arctic samples into their dinoflagellate data set and produced a glacial-interglacial summer amplitude of *ca.* 10 °C for August, which is higher than any previous studies in the northeastern Pacific (e.g. Moore, 1973; Sabin and Pisias, 1996). Their reference data set, however, does not include Pacific samples (de Vernal et al., 1993; 1994), indicating no local analogs were detected. Additionally, a large number of Arctic samples could bias the reconstructions towards colder results.

Due to the dissolution of carbonates, paleo-SSSTs for glacial-interglacial changes based on calcareous fossils (e.g. foraminifera, coccolithophores) are quite rare in the northern North Pacific. The northwestern Pacific subarctic was cooler by only 1-4 °C annually during the LGM as estimated by several methods based on foraminifera data set (Kucera et al., 2005b). Kucera et al. (2005b) noted that although the high subarctic latitudes were not well represented, the results are reliable (medium reliability). More recent work shows a 2-4 °C cooling in the same area during the LGM summer (MARGO Project Members, 2009), including a SIMMAX reconstruction by Kiefer et al. (2001). Few alkenone records of the northern North Pacific have been studied. These records are characterized by alkenone concentrations below the detection limit prior to the end of Heinrich Event 1 (H1; Kienast and McKay, 2001; Caissie et al., 2010; Max et al., 2012), which hampers a full comparison with our study. Nevertheless, Max et al. (2012) show an early temperature increase between 3 and 5 °C from the end of the H1 to the B/A transition in the northwestern North Pacific including the Sea of Okhotsk and the western Bering Sea. In the eastern Bering Sea only 1 °C rise has been found in the corresponding period (Caissie et al., 2010). In the early Holocene, temperature increases of 5 °C and 3 °C were recorded in the northwestern North Pacific (Max et al., 2012) and the eastern Bering Sea (Caissie et al., 2010), respectively, while an abrupt jump of 6 °C was reconstructed in the northeastern North Pacific (Kienast and McKay, 2001). Despite the age uncertainties (e.g. Kienast and McKay, 2001), the alkenone records therefore have higher glacial-interglacial temperature amplitudes than those of the diatom transfer function in this study. It has been suggested that the alkenone SSST from the northern North Pacific should have even larger glacial-interglacial ranges (MARGO Project Members, 2009), which has been proven by a recent reconstruction for SSST in the

western Bering Sea, showing a ca. 6 °C abrupt SSST increase during Termination II (Max et al., 2014). The high LGM alkenone temperatures are probably due to a shift of the alkenone production season from modern early summer or autumn (Harada et al., 2003, 2006; Seki et al., 2007) or even winter (Prahl et al., 1995) to mid-summer, the warmest period, thanks to the longer duration of sea ice cover (Harada et al., 2012). On the contrary, one alkenone-derived SSST record from the northwestern North Pacific shows a colder SSST of ca. 3 °C in the B/A than in the LGM (Minoshima et al., 2007). This is probably caused by alkenones from the physiological processes of coccolithophorids influenced by nutrient stress (Prahl et al., 2003; Minoshima et al., 2007). These different hypotheses indicate that SSSTs calculated from alkenones are very complex and sometimes misleading (Minoshima et al., 2007), making a comparison between SSST estimates by diatom and alkenone more difficult. However, a newly alkenone-derived SSST from the nearby coring site of MD01-2416 (SO202-07-6, 51.272°N, 167.700°E, 2340 m water depth), shows a similar glacial-interglacial temperature amplitudes with our diatom-based SSST (Méheust, 2014; Maier et al., 2015). If these reconstructions are not biased by changes of production seasonality or nutrient pressure, they can prove the accuracy of the diatom transfer function developed in this study.

Based on siliceous and calcareous fossils, the whole North Pacific glacial-interglacial summer sea surface temperature differences were reconstructed by the CLIMAP project members (1976) and Moore et al. (1980), showing a smaller amount of cooling compared to that in the North Atlantic. This minor cooling (2.3 °C by CLIMAP, 1976 and 2-4 °C by Moore et al., 1980) is in agreement with our results, although the radiolarian-based results could be biased by questionable living depths (Sancetta, 1979).

The freshwater hosing experiments from the LGM control experiments by different ocean-atmosphere coupled general circulation models (GCMs) show maximum annual SST cooling of 3-5°C along 40°-45°N, near the Subarctic Front where the Kuroshio and Oyashio Currents meet (Okumura et al., 2009). North of the front, the climate deterioration is milder (Okumura et al., 2009; Chikamoto et al., 2012). These model results are concordant with our reconstructions.

Accordingly, the SSST reconstructions based on the diatom data set in the northern North Pacific are generally in line with previous studies and estimates, showing a slight cooling during the LGM in this area.

4.5.2. Interpretation of the low glacial-interglacial SSST amplitudes

Our SSST reconstructions based on three different techniques show relative low glacial-interglacial SSST amplitudes of ca. 2 °C, which is inconsistent with SSST records with significant temperature ranges elsewhere (e.g. Zielinski et al., 1998; de Vernal et al., 2000; Trend-Staid and Prell, 2002).

Diatoms often bloom during several different seasons (e.g. Takahashi, 1986). Therefore, seasonal signals may be preserved in the sediments. If we reconstruct the summer temperature using samples that include signals from other seasons, the estimates are, to some extent, biased. In general, the archives of sediment traps located in the northern North Pacific statistically indicate a spring-to-early-autumn flux and hence the corresponding seasonal signals (*Chapter 3*). However, the sediment traps in the northwestern

North Pacific, where the core in this study is located, show mostly a spring flux (Tsoy and Wong, 1999; Onodera et al., 2005; see discussion in **Chapter 3**). This may increase the reconstructed temperature by using the warmer (summer) temperature instead of the colder (spring) ones. Minoshima et al. (2007) and Harada et al. (2012) suggested a shift of the alkenone production season during the LGM which resulted in higher estimated temperatures. This also could be applied to diatoms if the warm temperature for diatom blooming occurred later in the year during the glacial period. This would result in higher temperature during the glacial time and lower temperature during the interglacial time and therefore reduce the glacial-interglacial temperature amplitudes.

Additionally, selective dissolution of diatom species may also play a role. The sea-ice-related species (*F. cylindrus* and *F. oceanica*; **Chapter 3**), which are abundant in the surface samples on the Bering Shelf indicating sea ice cover, are very rare (< 10%) during the glacial period in MD01-2416 (Fig. 4.8). These species are weakly silicified and are prone to dissolution in the sediments. Meanwhile, the heavily silicified species (*A. curvatulus* and *T. trifulta*; **Chapter 3**), resistant to the dissolution, accumulated in the glacial sediments (Fig. 4.8). These species prefer a relatively warmer environment compared to the sea ice conditions (**Chapter 3**). Hence, a loss of cold signals and increase of relatively warm signals may reduce the temperature amplitudes between glacial and interglacial periods, although the MAT is thought to be nearly independent of local preservation (Pflaumann et al., 1996). The high temperatures reconstructed during MIS 3 and MIS 4 are likely due to the same effects.

The lack of cold endmembers in the reference data set may also have an impact

These problems may limit the accuracy of the diatom-based transfer function in the northern North Pacific and indicate that more care should be taken when reconstructing the paleo-SSSTs in this area, especially for the glacial period.

4.6. Conclusions

The development of the diatom reference data set with 206 samples and 32 taxa and taxa groups leads to a reliable diatom transfer function for paleotemperature reconstructions in the northern North Pacific. The sea surface temperature estimates based on the IKM, MAT and ANN are highly correlated with the measured SSSTs, with the lowest correlation coefficient by the IKM and the highest one by the ANN.

These three methods have been applied to a sediment core in the study area, showing the same trends with a similar degree of variability for the last 180 ka. The SSSTs by IKM and MAT are more constant during the glacial period, while the ANN record displays higher fluctuations. The average estimate of the MAT and ANN correlates well with the local planktic $\delta^{18}\text{O}$ record and the NGRIP $\delta^{18}\text{O}$ profile and therefore is suggested for paleotemperature reconstruction in the future. All estimates show a clear glacial-interglacial pattern, although the amplitudes of 1.5-2 °C, are quite low. These low amplitudes are in line with previous estimates based on various proxies in the same area. The robustness test also shows the reliability and the robustness of the SSST reconstructions based on the calibration data set.

During the glacial period, a shift of the diatom blooming seasons and the dissolution of weakly silicified species could bias the diatom-based reconstructions towards warmer temperatures. The lack of cold endmembers in the reference data set may also play a role. All these might result in low glacial-interglacial amplitudes. Therefore, care should be taken when applying a diatom-based transfer function to paleotemperature reconstructions, especially the glacial SSTs, in the northern North Pacific.

Acknowledgements

This paper is a contribution to the INOPEX (Innovative North Pacific Experiment) project funded by the Bundesministerium für Bildung und Forschung (the German Ministry of Education and Research). We thank M. Sarnthein and R. Tiedemann for helpful discussion. We are also grateful to U. Bock from Alfred Wegener Institute for the technical assistance.

Chapter 5. Late Pleistocene palaeoceanographic variability in the northern North Pacific for the last 160 ka: evidence from diatom records

Jian Ren^a, Rainer Gersonde^a, Oliver Esper^a, Constance Sancetta^b, Ralf Tiedemann^a

^a Alfred Wegener Institute Helmholtz Centre for Polar and Marine Research, Am Handelshafen 12, D-27570 Bremerhaven, Germany (Correspondence to J. Ren: jian.ren@awi.de)

^b Moreland Hills, OH 44022, U.S.A.

In preparation to submit to Quaternary Research

Abstract

The North Pacific is a critical area for understanding past and present global climate variability. Yet sea surface temperature and sea ice development in the Late Pleistocene are not sufficiently studied. Here we present records of diatom records and diatom-derived summer sea surface temperature (SSST_{diat}) from both the eastern and western North Pacific for the last 160 ka. The SSST_{diat} is estimated by a newly developed transfer function based on a diatom data set of 206 surface samples. Our SSST_{diat} estimate, for the first time, shows an uninterrupted temperature reconstruction in the northern North Pacific, which covers the whole last glacial-interglacial cycle. The variabilities of diatom composition and SSST_{diat} show similar pattern to paleoclimate and paleoceanography records elsewhere, corresponding to the Northern Hemisphere climate change. The sea ice diatom and cold water species together indicate an ice-free environment nearly for the last 160 ka in the eastern and western North Pacific open ocean. An only possible sea ice expansion during Heinrich Event 1 is revealed by significant abundance of cold water diatoms and high value of biomarker for sea ice (IP₂₅) from previous studies. A basin-wide east-lead-and-west-lag phenomenon has been discovered in the eastern and western North Pacific during the terminations. It is likely that eastern North Pacific responses more quickly to the increased summer insolation at terminations, driving the nearby mountain glaciers to collapse and hence huge amount of melting water to discharge into the open ocean, thus changing the surface environment earlier. The occurrence of abundant coastal species in the deep ocean in the mid to late MIS 5, might be applied as a stratigraphic marker in the northern North Pacific open ocean.

5.1. Introduction

The North Pacific is featured by a permanent surface stratification, preventing ocean-atmosphere gas and heat exchanges and hence influencing global CO₂ budget (Haug et al., 1999). Therefore this region is believed to be sensitive to global climate change and to play a significant role in it (Keigwin and Cook, 2007). In order to understand the mechanism behind the glacial-interglacial climate change during the Late Pleistocene, it is of special importance to investigate the teleconnections between the North Pacific and the North Atlantic via either oceanic conveyor belt (e.g. Keigwin et al., 1992; Kim et al., 2004) and/or

atmospheric circulation (e.g. Keigwin and Cook, 2007; Jaccard, 2012; Max et al., 2012). Development of the summer sea surface temperature (SSST) provides essential information on glacial-interglacial climate variability, therefore it is a key research target for paleoceanography study in the North Pacific.

However, only a few SSST reconstructions in the subarctic North Pacific are available, most of which only extending to the last deglaciation (ca. 20 ka BP; e.g. Sancetta, 1979; de Vernal et al., 1997; Ternois et al., 2000; Barron et al., 2003; Sarnthein et al., 2004, 2006; Caissie et al., 2010; Max et al., 2012). Harada et al. (2004, 2012) show an alkenone-derived sea surface temperature (SST) from western North Pacific covering the last 40 ka with low resolution, while Gebhardt et al. (2008) reconstructed the SSSTs back to Termination V, although the records are broken between the terminations. A recent study reconstructed alkenone-derived SST in the western Bering Sea for MIS 5 and late MIS 6 (Max et al., 2014). On the other hand, the SSST records based on a variety of proxies are prone to be biased by different seasonal signal or the dwelling water depths, preventing the comparison between records. Nevertheless, these records, displaying abrupt oscillations during the deglaciation, are in consistent with the archives from the Northern Hemisphere (e.g. NGRIP members, 2004), despite that some may show major deglacial events leading or lagging for thousand years due to the uncertainty of the ^{14}C datings or different dating techniques (e.g. Kienast and McKay, 2001; Sarnthein et al., 2006; Gebhardt et al., 2008; Rella et al., 2012). Recent study also indicates a synchronized SSST history of the North Pacific and the North Atlantic during the mid- to late-Holocene (Jaccard, 2012; Max et al., 2012) rather than a temperature seesaw between two ocean basins by previous study (Kim et al., 2004), which implies an atmosphere derived inter-basin teleconnection.

The sea ice is a fast amplifier of climate change. Its wax and wane influence the latitudinal temperature gradients and as well insulate the sea-atmosphere heat and moisture exchange (Zhao et al., 2004; Gersonde et al., 2005). For instance, shrinking of sea ice extent results in the increase of summer monsoon rainfall in southeastern China (Zhao et al., 2004). However, the sea ice history in the Late Pleistocene in the North Pacific remains unclear, except few studies in eastern and western North Pacific by the transfer function based on dinoflagellate cysts and a novel developed biomarker IP₂₅ (C₂₅ monounsaturated hydrocarbon), respectively (de Vernal and Pedersen, 1997; Max et al., 2012; Méheust, 2014; Maier et al., 2015).

The sparse paleoceanographic studies on SSST in the northern are mainly due to the relatively shallow carbonate compensation depth and the lack of the planktonic foraminifers for ^{14}C dating (e.g. Zahn et al., 1991; Sarnthein et al., 2004; Max et al., 2012). Furthermore, the ^{14}C reservoir ages of surface ocean in the area are poorly studied and even the estimates are variable (700-900 a; Southon et al., 1990; Zahn et al., 1991; Keigwin et al., 1992; McDonald, 1997; de Vernal and Pedersen, 1997; Keigwin, 1998; Kienast and McKay, 2001; Cook et al., 2005; Cook, 2006; Galbraith 2006; Cassie et al., 2010; Davies et al., 2011; Max et al., 2012; Rella et al., 2012), hampering accurate age models. Recently, inconstant reservoir ages were developed based on ^{14}C -plateau theory (Sarnthein et al., 2006, 2007, 2013, 2015; Gebhardt et al., 2008), providing an opportunity to establish reliable ^{14}C age models in the northern North Pacific.

Here we present diatom assemblage composition, sea ice species abundance and diatom-derived SSST

records based on newly developed transfer functions (*Chapter 4*) from sediment cores retrieved from the western and eastern North Pacific, covering up to the last 160 ka BP (Fig. 5.1). Our results provide basin-wide information on a continuous glacial-interglacial paleoceanography history in the northern North Pacific, making it possible to investigate the role the North Pacific played in the global glacial-interglacial cycle.

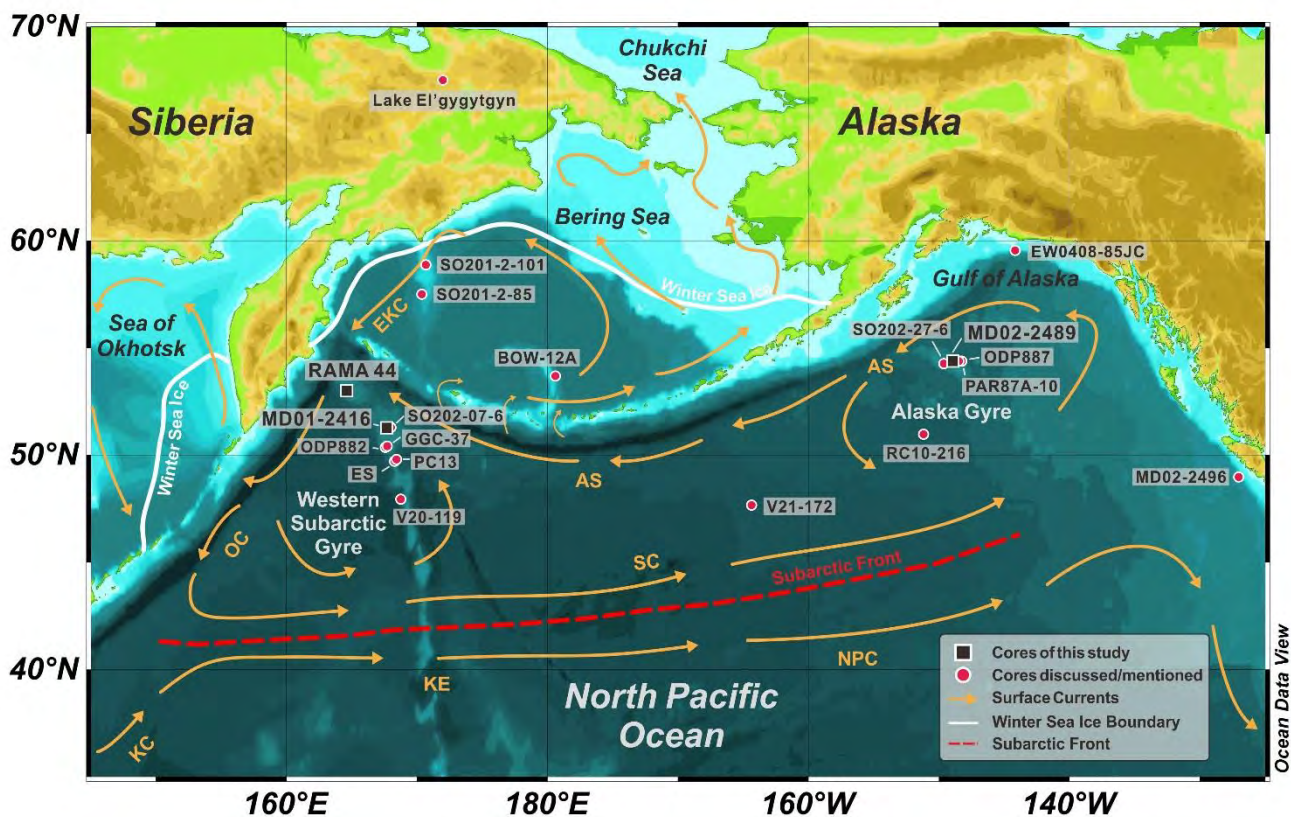


Fig. 5.1 Map of the northern North Pacific and the Bering Sea with core sites of this study (black squares) as well as other cores mentioned in the text (red dots): ES (Katsuki and Takahashi, 2005); EW0408-85JC (Davies et al., 2012); GGC-37 (Lam et al., 2013); MD02-2496 (Taylor et al., 2014); ODP882 and ODP887 (Galbraith, 2006; Galbraith et al., 2008); PAR87A-10 (de Vernal and Pedersen, 1997); PC13 (Brunelle et al., 2010); RC10-216, V20-119 and V21-172 (Sancetta and Silvestri, 1984); SO201-2-85 (Max et al., 2014); SO201-2-101 (Riethdorf et al., 2013a); SO202-07-6 and SO202-27-6 (Méheust, 2014; Maier et al., 2015). The Winter Sea Ice boundary (Averaged 15% sea ice concentration of March of 1982-1991; Raynolds et al., 2002) and the Subarctic Front (Aydin et al., 2004) are indicated by the white lines and red dash line, respectively. Currents system in the North Pacific Ocean is shown as well (orange arrows): AS-Alaska Stream; EKC-East Kamchatka Current; KC-Kuroshio Current; NPC-North Pacific Current; OC-Oyashio Current; SC-Subarctic Current.

5.2. Oceanography settings

The surface circulation of the northern North Pacific is dominated by the Subarctic Gyre, a large scale cyclonic system, which consists of two subgyres, the Alaska Gyre (AG) in the east and the Western Subarctic Gyre (WSG) in the west (Fig. 5.1). The Kuroshio Extension (KE) and the North Pacific Current (NPC), originated from the Kuroshio Current (KC), bring warm and salty water mass from the tropical

Pacific into the Subarctic Gyre via the Alaska Gyre (White et al., 1982; Qiu, 2000, 2002). The Alaska Gyre generates the Alaska Stream (AS), which flows southwestward along the Aleutian Islands, transporting the fresher North Pacific surface water into the Bering Sea mainly through the western Aleutian Islands. These inflows form another anticlockwise gyre, the Bering Sea Gyre (BSG), in the Bering Sea. Here, a part of the water mass joins the northerly outflow from the Bering Strait unidirectionally into the Chukchi Sea of the Arctic Ocean with an amount of 0.85 Sverdrups (Sv; Coachman, 1993; Takahashi, 2005), while the other part turns westward to originate the East Kamchatka Current (EKC) along the Kamchatka peninsula, forming the western boundary of the Western Subarctic Gyre. The straits of Kurile Islands allow the water mass from the East Kamchatka Current to flow into the Sea of Okhotsk, joining the cyclonic Okhotsk Gyre (OG). A part of the surface water runs back into the North Pacific to form the Oyashio Current (OC; Favorite et al., 1976; Alfultis and Martin, 1987; Ternois et al., 2001). In addition to the North Pacific water, the Sea of Okhotsk receives another warmer and saltier water source from the Japan Sea through Soya Strait (Takizawa, 1982).

While no sea ice is found in the open ocean (Dodimead et al., 1963), the seasonal sea ice in the Bering Sea and the Sea of Okhotsk starts in November and extends to its maximum in March-April and disappears in June-July (Niebauer, 1980, 1983; Parkinson and Gratz, 1983; Parkinson et al., 1987). Most of the Bering Shelf is covered by sea ice in winter, approximately 1/3 of the Bering Sea. In contrast, the Bering Basin experiences no ice cover, although it may be influenced by drifting ice (Sancetta, 1981). The Sea of Okhotsk has seasonal sea ice in winter, covering about 75% of the sea (Fig. 5.1; Parkinson et al., 1987).

Table 5.1 Core locations and corresponding modern SSST.

Sediment Cores ^a	Latitude	Longitude	Water Depth	Locations	Length studied	Modern SSST ^b
MD01-2416 GC	51.27°N	167.73°E	2317 m	NW Pacific	1200 cm	9.06 °C
MD02-2489 GC	54.39°N	148.92°W	3640 m	NE Pacific	1900 cm	11.30 °C
RAMA44 PC	53.00°N	164.65°E	2980 m	NW Pacific	80 cm	9.68 °C

^a GC: giant piston core; PC: piston core

^b Modern SSST derived from World Ocean Atlas 1994 at 10m water depth for July, August and September (WOA94; Levitus et al., 1994)

5.3. Material and methods

5.3.1. Material

Three deep sea sediment cores were studied (Fig. 5.1). MD01-2416 and RAMA44 were retrieved respectively from Detroit Seamount and Meiji Seamount, western North Pacific (WNP), whereas MD02-2489 was recovered from Patton Seamount, eastern North Pacific (ENP; Table 5.1; Fig. 5.1). These cores were taken during the cruises RAMA03 by R/V *Thomas Washington* in 1980, IMAGES VII WEPAMA by R/V *Marion Dufresne* in 2001 and 2002, respectively (Keigwin, 1987; Bassinot and Baltzer, 2002).

The sediment of all three cores is composed of diatom bearing and diatomaceous olive gray clay and silty clay interrupted by diatomaceous ooze (Keigwin, 1987; Bassinot and Baltzer, 2002).

Top 1200 cm of MD01-2416 and 1900 cm of MD02-2489 were used in this study. For RAMA44, upper 78 cm were selected (Table 5.1). For diatom analysis, sub-samples were collected as 1-cm slices at 5 cm and 10 cm interval throughout the cores. In total 260 samples were taken for diatom study (131 from MD01-2416, 119 from MD02-2489 and 10 from RAMA44). All the samples were firstly freeze-dried. 0.5 g of subsamples were made quantitatively into permanent slides for diatom identification and counting according to the standard procedure established at the Alfred-Wegener-Institute (Gersonde and Zielinski, 2000).

5.3.2. Diatom identification and data processing

Diatom identification was following the steps described by Schrader and Gersonde (1978). An average of 400 diatom valves was counted for each sample with a Zeiss Axioskop microscope at $\times 1000$ magnification. Diatoms were identified to species or species group level. Followed taxonomies can be found in **Chapter 3**. According to **Chapter 3**, 49 taxa were selected for this study, among which, 32 species and species groups were applied to the SSST reconstruction (**Chapter 4**).

The diatom valve concentration (valves per gram dry sediment) was calculated according to Esper et al. (2010) with the following equation:

$$\text{Diatom valves/gram} = (1/w) \times (csa/ta) \times (sv/split) \times (dvn/tn),$$

Where w is the dried sample weight in grams, csa is the area of the cover slide (254.5 mm^2), ta is the area of one counted traverse (3.6 mm^2), sv is the volume of processed diatom suspension (50 ml), $split$ is the volume of suspension split onto the cover slide (from 1.4 to 9.8×10^{-2} ml), dvn is the total counted diatom valve number and the tn is the number of fully counted traverses.

5.3.3. Sea ice and productivity indicators

Here we use the combined relative abundance of sea ice species *Fragilariopsis cylindrus* and *F. oceanica* as a sea ice indicator. A 20% of abundance was set as the threshold of the occurrence of the winter sea ice in the Bering Sea (**Chapter 3**). However, the relationship between the abundance of sea ice species and the distance to the winter sea ice edge (**Chapter 3**) might be applied in the North Pacific open ocean. The diatom valve concentration (valves per gram dry sediment) may indicate export production. Furthermore, a mesoscale iron enrichment experiment in the North Pacific shows the increase of *Chaetoceros debilis* and hence the corresponding resting spores in relation to the iron supply (Tsuda et al., 2003). It implies the abundance of *Chaetoceros* resting spores (*r. sp.*) may relate to the iron supply from the nearby continents and shelves in the northern North Pacific, which is a high-nutrient, low-chlorophyll area. Hereby we take *Chaetoceros r. sp.* as an indicator of iron input, which results in increased iron-induced fertilization.

5.3.4. Transfer functions for SSST reconstruction

Due to their wide distribution and dwelling in the photic zone, diatom assemblages are sensitive to environmental variability of the surface water. In the northern North Pacific, the diatom biogeographic distribution patterns are closely related to the SSST (**Chapter 3**), which allows us to establish a diatom-based transfer function in the region (**Chapter 4**).

In order to reduce the bias of the high abundant species, such as *Neodenticula seminae*, which accounts for 80% of the total assemblage of some samples, in the SSST reconstructions, a logarithm-based transformation on percentage abundance, as suggested by Zielinski et al. (1998), was employed in order to down-weight these species. The following equation is used:

$$L = \text{LOG}_{10} (\text{relative abundance} \times 10 + 1)$$

The summer sea surface temperature (SSST) was chosen as a target for paleoenvironmental reconstruction due to the fact that diatom export peaks in the northern North Pacific and its marginal seas usually occur in summer (July, August and September; see **Chapter 3**). The sea surface temperature data (at 10m water depth) were obtained from World Ocean Atlas 1994 (WOA94; Levitus et al., 1994), of which the measurements represent the temperature in the 1970s' before the onset of warming in the Bering Sea (Levitus et al., 1994).

Developed in **Chapter 4**, a reference dataset of 206 surface samples, covering the northern North Pacific and its marginal seas, with 32 species and species groups, is applied to reconstruct the SSST variability in the sediment core records. As tested in **Chapter 4**, the average of the estimates by the Modern Analog Technique (MAT) and the Artificial Neural Network (ANN) were used for SSST estimates in this study, owing to their better performances on reconstruction than that of the Imbrie and Kipp Method (IKM). Squared Chord Distance and 5 analogs are chosen for the MAT reconstructions, while one hidden layer and 20 hidden neurons are set for the SSST estimates by ANN, as suggested in **Chapter 4**. The systematic error is ± 1.28 °C (see **Chapter 4**), resulting from combined errors of two methods.

5.3.5. Age model

The age models of MD01-2416 and MD02-2489 have been developed by Sarnthein et al. (2005; 2007; 2013; 2015) and Gebhardt et al. (2008) by using the ^{14}C plateau boundaries and the joint geomagnetic and $\delta^{18}\text{O}$ records. Galbraith et al. (2008) generated another age model for MD01-2416 by the minimally constrained tuning of the Ca/Ti ratios to the carbonate record of nearby core ODP882, which has been dated by visual correlation between its Ba/Al ratios and the δD records of the EPICA Dome C ice core (EDC; EPICA Community Members, 2004). These two age models, however, are different from each other on several Marine Isotope Stages (MIS; Gebhardt et al., 2008). Besides, the age models are correlated either with low resolution planktonic $\delta^{18}\text{O}$ records (Imbrie et al., 1992; Bassinot et al., 1994) or with the EDC records in the Southern Hemisphere (EPICA Community Members, 2004), both of which may bias

Table 5.2 Age control points for MD02-2489.

Depth (cm)	Calendar Ages (ka BP)	Sedimentation rates (cm/ka)	Dating methods	References
59	8.003		¹⁴ C calibration ^a	Gebhardt et al., 2008; Maier et al., 2015
66.5	9.310	5.738	¹⁴ C calibration ^a	Gebhardt et al., 2008; Maier et al., 2015
76.5	9.933	16.051	¹⁴ C calibration ^a	Gebhardt et al., 2008; Maier et al., 2015
86.5	11.135	8.319	¹⁴ C calibration ^a	Gebhardt et al., 2008; Maier et al., 2015
96	12.445	7.252	¹⁴ C calibration ^a	Gebhardt et al., 2008; Maier et al., 2015
110	13.297	16.432	¹⁴ C calibration ^a	Gebhardt et al., 2008; Maier et al., 2015
119	13.567	33.333	¹⁴ C calibration ^a	Gebhardt et al., 2008; Maier et al., 2015
130	14.05	22.774	Suigetsu varve ^b	Sarnthein et al., 2013
165.5	14.92	40.805	Suigetsu varve ^b	Sarnthein et al., 2013
171.5	15.25	18.182	Suigetsu varve ^b	Sarnthein et al., 2013
189.5	16.05	22.500	Suigetsu varve ^b	Sarnthein et al., 2013
200.5	16.4	31.429	Suigetsu varve ^b	Sarnthein et al., 2013
208	16.9	15.000	Suigetsu varve ^b	Sarnthein et al., 2013
219	17.3	27.500	Suigetsu varve ^b	Sarnthein et al., 2013
231	18	17.143	Suigetsu varve ^b	Sarnthein et al., 2013
260	18.980	29.592	Suigetsu varve ^b	Sarnthein et al., 2015
268	19.130	53.333	Suigetsu varve ^b	Sarnthein et al., 2015
520	31.131	20.998	¹⁴ C calibration ^a	Gebhardt et al., 2008; Maier et al., 2015
532	35.2555	2.909	LR04/ODP 887 ^c	Galbraith et al., 2008; this study
608	40.985	13.265	LR04/ODP 887 ^c	Galbraith et al., 2008; this study
694	46.2435	16.354	LR04/ODP 887 ^c	Galbraith et al., 2008; this study
832	56.948	12.892	LR04/ODP 887 ^c	Galbraith et al., 2008; this study
1082	74.468636	14.269	LR04/ODP 887 ^c	Galbraith et al., 2008; this study
1296	91.0657	12.894	LR04/ODP 887 ^c	Galbraith et al., 2008; this study
1460	103.38	13.318	LR04/ODP 887 ^c	Galbraith et al., 2008; this study
1558	108.56533	18.899	LR04/ODP 887 ^c	Galbraith et al., 2008; this study
1760	133.49	8.104	LR04/ODP 887 ^c	Galbraith et al., 2008; this study
2034	172.9155	6.950	LR04/ODP 887 ^c	Galbraith et al., 2008; this study
2072	176.80783	9.763	LR04/ODP 887 ^c	Galbraith et al., 2008; this study
2422	227.1035	6.959	LR04/ODP 887 ^c	Galbraith et al., 2008; this study
2510	239.308	7.210	LR04/ODP 887 ^c	Galbraith et al., 2008; this study
2844	289.8416	6.609	LR04/ODP 887 ^c	Galbraith et al., 2008; this study

^a ¹⁴C ages of upper 7 samples were corrected for 440 ± 285 yr reservoir age and 1560 ± 310 yr for the lowest 1 sample. Reservoir ages were determined by Sarnthein et al. (2015) according to the nearest ¹⁴C plateau, and converted into calendar ages by CALIB 7.0 (Stuiver and Reimer, 1993) with the Marine13 calibration curve (Reimer et al., 2013).

^b ¹⁴C plateaus were correlated to atmospheric ¹⁴C plateaus from Lake Suigetsu (Bronk Ramsey et al., 2012) to determine the plateau boundaries (Sarnthein et al., 2013; 2015).

^c Graphic correlation were applied between the calcium (Ca; Gebhardt et al., 2008) and iron (Fe; Schmieder et al., unpub. data) XRF counts of MD02-2489 and the carbonate content and magnetic susceptibility of nearby ODP 887 (Rea et al., 1995; McDonald, 1997), which has been dated with the global benthic $\delta^{18}\text{O}$ stack (Lisiecki and Raymo) by Galbraith et al. (2008).

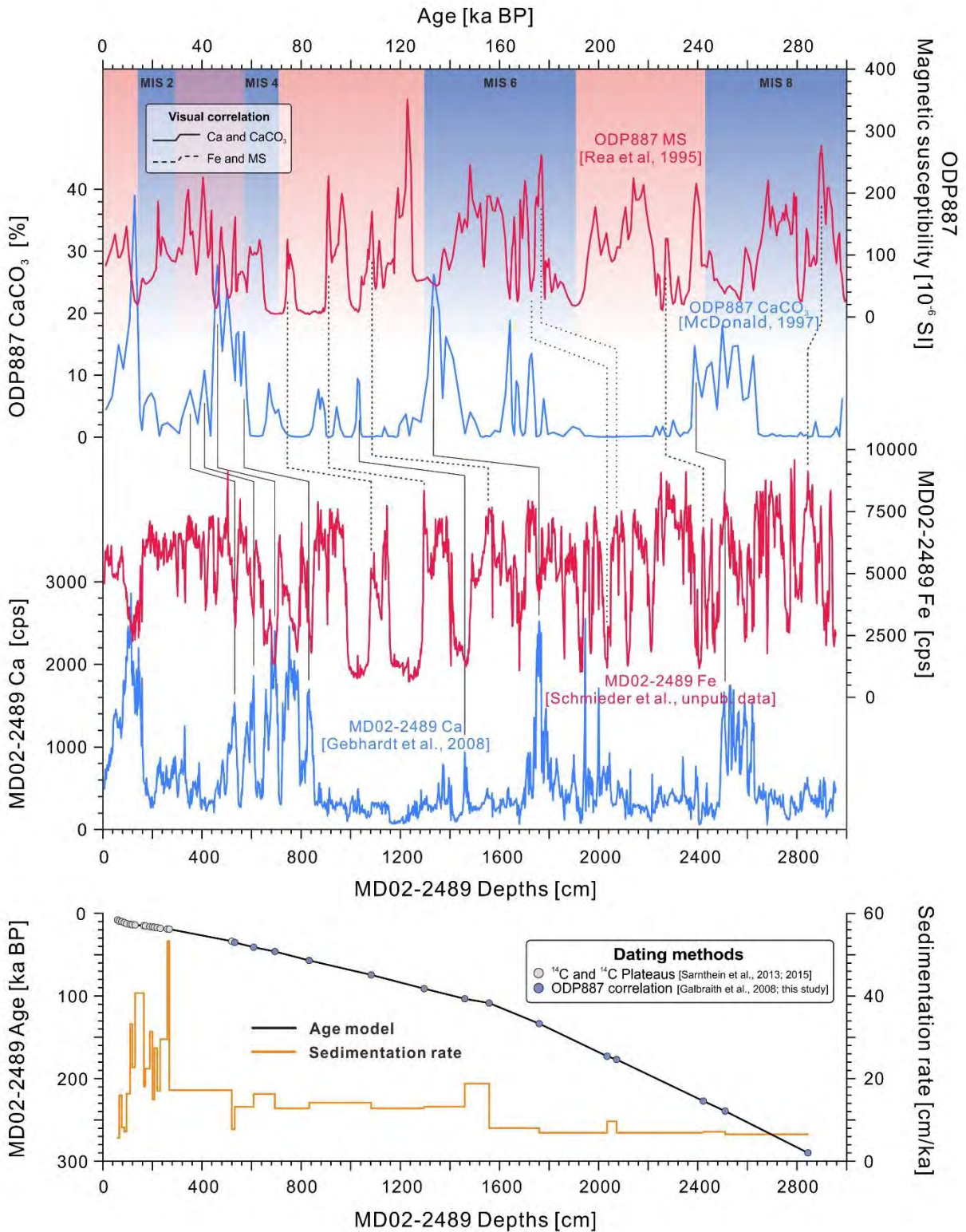


Fig. 5.2 (Top) Graphic correlations between the XRF Ca and Fe counts of MD02-2489 (Gebhardt et al., 2008; Schmiieder et al., unpub. data) and CaCO₃ (%) and magnetic susceptibility of nearby ODP 887 (McDonald, 1997; Rea et al., 1995) with straight lines (Ca and CaCO₃) and dash lines (Fe and MS), respectively. Shaded bars indicate the Marine Isotope Stages according to Lisiecki and Raymo (2005). **(Bottom)** Age model of MD02-2489. The gray circles are ¹⁴C dating points and ¹⁴C plateau boundaries listed in Table 5.2, while the blue circles display the graphic correlations. The sedimentation rates are shown in the bottom panel as well.

the accuracy of the age model. Additionally, the age model of MD02-2489 beyond 30 ka BP is not well constrained (see Gebhardt et al., 2008).

For MD01-2416, in order to avoid the contradiction of two age models, we proposed a new age model. The age of the upper part is established by AMS ^{14}C dating (Sarnthein et al., 2004) and ^{14}C plateau boundaries developed by Sarnthein et al. (2007; 2013, 2015), which has been correlated with atmospheric ^{14}C plateaus records from Lake Suigetsu (Bronk Ramsey et al., 2012), for the last 18 ka BP (see Maier et al., 2015). The age beyond the ^{14}C limits is established by visual correlation between benthic $\delta^{18}\text{O}$ records of MD01-2416 and LR04 global stack (Lisiecki and Raymo, 2005) as well as by independently dated geomagnetic paleointensity and inclination events (Gebhardt et al., 2008) for the last 180 ka BP (see Table 4.1 and Fig. 4.2 as well as the corresponding parts in **Chapter 4**). Additionally, for uppermost part, where no ^{14}C plateau is found, four AMS ^{14}C dating points with a reservoir age of 570 ± 140 year, according to the nearest ^{14}C plateau determined by Sarnthein et al. (2013; 2015), was applied to CALIB 7.0 (Stuiver and Reimer, 1993) with the Marine13 calibration curve (Reimer et al., 2013). The paleomagnetic intensity minima events with high quality, as defined by Gebhardt et al. (2008), were chosen as dating points, including the Mono Lake (28.4 ka BP), Laschamp (41 ka BP) and Icelandic Basin (184 ka BP). Linear interpolation was applied between the dating points. The age model of last 18 ka BP are established in Sarnthein et al. (2013, 2015) and Maier et al. (2015), while the age model beyond 18 ka BP is discussed in **Chapter 4**. The sedimentation rates are also described in **Chapter 4**.

For MD02-2489, we also used the AMS ^{14}C dating (Gebhardt et al., 2008) and ^{14}C plateau boundaries developed by Sarnthein et al. (2007, 2013, 2015) for the last 30 ka BP. For the AMS ^{14}C dating, we used same reservoir ages of closest ones calculated by ^{14}C plateau boundaries (Sarnthein et al., 2013, 2015). We correlated the Ca and Fe intensity (Gebhardt et al., 2008; Schmieder et al., unpublished data), measured by the X-Ray Fluorescence (XRF) Core Scanner I at Bremen University (Röhl and Abrams, 2000), with the carbonate content and the magnetic susceptibility (Rea et al., 1995; McDonald, 1997; McDonald et al., 1999), respectively, of the nearby ODP887 (54°21.92'N, 148°26.78'W, water depth 3647 m). The age model of ODP887, beyond the limit of ^{14}C dating, has been determined on correlation of $\delta^{18}\text{O}$ profile with the SPECMAP stacked $\delta^{18}\text{O}$ curve (Imbrie et al., 1984; McDonald, 1997). Galbraith et al. (2008) re-made the age model of ODP887 by assigning it to the newly developed LR04 $\delta^{18}\text{O}$ record (Lisiecki and Raymo, 2005). Here we use the LR04-based age of MD02-2489 (Table 5.2), in order to accord with the age of MD01-2416, which has the same basis. Similar with MD01-2416, high sedimentation rates are found during the Bølling/Allerød (B/A; 14.7-12.9 ka BP) warm period (ca. 40 cm/ka; Fig. 5.2) probably due partly to high productivity and to oversampling by the coring equipment on the R/V *Marion Dufresne* (Székely et al., 2004). The sedimentation rates are lower than 20 cm/ka before the Heinrich Event 1 (H1; 19-14.7 ka BP; Fig. 5.2).

The age model of RAMA44 was presented by Keigwin et al. (1992) by ^{14}C dating based on *Globigerina bulloides* and mix planktonic foraminifer with 700 yr reservoir age. Here we recalibrated this

age model with CALIB 7.0 (Stuiver and Reimer, 1993) and the MARINE13 calibration curve (Reimer et al., 2013), using a constant reservoir age of 700 yr. It extends to 17 ka BP.

All the age models were established by linear interpolation between the calibrated calendar ages.

5.4. Results

5.4.1. Diatom Assemblages

In total 48 marine diatom taxa were identified from the studied cores.

In the WNP, the diatom record of MD01-2416 has been shown in **Chapter 4**, with high abundance of relative warm water species *Neodenticula seminae* and *Coscinodiscus marginatus* during the interglacial. *Chaetoceros* resting spores, *Thalassiosira trifulta*, *Actinocyclus curvatulus*, cold water species (*Bacterosira bathyomphala*, *Porosira glacialis*, *T. antarctica* var. *borealis* resting spores, *T. hyalina* and *T. nordenskiöldii*) and sea ice species (*Fragilariopsis cylindrus* and *F. oceanica*) are more abundant during the glacial (Fig. 5.3). The RAMA44 record for the last 14 ka BP shows a gradual decrease of *N. seminae*, from 70% to 40%. Meanwhile, *Chaetoceros* resting spores and some cold species (mainly *T. antarctica* var. *borealis* resting spores and *T. nordenskiöldii*; Fig. 5.3) increase moderately. Sea ice species are rarely found in the Holocene records.

In the ENP, the diatom compositions of MD02-2489 are characterized by dominant *Neodenticula seminae* (~70%) in MIS 5 (130-71 ka BP) and the Holocene, while *A. curvatulus*, *T. trifulta* and cold water species are more frequently encountered during MIS 2, 3 and 4 (Fig. 5.3).

In general, diatom variabilities from the ENP and WNP show similar glacial-interglacial patterns. However, obvious regional differences of diatom composition are found:

1) *Chaetoceros* resting spores are generally less common in the ENP with a maximum abundance <30%, whereas they are up to 60% in the WNP. It is likely due to its location far away from the Asian dust sources (e.g. Serno et al. 2014), which has been reflected by the surface diatom records from the northern North Pacific (**Chapter 3**).

2) *Neodenticula seminae* is abundant during MIS 3 (57-29 ka BP) in the ENP, while it drops to <20% in the WNP, showing a basin-wide paleoceanographic contrast (Fig. 5.3).

The diatom concentrations range from 10 to 80×10^6 valves/g dry sediment in both the ENP and WNP (Fig. 5.3). While low diatom abundances occur in the cold period and the Holocene (< 20×10^6 valves/g in the WNP and < 10×10^6 valves/g in the ENP), high concentration events are found during the B/A and MIS 5 (60 to 80×10^6 valves/g in the WNP and 50×10^6 valves/g in the ENP). In particular, two concentration maxima at ca. 86 to 89 ka BP and 102 to 108 ka BP, are identified in both the ENP and WNP (Fig. 5.3).

In addition, the diatoms in the samples of the LGM (23-19 ka BP) and MIS 4 (71-57 ka BP) suffers extreme dissolution and therefore are mostly moderately dissolved, especially the fragile sea ice indicators (*F. cylindrus* and *F. oceanica*). The heavily silicified species (*A. curvatulus* and *T. trifulta*), which are resistant to dissolution, by contrast, reach their abundance peaks in the same period (Fig. 5.3).

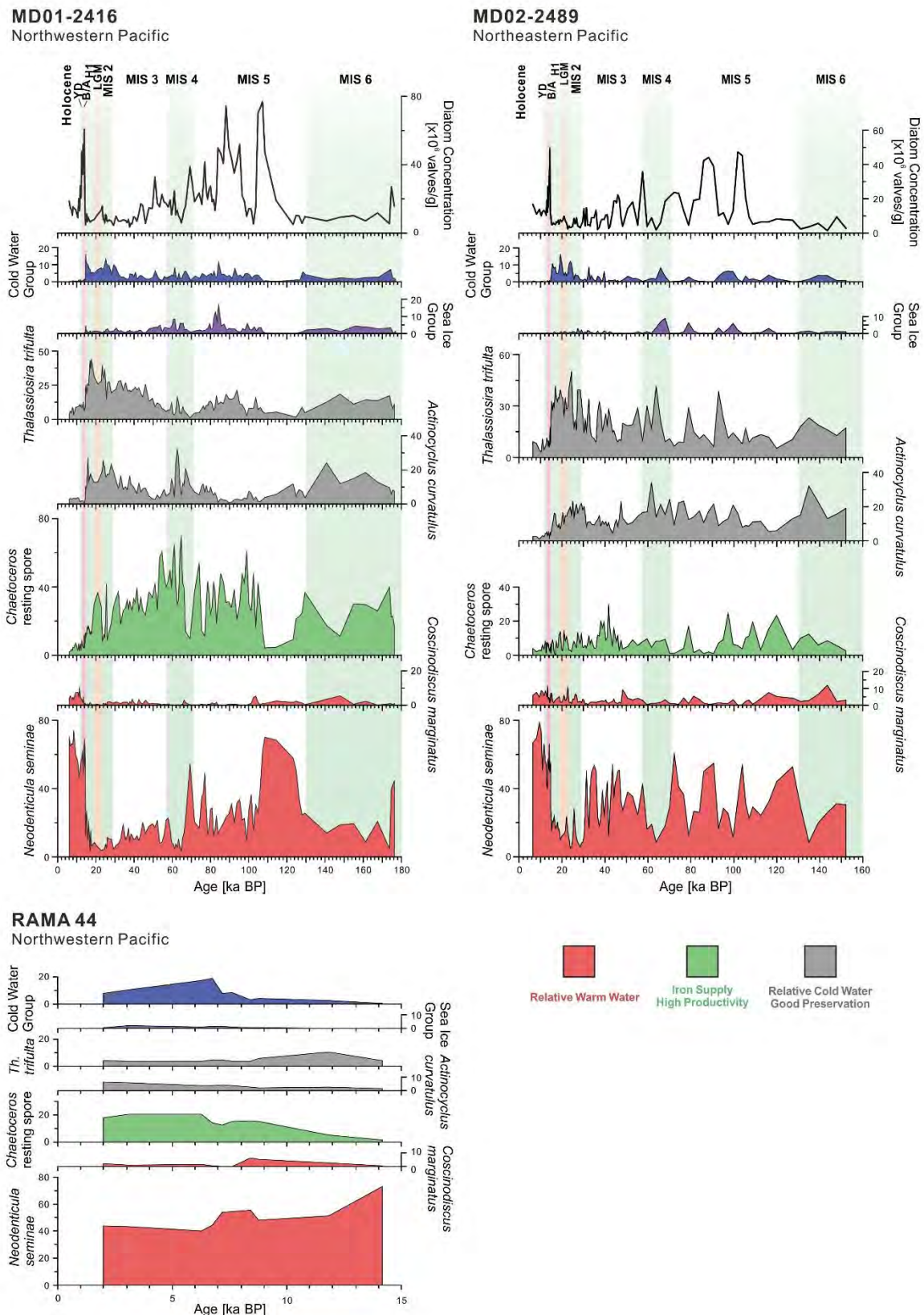


Fig. 5.3 Diagram of relative abundances of selected diatom species and species groups of MD01-2416, MD02-2489 and RAMA44. The cold water group includes *Bacterosira bathyomphala*, *Porosira glacialis*, *Thalassiosira antarctica* var. *borealis* r. sp., *T. bulbosa*, *T. hyaline*, *T. nordenskiöldii* (**Chapter 3**). The sea ice group consists of *Fragilariopsis cylindrus* and *F. oceanica* (**Chapter 3**). The Marine Isotope Stages and climate events are indicated in shaded bars: LGM-Last Glacial Maximum, H1-Heinrich Event 1, B/A- Bølling/Allerød, YD-Younger Dryas.

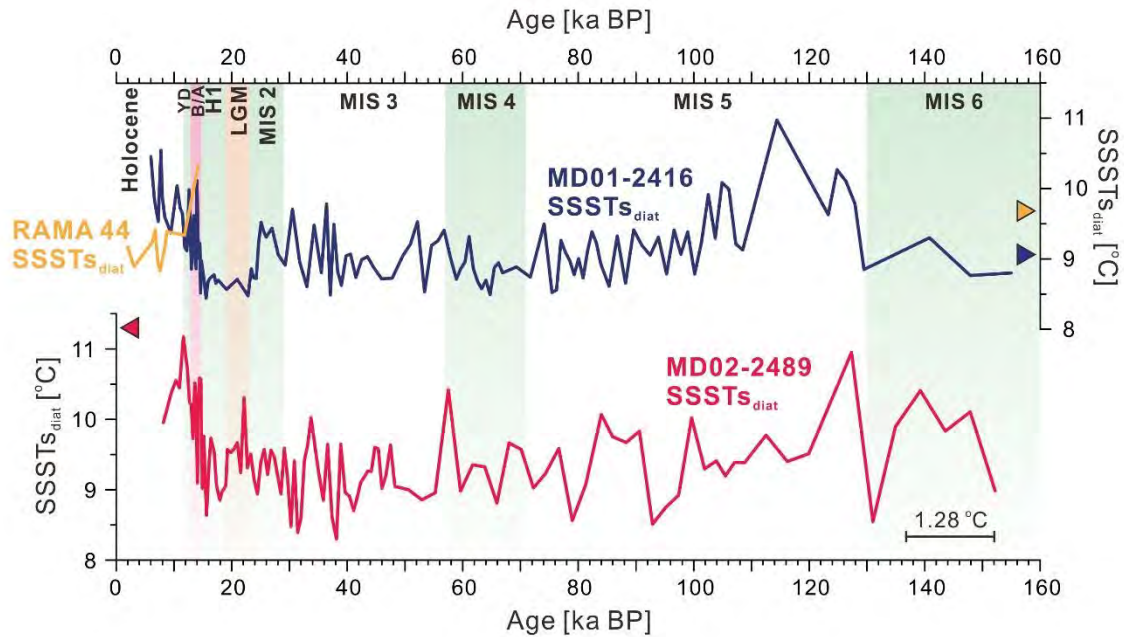


Fig. 5.4 Reconstructed SSST variability of MD01-2416 (in blue), MD02-2489 (in red) and RAMA44 (in orange). The modern SSST of the coring sites as well as the systematic error bar are displayed. The Marine Isotope Stages and climate events are shown in shaded bars: LGM-Last Glacial Maximum, H1-Heinrich Event 1, B/A-Bølling/Allerød, YD-Younger Dryas.

5.4.2. SSST reconstruction

The diatom-derived SSST (SSST_{diat} hereafter) is reconstructed based on the diatom data set of 206 samples, which is developed in **Chapter 4**. The results are averaged estimates by the ANN and MAT, with a combined systematic error of ± 1.28 °C, according to **Chapter 4**.

The SSST_{diat} of the WNP reaches 10.5 to 11 °C in MIS 5 and the early Holocene, whereas its minimum, 8.5 °C, is found in the LGM and H1. Abrupt warming is recorded in both Termination I and II, indicating temperature rises of 2 °C. During the Holocene, two temperature records of the WNP show different trends: while SSST_{diat} of RAMA44 decreases from 10 to 9 °C, the temperature of MD01-2416 increases from 9.5 to 10.5 °C (Fig. 5.4). The warmest surface environment of the ENP, ca. 11 °C, occurs in the early MIS 5 and the onset of the Holocene, which is as warm as the modern SSST. The lowest SSST_{diat} is recorded in MIS 3. Sudden SSST increases are encountered in the terminations, rising from 9 to 11 °C (Fig. 5.4).

The SSST_{diat} from both the ENP and WNP show a similar pattern, indicating warm environments during MIS 5, the B/A and the early Holocene and cooling in the H1, MIS 2 and 4. Both long records (MD01-2416 and MD02-2489) indicate a glacial-interglacial SSST amplitude of ca. 2 °C. An insignificant cooling pulse of Younger Dryas (YD; 12.9-11.7 ka BP) is only visible in the WNP (Fig. 5.4). A slight increase of temperature was reconstructed in MIS 3 in both records, while another warming is detected in MIS 6 in the ENP (Fig. 5.4). However, temporal discrepancies of ENP and WNP records are found during the terminations. The onsets of warming are hundred years earlier in the ENP than its western counterpart

during both Termination II and I (Fig. 5.4). During the Holocene, a continuous decreasing of $SSST_{diat}$ is reconstructed in MD02-2489 and RAMA44, while a general warming in MD01-2416.

5.5. Discussion

5.5.1. Paleoceanographic changes in the northern North Pacific

5.5.1.1. Marine Isotope Stage 5 and 6

A warming is encountered in both the ENP and WNP during Termination II (Fig. 5.5c). While the $SSST_{diat}$ increasing is more gradual in the WNP, the ENP, however, is featured by a pre-warming, between 152 to 130 ka BP, with an amplitude of 1.5 °C (Fig. 5.5c). This “pre-warming” has also been reconstructed by recent studies in the western Bering Sea (Max et al., 2014) and in the Arctic Lake El’gygytgyn in northeastern Russia (Melles et al., 2012), in spite of the different timing of the warming periods (Fig. 5.5a and 5.5b). Interestingly, these records are located more closely to the WNP, where no similar pre-warming is found. This phenomenon is probably due partly to the low sampling resolution and partly to the uncertainty of the age model. More works are needed for further study to confirm whether there is a pre-warming in the entire northern North Pacific in terminations or an eastern-western asynchronicity as we found during Termination I (see discussion 5.2).

During MIS 5.5 (128.5-115 ka BP; NEEM community members, 2013), the $SSST_{diat}$ of the WNP displays a ca. 2 °C warmer environment than modern $SSST$, which is in agreement with records from the western Bering Sea (Max et al., 2014) regardless of the different $SSST$ amplitudes (Fig. 5.5a and 5.5c). Additionally, if we disregard the result that the whole $SSST_{diat}$ of the ENP are below the modern $SSST$, which might be a systematic bias (**Chapter 4**), the ENP also shows a ca. 2 °C warmer MIS 5.5 than MIS 4 (Fig. 5.5c). Furthermore, NEEM ice core record shows that the air temperature in MIS 5.5 is 8 ± 4 °C higher than the mean of the past millennium at the surface of the Greenland ice sheet (Fig. 5.5j; NEEM community members, 2013). Warming in MIS 5.5 is also found in the lake record from the Siberia (Melles et al., 2012). All these results indicate an atmosphere-ocean coupled Arctic/Subarctic warming in MIS 5.5.

High diatom concentrations are recorded in both the ENP and WNP in MIS 5 extending to early MIS 4 (Fig. 5.5d), which are synchronous with a substantial opal peak from the ODP882, WNP (Fig. 5.1; Jaccard et al., 2009). This may indicate high export production and/or good preservation. Diatom blooms are generally limited by nutrients, including macronutrients (nitrate, phosphate and silicate) and micronutrients (e.g. iron), lights, sea surface temperatures and duration of sea ice cover. The North Pacific is a High-Nutrient-Low-Chlorophyll (HNLC) ocean, of which the primary productivity is controlled by iron supply. However, an iron supply indicator, *Chaetoceros* resting spores, did not correlate to the diatom concentration variability (Fig. 5.5h). In addition, no corresponding increase of eolian dust is recorded in a nearby core (Station 3; 50°00’N, 164°59’E; Shigemitsu et al., 2007) and only slight dust flux from the Greenland ice core has been found during these periods (Fig. 5.5k; Ruth et al., 2007). Therefore iron input

might only play a minor role in these productivity events. By using diatom-derived silicon isotope ($\delta^{30}\text{Si}$), a recent study on ODP882 associates these productivity events in MIS 5 with the collapse of the stratification and hence increased nutrient supply from the deep ocean to the surface layer in the study region (Swann and Snelling, 2015).

Interestingly, two peaks of diatom concentration in the WNP occur several thousand years earlier than that of the ENP (Fig. 5.5). The reason of that remains unclear. As discussed above, although iron only has minor impact on these productivity events (Lam et al., 2013; Swann and Snelling, 2015), iron fertilization experiments *in situ* indicate that iron limitation do control diatom blooms (e.g. Tsuda et al., 2003). The modern dust flux pattern from the surface samples indicate different dust sources in the northern North Pacific (Serno et al., 2014), implying a possible east-west dust source asymmetry (e.g. eolian dust dominates the WNP while lithogenic components prevail in the ENP), which too has been modeled (Mahowald et al., 2005). Crusius et al. (2011) also suggest a dust source from the glacially-derived sediment at the mouths of nearby rivers of the Gulf of Alaska in the ENP. Thus, different sources of iron may trigger diatom blooms in the ENP and WNP, resulting in a lead-and-lag pattern of diatom productivity on millennial scale. However, the lead-and-lag pattern may switch due to the variation of iron inputs from different sources. Therefore, we saw earlier diatom concentration peaks in the WNP in MIS 5 and a leading diatom bloom in the ENP during Termination I (Fig. 5.5d). Silicate is another factor that controls the growth of diatoms (e.g. Hoffmann et al., 2008). In the modern northern North Pacific, silicate is abundant in the WNP and the western Bering Sea (Fig. 3.2a; Garcia et al., 2006). Similar to iron, the uneven distribution of silicate may also cause the lead-and-lag pattern of diatom productivity in the ENP and WNP.

Our recent study suggests that the cumulative relative abundance of sea ice diatom of 20% may represent the winter sea ice extent in the Bering Sea (**Chapter 3**). This assumption, however, may not be applied to the northern North Pacific due to no presence of modern winter sea ice. But the modern relationship between the relative abundance of sea ice indicators and the distance from the winter sea ice edge may imply the past sea ice extent in the area (**Chapter 3**). During MIS 5, sea ice indicators are mostly in low abundance (<5%; Fig. 5.5), suggesting a distance of ca. 500 km from the core locations to the past winter sea ice edge (Fig. 3.10), which is similar to the modern distance. Therefore, it is likely that no sea ice expanded to the open ocean of the northern North Pacific during the entire MIS 5. However, a peak abundance of sea ice and cold water species is recorded at the boundary of MIS 5.2 and 5.1 (ca. 84 ka BP) in the WNP (Fig. 5.5). This cold event is also recorded in the western Bering Sea by high value of IP_{25} (Max et al., 2014). But no corresponding evidences found in the ENP may suggest it might be a local signal of drifting sea ice.

5.5.1.2. Marine Isotope Stage 3 and 4

The Greenland ice core records show that MIS 3 and 4 are characterized by rapid climate fluctuations, named as Dansgaard-Oeschger events (D-O events; e.g. Dansgaard et al., 1993; NGRIP members, 2004). Diatom abundances of certain species, for instance *N. seminae*, display a possible correlation with these

climate fluctuations (Fig. 5.5g). It seems that *N. seminae* mirrors not only the scale of glacial-interglacial marine isotope variability (Sancetta and Silverstri, 1984) but also parts of the D-O oscillations. This rapid variability of *N. seminae* is not a consequence of dissolution, since most samples of MIS 3 and 4 are moderately preserved. Instead, it is likely caused by a reorganization of the atmosphere system as well as the shifts of discharge due to the advance and retreat in mountain glacier in the Alaska. This may explain why the correlation between *N. seminae* and D-O events is better in the ENP, where the Aleutian mountain glacier were located, than the WNP (Fig. 5.5g and 5.5i). Recently, a study attributes the D-O events to the height changes of the Northern Hemisphere Ice Sheets and the consequent altered atmospheric system (Zhang et al., 2014). Therefore, the reorganized atmosphere system was also likely to influence the northern North Pacific. The XRF calcium (Ca) peaks also corresponds to the D-O events, which may imply high productivity events. However, further discussion is hampered by the relatively low resolution of our samples. On the other hand, although *Chaetoceros* resting spore occurrence is influenced by iron input (Tsuda et al., 2003; **Chapter 3**), it do not show clear response to the Greenland dust records (Ruth et al, 2007), indicating other unknown factors controlling the blooming and preservation of the spores (Fig. 5.5h).

Sea ice diatoms, together with cold water diatoms, increase in abundance during MIS 4, especially in the ENP, reaching there its maximum of the entire record (Fig. 5.5e-f). But according to the relationship of the distance to the winter sea ice edge and the abundance of sea ice diatoms, the core locations might still be 500 km far away from the past sea ice edge in MIS 4. Thus, these events indicate a sea ice expansion event, driving more floating sea ice to the core locations, rather than an environment of winter ice coverage.

5.5.1.3. The LGM and Termination I

A less cold LGM is found in the ENP with a ca. 0.5 °C higher SSST_{diat} than the subsequent H1 cold period, in spite that warm water indicator *N. seminae* are constantly rare in both periods, while the WNP SSST_{diat} of the LGM is as low as that of the H1 (Fig. 5.6a-b). Comparable alkenone-derived SSST estimates, on the contrary, are to some extent different, indicating the LGM warmer than the H1 in the ENP (Fig. 5.6c; Méheust, 2014; Maier et al., 2015). However, as argued by Harada et al. (2012), the warmer alkenone-derived SSST records in the LGM are probably biased by the change of blooming season of coccolithophore (*Emiliana huxley*). The subsurface temperatures reconstructed from nearby cores also show a warmer LGM relative to the following H1 (Riethdorf et al., 2013b). The LGM subsurface warming of 2 °C has been reconstructed in western North America (Taylor et al., 2014). This relative warm also corresponds to a light $\delta^{18}\text{O}$ excursion of subsurface *Neogloboquadrina pachyderma* (s) (Fig. 5.6d; Gebhardt et al., 2008). It seems that in the LGM both the surface and subsurface ocean turned warm in the ENP, which might relatively reduce the stratification compared to the H1.

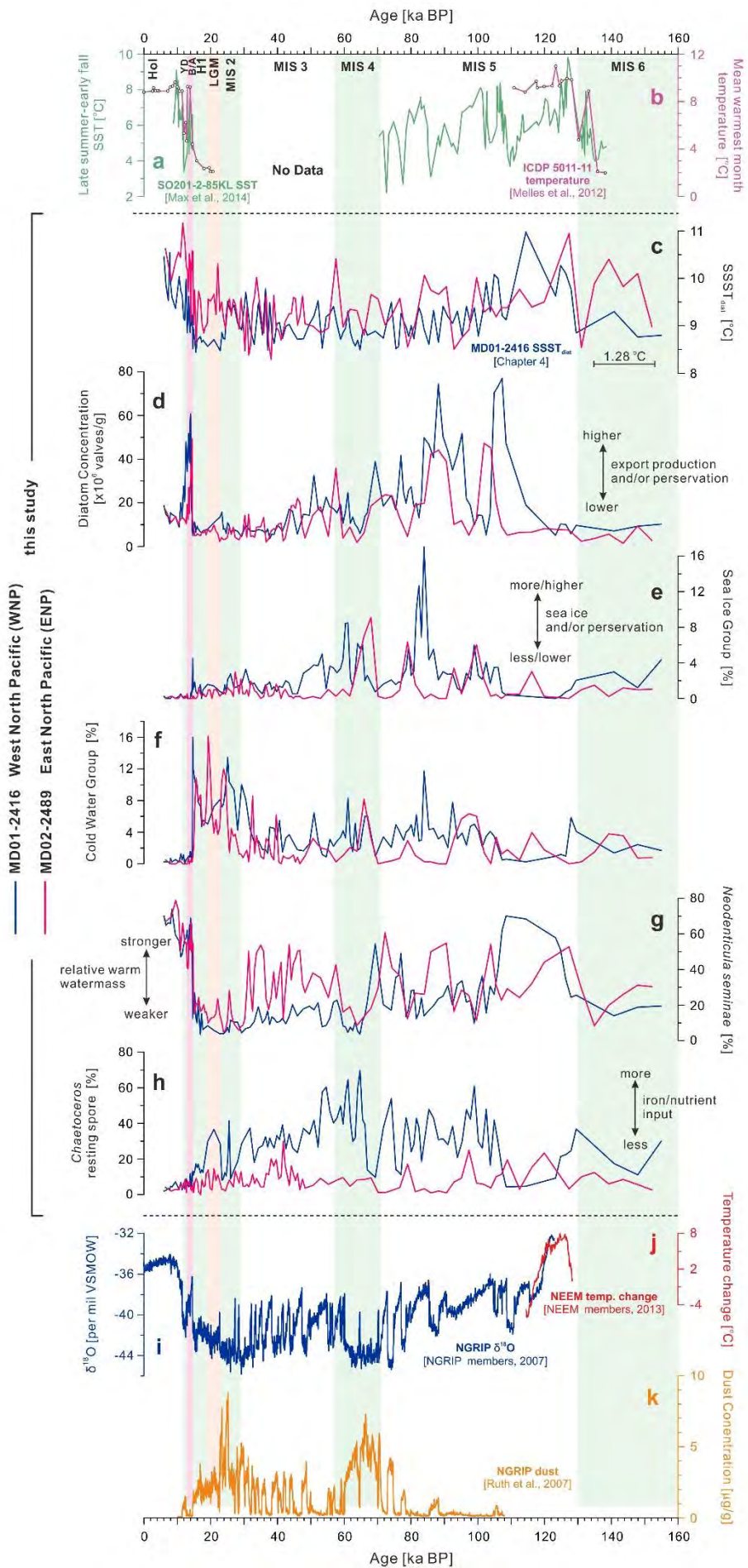
Sea ice species are abundant in neither the LGM nor H1, while the cold water species reach maximum abundance showing a cold environment (Fig. 5.4; Fig. 5.6e-f). The diatom preservation is poor during this period, implying the dissolution of sea ice diatoms which might reduce the sea ice signal. However, most cold water species, mainly *Thalassiosira antarctica* var. *borealis* resting spore with heavily silicified valves,

are resistant to dissolution. Although they are not true sea ice inhabitant species, they are related to the cold water mass produced in the sea ice area. Thus, the abundant occurrences of these species at least indicate an environmental deterioration. In addition, the sea ice indicator IP₂₅ derived from ENP cores display fluctuations similar to the cold water diatom rather than to the sea ice diatom (Fig. 5.6g), indicating a possible close relationship between IP₂₅ and cold water species. Further studies are needed to establish a quantitative relationship between cold-water species and sea ice conditions, in order to compensate the loss of sea ice diatoms due to the dissolution effect. Nevertheless, all sea ice indicators reach high values in the H1 during Termination I, including the IRD records (Fig. 5.6h), implying a possible sea ice expansion in the entire northern North Pacific area, which is in agreement with previous studies (Max et al., 2012; Méheust, 2014).

Abrupt changes in diatom composition at the H1-B/A boundary (ca. 14.7 ka BP) are found in the entire northern North Pacific as well as in the Bering Sea (Fig. 5.6b; 5.6e-f; Sancetta, 1983b; Katsuki and Takahashi, 2005; Max et al., 2012; this study). *Neodenticula seminae* jumped from 10% to 60%, while the cold water and sea ice species almost disappeared (Fig. 5.6e-f), indicating a warmer sea surface environment. These events correspond to a rapid rise of sea surface and subsurface temperatures (Fig. 5.6a, c, d). SSST_{diat} of the ENP increases ca. 1.5 to 2 °C and a similar but more gradual increase of SSST_{diat} is reconstructed in the WEP (Fig. 5.6a), although the amplitude of SSST_{diat} increases are smaller compared to those temperatures derived from other proxies. This rather low amplitude is likely due to the shift of the blooming seasons from late spring/early summer in the interglacial to summer in the glacial as well as to the dissolution of weakly silicified species, which may reduce the cooling signal of the glacial period (**Chapter 4**). The diatom concentration, which peaks in the B/A and early YD, corresponds to the maximum SSST_{diat} in Termination I (Fig. 5.6i). This is in agreement with the maximum opal content from the same cores (Fig. 5.6j; Gebhardt et al., 2008), indicating a preferential environment for diatom blooming, which has also been revealed by silicon isotope derived from diatom frustules ($\delta^{30}\text{Si}$; Maier et al., 2015).

These sudden shifts are also reflected by different proxies elsewhere in the North Pacific (e.g. Kiefer and Kienast, 2005; Gebhardt et al., 2008; Caissie et al., 2010; Max et al., 2012; Lam et al., 2013; Méheust, 2014; Rae et al., 2014; Maier et al., 2015). They are widely accepted as a response to the abrupt deglacial changes at the H1-B/A boundary found in the northern Hemisphere (Alley and Clark, 1999; Denton et al., 2010). However, several studies have argued that these fast climate shifts in the northern North Pacific

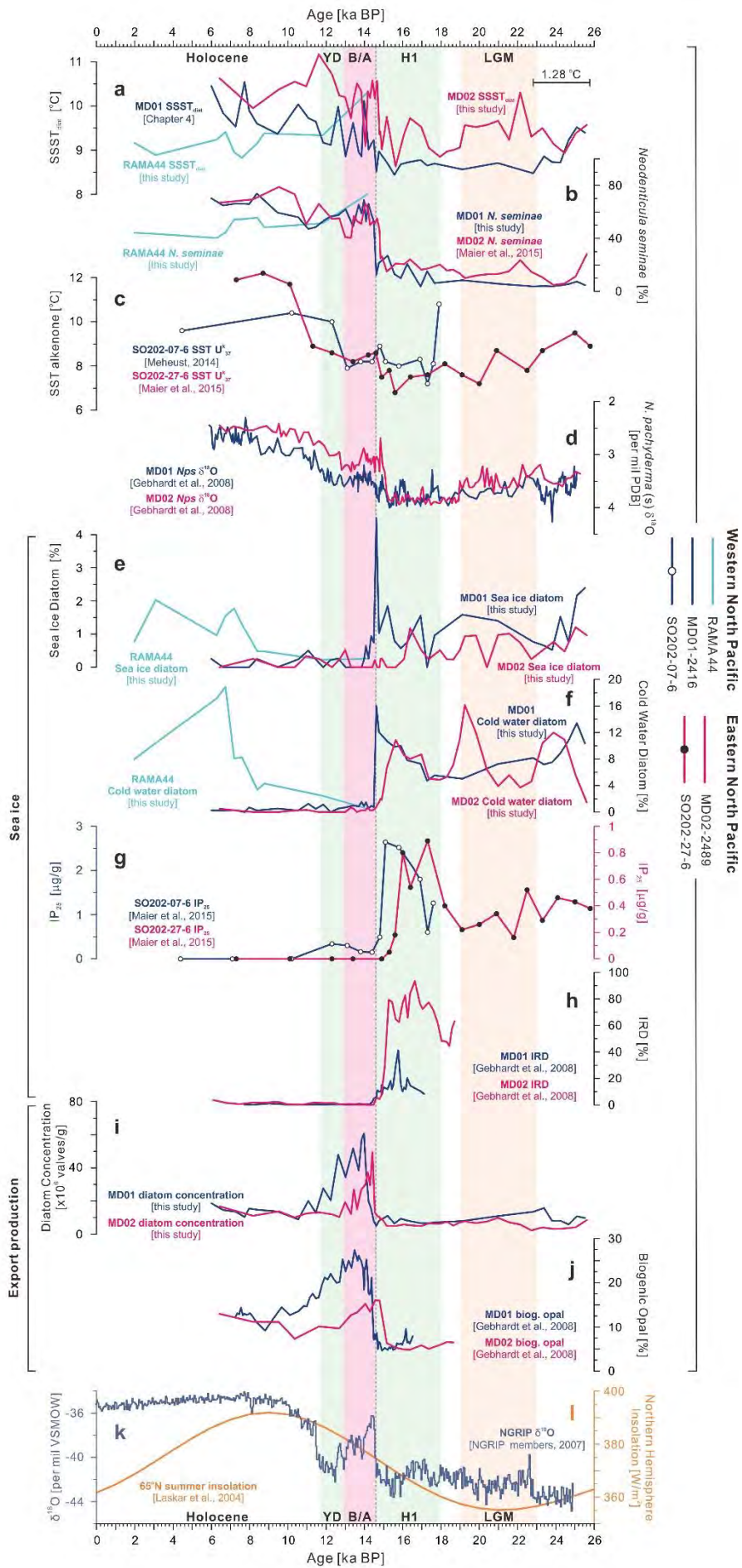
Fig. 5.5 Comparison of diatom-based proxy records of MD01-2416 (in blue) and MD02-2489 (in red), including (c) reconstructed SSST_{diat} (°C), (d) diatom concentration (x10⁶ valves/g), (e) sea ice diatom group (%), (f) cold water diatom group (%), (g) *Neodenticula seminae* (%) and (h) *Chaetoceros* resting spores (%), with (a) late-summer-early-fall sea surface temperature from the western Bering Sea (Max et al., 2014), (b) mean warmest month temperature from arctic Lake El'gygytyn (Melles et al., 2012), (i) $\delta^{18}\text{O}$ and (k) dust concentration of NGRIP (NGRIP members, 2007; Ruth et al., 2007) and (j) Greenland air temperature change (NEEM members, 2013) for the last 160 ka BP. The Marine Isotope Stages and other climate events are shown in shaded bars: LGM-Last Glacial Maximum, H1-Heinrich Event 1, B/A- Bølling/Allerød, YD-Younger Dryas.



starts earlier than the H1-B/A boundary (Sarnthein et al., 2006; Gebhardt et al., 2008; Maier et al., 2015; this study), while other results from the same area (Max et al., 2012; Riethdorf et al., 2013b; Lam et al., 2014) and the Greenland records (Fig. 5.6k; NGRIP members, 2007) show abrupt changes sharply at the H1-B/A boundary. Although this discordance is probably due to the age models used in different cores, pollen records from the annually laminated sediment in Lake Suigetsu, Japan show the onset of Bølling event with a few centuries earlier (Nakagawa et al., 2003), which may imply the northern North Pacific responded more quickly to intensified solar insolation during Termination I (Fig. 5.6l; Laskar et al., 2004).

In spite of a small cooling of SSST_{diat} in MD01-2416 from the WNP, a clear YD pattern is reflected neither by the diatom compositions nor by the SSST_{diat} of MD02-2416 and RAMA44 (Fig. 5.6a-b; 5.6e-f). Alkenone-derived SSST from nearby cores (SO202-07-6 and SO202-27-6; Fig. 5.1) also do not show obvious YD cooling (Fig. 5.6c; Harada et al., 2012; Méheust, 2014; Maier et al., 2015). Neither do the summer and winter sea surface temperature based on dinoflagellate cysts (de Vernal and Pedersen, 1997). However, other studies from the northern North Pacific and the Bering Sea do indicate obvious low SSST in the YD (e.g. Kallel et al., 1988; Cassie et al., 2010; Max et al., 2012). For the discrepancy, there are two possible causes. One is the relative low resolution of our samples, which may fail in resolving the cold signal of YD. The other reason is the seasonality of different proxies, as diatom reconstructions mainly derived for summer (**Chapter 3**, **Chapter 4**) and alkenone based SSST estimates are for annual temperature (e.g. Müller et al., 1998) or late summer-fall environment (e.g. Harada et al., 2003, 2006). However, the abrupt climate changes such as YD are more weighted toward the winter season, with no substantial summer changes (Denton et al., 2005). This hypothesis has been strengthened by the records for 8.2 ka BP cooling event, which show sharp signals in winter-dominated proxies and broad or reduced anomaly in summer-dominated ones (Rohling and Pälike, 2005). Therefore, besides the low sampling resolution, our diatom records which mainly represent the summer environment (**Chapter 3**) may consequently fail to resolve the abrupt YD cold event.

Fig. 5.6 Comparison of proxy records from the Northwestern Pacific (WNP; MD01-2416, SO202-07-6 and RAMA44 in dark blue, dark blue with dots and light blue, respectively) and the Northeastern Pacific (ENP; MD02-2489 and SO202-27-6 in red and red with dots, respectively) for the last 26 ka BP: **(a)** SSST_{diat} (°C; Chapter 4; this study); **(b)** *N. seminae* (%; Maier et al., 2015; this study); **(c)** alkenone-SST (°C; Méheust 2014; Maier et al., 2015); **(d)** $\delta^{18}\text{O}$ of *N. pachyderma* (s) (‰PDB; Gebhardt et al., 2008); **(e)** sea ice diatom (%; this study); **(f)** cold water diatom (%; this study); **(g)** IP₂₅ ($\mu\text{g/g}$; Maier et al., 2015); **(h)** IRD (%; Gebhardt et al., 2008); **(i)** diatom concentration ($\times 10^6$ valves/g; this study); **(j)** biogenic opal (%; Gebhardt et al., 2008). The $\delta^{18}\text{O}$ of NGRIP (in gray blue; NGRIP members, 2007) and Northern Hemisphere insolation (in orange; Laskar et al., 2004) are plotted in **(g)** as references. Sea ice and export production proxies are indicated in the left panel. Climate events are shown in shaded bars: LGM-Last Glacial Maximum, H1-Heinrich Event 1, B/A- Bølling/Allerød, YD-Younger Dryas.



5.5.1.4. The Holocene

Our records only cover part of the Holocene. While MD01-2416 shows continuous warming with fluctuations, RAMA44 and MD02-2486 display cooling towards the mid-Holocene (Fig. 5.6a). Diverse response to the Holocene climate in the North Pacific has been reviewed by Max et al. (2012), showing a consistent cooling trend for the last 7 ka, which is in line with the $SSST_{diat}$ record of RAMA44. The records of MD01-2416 and MD02-2489 from the ENP and WNP lack the late Holocene interval, preventing a basin-wide comparison for the whole Holocene. However, we do see an opposite $SSST_{diat}$ trend between the ENP and WNP (Fig. 5.6a), implying a possible basin-wide seesaw or inconsistency, which has been discovered during the terminations (see 5.2). High resolution sediment and accurate age models are needed for more detailed investigation. The $SSST_{diat}$ contradiction between the nearby RAMA44 and MD01-2416 might be partly attributed to the different influencing water mass in the WNP, such as changes in the East Kamchatka Current (Fig. 5.1).

Sea ice indicators and cold water species almost disappeared in the Holocene (Fig. 5.6e-f). Dissolution effect may be ruled out since the preservation condition in the Holocene is moderate to good. Therefore, these signals, as well as the absence of IP_{25} , indicate an ice-free sea surface environment.

5.5.2 Asynchronous deglaciation in the eastern and western North Pacific

Our diatom results of MD01-2416 and MD02-2489 from the WNP and ENP, respectively, show a clear basin-wide climate variability over the last 160 ka (Fig. 5.5). However, within the age uncertainties, Termination I occurs 0.25 ka and Termination II 3.5 ka earlier in the ENP than in the WNP (Fig. 5.7a-b). *Neodenticula seminae*, an endemic North Pacific species indicating subarctic water mass (**Chapter 3**), is in phase with the LR04 stack (Lisiecki and Raymo, 2005) in the ENP at Termination II while its abundance increase occurs 3.5 ka later in the WNP (Fig. 5.7b). This lead-and-lag phenomenon is also recorded in the $SSST_{diat}$ (this study) and XRF Ca profiles (Gebhardt et al., 2008; Fig. 5.7b). Earlier Ca rises are also found in Termination II in the western Bering Sea, where the oceanographic environment is similar to the WNP (Riethdorf et al., 2013a). Galbraith (2006) also shows a temporal discrepancy of $CaCO_3$ concentration at Termination II, during which the ENP records lead the WNP counterpart by ~ 7 ka. However, his age models were established by different chronological methods (Jaccard et al., 2005; Galbraith et al., 2008), which may increase the uncertainties (E. Galbraith, personal communication). A carbonate record from the WNP, which shows synchronous increase with our record from the ENP, is also probably due to the age uncertainties resulting from the lack of age control points at Termination II (Brunelle et al., 2010). On the contrary, our age models, which were directly or indirectly based on LR04, are more reliable, although the chronology of MD02-2489 relies on the correlation method by Galbraith (2006), which may introduce age uncertainties (E. Galbraith, personal communication). Furthermore, an eastern-lead/western-lag mode (Fig. 5.7a) is also observed from our results during Termination I, of which the age models are more precisely established (see Material and Methods). The diatom assemblages of MD02-2489 shows an abrupt change

0.25 ka before the H1- B/A boundary, leading the corresponding changes in the diatom record of MD01-2416, which occur at the onset of B/A warming (Fig. 5.7a). In the southern part of the Gulf of Alaska, earlier peaks of carbonate and opal were recorded precisely before the B/A (Cosma et al., 2008; Hendy and Cosma, 2008; Kohfeld and Chase, 2011). Regardless of the uncertainties brought into the age models by visual correlation, earlier deglaciation in the ENP than in the WNP is encountered in several records during Termination I (Fig. 5.6; 5.7a), including diatom composition, diatom based SSST (this study), IRD (Gebhardt et al., 2008), biogenic opal (Gebhardt et al., 2008), diatom-bound $\delta^{30}\text{Si}$ and $\delta^{18}\text{O}$ (Maier et al., 2015) and IP_{25} (Méheust, 2014).

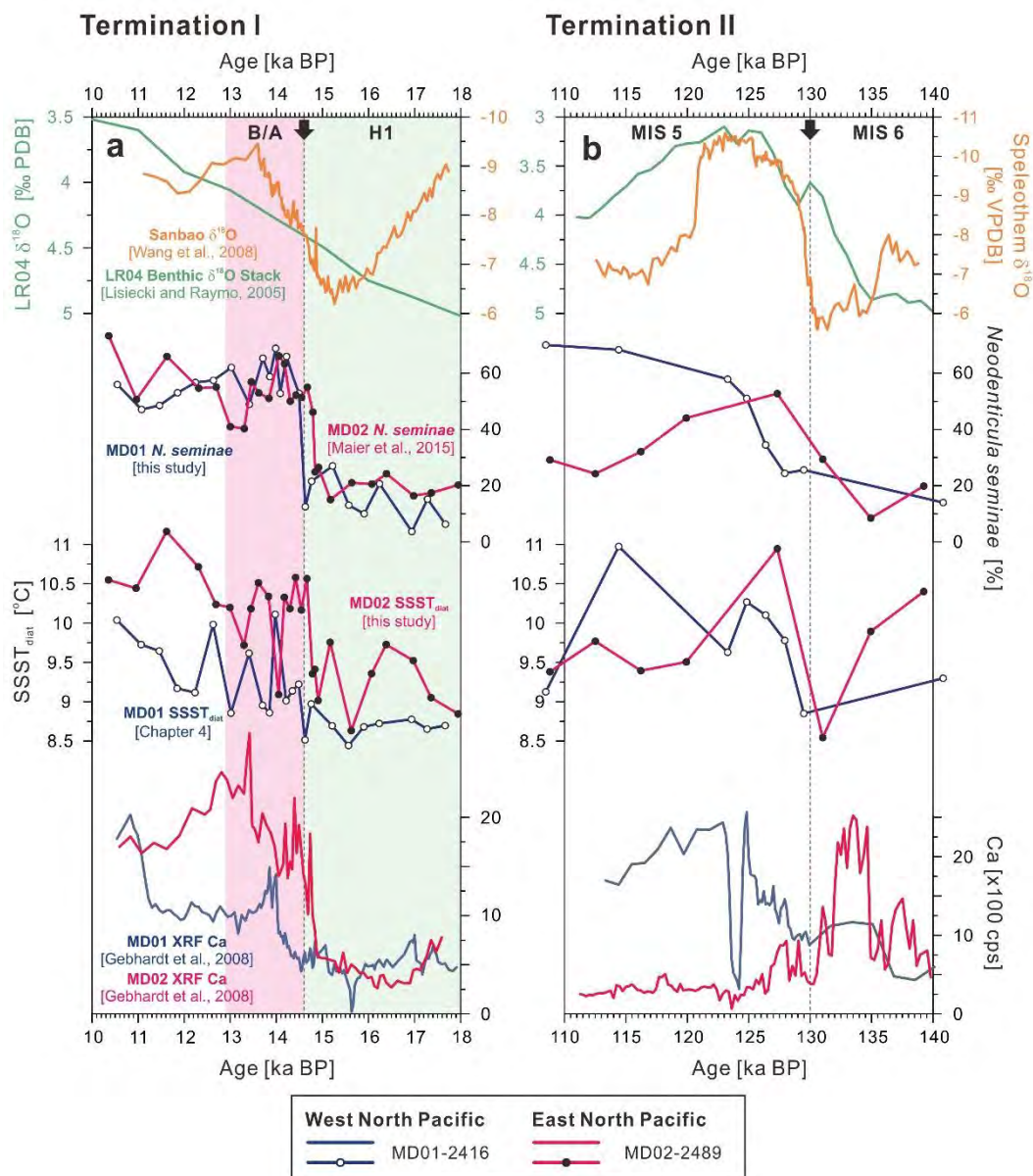


Fig. 5.7 Selected proxies of MD01-2416 (in blue) and MD02-2489 (in red) across Termination I (a) and II (b), including *N. seminae* (%; Maier et al., 2015; this study), SSST_{diat} (°C; Chapter 4; this study) and XRF Ca counts (cps; Gebhardt et al., 2008). Global benthic $\delta^{18}\text{O}$ stack (in green; Lisiecki and Raymo, 2005) and southwest China speleothem $\delta^{18}\text{O}$ record (in orange; Wang et al., 2008) are shown in the upper panel as references. Climate events are shown in shaded bars in a): H1-Heinrich Event 1, B/A- Bølling/Allerød. Black arrows and dash lines indicate abrupt climate change boundaries in the Northern Hemisphere.

To explain this eastern-lead/western-lag deglaciation phenomenon, one might assume a delay of hundred and thousand years for current transportation from the ENP to the WNP. However, it is impossible, considering that studied sediment records are from the same ocean basin. Besides, the atmosphere overlaid above the northern North Pacific is a large-scale system, which has a synchronous teleconnection with the North Atlantic atmospheric system. This teleconnection has been recorded in a laminated sediment core located on the Bering Slope (Kuehn et al., 2014), in which the varve-like laminae show a tight correlation with the Greenland ice core record (NGRIP group members, 2004), as well as in sediment cores from the southeast Alaska margin (Davies et al., 2011) and from off the western North American (Hendy and Cosma, 2008). A recent study suggests, this trans-ocean-basin (i.e. North Pacific and North Atlantic) synchronization occurred from 15.5 to 11 ka BP, corresponding to Termination I (Praetorius and Mix, 2014). Therefore it is unreasonable to assume that the environmental variability in the WNP is concurrent with that of the North Atlantic, while that in the ENP from the same ocean basin are hundred to thousand years earlier (according to this study). Accordingly, neither the ocean currents nor the atmospheric system above the ocean could generate such an eastern-lead/western-lag deglaciation phenomenon. We therefore suggest local signals may drive the onset of the deglaciation in the ENP earlier than that in the WNP. During the last glacial periods, the western North America, including British Columbia, southern Yukon Territory and parts of Alaska, was covered by the Cordilleran Ice Sheet (CIS; e.g. Clague and James, 2002). A record from the offshore western Canada shows the retreat of the CIS after the LGM started at 17.2 ka BP, which was destabilized by a ca. 2 °C ocean warming due to the increasing of Northern Hemisphere summer insolation at mid to high-latitudes (MD02-2496; Taylor et al., 2014). The collapse of the CIS would result in megafloods discharging into ocean and freshening surface layers by as much as 6 psu (practical salinity units; e.g. Lopes and Mix, 2009). Consequently, these huge and intermittent pulse of fresh water may be transported to the Gulf of Alaska via the Alaska Current (Fig. 5.1) and hence introduce the earlier oceanographic changes. However, it is questionable how the signal from the western offshore Canada was transported to the distant Gulf of Alaska. Indeed, these kind of pre-B/A megafloods originally from the CIS were also recorded in the southern Alaska (Wiedmer et al., 2010), which released fresh water to the nearby Gulf of Alaska and reduced the $\delta^{18}\text{O}$ by 0.8‰ on the continental slope (Davies et al., 2011). Our study shows a sudden increase of a littoral species, *Cocconeis costata* (Hendey, 1964), from none to 3% in the MD02-2489 at 16.97 ka BP, which coincides with the surface freshening in the offshore western Canada and southeast Alaska margin, indicating a possible influence on the coring site from the ENP (Fig. 5.8). This has been recently proved by a freshening sea water $\delta^{18}\text{O}$ pulse derived from diatom bound $\delta^{18}\text{O}$ from a nearby core (SO202-27-6; Maier et al., 2015). On the other hand, the $\delta^{18}\text{O}$ of subsurface *Neogloboquadrina pachyderma* from the ENP and WNP decrease synchronously may indicate that the eastern-lead/western-lag deglaciation phenomenon is only constrained in the surface layer, which conforms to our hypothesis of megafloods (Fig. 5.6d).

5.5.3. Coastal species occurrence event

Abundant coastal species, i.e. *Cocconeis costata* and *Rhabdonema* spp. as well as their copula, are encountered in the northern North Pacific during the middle to late MIS 5 (~5% in the WNP and ~15% in the ENP; Fig. 5.8). These species are either absent or rather rare in the other periods of the records. The phenomena have been recorded by other cores in the same area (C. Sancetta, personal communication). In the northern North Pacific, *Cocconeis costata* is found in the coasts of western North America (Lopes et al., 2006; **Chapter 3**) and the Bering Sea (Ren et al., unpub. data) with low abundance, while *Rhabdonema* spp. is less common as a littoral epiphytic species around all coasts (Round et al., 1990). It is still a mystery why these coastal diatoms occur in the sediments which are > 500 km away from the coasts (Fig. 5.1). They might be transported by sea ice or icebergs, which have capacity for long-distance transportation (Lisitzin, 1972). However, the SSST_{diat} and sea ice/cold water diatom abundance do not indicate cold environments suitable for sea ice or icebergs for these periods (Fig. 5.5c; 5.5e-f). On the contrary, our records and the study from the western Bering Sea show relative warm sea surface environment (Max et al., 2014; this study), discarding the sea ice/iceberg transportation. Previous studies also show these coastal epiphytic species might be carried to the core locations by gigantic algae, i.e. kelps, which are tens to hundreds meters long maintaining enough buoyancy to move algae and rocks from coasts to ocean hundreds kilometers further away (Lisitzin, 1972). If this is the case, the occurrence of abundant coastal species events might be attributed to the reorganization of surface current system and/or the variation of

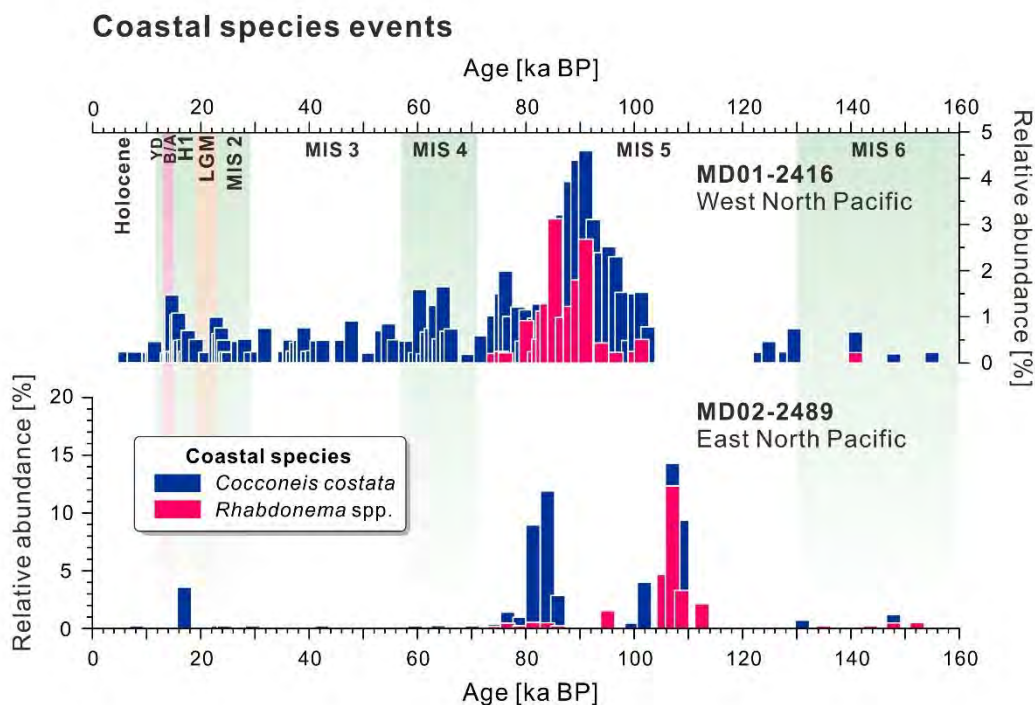


Fig. 5.8 Coastal species events of MD01-2416 and MD02-2489. The blue histograms represent *Cocconeis costata* and the red ones indicate *Rhabdonema* spp. The Marine Isotope Stages and other climate events are shown in shaded bars: LGM-Last Glacial Maximum, H1-Heinrich Event 1, B/A- Bølling/Allerød, YD-Younger Dryas. Note that MD01-2416 and MD02-2489 are in different scales.

productivity of kelps in the area, which in turn are controlled by surface environment and nutrient supply. Therefore, if we clarify the driving mechanism behind, these coastal species occurrence events may be indicators of certain environmental changes. In addition, the events occur asynchronously in the WNP and the ENP (Fig. 5.8), probably due either to the uncertainty of the age models or to the different surface environment and circulation system in two areas. Thus further investigation on these phenomena may improve our understanding of the ocean-atmosphere system in the northern North Pacific. Moreover, if these are basin-wide events, they might be applied as stratigraphic markers for correlation of marine sediments in the study area.

5.6. Conclusions

Our study, for the first time, reconstructs uninterrupted diatom-derived SSST ($SSST_{\text{diat}}$) records of the whole last glacial-interglacial cycle in the northern North Pacific, where calcareous fossils are rare during glacial period. In the western North Pacific (WNP), the highest $SSST_{\text{diat}}$ is found in MIS 5 and the early Holocene, and the lowest temperature occurs in the LGM and H1. The eastern North Pacific (ENP) is warmest in MIS 5 and the onset of Holocene, while the coldest environment of 8.5 °C is encountered in MIS 3. $SSST_{\text{diat}}$ records from both the ENP and WNP indicate a glacial-interglacial SSST amplitude of ca. 2 °C. Diatom compositions and $SSST_{\text{diat}}$ from both the ENP and WNP display continuous glacial-interglacial history for the last 160 ka, corresponding to the global climate change, implying fast teleconnections between ocean basins in the Northern Hemisphere.

With the exception of possible sea ice expansion in H1, the sea ice and cold water diatoms together indicate winter-ice-free environment for the last 160 ka in the ENP and WNP open ocean. Relative high sea ice diatom abundances are found at the boundary of MIS 5.2 and 5.1 in the WNP and in MIS 4 in the entire northern North Pacific, suggesting the influence of drifting ice.

A basin-wide lead-and-lag phenomenon has been discovered in the eastern and western North Pacific during the terminations. The reason that ENP responds to the global change earlier than the WNP is probably due to the faster response to the increase of Northern Hemisphere insolation which causes the nearby mountain glaciers to collapse and hence huge amount of melting water to discharge into the open ocean, thus changing the surface environment earlier.

Abundant coastal species are found in the mid to late MIS 5. The mechanism behind remains unknown. If this is a basin-wide event, we suggest to apply it as a stratigraphic marker in the northern North Pacific open ocean.

In this study, we established an age model of MD02-2489 from the ENP for the last 160 ka. In order to reduce the age uncertainties, which hamper deeper investigation, newly developed dating and correlation methods or techniques in the northern North Pacific (e.g. Kuehn et al., 2014; Sarnthein et al., 2015; Serno et al., 2015) are suggested to apply to the future researches.

Acknowledgements

This paper is a contribution to the INOPEX (Innovative North Pacific Experiment) project funded by the Bundesministerium für Bildung und Forschung (the German Ministry of Education and Research). We thank M. Sarnthein from University of Kiel, Germany, for offering samples of two R/V *Marion Dufresne* cores and A. Hangsterfer from Scripps Institution of Oceanography, USA, for material of RAMA44. E. Galbraith and H. Gebhardt are acknowledged for helpful discussion. We are also grateful to U. Bock from Alfred Wegener Institute for the technical assistance.

Chapter 6. Conclusions and perspectives

6.1. Conclusions

The main aim of this thesis was to improve the understanding of Late Pleistocene glacial-interglacial paleoceanographic variability in the northern North Pacific by studying diatom assemblage changes and by reconstructing summer sea surface temperature (SSST) based on diatom records. To achieve this goal, a total of 422 surface sediment samples were firstly selected to map the modern diatom distribution in the study area (**Chapter 3**). Secondly, 206 of them were chosen as the base of a diatom reference data set for SSST reconstruction (**Chapter 4**), and thirdly diatom-based transfer function was applied to three sediment cores in the northern North Pacific to investigate the Late Pleistocene paleoceanographic variability, providing for the first time continuous SSSTs for the last 160 ka BP in the study region (**Chapter 5**).

In **Chapter 3**, a new diatom data set of 422 surface sediments was generated, covering the northern North Pacific, the Sea of Okhotsk, the Bering Sea and southern part of the Chukchi Sea. The diatom distribution patterns of 38 diatom species and species groups were mapped. Q-mode factor analysis shows three diatom assemblages to be associated with the Arctic, Subarctic and Subtropical water masses, respectively, implying a close relationship between the diatom composition and the sea surface temperatures. Canonical Correspondence Analysis (CCA) indicates 32 diatom species and species groups have stronger correspondence with the pattern of summer sea surface temperature (SSST), than other eight environmental variables, i.e. the summer sea surface salinity, annual surface nutrient concentration (nitrate, phosphate, silicate), summer and winter mixed layer depth and summer and winter sea ice concentrations. Additionally, the total diatom flux data from 10 sediment traps from the northern North Pacific and the Bering Sea demonstrate that the seasonal signals preserved in the surface sediments represent primarily from spring through autumn (Takahashi, 1997; Tsoy and Wong, 1999; Onodera et al., 2005; Onodera and Takahashi, 2009). Therefore, a transfer function in the northern North Pacific for the quantitative paleoceanographic studies might be based on this close relationship between diatom composition and the summer sea surface temperature. Moreover, the relative abundance of the sea ice indicator diatoms *Fragilariopsis cylindrus* and *F. oceanica* of >20% in the diatom composition is employed to represent the winter sea ice edge in the Bering Sea.

According to the close relationship of diatom and SSST in **Chapter 3**, a new diatom-based transfer function for SSST reconstructions was developed from 206 surface sediment samples with 32 taxa and taxa groups recovered in the northern North Pacific and its marginal seas in **Chapter 4**. Three transfer function methods, the Imbrie and Kipp Method (IKM; Imbrie and Kipp, 1971; Klován and Imbrie, 1971), the Modern Analog Technique (MAT; Huston, 1980) and Artificial Neural Network (ANN; Malmgren et al., 2001), were employed to reconstruct SSSTs. The modern SSST estimates are highly correlating with the observations. The transfer functions were then applied to a sediment core from the northwestern North Pacific for the last 180 ka. All three estimates show a clear glacial-interglacial pattern, correlating well

with the local planktonic $\delta^{18}\text{O}$ record (Gebhardt et al., 2008) as well as the NGRIP $\delta^{18}\text{O}$ profile (NGRIP members, 2004). The MAT and ANN display better performance than IKM, thus are suggested for Late Quaternary paleotemperature reconstructions in the northern North Pacific. However, the SSST estimates show low glacial-interglacial temperature amplitudes of 1.5-2 °C, which are similar with previous estimates based on different proxies and methods in the study area. The low glacial-interglacial SSST amplitude is likely due to a shift of the diatom blooming seasons during glacial period and the dissolution of weakly silicified species which could bias the diatom based reconstructions towards warmer temperatures.

Diatom derived SSST reconstruction based on surface diatom data set developed in *Chapter 4* and diatom assemblages were applied to investigate sediment cores from both the eastern and western North Pacific, providing insight on continuous glacial-interglacial variability for the last 160 ka in *Chapter 5*. The diatom derived SSSTs, for the first time, show an uninterrupted temperature reconstruction in the northern North Pacific, covering the whole last glacial-interglacial cycle. Due to the lack of calcareous fossil based SSST in the glacial North Pacific, the reconstruction indicates how temperature fluctuates in the glacial period. The sea ice and cold water species imply ice-free environment in the northern North Pacific open ocean for the last 160 ka with an exception that a possible sea ice expansion during Heinrich Event 1. Interestingly, a basin-wide east-lead-and-west-lag phenomenon has been found in the eastern and western North Pacific during the terminations. It is likely that the faster response to the increased summer insolation in the North Hemisphere caused the mountain glaciers in the Northwestern America to collapse and hence huge amount of melting water to discharge into the eastern North Pacific, thus changed the surface environment earlier than its counterpart.

In addition to results from diatom, age models of MD01-2416 and MD02-2489 for the last 160 ka to 30 ka are established by visual correlation with LR04 benthic $\delta^{18}\text{O}$ stack (*Chapter 4*; Lisiecki and Raymo, 2005) and XRF counts of Ca and Fe from nearby dated cores (*Chapter 5*; Rea et al., 1995; McDonald, 1997; Galbraith et al., 2008), respectively.

In conclusion, the results of this thesis demonstrate that diatom assemblages from sediments are a useful proxy for quantitatively reconstruction of glacial-interglacial surface paleoceanographic variability in the northern North Pacific, where calcareous fossils are poorly preserved. The information of diatom distribution in surface sediments and the close relationship between the sea ice diatom abundance and the observed sea ice concentration in the Bering Sea also allows us to develop a sea ice transfer function in this region. To improve the understanding of the paleoceanography in the northern North Pacific, high resolution and accurately dated samples are demanded for future study.

6.2. Future perspectives

6.2.1. Improvement of SSST reconstruction

The SSST reconstruction performed in *Chapter 4* indicates a low glacial-interglacial temperature

amplitude, which is consistent with some SSST estimates from other proxies in the northern North Pacific. However, the new alkenone SSST records from nearby coring sites, whose Holocene reconstructions are closer to the modern ones, implying a possible reliable estimation, show higher amplitudes (Fig. 5.6a, c; Méheust, 2014; Maier et al., 2015). Therefore the diatom-based SSST still need to be improved for more accurate estimations.

As discussed in **Chapter 4**, the low SSST estimations based on diatom might be technically attributed to the lack of cold end-members in the surface data set and to the dissolution of sea ice related species in the sediment cores. Therefore, diatom distribution data from the Chukchi Sea, of which the diatom compositions are similar to those of the northern North Pacific (Obrezkova et al., 2014), is suggested to be integrated with the diatom data set developed in **Chapter 4**. A recent study of diatom distribution in the Chukchi Sea (Ran et al., 2012) might provide adequate data for extending our data set towards cold environment.

In addition, transfer function techniques besides IKM, MAT and ANN should be tested as well. The weighted averaging with partial least squares (WAPLS) has been successfully applied to develop SSST and sea ice reconstructions in the North Atlantic (e.g. Jiang et al., 2005; Sha et al., 2014) and the Southern Ocean (Esper and Gersonde, 2014a). If the WAPLS reconstructions also show as low SSST amplitudes as those of IKM, MAT and ANN, the results from **Chapter 4** will be strengthened.

To rule out the dissolution effect of sea ice species, sediment cores with better glacial diatom preservation too should be considered for future studies.

6.2.2. Sea ice reconstruction

Sea ice diatoms are a useful tool for sea ice reconstructions in both the Southern and the Northern Hemisphere (e.g. Crosta et al., 2004; Gersonde et al., 2005; Esper and Gersonde, 2014a; Sha et al., 2014). Although the marginal seas of the North Pacific, the Bering Sea and the Sea of Okhotsk, are areas of seasonal sea ice coverage and a region of abundant sea ice diatoms (**Chapter 3**), a sea ice diatom based transfer function has not been developed. However, a close relationship between sea ice diatom abundance and modern winter sea ice concentration discovered in the Bering Sea (Fig. 3.9; 6.1a; **Chapter 3**). CCA results also indicate this relationship (Fig. 3.7), which allows the establishment of a transfer function for sea ice concentration reconstruction derived from sea ice species. In addition, the surface diatom data of the Bering Sea (**Chapter 3**) as well as data of the Chukchi Sea (Ran et al., 2012) provide sufficient information for sea ice reconstruction.

The novel sea ice biomarker IP₂₅ has been recently studied in the northern North Pacific, showing a good correlation with sea ice concentration and extent (Fig. 6.1b; Caisse, 2012; Max et al., 2012; Stoyanova et al., 2013; Méheust, 2013, 2014; Maier et al., 2015; Xiao et al., 2015). As an independent sea ice estimation tool, IP₂₅ is useful to verify the reconstructions derived from sea ice diatom transfer function and hence improve it. Thus, IP₂₅ and sea ice diatom transfer function together would provide a more reliable

sea ice concentration reconstructions in the northern North Pacific.

Interestingly, a sediment core retrieved from the shelf break of the Bering Shelf (Fig. 2.1) presents reverse trends of IP₂₅ and sea ice diatom during the early Holocene (Fig. 6.2). This period is characterized by laminae sediments, in which diatom valves are well preserved (Kuehn et al., 2014). Therefore sea ice diatoms are abundant, reaching 40%, much higher than that of the YD. On the contrary, the IP₂₅ and P_BIP₂₅ (a ratio of IP₂₅ to the combined IP₂₅ and phytoplankton marker content; Müller et al., 2011) peak in the YD and almost disappear in the early Holocene (Fig. 6.2). This contrasting phenomenon might raise the question why no IP₂₅ signal is recorded in the laminae of SO202-18-6, whereas sea ice diatoms are abundant? Since IP₂₅ is produced by especially by a sea ice diatom, *Haslea* spp. (Belt et al., 2007), our study might help to improve the understanding the behavior of sea ice diatoms and hence IP₂₅. This, in turn, will benefit the diatom based transfer function for sea ice reconstruction.

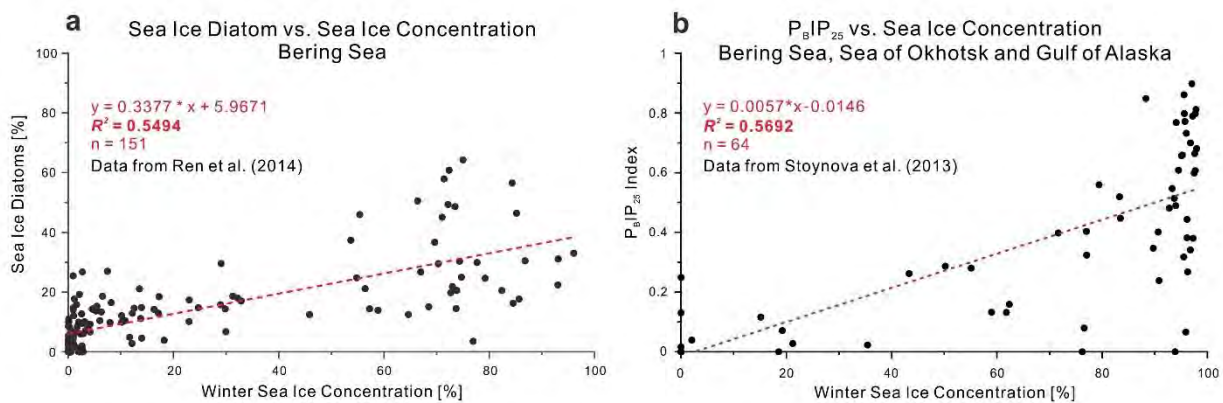


Fig. 6.1 a) Correlation between sea ice diatom abundance and sea ice concentration in the Bering Sea. Sea ice diatom data are from Ren et al. (2014); **b)** Correlation between P_BIP₂₅ and sea ice concentration. P_BIP₂₅ is a phytoplankton-IP₂₅ index, representing the fraction of IP₂₅ to the combined IP₂₅ and phytoplankton marker (brassicasterol) content. It indicates the algal activity beneath the sea ice and hence indicates the spatial extent of the sea ice cover (Müller et al., 2011). P_BIP₂₅ is calculated from Stoyanova et al. (2013) according to the method proposed by Müller et al. (2011). Modern winter sea ice concentration is derived from NOAA Optimum Interpolation (OI) Sea Surface Temperature Version 2 (Reynolds et al., 2002).

6.2.3. Paleooceanography in the Bering Sea

In the thesis, the Late Pleistocene paleooceanographic variability of the northern North Pacific open ocean is studied and discussed (**Chapter 5**). In order to obtain a comprehensive understanding of paleoceanographic development in the area, two sediment cores retrieved from the Bering Sea were investigated (SO202-12-1 and SO202-18-6; Table 2.1; Fig. 2.1) in addition to three cores studied in **Chapter 5**.

SO202-12-1 and SO202-18-6 are located on the Bowers Ridge and the shelf break of Bering Shelf, respectively (Fig. 2.1). The age controls of two cores were provided by accelerator mass spectrometry (AMS) ¹⁴C dates on planktonic monospecific *Neogloboquadrina pachyderma* sinistral measured by the National Ocean Science Accelerator Mass Spectrometry Facility (NOSAMS) at Woods Hole

Oceanographic Institute (Abelmann et al., unpub. data). The annual laminae of SO202-18-6, which occurred in the B/A and the early Holocene, were correlated to the NGRIP $\delta^{18}\text{O}$ record (NGRIP members, 2004) to establish a reasonable age model (Kuehn et al., 2014). Further core-core correlations based on XRF counts were applied to SO202-12-1 (Kuehn et al., 2014). The age models of SO202-12-1 and SO202-18-6 cover the last 70 ka and 13 ka, respectively.

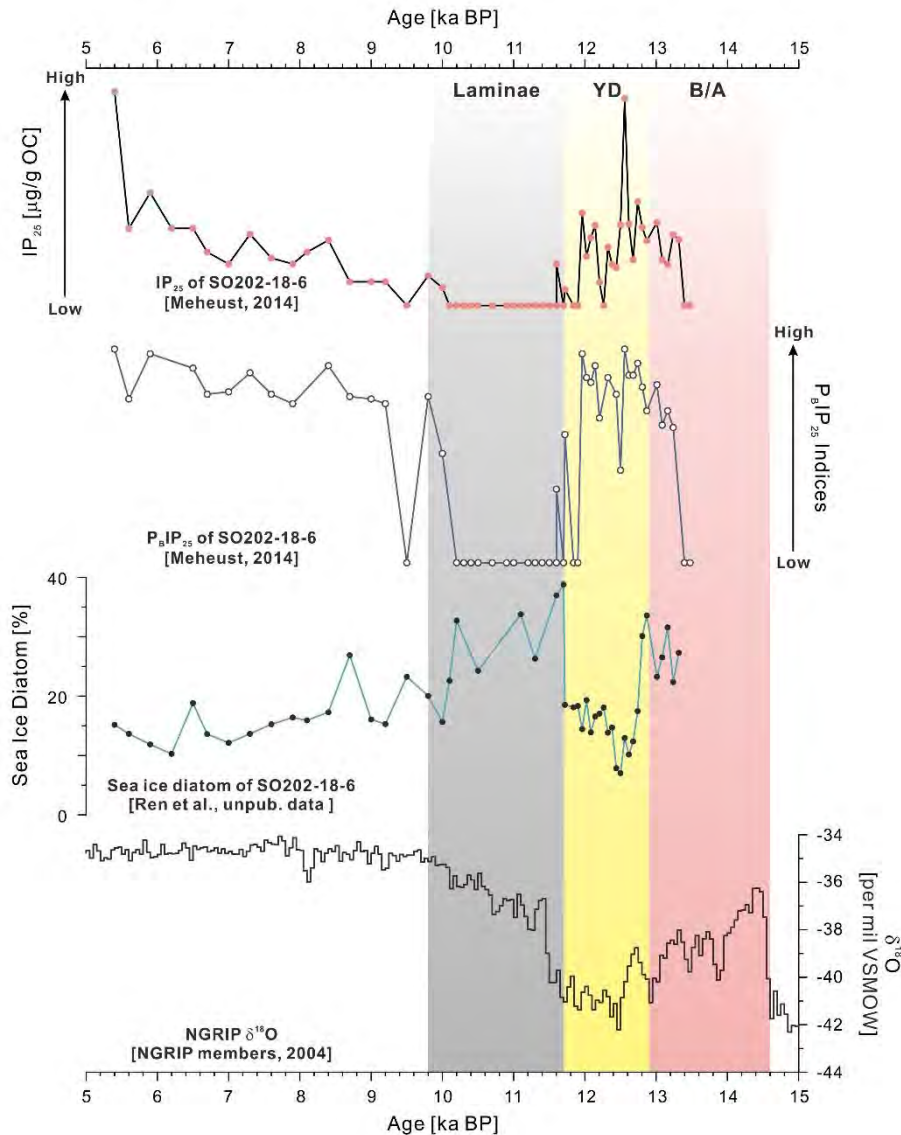


Fig. 6.2 Sea ice diatom abundance and IP_{25} content from SO202-18-6 in the Bering Sea. IP_{25} and $\text{P}_{\text{B}}\text{IP}_{25}$ are from Méheust (2014). $\text{P}_{\text{B}}\text{IP}_{25}$ is a phytoplankton- IP_{25} index, calculated as a ratio of IP_{25} to the combined IP_{25} and phytoplankton marker (brassicasterol) content (Müller et al., 2011). Sea ice diatom abundances are from Ren et al. (unpub. data), including *Fragilariopsis cylindrus* and *F. oecania*. A Greenland $\delta^{18}\text{O}$ record is displayed at the bottom panel as a reference (NGRIP members, 2004). Climate events are shown in shaded bars: B/A-Bølling/Allerød, YD-Younger Dryas. Laminae sediments are marked in gray according to Kuehn et al. (2014).

The diatom compositions of SO202-12-1 show an abrupt change at the boundary from H1 to B/A, characterized by a sudden increase of *N. seminae* and a drop of sea ice diatoms (Fig. 6.3). This might improve our understanding of the east-lead-and-west-lag phenomenon in the northern North Pacific

(discussed in *Chapter 5*). In addition, the immediate decrease of coastal species *Cocconeis* spp. at the H1-B/A boundary, may indicate sea level increase resulted from the Melt Water Pulse 1A. Therefore, *Cocconeis* spp. together with other coastal species (e.g. *Paralia sulcata*, *Rhabdonema* spp.) might be used to reconstruct the sea level change for the last 70 ka in the southern Bering Sea.

The variability of diatom assemblages for the last 13 ka from SO202-18-6 are interrupted by a thick laminae (Fig. 6.2) with extremely good preservation of diatoms. However, the laminae allow a close investigation on annually deposited diatoms, which may help to get more comprehensive knowledge of diatom signals in the sediments. Furthermore, thanks to its close location to the modern winter sea ice boundary, SO202-18-6 also a proper core for sea ice transfer function (Fig. 6.2).

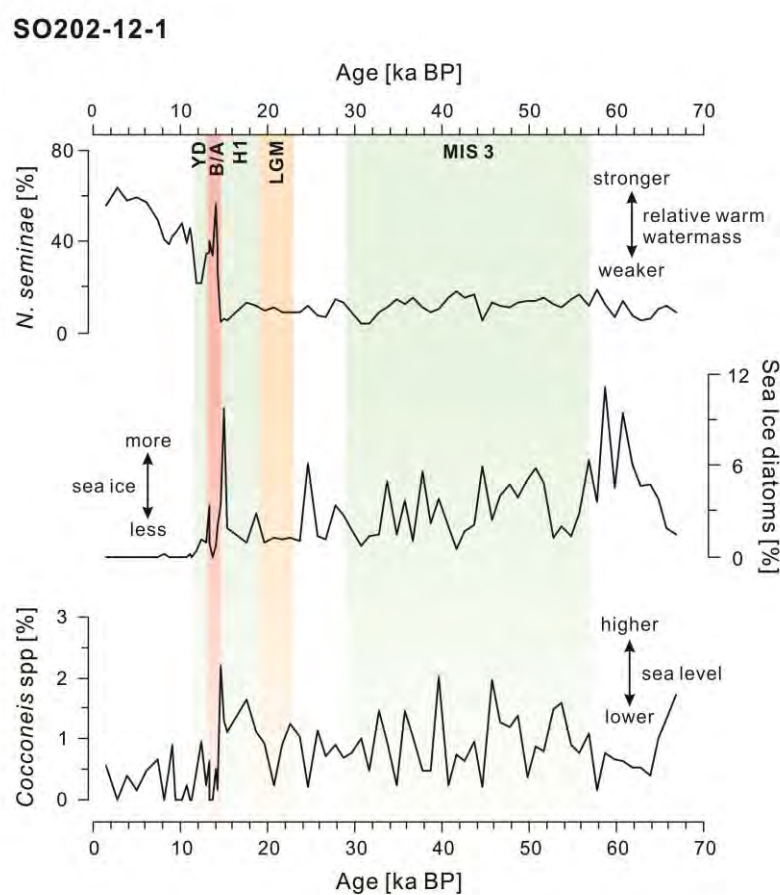


Fig. 6.3 Selected diatom relative abundance of SO202-12-1 (Ren et al., unpub. data). Sea ice diatom are *Fragilariopsis cylindrus* and *F. oecania*. Climate events are shown in shaded bars: MIS 3-Marine Isotope Stage 3, LGM- Last Glacial Maximum, H1-Heinrich event 1, B/A- Bølling/Allerød, YD-Younger Dryas.

Data handling

All data presented in this study will be stored electronically and will be available online in the PANGAEA database (<http://www.pangaea.de>).

References

- Abelmann, A., Nimmergut, A., 2005. Radiolarians in the Sea of Okhotsk and their ecological implication for paleoenvironmental reconstructions. *Deep Sea Research II*, 52, 2302–2331.
- Abelmann, A., Brathauer, U., Gersonde, R., Sieger, R., Zielinski, U., 1999. Radiolarian - based transfer function for the estimation of sea surface temperatures in the Southern Ocean (Atlantic Sector). *Paleoceanography*, 14, 410-421.
- Abrantes, F., 1988. Diatom assemblages as upwelling indicators in surface sediments off Portugal. *Marine Geology*, 85, 15-39.
- Abrantes, F., Lopes, C., Mix, A., Pisias, N., 2007. Diatoms in Southeast Pacific surface sediments reflect environmental properties. *Quaternary Science Reviews*, 26, 155-169.
- Akiba, F., 1986. Middle Miocene to Quaternary diatom biostratigraphy in the Nankai Trough and Japan Trench, and modified lower Miocene through Quaternary diatom zones for middle-to-high latitudes of the latitudes of the North Pacific. *Initial Reports of the Deep Sea Drilling Project* 87, 393-481.
- Alfultis, M. A., Martin, S., 1987. Satellite passive microwave studies of Sea of Okhotsk ice cover and relation to oceanic processes, 1987-1982. *Journal of Geophysical Research*, 92, 13,013-13,028.
- Alley, R.B., Clark, P.U., 1999. The deglaciation of the northern hemisphere: a global perspective. *Annual Review of Earth Planetary Science*, 27, 149-182.
- Andersen, C., Koç, N., Jennings, A., Andrews, J.T., 2004. Nonuniform response of the major surface currents in the Nordic Seas to insolation forcing: Implications for the Holocene climate variability. *Paleoceanography*, 19, PA2003, doi: 10.1029/2002PA000873.
- Antonov, J. I., Locarnini, R.A., Boyer, T.P., Mishonov, A.V., Garcia, H.E., 2006. World Ocean Atlas 2005. In: Levitus, S. (Ed.), *Salinity: NOAA Atlas NESDIS 62*, U.S. Government Printing Office, Washington, D.C., Vol. 2. 182 pp.
- Aydin, M., Top, Z., Olson, D.B., 2004. Exchange processes and watermass modification along the subarctic front in the North Pacific: oxygen consumption rates and net carbon flux. *Journal of Marine Research*, 62, 153-167.
- Banse, K. and English, D.C., 1999. Comparing phytoplankton seasonality in the eastern and western subarctic Pacific and the western Bering Sea. *Progress in Oceanography*, 43, 235-288.
- Barron, J.A., 1992. Pliocene paleoclimatic interpretations of DSDP Site 580 (NW Pacific) using diatoms. *Marine Micropaleontology*, 20, 23-44.
- Barron, J.A., 1995. High-resolution diatom paleoclimatology of the middle part of the Pliocene of the northwest Pacific. In: Rea, D.K., Basov, I.A., Allan, J.F. (Eds), *Proceedings of the Ocean Drilling Program, Scientific results*, College Station, TX (Ocean Drilling Program), vol. 145, pp. 43-53.
- Barron, J.A., Bukry, D., 2007. Development of the California Current during the past 12,000 yr based on diatoms and silicoflagellates. *Palaeogeography, Palaeoclimatology, Palaeoecology*, 248, 313-338.
- Barron, J.A., Anderson, L., 2011. Enhanced Late Holocene ENSO/PDO expression along the margins of the eastern North Pacific. *Quaternary International*, 235, 3-12.
- Barron, J. A., Heusser, L., Herbert, T., Lyle, M., 2003. High-resolution climatic evolution of coastal northern California during the past 16,000 years, *Paleoceanography*, 18, PA1020, doi:10.1029/2002PA000768.
- Barron, J.A., Bukry, D., Dean, W.E., Addison, J.A., Finney, B., 2009. Paleoceanography of the Gulf of Alaska during the past 15,000 years: Results from diatoms, silicoflagellates, and geochemistry. *Marine Micropaleontology*, 72, 176–195.
- Bassinot, F., Baltzer, A., 2002. Scientific Report of the WEPAMA Cruise, MD122/IMAGES VII (Leg 1 and Leg 2), 453pp.

- Bassinot, F.C., Labeyrie, L.D., Vincent, E., Quidelleur, X., Shackleton, N.J., Lancelot, Y., 1994. The astronomical theory of climate and the age of the Brunhes-Matuyama magnetic reversal. *Earth and Planetary Science Letters*, 162, 91–108.
- Belt, S.T., Massé, G., Rowland, S.J., Poulin, M., Michel, C., LeBlanc, B., 2007. A novel chemical fossil of palaeo sea ice: IP₂₅. *Organic Geochemistry*, 38, 16-27.
- Berger, W.H., Winterer, E.L., 1974. Plate stratigraphy and the fluctuating carbonate line, Pelagic Sediments on Land and Under the Sea. In: Hsu, K.J., Jenkyns, H.C. (Eds), *International Association of Sedimentology Special Publication*, 1, pp. 59-96.
- Birks, H.J.B., 2010. Numerical methods for the analysis of diatom assemblage data. In: Smol, J.P., Stoermer E.F. (Eds), *The Diatoms Applications for the Environmental and Earth Sciences*, Cambridge University Press, Cambridge, pp. 23-54.
- Birks, H.J.B., Juggins, S., Line, J.M., 1990. Lake surface-water chemistry reconstructions from palaeolimnological data. In: Mason, B.J. (Ed.), *The Surface Water Acidification Programme*. Cambridge University Press, Cambridge, pp. 301-313.
- Bonnet, S., de Vernal, A., Hillaire-Marcel, C., Radi, T., Husum, K., 2010. Variability of seasurface temperature and sea-ice cover in the Fram Strait over the last two millennia. *Marine Micropaleontology*, 74, 59 – 74.
- Bonnet, S., de Vernal, A., Gersonde, R., Lembke-Jene, L., 2012. Modern distribution of dinocysts from the North Pacific Ocean (37–64°N, 144°E–148°W) in relation to hydrographic conditions, sea-ice and productivity. *Marine Micropaleontology*, 84–85, 87–113.
- Bronk Ramsey, C., Staff, R.A., Bryant, C.L., Brock, F., Kitagawa, H., van der Plicht, J., Schlolaut, G., Marshall, M.H., Brauer, A., Lamb, H.F., Payne, R.L., Tarasov, P.E., Haraguchi, T., Gotanda, K., Yonenobu, H., Yokoyama, Y., Tada, R., Nakagawa, T., 2012. A complete terrestrial radiocarbon record for 11.2 to 52.8 kyr B.P. *Science*, 338, 370-374.
- Brunelle, B.G., Sigman, D.M., Cook, M.S., Keigwin, L.D., Haug, G.H., Plessen, B., Schettler, G., Jaccard, S., 2007. Evidence from diatom-bound nitrogen isotopes for Subarctic Pacific stratification during the last ice age and a link to North Pacific denitrification changes. *Paleoceanography*, 22, doi: 10.1029/2005PA001205.
- Brunelle, B.G., Sigman, D.M., Jaccard, S.L., Keigwin, L.D., Plessen, B., Schettler, G., Cook, M.S., Haug, G.H., 2010. Glacial/interglacial changes in nutrient supply and stratification in the western subarctic North Pacific since the penultimate glacial maximum. *Quaternary Science Review*, 29, 2579–2590.
- Caisse, B., 2012. Diatoms as recorders of sea ice in the Bering and Chukchi seas: proxy development and application. PhD dissertation, University of Massachusetts-Amherst, 213pp.
- Caisse, B. E., Brigham-Grette, J., Lawrence, K.T., Herbert, T.D., Cook, M.S., 2010. Last Glacial Maximum to Holocene sea surface conditions at Umnak Plateau, Bering Sea, as inferred from diatom, alkenone, and stable isotope records, *Paleoceanography*, 25, PA1206, doi:10.1029/2008PA001671.
- Chen, M.-T., Huang, C.-C., Pflaumann, U., Waelbroeck, C., Kucera, M., 2005. Estimating glacial western Pacific sea-surface temperature: methodological overview and data compilation of surface sediment planktic foraminifer faunas. *Quaternary Science Review: Multiproxy Approach for the Reconstruction of the Glacial Ocean surface*, 24, 951–998.
- Chikamoto, O.M., Menviel, L., Abe-Ouchi, A., Ohgaito, R., Timmermann, A., Okazaki, Y., Harada, N., Oka, A., 2012. Variability in North Pacific intermediate and deep water ventilation during the Heinrich events in two coupled climate models. *Deep Sea Research, Part II*, 61–64, 114–126.
- Clague, J.J., James, T.S., 2002. History and isostatic effects of the last ice sheet in southern British Columbia. *Quaternary Science Review*, 21, 71–87.
- CLIMAP Project Members, 1976. The Surface of the Ice-Age Earth. *Science*, 191, 1131-1137.
- CLIMAP Project Members, 1984. The Last Interglacial Ocean. *Quaternary Research*, 21, 123-224.

- Coachman, L.K., 1993. On the flow field in the Chirikov Basin. *Continental Shelf Research*, 13, 481-508.
- Cook, M.S., 2006. The paleoceanography of the Bering Sea during the last glacial cycle. PhD dissertation, Massachusetts Institute of Technology and Woods Hole Oceanographic Institution. 126pp.
- Cook, M.S., Keigwin, L.D., Sancetta, C.A., 2005. The deglacial history of surface and intermediate water of the Bering Sea. *Deep-Sea Research II*, 52, 2163-2173.
- Cooke-Poferl, K., Burckle, L.H., Riley, S., 1975. Diatom evidence bearing on Late Pleistocene climatic changes in the equatorial Pacific. *Geological Society of America Abstract with Programs*, 7, 1038-1039.
- Cosma, T., Hendy, I.L., Chang, A., 2008. Chronological constraints on Cordilleran Ice Sheet glaciomarine sedimentation from MD02-2496 off Vancouver Island (western Canada). *Quaternary Science Review*, 27, 941-955.
- Crawford, R. M. 1979. Taxonomy and frustular structure of the marine centric diatom *Paralia sulcata*. *Journal of Phycology*, 15, 200-210.
- Crosta, X., Koc, N., 2007. Diatoms: From micropaleontology to isotope geochemistry, In: Hillaire-Marcel, C., de Vernal, A. (Eds), *Methods in Late Cenozoic Paleooceanography*, Elsevier, pp. 327-369.
- Crosta, X., Pichon, J.-J., Burckle, L.H., 1998. Application of modern analog technique to marine Antarctic diatoms: reconstruction of maximum sea-ice extent at the Last Glacial Maximum. *Paleoceanography*, 13, 284-297.
- Crosta, X., Sturm, A., Armand, L., Pichon, J.-J., 2004. Late Quaternary sea ice history in the Indian sector of the Southern Ocean as recorded by diatom assemblages. *Marine Micropaleontology*, 50, 209-223.
- Crusius, J., Schroth, A.W., Gassó, S., Moy, C.M., Levy, R.C., Gatica, M., 2011. Glacial flour dust storms in the Gulf of Alaska: Hydrologic and meteorological controls and their importance as a source of bioavailable iron. *Geophysical Research Letters*, 38, L06602.
- Dansgaard, W., Johnsen, S.J., Clausen, H.B., Dahl-Jensen, D., Gundestrup, N.S., Hammer, C.U., Hvidberg, C.S., Steffensen, J.P., Sveinbjörnsdóttir, A.E., Jouzel, J., Bond, G., 1993. Evidence for general instability of past climate from a 250-kyr ice-core record. *Nature*, 364, 218-220.
- Davies, M.H., Mix, A.C., Stoner, J.S., Addison, J.A., Jaeger, J., Finney, B., Wiest, J., 2011. The deglacial transition on the southeastern Alaska Margin: Meltwater input, sea level rise, marine productivity, and sedimentary anoxia. *Paleoceanography*, 26, PA2223, doi:10.1029/2010PA002051.
- De La Rocha, C.L., Brzezinski, M.A., DeNiro, M.J., Shemesh, A., 1998. Silicon-isotope composition of diatoms as an indicator of past oceanic change. *Nature*, 395, 680-683.
- de Vernal, A., Pedersen, T.F., 1997. Micropaleontology and palynology of core PAR87A-10: A 23,000 year record of paleoenvironmental changes in the Gulf of Alaska, northeast North Pacific. *Paleoceanography*, 12, 821-830.
- de Vernal, A., Rochon, A., Hillaire-Marcel, C., Turon, J.-L., Guiot, J., 1993. Quantitative reconstruction of sea-surface conditions, seasonal extent of sea-ice cover and meltwater discharges in high latitude marine environments from dinoflagellate cyst assemblages, in *Proceedings of the NATO Workshop on Ice in the Climate System*, edited by W.R. Peltier, NATO ASI Ser., 112, 611-621.
- de Vernal, A., Turon, J.-L., Guiot, J., 1994. Dinoflagellate cyst distribution in high latitude environments and quantitative reconstruction of sea-surface temperature, salinity and seasonality. *Canadian Journal of Earth Science*, 31, 48-62.
- de Vernal, A., Hillaire-Marcel, C., Turon, J.-L., Matthiessen, J., 2000. Reconstruction of sea-surface temperature, salinity, and sea-ice cover in the northern North Atlantic during the last glacial maximum based on dinocyst assemblages. *Canadian Journal of Earth Sciences*, 37, 725-750.
- de Vernal, A., Henry, M., Matthiessen, J., Mudie, P.J., Rochon, A., Boessenkool, K., Eynaud, F., Grøsfjeld, K., Guiot, J., Hamel, D., Harland, R., Head, M.J., Kunz-Pirrung, M., Levac, E., Loucheur, V., Peyron, O.,

- Pospelova, V., Radi, T., Turon, J.-L., Voronina, E., 2001. Dinoflagellate cyst assemblages as tracers of sea-surface conditions in the northern North Atlantic, Arctic and sub-Arctic seas: the new “n=677” database and application for quantitative paleoceanographical reconstruction. *Journal of Quaternary Science*, 16, 681–699.
- de Vernal, A., Eynaud, F., Henry, M., Hillaire-Marcel, C., Londeix, L., Mangin, S., Matthiessen, J., Marret, F., Radi, T., Rochon, A., 2005. Reconstruction of sea-surface conditions at middle to high latitudes of the Northern Hemisphere during the Last Glacial Maximum (LGM) based on dinoflagellate cyst assemblages. *Quaternary Science Reviews*, 24, 897–924.
- Denton, G.H., Alley, R.B., Comer, G., Broecker, W.S., 2005. The role of seasonality in abrupt climate change. *Quaternary Science Reviews*, 24, 1159–1182.
- Denton, G.H., Anderson, R.F., Toggweiler, J.R., Edwards, R.L., Schaefer, J.M., Putnam, A.E., 2010. The last glacial termination. *Science*, 328, 1652–1656.
- Dodimead, A.J., Favorite, F., Hirano, T., 1963. Salmon of the North Pacific Ocean: part II. review of oceanography of the subarctic Pacific region. *International North Pacific Fisheries Commission Bulletin* 13, 1–195.
- Dullo, W.-C., Biebow, N., Georgeleit, K., 2004. SO178-KOMEX Cruise Report: Mass exchange processes and balances in the Okhotsk Sea. IFM-GEOMAR, Kiel, 125 pp.
- Dullo, W.-C., Baranov, B., van den Bogaard, C., 2009. FS Sonne Cruise Report SO201-2 KALMAR: Kurile-Kamchatka and Aleutian Marginal sea-island arc systems: geodynamic and climate interaction in space and time. IFM-GEOMAR Report, 35, IFM-GEOMAR, Kiel, 233 pp.
- Emile-Geay, J., Cane, M.A., Naik, N., Seager, R., Clement, A.C., van Geen, A., 2003. Warren revisited: Atmospheric freshwater fluxes and "Why is no deepwater formed in the North Pacific". *Journal of Geophysical Research*, 108, doi: 10.1029/2001JC001058.
- EPICA Community Members, 2004. Eight glacial cycles from an Antarctic ice core. *Nature*, 429, 623–628.
- Esper, O., Gersonde, R., 2014a. New tools for the reconstruction of Pleistocene Antarctic sea ice. *Palaeogeography, Palaeoclimatology, Palaeoecology*, <http://dx.doi.org/10.1016/j.palaeo.2014.01.019>.
- Esper, O., Gersonde, R., 2014b. Quaternary surface water temperature estimations: New diatom transfer functions for the Southern Ocean. *Palaeogeography, Palaeoclimatology, Palaeoecology*, 414, 1–19.
- Esper, O., Gersonde, R., Kadagies, N., 2010. Diatom distribution in southeastern Pacific surface sediments and their relationship to modern environmental variables. *Palaeogeography, Palaeoclimatology, Palaeoecology*, 287, 1–27.
- Expedition 323 Scientists, 2009. Bering Sea paleoceanography: Pliocene–Pleistocene paleoceanography and climate history of the Bering Sea. IODP Preliminary Report, 323. doi:10.2204/iodp.pr.323.2010.
- Expedition 341 Scientists, 2014. Southern Alaska Margin: interactions of tectonics, climate, and sedimentation. IODP Preliminary Report, 341. doi:10.2204/iodp.pr.341.2014.
- Favorite, F., Dodimead, A.J., Nasu, K., 1976. Oceanography of the subarctic Pacific region, 1962–72. *Bulletin of the International North Pacific Fishery Committee*, 33, 1–187.
- Fronval, T., Jansen, E., 1997. Eemian and early Weichselian (140–60 ka) paleoceanography and paleoclimate in the Nordic seas with comparisons to Holocene conditions. *Paleoceanography*, 12, 443–462.
- Galbraith, E.D., 2006. Interactions between climate and the marine nitrogen cycle on glacial/interglacial timescales. Ph.D. dissertation, University of British Columbia. 228 pp.
- Galbraith, E.D., Jaccard, S.L., Pedersen, T.F., Sigman, D.M., Haug, G.H., Cook, M., Southon, J.R., Francois, R., 2007. Carbon dioxide release from the North Pacific abyss during the last deglaciation. *Nature*, 449, 890–893.
- Galbraith, E.D., Kienast, M., Jaccard, S.J., Pedersen, T.F., Brunelle, B.G., Sigman, D.M., Kiefer, T., 2008.

- Consistent relationship between global climate and surface nitrate utilization in western Subarctic Pacific throughout last 500 ka. *Paleoceanography*, 23, PA2212, doi:10.1029/2007PA001518.
- Garcia, H.E., Locarnini, R.A., Boyer, T.P., Antonov, J.I., 2006. World Ocean Atlas 2005. In: Levitus, S. (Ed.), Nutrients (Phosphate, Nitrate, Silicate). NOAA Atlas NESDIS 64, U.S. Government Printing Office, Washington, D.C., Vol. 4. 396 pp.
- Gargett, A.E., 1991. Physical processes and the maintenance of nutrient-rich euphotic zones. *Limnology and Oceanography*, 36, 1527–1545.
- Gebhardt, H., Sarnthein, M., Grootes, P.M., Kiefer, T., Kuehn, H., Schmieder, F., Röhl, U., 2008. Paleonutrient and productivity records from the subarctic North Pacific for Pleistocene glacial terminations I to V. *Paleoceanography*, 23, PA4212, doi:10.1029/2007PA001513.
- Gersonde, R., 1990. The paleontological significance of fossil diatoms from the high-latitude oceans. In: Medlin, L.K., Priddle, J. (Eds.), *Polar marine diatoms*, Cambridge, British Antarctic Survey, pp. 57–63.
- Gersonde, R., 2012. The expedition of the research vessel "Sonne" to the subpolar North Pacific and the Bering Sea in 2009 (SO202-INOPEX), *Berichte zur Polar- und Meeresforschung* (Reports on polar and marine research), Bremerhaven, Alfred Wegener Institute for Polar and Marine Research, 643, 323 p.
- Gersonde, R., Zielinski, U., 2000. The reconstruction of late Quaternary Antarctic sea ice distribution - the use of diatoms as a proxy for sea ice. *Palaeogeography, Palaeoclimatology, Palaeoecology*, 162, 263–286.
- Gersonde, R., Abelmann, A., Brathauer, U., Becquey, S., Bianchi, C., Cortese, G., Grobe, H., Kuhn, G., Niebler, H.-S., Segl, M., Sieger, R., Zielinski, U., Fütterer, D.K., 2003. Last glacial sea-surface temperatures and sea-ice extent in the Southern Ocean (Atlantic-Indian sector) -- A multiproxy approach. *Paleoceanography*, 18, 1061 doi: 1029/2002PA000809.
- Gersonde, R., Crosta, X., Abelmann, A., Armand, L., 2005. Sea-surface temperature and sea ice distribution of the Southern Ocean at the EPILOG Last Glacial Maximum—a circum-Antarctic view based on siliceous microfossil records. *Quaternary Science Reviews*, 24, 869–896.
- Grant, W.S. and Horner, R.A., 1976. Growth responses to salinity variation in four arctic ice diatoms. *Journal of Phycology*, 12, 180–185.
- Grebmeier, J.M., Overland, J.E., Moore, S.E., Farley, E.V., Carmack, E.C., Cooper, L.W., Frey, K.E., Helle, J.H., McLaughlin, F.A., McNutt, S.L., 2006. A major ecosystem shift in the northern Bering Sea. *Science*, 311, 1461–1464.
- Guillard, R.R.L. and Kilham, P., 1977. The ecology of marine planktonic diatoms. In: Werner, D. (Ed), *The Biology of Diatoms*, Blackwell, London, pp.372–469.
- Guiot, J., de Vernal, A., 2007. Transfer functions: methods for quantitative paleoceanography based on microfossils. In: Hillaire-Marcel, C., de Vernal, A. (Eds.), *Proxies in Late Cenozoic paleoceanography: Developments in Marine Geology*. Elsevier, pp. 523 – 563.
- Günther, F., Fritsch, S., 2010. Neuralnet: Training of neural networks. *R Journal*, 2, 30–38.
- Harada, N., Shin, K.H., Murata, A., Uchida, M., Nakatani, T., 2003. Characteristics of alkenones synthesized by a bloom of *Emiliania huxleyi* in the Bering Sea. *Geochimica et Cosmochimica Acta*, 67, 1507–1519.
- Harada, N., Ahagon, N., Uchida, M., Murayama, M., 2004. Northward and southward migrations of frontal zones during the past 40 kyr in the Kuroshio-Oyashio transition area. *Geochemistry Geophysics Geosystem*, 5, Q09004, doi:10.1029/2004GC000740.
- Harada, N., Ahagon, N., Sakamoto, T., Uchida, M., Ikehara, M., Shibata, Y., 2006. Rapid fluctuation of alkenone temperature in the southwestern Okhotsk Sea during the past 120 ky. *Global and Planetary Change*, 53, 29–46.
- Harada, N., Sato, M., Sakamoto, T., 2008. Freshwater impacts recorded in tetraunsaturated alkenones and alkenone sea surface temperatures from the Okhotsk Sea across millennial-scale cycles. *Paleoceanography*,

- 23, PA3201, doi: 10.1029/2006PA001410.
- Harada, N., Sato, M., Seki, O., Timmermann, A., Moossen, H., Bendle, J., Nakamura, Y., Kimoto, K., Okazaki, Y., Nagashima, K., Gorbarenko, S.A., Ijiri, A., Nakatsuka, T., Menviel, L., Chikamoto, M.O., Abe-Ouchi, A., Schouten, S., 2012. Sea Surface temperature changes in the Okhotsk Sea and adjacent North Pacific during the last glacial maximum and deglaciation. *Deep Sea Research, Part II*, 61–64, 93–105.
- Harrison, P.J., Boyd, P.W., Varela, D.E., Takeda, S., 1999. Comparison of factors controlling phytoplankton productivity in the NE and NW subarctic Pacific gyres. *Progress in Oceanography*, 43, 205-223.
- Hasle, G.R., 1990. Arctic plankton diatoms: dominant species, biogeography. In: Medlin, L.K., Priddle, J. (Eds.), *Polar marine diatoms*, Cambridge: British Antarctic Survey, pp. 53-56.
- Hasle, G.R., 2001. The marine, planktonic diatom Family Thalassionemataceae: morphology, taxonomy and distribution. *Diatom Research*, 16, 1-82.
- Hasle, G.R., Syvertsen, E.E., 1997. Marine diatoms. In: Tomas, C.R. (Ed.), *Identifying Marine Phytoplankton*. Academic Press, New York, pp. 5-385.
- Haug, G., Sarnthein, M., 2005. U^{k}_{37} , Sea surface temperature and pigment data of ODP Site 145-882. doi:10.1594/PANGAEA.315092.
- Haug, G., Sigman, D., Tiedemann, R., Pedersen, T., Sarnthein, M., 1999. Onset of permanent stratification in the subarctic Pacific Ocean. *Nature*, 401, 779–782.
- Haug, G., Ganopolski, A., Sigman, D., Rosell-Mele, A., Swann, G., Tiedemann, R., Jaccard, S., Bollmann, J., Maslin, M., Leng, M., Eglinton, G., 2005. North Pacific seasonality and the glaciation of North America 2.7 million years ago. *Nature*, 433, 821–825.
- Hendey, N.I., 1964. An introductory account of the smaller algae of British coastal waters: Part V. Bacillariophyceae (Diatoms). *Fishery Investigations, London*. Ser. 4. 317 pp.
- Hendy, I.L., and Kennett, J.P., 1999. Latest Quaternary North Pacific surface-water responses imply atmosphere-driven climate instability. *Geology*, 27, 291-294.
- Hendy, I.L., and Cosma, T., 2008. Vulnerability of the Cordilleran Ice Sheet to iceberg calving during late Quaternary rapid climate change events. *Paleoceanography*, 23, PA2101, doi: 10.1029/2008PA001606.
- Hoffman, L., Peeken, I., Lochte, K., 2008. Iron, silicate, and light co-limitation of three Southern Ocean diatom species. *Polar Biology*, 31, 1067–1080.
- Horner, R., Alexander, V., 1972. Algal populations in Arctic sea-ice: an investigation of heterotrophy. *Limnology and Oceanography*, 17, 454-458.
- Huang, Y., Jiang, H., Sarnthein, M., Li, D.L., 2009. Diatom response to changes in palaeoenvironments of the northern South China Sea during the last 15000 years. *Marine Micropaleontology*, 72, 99-109,
- Hutson, W.H., 1980. The Agulhas Current during the Late Pleistocene: Analysis of modern faunal analogs. *Science*, 207, 64-66.
- Imbrie, J., Kipp, N.G., 1971. A new micropaleontological method for quantitative micropaleontology: application to a Late Pleistocene Caribbean core. In: Turekian, K.K. (Ed.), *The Late Cenozoic Glacial Ages*. Yale University Press, New Haven, pp. 71–181.
- Imbrie, J., Hays, J.D., Martinson, D.G., McIntyre, A., Mix, A.C., Morley, J.J., Pisias, N.G., Prell, W.L., Shackleton, N.J., 1984. The orbital theory of Pleistocene climate: support from a revised chronology of the marine $\delta^{18}O$ record. In *Milankovitch and Climate*, A. L. Berger (Ed.). D. Reidel Publishing, pp. 269-305.
- Imbrie, J., McIntyre, A., Mix, A., 1992. Oceanic response to orbital forcing in the Late Quaternary: Observational and experimental strategies. *Paleoceanography*, 7, 701–738.
- Ingalls, A.E., Anderson, R.F., Pearson, A., 2004. Radiocarbon dating of diatom-bound organic compounds. *Marine Chemistry*, 92, 91-105.
- Jaccard, S.L., 2012. Pacific and Atlantic synchronized. *Nature Geoscience*, 5, 594-596.

- Jaccard, S.L., Haug, G.H., Sigman, D.M., Pedersen, T.F., Thierstein, H.R., Röhl, U., 2005. Glacial/interglacial changes in Subarctic North Pacific stratification. *Science*, 308, 1003-1006.
- Jiang, H., Seidenkrantz, M.S., Knudsen, K.L., Eiriksson, J., 2001. Diatom surface sediment assemblages around Iceland and their relationships to oceanic environmental variables. *Marine Micropaleontology*, 41, 73-96.
- Jiang, H., Seidenkrantz, M.-S., Knudsen, K.L., Eiriksson, J., 2002. Late Holocene summer sea-surface temperature based on a diatom record from the North Icelandic shelf. *The Holocene*, 12, 137-147.
- Jiang, H., Zheng, Y., Ran, L., Seidenkrantz, M.S., 2004. Diatoms from the surface sediments of the South China Sea and their relationships to modern hydrography. *Marine Micropaleontology*, 53, 279-292.
- Jiang, H., Eiriksson, J., Schulz, M., Knudsen, K. L., Seidenkrantz, M. S., 2005. Evidence for solar forcing of sea-surface temperature on the North Icelandic Shelf during the late Holocene. *Geology*, 33, 73-76.
- Jiang, H., Björck, S., Ran, L., Huang, Y., Li, J., 2006. Impact of the Kuroshio Current on the South China Sea based on a 115000 year diatom record. *Journal of Quaternary Science*, 21, 377-385.
- Jousé, A.P., Kozlova, O.G., Muhina, V.V., 1971. Distribution of diatoms in the surface layer of sediment from the Pacific Ocean. In: Funnell, B.M., Riedel, W.R. (Eds.), *The Micropalaeontology of Oceans*. Cambridge University Press, London, pp. 263- 269.
- Kallel, N., Labeyrie, L.D., Arnorid, M., Okada, H., Dudley, W.C., Duplessy, J.-C., 1988. Evidence of cooling during the Younger Dryas in the western North Pacific. *Oceanologica Acta*, 11, 369- 375.
- Kanaya, T., Koizumi, I., 1966. Interpretation of diatom thanatocoenoses from the North Pacific applied to a study of core V20-130 (Studies of a deep-sea core V20-130, part IV), *Science Reports of the Research Institutes, Tohoku University*, 2nd serie (Geology), 37, 89-130.
- Katsuki, K., Takahashi, K., 2005. Diatoms as paleoenvironmental proxies for seasonal productivity, sea-ice and surface circulation in the Bering Sea during the late Quaternary. *Deep Sea Research Part II: Topical Studies in Oceanography*, 52, 2110-2130.
- Katsuki, K., Takahashi, K., Okada, M., 2003. Diatom Assemblage and Productivity Changes during the Last 340,000 Years in the Subarctic Pacific. *Journal of Oceanography*, 59, 695-707.
- Katsuki, K., Khim, B.-K., Itaki, T., Harada, N., Sakai, H., Ikeda, T., Takahashi, K., Okazaki, Y., Asahi, H., 2009. Land-sea linkage of Holocene paleoclimate on the southern Bering continental shelf. *The Holocene*, 2009, 19, 747-756.
- Katsuki, K., Khim, B.K., Itaki, T., Okazaki, Y., Ikehara, K., Shin, Y., Yoon, H.I., Kang, C.Y., 2010. Sea-ice distribution and atmospheric pressure patterns in southwestern Okhotsk Sea since the Last Glacial Maximum. *Global and Planetary Change*, 72, 99-107.
- Kawai, H., 1972. Hydrography of the Kuroshio Extension. In: Stommel, H., Yoshida, K., (Eds.), *Kuroshio: its physical aspects*. University of Tokyo Press, Tokyo, pp. 235-354.
- Kazarina, G.K., Yushina, I.G., 1999. Diatoms in recent and Holocene sediments of the North Pacific and the Bering Sea. In: Spielhagen, R.F., Barash, M.S., Ivanov, G.I., Thiede, J. (Eds), *German-Russian Cooperation: Biogeographic and biostratigraphic investigations on selected sediment cores from the Eurasian continental margin and marginal seas to analyze the Late Quaternary climatic variability*. *Berichte zur Polarforschung*, Bremerhaven, Alfred Wegener Institute for Polar and Marine Research, 306, pp 134-148.
- Keigwin, L.D., 1987. North Pacific deep water formation during the latest glaciation. *Nature*, 330, 362-364.
- Keigwin, L.D., 1998. Glacial-age hydrography of the far northwest Pacific Ocean. *Paleoceanography*, 13, 323-339.
- Keigwin, L.D., Cook, M. S., 2007. A role for North Pacific salinity in stabilizing North Atlantic climate. *Paleoceanography*, 22, PA3102, doi:10.1029/2007PA001420.
- Keigwin, L.D., Jones, G.A., Froelich, P. N., 1992. A 15,000 year paleoenvironmental record from Meiji Seamount, far northwestern Pacific. *Earth Planetary Science Letters*, 111, 425-440.

- Kiefer, T., Sarnthein, M., Erlenkeuser, H., Grootes, P., Roberts, A., 2001. North Pacific response to millennial-scale changes in ocean circulation over the last 60 ky. *Paleoceanography*, 16, 179–189.
- Kiefer, T., Kienast, M., 2005. Patterns of deglacial warming in the Pacific Ocean: a review with emphasis on the time interval of Heinrich event 1. *Quaternary Science Reviews*, 24, 1063–1081.
- Kienast, S.S. and McKay, J.L., 2001. Sea surface temperatures in the subarctic northeast Pacific reflect millennial-scale climate oscillations during the last 16 kyrs. *Geophysical Research Letters*, 28, 1563–1566.
- Kim, J.H., Rambu, N., Lorenz, S.J., Lohmann, G., Nam, S.I., Schouten, S., Ruhlemann, C., Schneider, R.R., 2004. North Pacific and North Atlantic sea-surface temperature variability during the Holocene. *Quaternary Science Review*, 23, 2141–2154.
- Klovan, J.E., Imbrie, J., 1971. An algorithm and FORTRAN-IV program for large scale Q mode factor analysis and calculation of factor scores. *Mathematical Geology*, 3, 61–77.
- Koblentz-Mishke, O.J., Volkovinsky, V.V., Kabanova, G. 1970. Plankton primary production of the world ocean. In: Wooster, W. (Ed), *Scientific exploration of the south Pacific*. National Academy of Science, Washington, D.C., pp. 183–193.
- Koç Karpuz, N., Schrader, H., 1990. Surface sediment diatom distribution and Holocene paleotemperature variations in the Greenland, Iceland and Norwegian Sea. *Paleoceanography*, 5, 557–580.
- Kohfeld, K.E., Chase, Z., 2011. Controls on deglacial changes in biogenic fluxes in the North Pacific Ocean. *Quaternary Science Review*, 30, 3350–3363.
- Koizumi, I, Sakamoto, T., 2003. Paleoceanography off Sanriku, Northeast Japan, based on diatom flora. In: Suyehiro, K., Sacks, I.S., Acton, G.D., Oda, M. (Eds), *Proceeding of Ocean Drilling Program Scientific Results 186*, Texas A & M University, Texas, pp. 1–21.
- Koizumi, I., Yamamoto, H., 2015. Diatom records in the Quaternary marine sequences around the Japanese Islands. *Quaternary International*, doi: 10.1016/j.quaint.2015.03.043.
- Koizumi, I., 2008. Diatom-derived SSTs (Td' ratio) indicate warm seas off Japan during the middle Holocene (8.2–3.3 ka BP). *Marine Micropaleontology*, 69, 263–281.
- Kotilainen, A.T., Shackleton, N.J., 1995. Rapid climate variability in the North Pacific Ocean during the past 95,000 years. *Nature*, 377, 323–326.
- Kucera, M., Rosell-Mele, A., Schneider, R.R., Waelbroeck, C., Weinelt, M., 2005a. Multiproxy approach for the reconstruction of the glacial ocean surface (MARGO). *Quaternary Science Review*, 24, 813–819.
- Kucera, M., Weinelt, M., Kiefer, T., Pflaumann, U., Hayes, A., Weinelt, M., Chen, M.-T., Mix, A.C., Barrows, T.T., Cortijo, E., Duprat, J., Juggins, S., Waelbroeck, C., 2005b. Reconstruction of Sea-surface temperatures from assemblages of planktonic foraminifera: multitechnique approach based on geographically constrained calibration data sets and its application to glacial Atlantic and Pacific Oceans. *Quaternary Science Reviews: Multiproxy Approach for the Reconstruction of the Glacial Ocean surface*, 24, 951–998.
- Kuehn, H., Lembke-Jene, L., Gersonde, R., Esper, O., Lamy, F., Arz, H., Tiedemann, R., 2014. Laminated sediments in the Bering Sea reveal atmospheric teleconnections to Greenland climate on millennial to decadal timescales during the last deglaciation. *Climate of the Past Discussion*, 10, 2467–2518, doi:10.5194/cpd-10-2467-2014.
- Lam, P.J., Bishop, J.K.B., 2008. The continental margin is a key source of iron to the HNLC North Pacific Ocean. *Geophysical Research Letters*, 35, L07608, doi:10.1029/2008GL033294.
- Lam, P.J., Bishop, J.K.B., Henning, C.C., Marcus, M.A., Waychunas, G.A., Fung, I.Y., 2006. Wintertime phytoplankton bloom in the subarctic Pacific supported by continental margin iron. *Global Biogeochemical Cycles*, 20, GB1006, doi:10.1029/2005GB002557.
- Lam, P.J., Robinson, L.F., Blusztajn, J., Li, C., Cook, M.S., McManus, J.F., Keigwin, L.D., 2013. Transient stratification as the cause of the North Pacific productivity spike during deglaciation. *Nature Geoscience*, 6,

- 622-626, doi: 10.1038/NGEO1873
- Levitus, S., Boyer, T., 1994. World Ocean Atlas 1994, Vol. 4: Temperature. NOAA Atlas NESDIS 4, U.S. Government Printing Office, Washington, D.C., 117 pp.
- Lisiecki, L.E., and Raymo, M.E., 2005. A Pliocene-Pleistocene stack of 57 globally distributed benthic $\delta^{18}\text{O}$ records. *Paleoceanography*, 20, PA1003, doi: 10.1029/2004PA001071.
- Lisitzin, A.P., 1972. Sedimentation in the world ocean: with emphasis on the nature, distribution and behavior of marine suspensions. SEPM Special Publication, 17, Tulsa, Oklahoma, 218pp.
- Lopes, C., Mix, A., Abrantes, F., 2006. Diatoms in northeast Pacific surface sediments as paleoceanographic proxies. *Marine Micropaleontology*, 60, 45-65.
- Lopes, C., Mix, A.C., 2009. Pleistocene megafloods in the northeast Pacific. *Geology*, 37, 79–82.
- Luchin, V.A., Semiletov, I.P., Weller, G.E., 2002. Changes in the Bering Sea region: atmosphere–ice–water system in the second half of the twentieth century. *Progress in Oceanography*, 55, 23–44.
- Lundholm, N., Hasle, G.R., 2010. *Fragilariopsis* (Bacillariophyceae) of the Northern Hemisphere - morphology, taxonomy, phylogeny and distribution, with a description of *F. pacifica* sp. nov. *Phycologia*, 49, 438-460.
- Mahowald, N. M., Baker, A. R., Bergametti, G., Brooks, N., Duce, R. A., Jickells, T. D., Kubilay, N., Prospero, J. M., Tegen, I., 2005. Atmospheric global dust cycle and iron inputs to the ocean. *Global Biogeochemical Cycles*, 19, GB4025, doi: 10.1029/2004GB002402.
- Maier, E., Chaplignin, B., Abelmann, A., Gersonde, R., Esper, O., Ren, J., Friedrichsen, H., Meyer, H., Tiedemann, R., 2013. Combined oxygen and silicon isotope analysis of diatom silica from a deglacial subarctic Pacific record. *Journal of Quaternary Science*, 28, 571–581.
- Maier, E., Méheust, M., Abelmann, A., Gersonde, R., Chaplignin, B., Ren, J., Stein, R., Meyer, H., Tiedemann, R., 2015. Deglacial subarctic Pacific surface water hydrography and nutrient dynamics and links to North Atlantic climate variability and atmospheric CO_2 . *Paleoceanography*, doi: 10.1002/2014PA002763.
- Malmgren, B.A., Nordlund, U., 1997. Application of artificial neural networks to paleoceanographic data. *Palaeogeography, Palaeoclimatology, Palaeoecology*, 136, 359-373.
- Malmgren, B.A., Kucera, M., Nyberg, J., Waelbroeck, C., 2001. Comparison of statistical and artificial neural network techniques for estimating past sea surface temperatures from planktonic foraminifer census data. *Paleoceanography*, 16, 520–530, doi:10.1029/2000PA000562.
- Mantua, N.J., Hare, S.R., 2002. The Pacific decadal oscillation. *Journal of Oceanography*, 58, 35–44.
- Mantua, N.J., Hare, S.R., Zhang, Y., Wallace, J.M., Francis, R.C., 1997. A Pacific interdecadal climate oscillation with impacts on salmon production, *Bulletin of the American Meteorological Society*, 78, 1069–1079,
- Margalef, R., 1978. Life-forms of phytoplankton as survival alternatives in an unstable environment. *Oceanologica Acta*, 1, 493-508.
- MARGO Project Members, 2009. Constraints on the magnitude and patterns of ocean cooling at the Last Glacial Maximum. *Nature Geoscience*, 2, 127 - 132.
- Martin, J.H., Fitzwater, S.E., 1988. Iron deficiency limits phytoplankton growth in the northeast Pacific subarctic. *Nature*, 331, 341-343.
- Max, L., Riethdorf, J.-R., Tiedemann, R., Smirnova, M., Lembke-Jene, L., Fahl, K., Nürnberg, D., Matul, A., Mollenhauer, G., 2012. Sea surface temperature variability and sea-ice extent in the subarctic northwest Pacific during the past 15,000 years. *Paleoceanography*, 27, PA3213, doi:10.1029/2012PA002292.
- Max, L., Belz, L., Tiedemann, R., Fahl, K., Nürnberg, D., Riethdorf, J.-R., 2014. Rapid shifts in subarctic Pacific climate between 138 and 70 ka. *Geology*, doi:10.1130/G35879.1
- McDonald, D., 1997. The Late Quaternary History of Primary Productivity in the Subarctic East Pacific, Master Thesis, University of British Columbia. 201pp.

- McDonald, D., Pedersen, T.F., Crusius, J., 1999. Multiple late Quaternary episodes of exceptional diatom production in the Gulf of Alaska. *Deep Sea Research Part II: Topical Studies in Oceanography*, 46, 2993-3017.
- Medlin, L.K., Priddle, J., 1990. *Polar Marine Diatoms*. British Antarctic Survey, Cambridge.
- Méheust, M., 2014. Late Quaternary variability of sea-ice cover, surfacewater temperature and terrigenous input in the subarctic North Pacific and the Bering Sea: A biomarker approach. PhD dissertation, Universität Bremen, 98pp.
- Méheust, M., Fahl, K., Stein, R., 2013. Variability in modern sea surface temperature, sea ice and terrigenous input in the sub-polar North Pacific and Bering Sea: Reconstruction from biomarker data. *Organic Geochemistry*, 57, 54-64.
- Melles, M., Brigham-Grette, J., Minyuk, P.S., Nowaczyk, N.R., Wennrich, V., DeConto, R.M., Anderson, P.M., Andreev, A.A., Coletti, A., Cook, T.L., Haltia-Hovi, E., Kukkonen, M., Lozhkin, A.V., Rosen, P., Tarasov, P., Vogel, H., Wagner, B., 2012. 2.8 million years of arctic climate change from Lake El'Gygytgyn, NE Russia. *Science*, 337, 315–320.
- Menviel, L., Timmermann, A., Timm, O. E., Mouchet, A., 2011. Deconstructing the Last Glacial termination: the role of millennial and orbital-scale forcings. *Quaternary Science Reviews*, 30, 1155-1172.
- Minoshima, K., Kawahata, H., Ikehara, K., 2007. Changes in biological production in the mixed water region (MWR) of the northwestern North Pacific during the last 27 kyr. *Palaeogeography, Palaeoclimatology, Palaeoecology*, 254, 430-447.
- Monterey, G., Levitus, S., 1997. Seasonal variability of mixed layer depth for the world ocean. NOAA Atlas NESDIS, Vol. 14. U.S. Gov. Printing Office, Washington, D.C. 96 pp.
- Moore, T. C., 1978. The distribution of radiolarian assemblages in the modern and ice-age Pacific. *Marine Micropaleontology*, 3, 229–266.
- Moore, T.C., Burckle, L.H., Geitzenauer, K., Luz, B., Molina-Cruz, A., Robertson, J.H., Sachs, H., Sancetta, C., Thiede, J., Thompson, P., Wenkam, C., 1980. The reconstruction of sea surface temperatures in the Pacific Ocean of 18,000B.P. *Marine Micropaleontology*, 5, 215-247.
- Muhina, V.V., 1971. Problems of diatom and silicoflagellate Quaternary stratigraphy in the equatorial Pacific Ocean. In: Funnell, B.M., Riedel, W.R. (Eds.), *The Micropalaeontology of Oceans*. Cambridge University Press, London, pp. 423-431.
- Müller, P.J., Kirst, G., Ruhland, G., von Storch, I., Rosell-Mele, A., 1998. Calibration of the alkenone paleotemperature index $U_{37}^{K'}$ based on core-tops from the eastern South Atlantic and the global ocean (60 °N–60 °S). *Geochimica et Cosmochimica Acta*, 62, 1757–1772.
- Müller, J., Wagner, A., Fahl, K., Stein, R., Prange, M., Lohmann, G., 2011. Towards quantitative sea ice reconstructions in the northern North Atlantic: a combined biomarker and numerical modelling approach. *Earth and Planetary Science Letters*, 306, 137-148.
- Nakagawa, T., Kitagawa, H., Yasuda, Y., Tarasov, P.E., Nishida, K., Gotanda, K., Sawai, Y., Yangtze River Civilization Program Members, 2003. Asynchronous climate changes in the North Atlantic and Japan during the last termination. *Science*, 299, 688-691.
- Nakatsuka, T., Fujimune, T., Yoshikawa, C., Noriki, S., Kawamura, K., Fukamachi, Y., Mizuta, G., Wakatsuchi, M., 2004. Biogenic and lithogenic particle fluxes in the western region of the Sea of Okhotsk: Implications for lateral material transport and biological productivity. *Journal of Geophysical Research*, 109, C09S13, doi:10.1029/2003JC001908.
- NGRIP-Members, Andersen, K.K., Azuma, N., Barnola, J.M., Bigler, M., Biscaye, P., Caillon, N., Chappellaz, J., Clausen, H.B., Dahl-Jensen, D., Fischer, H., Flückiger, J., Fritzsche, D., Fujii, Y., Goto-Azuma, K., Gronvold, K., Gundestrup, N.S., Hansson, M., Huber, C., Hvidberg, C.S., Johnsen, S.J., Jonsell, U., Jouzel,

- J., Kipfstuhl, S., Landais, A., Leuenberger, M., Lorrain, R., Masson-Delmotte, V., Miller, H., Motoyama, H., Narita, H., Popp, T., Rasmussen, S.O., Raynaud, D., Röthlisberger, R., Ruth, U., Samyn, D., Schwander, J., Shoji, H., Siggard-Andersen, M.L., Steffensen, J.P., Stocker, T., Sveinbjornsdottir, A.E., Svensson, A., Takata, M., Tison, J.L., Thorsteinsson, T., Watanabe, O., Wilhelms, F., and White, J.W.C., 2004. High-resolution record of Northern Hemisphere climate extending into the last interglacial period. *Nature*, 431, 147–151.
- Niebauer, H., 1980. Sea ice and temperature variability in the Eastern Bering Sea and the relation to atmospheric fluctuations. *Journal of Geophysical Research*, 85(C12), 7507-7515.
- Niebauer, H., 1983. Multiyear sea ice variability in the Eastern Bering Sea: an update. *Journal of Geophysical Research*, 88(C5), 2733-2742.
- Niebauer, H.J., 1998. Variability in Bering Sea ice cover as affected by a regime shift in the Pacific in the period 1947–1996. *Journal of Geophysical Research*, 103, 27717-27737.
- North Greenland Ice Core Project members, 2004. High-resolution record of Northern Hemisphere climate extending into the last interglacial period. *Nature*, 431, 147-151.
- Obrezkova, M.S., Kolesnik, A.N., Semiletov, I.P., 2014. The diatom distribution in the surface sediments of the eastern Arctic seas of Russia. *Russian Journal of Marine Biology*, 40, 465-472.
- Ohtani, K., Akiba, Y., Takenouti, A.Y., 1972. Formation of western subarctic water in the Bering Sea. In: Takenouti, A.Y. (Ed.), *Biological oceanography of the northern North Pacific Ocean*. Idemitsu Shoten Publishing Corporation, Tokyo, pp. 32-44.
- Okazaki, Y., Takahashi, K., Katsuki, K., Ono, A., Hori, J., Sakamoto, T., Uchida, M., Shibata, Y., Ikehara, M., Aoki, K., 2005. Late Quaternary paleoceanographic changes in the southwestern Okhotsk Sea: evidence from geochemical, radiolarian, and diatom records. *Deep-Sea Research II*, 52, 2332–2350.
- Okazaki, Y., Timmermann, A., Menviel, L., Harada, N., Abe-Ouchi, A., Chikamoto, M., Mouchet, A., Asahi, H., 2010. Deep water formation in the North Pacific during the last glacial termination. *Science*, 329, 200–204.
- Okumura, Y.M., Deser, C., Hu, A., Timmermann, A., Xie, S.P., 2009. North Pacific climate response to fresh water forcing in the subarctic North Atlantic: Ocean and atmospheric pathways. *Journal of Climate*, 22, 1424–1445.
- Onodera, J., Takahashi, K., 2007. Diatoms and Siliceous Flagellates (Silicoflagellates, Ebridians, and Endoskeletal Dinoflagellate Actiniscus) from the Subarctic Pacific. *Memoir of the Faculty of Science, Kyushu University, Series D, Earth & Planetary Science*, XXXI, 105-136.
- Onodera, J., Takahashi, K., 2009. Long-term diatom fluxes in response to oceanographic conditions at Stations AB and SA in the central subarctic Pacific and the Bering Sea, 1990-1998. *Deep-Sea Research I*, 56, 189-211.
- Onodera, J., Takahashi, K., Honda, M.C., 2005. Pelagic and coastal diatom fluxes and the environmental changes in the northwestern North Pacific during December 1997-May 2000. *Deep-Sea Research II*, 52, 2218-2239.
- Overland, J.E., Pease, C.H., 1982. Cyclone climatology of the Bering Sea and its relation to sea ice extent. *Monthly Weather Review*, 110, 5–13.
- Overland, J.E., Adams, J.M., Bond, N.A., 1999. Decadal variability of the Aleutian Low and its relation to highlatitude circulation. *Journal of Climate*, 12, 1542–1548.
- Overland, J.E., Bond, N.A., Adams, J.M., 2002. The relation of surface forcing of the Bering Sea to large-scale climate patterns. *Deep Sea Research, Part II*, 49, 5855–5868.
- Overland, J.E., Stabeno, P.J., 2004. Is the climate of the Bering Sea warming and affecting the ecosystem? *EOS*, 85, 309-316.

- Overpeck, J.T., Webb III, T., Prentice, I.C., 1985. Quantitative interpretation of fossil pollen spectra: Dissimilarity coefficients and the method of modern analogs. *Quaternary Research*, 23, 87 - 108.
- Parkinson C. L., Comiso J. C., Zwally H. J., Cavallieri D. J., Gloersen P., and Campbell W. J., 1987. Arctic Sea Ice, 1973–1976 Satellite Passive-Microwave Observations, NASA Special Publication SP-489, pp 296.
- Parkinson, C.L., Gratz, A.J., 1983. On the Seasonal Sea Ice Cover of the Sea of Okhotsk. *Journal of Geophysical Research*, 88, 2793-2802.
- Pflaumann, U., Duprat, J., Pujol, C., Labeyrie, L., 1996. SIMMAX: A modern analog technique to deduce Atlantic sea surface temperatures from planktonic foraminifera in deep-sea sediments. *Paleoceanography*, 11, 15–35.
- Pflaumann, U., Sarnthein, M., Chapman, M., Duprat, J., Huels, M., Kiefer, T., Maslin, M., Schulz, H., van Kreveld, S., Vogelsang, E., Weinelt, M., 2003. North Atlantic: sea-surface conditions reconstructed by GLAMAP-2000. *Paleoceanography*, 18, doi:10.1029/2002PA000774.
- Pike, J., Crosta, X., Maddison, E.J., Stickley, C.E., Denis, D., Barbara, L., Renssen, H., 2009. Observations on the relationship between the Antarctic coastal diatoms *Thalassiosira antarctica* Comber and *Porosira glacialis* (Grunow) Jørgensen and sea ice concentrations during the Late Quaternary. *Marine Micropaleontology*, 73, 14–25.
- Poulin, M., 1990. Ice diatoms: the Arctic. In: Medlin, L.K, Priddle, J. (Eds), *Polar Marine Diatoms*. British Antarctic Survey, Cambridge, pp 15-18.
- Praetorius, S.L., Mix, A.C., 2014. Synchronization of North Pacific and Greenland climates preceded abrupt deglacial warming. *Science*, 345, 444-448.
- Prahl, F., Pisias, N., Sparrow, M., Sabin A., 1995. Assessment of sea-surface temperature at 42N in the California Current over the last 30,000 years. *Paleoceanography*, 10, 763-773.
- Prahl, F.G., Wolfe, G.V., Sparrow, M.A., 2003. Physiological impacts on alkenone paleothermometry. *Paleoceanography*, 18, doi:10.1029/2002PA000803.
- Prell, W.L., 1985. The stability of low-latitude sea-surface temperatures, an evaluation of the CLIMAP reconstruction with emphasis on the positive SST anomalies. Rep. TR025, US Dept. of Energy, Washington, DC. 60p.
- Qiu, B., 2000. Interannual variability of the Kuroshio Extension system and its impact on the wintertime SST field. *Journal of Physical Oceanography*, 30, 1486-1502.
- Qiu, B., 2002. Large-scale variability in the midlatitude subtropical and subpolar North Pacific Ocean: observations and causes. *Journal of Physical Oceanography*, 32, 353-375.
- Rae, J.W.B., Sarnthein, M., Foster, G.L., Ridgwell, A., Grootes, P.M., Elliott, T., 2014. Deep water formation in the North Pacific and deglacial CO₂ rise. *Paleoceanography*, 29, 645–667, doi: 10.1002/2013PA002570.
- Ran, L.H., Chen, J.F., Jin, H.Y., Li, H.L., Lu, Y., Wang, K., 2012. The distribution of surface sediment diatoms in the Bering Sea and Chukchi Sea. *Chinese Journal of Polar Research*, 24, 15-23 (in Chinese with English abstract).
- Rasmussen, S.O., Andersen, K.K., Svensson, A.M., Steffensen, J.P., Vinther, B.M., Clausen, H.B., Andersen, M.L., Johnsen, S.J., Larsen, L.B., Bigler, M., Röthlisberger, R., Fischer, H., Goto-Azuma, K., Hansson, M.E., Ruth, U., 2006. A new Greenland ice core chronology for the last glacial termination. *Journal of Geophysical Research (Atmospheres)*, 111, D06102, doi: 10.1029/2005JD006079.
- Rea, D.K., Basov, L.A., Krissek, L.A., 1995. Scientific results of drilling the North Pacific transect. In: Rea, D.K., Basov, I.A., Allan, J.F. (Eds), *Proceedings of the Ocean Drilling Program, Scientific results*, College Station, TX (Ocean Drilling Program), vol. 145, pp. 577-596.
- Reimer, P.J., Bard, E., Bayliss, A., Beck, J.W., Blackwell, P.G., Bronk Ramsey, C., Buck, C.E., Cheng, H., Edwards, R.L., Friedrich, M., Grootes, P.M., Guilderson, T.P., Haflidason, H., Hajdas, I., Hatté, C., Heaton,

- T.J., Hogg, A.G., Hughen, K.A., Kaiser, K.F., Kromer, B., Manning, S.W., Niu, M., Reimer, R.W., Richards, D.A., Scott, E.M., Southon, J.R., Turney, C.S.M., van der Plicht, J., 2013. IntCal13 and MARINE13 radiocarbon age calibration curves 0-50000 years calBP. *Radiocarbon*, 55, 1869–1887.
- Rella, S.F., Tada, R., Nagashima, K., Ikehara, M., Itaki, T., Ohkushi, K., Sakamoto, T., Harada, N., Uchida, M., 2012. Abrupt changes of intermediate water properties on the northeastern slope of the Bering Sea during the last glacial and deglacial period. *Paleoceanography*, 27, PA3203, doi:10.1029/2011PA002205.
- Ren, J., Gersonde, R., Esper, O., Sancetta, C., 2014. Diatom distributions in northern North Pacific surface sediments and their relationship to modern environmental variables. *Palaeogeography, Palaeoclimatology, Palaeoecology*, 402, 81-103.
- Reynolds, R.W., Rayner, N.A., Smith, T.M., Stokes, D.C., Wang, W., 2002. An improved in situ and satellite SST analysis for climate. *Journal of Climate*, 15, 1609-1625.
- Riethdorf, J.-R., Nürnberg, D., Max, L., Tiedemann, R., Gorbarenko, S.A., and Malakhov, M.I., 2013a. Millennial-scale variability of marine productivity and terrigenous matter supply in the western Bering Sea over the past 180 kyr. *Climate of the Past*, 9, 1345-1373, doi:10.5194/cp-9-1345-2013.
- Riethdorf, J.-R., Max, L., Nürnberg, D., Lembke-Jene, L., Tiedemann, R., 2013b. Deglacial development of (sub) sea surface temperature and salinity in the subarctic northwest Pacific: Implications for upper-ocean stratification. *Paleoceanography*, 28, 91–104, doi: 10.1002/palo.20014.
- Robertson, J.H., 1975. Glacial to Interglacial Oceanographic Changes in the Northwest Pacific, Including a Continuous Record of the Last 400,000 Years. Thesis, Columbia University, New York, N.Y., 355 pp.
- Rodionov, S.N., Bond, N.A., Overland, J.E., 2007. The Aleutian low, storm tracks, and winter climate variability in the Bering Sea. *Deep Sea Research Part II: Topical Studies in Oceanography*, 54, 2560–2577.
- Röhl, U., Abrams, L.J., 2000. High-resolution, downhole and non-destructive core measurements from sites 999 and 1001 in the Caribbean Sea: Application to the late Paleocene Thermal Maximum. *Proceedings of the Ocean Drilling Program, Scientific Results*, 165, 191–203.
- Rohling, E., Pälike, H., 2005. Centennial-scale climate cooling with a sudden cold event around 8,200 years ago. *Nature*, 434, 975–979.
- Round, F.E., Crawford, R.M., 1989. Phylum Bacillariophyta. In: Margulis, L., Corliss, J.O., Melkonian, M., Chapman, D.J. (Eds), *Handbook of Protozoa*, Jones and Barlett, Boston, pp. 574-596.
- Round, F.E., Crawford, R.M., Mann, D.G., 1990. *The Diatoms: biology and morphology of the genera*. Cambridge University Press, Cambridge, 747 pp.
- Ruth, U., Bigler, M., Röthlisberger, R., Siggaard-Andersen, M.-L., Kipfstuhl, S., Goto-Azuma, K., Hansson, M.E., Johnsen, S.J., Lu, H., Steffensen, J.P., 2007. Ice core evidence for a very tight link between North Atlantic and east Asian glacial climate. *Geophysical Research Letters*, 34, L03706, doi:10.1029/2006GL027876.
- Sabin, A.L., Pisias, N.G., 1996. Sea-surface temperature changes in the northeastern Pacific Ocean during the past 20,000 years and their relationship to climate changes in northwestern North America. *Quaternary Research*, 46, 48-61.
- Sachs, H.M., 1973a. North Pacific radiolarian assemblages and their relationship to oceanographic parameters. *Quaternary Research*, 3, 73-88.
- Sachs, H.M., 1973b. Late Pleistocene history of the North Pacific: Evidence from a quantitative study of radiolaria in core V21-173. *Quaternary Research*, 3, 89-98.
- Sachs, H.M., Webb III, T., Clark, D.R., 1977. Paleocological transfer functions. *Annual Review of Earth and Planetary Science*, 5, 159 – 178.
- Saenko, O.A., Schmittner, A., Weaver, A.J., 2004. The Atlantic-Pacific seesaw. *Journal of Climate*, 17, 2033–2038.

- Sancetta, C., 1979. Oceanography of the North Pacific during the last 18000 years - evidence from fossil diatoms. *Marine Micropaleontology*, 4, 103-123.
- Sancetta, C., 1981. Oceanographic and ecological significance of diatoms in surface sediments of the Bering and Okhotsk seas. *Deep-Sea Research*, 28A, 789-817.
- Sancetta, C., 1982. Distribution of diatom species in surface sediments of the Bering and Okhotsk seas. *Micropaleontology*, 28, 221-257.
- Sancetta, C., 1983a. Diatoms in sediments as indicators of the shelf-slope break. *SEPM Special Publication*, 33, 373-380.
- Sancetta, C., 1983b. Effect of Pleistocene glaciation upon oceanographic characteristics of the North Pacific Ocean and Bering Sea. *Deep Sea Research*, 30, 851-869.
- Sancetta, C., 1987. Three species of *Concinodiscus* Ehrenberg from North Pacific sediments examined in the light and scanning electron microscopes. *Micropaleontology*, 33, 230-241.
- Sancetta, C., 1992. Comparison of phytoplankton in sediment trap time series and surface sediments along a productivity gradient. *Paleoceanography*, 7, 183-194.
- Sancetta, C., 1999. Diatoms and marine paleoceanography. In: Stoermer, E.F., Smol, J.P. (Eds), *The Diatoms: Applications for the Environmental and Earth Sciences*. Cambridge University Press, Cambridge, pp. 374-386.
- Sancetta, C. and Silvestri, S., 1984. Diatom stratigraphy of the Late Pleistocene (Brunhes) subarctic Pacific. *Marine Micropaleontology*, 9, 263-274.
- Sancetta, C. and Silvestri, S., 1986. Pliocene-Pleistocene evolution of the North Pacific ocean-atmosphere system, interpreted from fossil diatoms. *Paleoceanography*, 1, 163-180.
- Sarnthein, M., Gebhardt, H., Kiefer, T., Kucera, M., Cook, M., Erlenkeuser, H., 2004. Mid Holocene origin of the sea surface salinity low in the subarctic North Pacific. *Quaternary Science Review*, 23, 2089–2099.
- Sarnthein, M., H. Gebhardt, T. Kiefer, H. Erlenkeuser, C. Kissel, F. Schmieder, 2005. 95-ky Cycles of ocean circulation in the far northwestern Pacific and South China Sea during the Brunhes Chron, in Milutin Milankovitch Anniversary Symposium: Paleoclimate and the Earth Climate System, Serbian Academy of Sciences and Arts, vol. 110, A. Berger, M. Ercegovac, F. Mesinger (Eds), pp. 135–140, Serbian Academy of Sciences and Arts, Belgrade.
- Sarnthein, M., Kiefer, T., Grootes, P.M., Elderfield, H., Erlenkeuser H., 2006. Warmings in the far northwestern Pacific promoted pre-Clovis immigration to America during Heinrich event 1. *Geology*, 34, 141–144.
- Sarnthein, M., Grootes, P. M., Kennett, J. P., Nadeau, M.-J., 2007. ^{14}C Reservoir ages show deglacial changes in ocean currents and carbon cycle, in *Past and Future Changes of the Oceanic Meridional Overturning Circulation: Mechanisms and Impacts*. AGU Monograph Series, 173, 175–196.
- Sarnthein, M., Schneider, B., Grootes, P. M., 2013. Peak glacial ^{14}C ventilation ages suggest major draw-down of carbon into the abyssal ocean. *Climate of the Past*, 9, 2595-2614, doi: 10.5194/cp-9-2595-2013.
- Sarnthein, M., Balmer, S., Grootes, P.M., Mudelsee, M., 2015. Planktic and benthic ^{14}C reservoir ages for three ocean basins, calibrated by a suite of ^{14}C plateaus in the glacial-to-deglacial Suigetsu atmospheric ^{14}C record. *Radiocarbon*, 57, 129-151.
- Sawada, K., Handa, N., 1998. Variability of the path of the Kuroshio ocean current over the past 25,000 years. *Nature*, 392, 592–595.
- Schrader, H.J., Gersonde, R., 1978. Diatoms and silicoflagellates. In: Zachariasse, W.J., et al. (Ed.), *Micropaleontological Methods and Techniques - an Exercise on an Eight Metres Section of the Lower Pliocene of Capo Rossello, Sicily: Utrecht micropaleontological bulletins*, 17, pp. 129–176.
- Schrader, H.J., Koç Karpuz, N.K., 1990. Norwegian-Iceland seas: Transfer functions between marine planktic diatoms and surface water temperature, In: U. Bleil and J. Thiede (Eds), *Geological History of the Polar*

- Oceans: Arctic versus Antarctic, NATO ASI Ser. C., vol.308, Kluwer Acad., Norwell, Mass. pp. 337-361.
- Seki, O., Nakatsuka, T., Kawamura, K., Saitoh S.-I., Wakatsuchi, M., 2007. Time-series sediment trap record of alkenones from the western Sea of Okhotsk. *Marine Chemistry*, 104, 253-265.
- Seki, O., Sakamoto, T., Sakai, S., Schouten, S., Hopmans, E.C., Sinninghe Damste, J.S., Pancost, R.D., 2009. Large changes in seasonal sea ice distribution and productivity in the Sea of Okhotsk during the deglaciations. *Geochemistry Geophysics Geosystems*. 10, Q10007.doi:10.1029/2009GC002613.
- Semina, H.J., 1981. Morphology and distribution of a tropical Denticulopsis. *Proceeding of 6th International Diatom Symposium*, Otto Koeltz, Koenigstein, West Germany, pp. 179-190.
- Serno, S., Winckler, G., Anderson, R.F., Hayes, C.T., McGee, D., Machalett, B., Ren, H., Straub, S.M., Gersonde, R., Haug, G.H., 2014. Eolian dust input to the Subarctic North Pacific, *Earth and Planetary Science Letters*, 387, 252-263.
- Sha, L., Jiang, H., Seidenkrantz, M.-S., Knudsen, K.L., Olsen, J., Kuijpers, A., Liu, Y., 2014. A diatom-based sea-ice reconstruction for the Vaigat Strait (Disko Bugt, West Greenland) over the last 5000 yr. *Paleogeography, Paleoclimatology, Paleoecology*, 403, 66-79.
- Sha, L.B., Jiang, H., Liu, Y.G., Zhao, M.X., Li, D.L., Chen, Z.L., Zhao, Y., 2015. Palaeo-sea-ice changes on the North Icelandic shelf during the last millennium: Evidence from diatom records. *Science China: Earth Sciences*, doi: 10.1007/s11430-015-5061-2
- Shiga, K., Koizumi, I., 2000. Latest Quaternary oceanographic changes in the Okhotsk Sea based on diatom records. *Marine Micropaleontology*, 38, 91-117.
- Shimada, C., Tanaka, Y., Tanimura, Y., 2006. Seasonal variation in skeletal silicification of *Neodenticula seminae*, a marine planktonic diatom - sediment trap experiments in the NW Pacific Ocean (1997-2001). *Marine Micropaleontology*, 60, 130-144.
- Shinji, F., 1972. Formation of western subarctic water in the Bering Sea, In: Takenouti, A.Y., (Eds), *Biological Oceanography of the Northern North Pacific Ocean*. Idemitsu Shoten, Tokyo. pp. 63–71.
- Shiomoto, A., Ishida, Y., Tamaki, M., Yamanaka, Y., 1998. Primary production and chlorophyll a in the northwestern Pacific Ocean in summer. *Journal of Geophysical Research*, 103, 24651-24661
- Sieger, R., Gersonde, R., Zielinski, U., 1999. A new extended software package for quantitative paleoenvironmental reconstructions. *EOS*, 80, 223.
- Sigman, D.M., Jaccard, S.L., Haug, G.H., 2004. Polar ocean stratification in a cold climate. *Nature* 428, 59–63.
- Simonsen, R., 1979. The diatom system: Ideas on phylogeny. *Bacillaria*, 2, 9-71.
- Simpson, G.L., 2007. Analogue Methods in Palaeoecology: Using the analogue Package *Journal of Statistical Software*, 22, 1-29.
- Simpson, G.L., Oksanen, J., 2011. analogue: Analogue matching and Modern Analogue Technique transfer function models. (R package version 0.7-0). (<http://cran.r-project.org/package=analogue>).
- Smayda, T.J., 1958. Biogeographical studies of marine phytoplankton. *Oikos*, 9, 158-191.
- Smirnova, M.A. Kazarina, G.Kh., Matul, A.G., Max, L., 2015. Diatom Evidence for Paleoclimate Changes in the Northwestern Pacific during the Last 20000 Years. *Okeanologiya*, 55, 425–431.
- Southon, J.R., Nelson, D.E., Vogel, J.S., 1990. A record of past ocean-atmosphere radiocarbon differences from the Northeast Pacific. *Paleoceanography*, 5, 197–206,
- Stabeno, P.J., Reed, R. K., 1994. Circulation in the Bering Sea Basin observed by satellite-tracked drifters: 1986-1993. *Journal of Physical Oceanography*, 24, 848-854.
- Stabeno, P.J., Schumacher, J.D., Ohtani, K., 1999. The physical oceanography of the Bering Sea. In: Loughlin, T.R., Ohtani, K. (Eds.), *Dynamics of the Bering Sea*. University of Alaska Sea Grant, Fairbanks, pp. 1–21.
- Stoermer, E.F., Smol, J.P., 2010. *The Diatoms: Applications for the Environmental and Earth Sciences*. Cambridge University Press, Cambridge, 667p.

- Stoynova, V., Shanahan, T.M., Hughen, K.A., de Vernal, A., 2013. Insights into Circum- Arctic Sea ice variability from molecular geochemistry. *Quaternary Science Reviews*, 79, 63-73.
- Stuiver, M., Reimer, P. J., 1993. Extended 14C database and revised CALIB radiocarbon calibration program. *Radiocarbon*, 35, 215-230.
- Swann, G.E.A., Leng, M.J., 2009. A review of diatom $\delta^{18}\text{O}$ in palaeoceanography. *Quaternary Science Reviews*, 28, 384-398.
- Swann, G.E.A. and Snelling, A.M., 2015. Photic zone changes in the north-west Pacific Ocean from MIS 4-5e. *Climate of the Past*, 11, 15-25.
- Syventsen, E.E., 1979. Resting spore formation in clonal cultures of *Thalassiosira antarctica* Comber, *T. nordenskiöldii* Cleve and *Detonula convolvacea* (Cleve). *Nova Hedwigia*, 64, 41-63.
- Széréméta, N., Bassinot, F., Balut, Y., Labeyrie, L., Pagel, M., 2004. Oversampling of sedimentary series collected by giant piston corer: Evidence and corrections based on 3.5-kHz chirp profiles. *Paleoceanography*, 19, PA1005, doi:10.1029/2002PA000795.
- Takahashi, K., 1986. Seasonal fluxes of pelagic diatoms in the subarctic Pacific, 1982-1983. *Deep Sea Research*, 33, 1225-1251.
- Takahashi, K., 1997. Siliceous microplankton fluxes in the eastern Subarctic Pacific, 1982-1986. *Journal of Oceanography*, 53, 455-466.
- Takahashi, K., 2005. The Bering Sea and paleoceanography. *Deep-Sea Research II*, 52, 2080-2091.
- Takenouti, A.Y., Ohtani, K., 1974. Currents and water masses in the Bering Sea: a review of Japanese work. In: Hood, D.W., Kelley, E.J. (Eds), *Oceanography of the Bering Sea*. Institute of Marine Sciences, University of Alaska, pp. 39-58.
- Takizawa, T., 1982. Characteristics of the Soya warm current in the Okhotsk Sea. *Journal of the Oceanography Society of Japan*, 38, 281-292.
- Talley, L.D., 1993. Distribution and Formation of North Pacific Intermediate Water. *Journal of Physical Oceanography*, 23, 517-537.
- Tanimura, Y., 1999. Varieties of a single cosmopolitan diatom species associated with surface water masses in the North Pacific. *Marine Micropaleontology*, 37, 199-218.
- Taylor, M.A., Hendy, I.L., Pak, D.K., 2014. Deglacial ocean warming and marine margin retreat of the Cordilleran Ice Sheet in the North Pacific Ocean. *Earth and Planetary Science Letters*, 403, 89-98.
- Telford, R.J., 2006. Limitations of dinoflagellate cyst transfer functions. *Quaternary Science Reviews*, 25, 1375-1382.
- Telford, R.J., Birks, H.J.B., 2005. The secret assumption of transfer functions: problems with spatial autocorrelation in evaluating model performance. *Quaternary Science Review*, 24, 2173-2179.
- ter Braak, C.J.F., Juggins, S., 1993. Weighted averaging partial least squares regression (WAPLS): an improved method for reconstructing environmental variables from species assemblages. *Hydrobiologia*, 269-270, 485-502.
- ter Braak, C.J.F., Prentice, I.C., 1994. A theory of gradient analysis. *Ecoscience*, 1, 127-140.
- ter Braak, C.J.F., Verdonschot, P.F.M., 1995. Canonical correspondence analysis and related multivariate methods in aquatic ecology. *Aquatic Science*, 57, 255-289.
- ter Braak, C.J.F., Smilauer, P., 2002. *CANOCO reference manual and CanoDraw Windows user's guide: software for canonical community ordination (version 4.5)*. Microcomputer Power, Ithaca, NY, USA, 500 pp.
- Ternois, Y., Kawamura, K., Ohkouchi, N., Keigwin, L., 2000. Alkenone sea surface temperature in the Okhotsk Sea for the last 15 kyr. *Geochemical Journal*, 34, 283-293.
- Ternois, Y., Kawamura, K., Keigwin, L., Ohkouchi, N., Nakatsuka, T., 2001. A biomarker approach for

- assessing marine and terrigenous inputs to the sediments of Sea of Okhotsk for the last 27000 years. *Geochimica et Cosmochimica Acta*, 65, 791-802.
- Trend-Staid, M., Prell, W.L., 2002. Sea surface temperature at the Last Glacial Maximum: a reconstruction using the modern analog technique. *Paleoceanography*, 17, doi:10.1029/2000PA000506.
- Tsoy, I.B., Wong, C.S., 1999. Diatom fluxes and preservation in the deep northwest Pacific Ocean. In: Mayama, S., Idei, M., Koizumi, I. (Eds.), *Proceedings of the 14th International Diatom Symposium*. Koeltz Scientific Books, Koenigstein, Germany, pp. 523-549.
- Tsoy, I.B., Obrezkova, M.S., Artemova, A.V., 2009. Diatoms in surface sediments of the Sea of Okhotsk and the Northwest Pacific Ocean. *Oceanology*, 49, 130-139.
- Tsuda, A., Takeda, S., Saito, H., Nishioka, J., Nojiri, Y., Kudo, I., Kiyosawa, H., Shiimoto, A., Imai, K., Ono, T., Shimamoto, A., Tsumune, D., Yoshimura, T., Aono, T., Hinuma, A., Kinugasa, M., Suzuki, K., Sohrin, Y., Noiri, Y., Tani, H., Deguchi, Y., Tsurushima, N., Ogawa, H., Fukami, K., Kuma, K., and Saino, T., 2003, A mesoscale iron enrichment in the western subarctic Pacific induces a large centric diatom bloom. *Science*, 300, 958-961.
- Tsuda, A., Takeda, S., Saito, H., Nishioka, J., Kudo, I., Nojiri, Y., Suzuki, K., Uematsu, M., Wells, M.L., Tsumune, D., Yoshimura, T., Aono, T., Aramaki, T., Cochlan, W.P., Hayakawa, M., Imai, K., Isada, T., Iwamoto, Y., Johnson, W.K., Kameyama, S., Kato, S., Kiyosawa, H., Kondo, Y., Levasseur, M., Machida, R.J., Nagao, I., Nakagawa, F., Nakanishi, T., Nakatsuka, S., Narita, A., Noiri, Y., Obata, H., Ogawa, H., Oguma, K., Ono, T., Sakuragi, T., Sasakawa, M., Sato, M., Shimamoto, N., Takata, H., Trick, C.G., Watanabe, Y.W., Wong, C.S., Yoshie, N., 2007. Evidence for the grazing hypothesis: grazing reduces phytoplankton responses of the HNLC ecosystem to iron enrichment in the western subarctic Pacific (SEEDS II). *Journal of Oceanography*, 63, 983-994.
- Venrick, E.L., 1971. Recurrent groups of diatom species in the North Pacific. *Ecology* 52, 614-625.
- Warren, B.A., 1983. Why is no deep water formed in the North Pacific? *Journal of Marine Research*, 41, 327-347.
- White, W. B., 1982. Traveling Wave-Like Mesoscale Perturbations in the North Pacific Current. *Journal of Physical Oceanography*, 12, 231-243.
- Xiao, X., Fahl, K., Müller, J., Stein, R., 2015. Sea-ice distribution in the modern Arctic Ocean: Biomarker records from trans-Arctic Ocean surface sediments. *Geochimica et Cosmochimica Acta*, 155, 16-29, doi:10.1016/j.gca.2015.01.029.
- Wiedmer, M., Montgomery, D.R., Gillespie, A.R., Greenberg, H., 2010. Late quaternary megafloods from glacial Lake Atna, southcentral Alaska U.S.A. *Quaternary Research*, 73, 413-424.
- Witkowski, A., Lange-Bertalot, H., Metzeltin, D., 2000. Diatom flora of marine coasts I. In: Lange-Bertalot, H. (Ed.), *Iconographia Diatomologica*, Vol. 7, 925pp.
- Wong, C.S., Whitney, F.A., Crawford, D.W., Iseki, K., Mearns, R.J., Johnson, W.K., Page, J.S., Timothy, D., 1999, Seasonal and interannual variability in particle fluxes of carbon, nitrogen and silicon from time series of sediment traps at Ocean Station P, 1982-1993: relationship to changes in subarctic primary productivity. *Deep-Sea Research II*, 46, 2735-2760.
- Yasuda, I., 2004. North Pacific Intermediate Water: progress in SAGE (SubArctic Gyre Experiment) and related projects. *Journal of Oceanography*, 60, 385 - 395.
- Yuan, W., Zhang, J., 2006. High correlations between Asian dust events and biological productivity in the western North Pacific. *Geophysical Research Letters*, 33, L07603, doi:10.1029/2005GL025174.
- Yuan, X., Talley, L., 1996. The subarctic frontal zone in the North Pacific: characteristics of frontal structure from climatological data and synoptic surveys. *Journal of Geophysical Research*, 101(C7), 16491-16508.
- Zahn, R., Pedersen, T.F., Bornhold, B.D., Mix, A.C., 1991. Water mass conversion in the glacial subarctic

- Pacific (54°N, 148°W): Physical constrains and the benthic-planktonic stable isotope record. *Paleoceanography*, 6, 543-560.
- Zhang, X., Lohmann, G., Knorr, G., Purcell, C., 2014. Abrupt glacial climate shifts controlled by ice sheet changes. *Nature*, 512, 290–294.
- Zhao, P., Zhang, X., Zhou, X., Ikeda, M., Yin, Y., 2004. The sea ice extent anomaly in the north pacific and its impact on the east Asian summer monsoon rainfall. *Journal of Climate*, 17, 3434-3447.
- Zielinski, U., 1993. Quantitative estimation of palaeoenvironmental parameters of the Antarctic Surface Water in the Late Quaternary using transfer functions with diatoms. *Reports on Polar Research*, vol. 126. Alfred Wegener Institute for Polar and Marine Research, Bremerhaven. 148 pp.
- Zielinski, U., Gersonde, R., 1997. Diatom distribution in Southern Ocean surface sediments (Atlantic sector): implications for paleoenvironmental reconstructions. *Palaeogeography, Palaeoclimatology, Palaeoecology*, 129, 213-250.
- Zielinski, U., Gersonde, R., Sieger, R., Fütterer, D., 1998. Quaternary surface water temperature estimations: Calibration of a diatom transfer function for the Southern Ocean. *Paleoceanography*, 13, 365-38

Appendix A1: Surface sample locations and corresponding environmental variables

The data set of 422 surface samples is not provided here due to its large size. Instead, it is available online at <http://dx.doi.org/10.1016/j.palaeo.2014.03.008>. (Table S1)

Appendix A2: Deglacial subarctic Pacific surface water hydrography and nutrient dynamics and links to North Atlantic climate variability and atmospheric CO₂

E. Maier¹, M. Méheust¹, A. Abelmann¹, R. Gersonde¹, B. Chaplignin², **J. Ren¹**, R. Stein¹, H. Meyer², R. Tiedemann¹

1 Alfred Wegener Institute Helmholtz Centre for Polar and Marine Research, 27568 Bremerhaven, Germany

2 Alfred Wegener Institute Helmholtz Centre for Polar and Marine Research, 14473 Potsdam, Germany

Paleoceanography, 2015, doi: 10.1002/2014PA002763

Abstract

The glacial-to-Holocene evolution of subarctic Pacific surface water stratification and silicic acid (Si) dynamics is investigated based on new combined diatom oxygen ($\delta^{18}\text{O}_{\text{diat}}$) and silicon ($\delta^{30}\text{Si}_{\text{diat}}$) isotope records, along with new biogenic opal, subsurface foraminiferal $\delta^{18}\text{O}$, alkenone-based sea surface temperature, sea-ice, diatom and core logging data from the NE Pacific. Our results suggest that $\delta^{18}\text{O}_{\text{diat}}$ values are primarily influenced by changes in freshwater discharge from the Cordilleran Ice Sheet (CIS), while corresponding $\delta^{30}\text{Si}_{\text{diat}}$ are primarily influenced by changes in Si supply to surface waters.

Our data indicate enhanced glacial to mid-HS1 NE Pacific surface water stratification, generally limiting the Si supply to surface waters. However, we suggest that an increase in Si supply during early HS1, when surface waters were still stratified, is linked to increased North Pacific Intermediate Water formation. The coincidence between fresh surface waters during HS1 and enhanced ice-rafted debris sedimentation in the North Atlantic indicates a close link between CIS and Laurentide Ice Sheet dynamics and a dominant atmospheric control on CIS deglaciation. The Bølling/Allerød (B/A) is characterized by destratification in the subarctic Pacific and an increased supply of saline, Si-rich waters to surface waters. This change towards increased convection occurred prior to the Bølling warming and is likely triggered by a switch to sea-ice-free conditions during late HS1. Our results furthermore indicate a decreased efficiency of the biological pump during late HS1 and the B/A (possibly also the Younger Dryas), suggesting that the subarctic Pacific has then been a source region of atmospheric CO₂.

Author's contribution: *I counted diatom composition of MD01-2146 from the western North Pacific and MD02-2489 from the eastern North Pacific and provided paleoceanographic information based on diatom variability.*

Appendix A3: Preliminary biostratigraphic dating of cores retrieved during Sonne202-INOPEX curise in the North Pacific

Rainer Gersonde¹, **Jian Ren**¹, Maria Obrezkova²

¹ Alfred Wegener Institute, Bremerhaven, Germany

² V.I. Il'ichev Pacific Oceanological Institute, Russia

In: Gersonde, R., 2012. *The expedition of the research vessel Sonne to the subpolar North Pacific and the Bering Sea in 2009 (SO202-INOPEX). Berichte zur Polar- und Meeresforschung = Reports on polar and marine research, 643. Alfred Wegener Institute for Polar and Marine Research, Bremerhaven (323 pp).*

Abstract

Microfossils are valuable as a primary tool for the establishment of age models of sediments. During SO202-INOPEX on-board biostratigraphy was based on the occurrence of diatoms. The siliceous microfossils are most significant for Cenozoic stratigraphy, especially in the North Pacific, where calcareous microfossils are generally rare in post-Eocene sediments (Gladenkov 2006). The North Pacific diatom zonation has been studied and established by several researchers (e.g. Koizumi 1973, Akiba 1986). During SO202-INOPEX we have used the zonation established by Gladenkov (2006) as a reference.

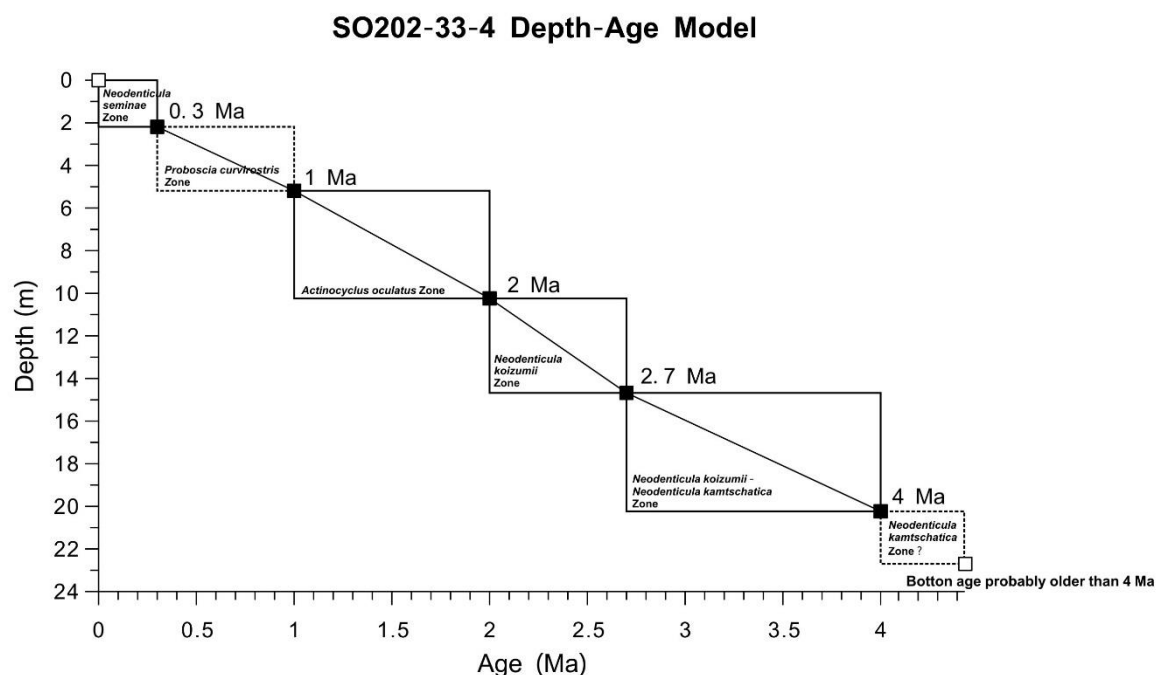


Figure Diatom biostratigraphic dating of SO202-33-4. *Proboscia curvirostris* is rare in the corresponding zone, which makes the upper boundary uncertain. The possible occurrence of the *Neodenticula kamtschatica* zone at the base of the core places the lowermost portion of the core at an age older than 4 Ma.

Author's contribution: I counted diatom composition of half of the INOPEX cores on board to establish biostratigraphic age frames.